EFFECT OF NEAR-FAULT GROUND MOTION ON DYNAMIC RESPONSE OF BUILDINGS ON HILLSLOPE

Ph. D. THESIS

by
PRABHAT KUMAR

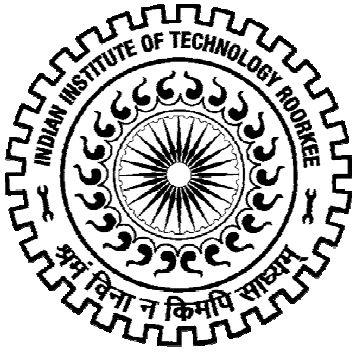

DEPARTMENT OF EARTHQUAKE ENGINEERING
INDIAN INSTITUTE OF TECHNOLOGY ROORKEE
ROORKEE-247 667 (INDIA)

JULY, 2015

EFFECT OF NEAR-FAULT GROUND MOTION ON DYNAMIC RESPONSE OF BUILDINGS ON HILLSLOPE

A THESIS
Submitted in partial fulfilment of the requirements for the award of the degree of
DOCTOR OF PHILOSOPHY
in
EARTHQUAKE ENGINEERING

by
PRABHAT KUMAR

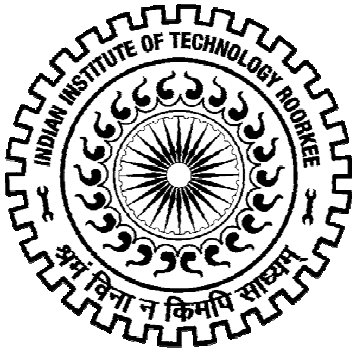

DEPARTMENT OF EARTHQUAKE ENGINEERING
INDIAN INSTITUTE OF TECHNOLOGY ROORKEE
ROORKEE-247 667 (INDIA)

JULY, 2015

INDIAN INSTITUTE OF TECHNOLOGY ROORKEE
ROORKEE

CANDIDATE'S DECLARATION

I hereby certify that the work which is being presented in this thesis entitled **"EFFECT OF NEAR-FAULT GROUND MOTION ON DYNAMIC RESPONSE OF BUILDINGS ON HILLSLOPE"** in partial fulfilment of the requirements for the award of the Degree of Doctor of Philosophy and submitted in the Department of Earthquake Engineering of the Indian Institute of Technology Roorkee is an authentic record of my own work carried out during a period from July, 2009 to July, 2015 under the supervision of Dr. Ashwani Kumar, Professor, and Sri. A.D. Pandey, Assistant Professor, Department of Earthquake Engineering of the Indian Institute of Technology Roorkee.

The matter presented in the thesis has not been submitted by me for the award of any other degree of this or any other Institute.

(PRABHAT KUMAR)

This is to certify that the above statement made by the candidate is correct to the best of our knowledge.

(Ashwani Kumar)
Supervisor

(A.D. Pandey)
Supervisor

Date:

ABSTRACT

The immense damage potential due to the near-fault ground motion (NFGM) has been recognized during the damage investigations associated with the 1971 San Fernando, 1979 Imperial Valley, 1989 Loma Prieta, 1992 Landers, 1994 Northridge, 1995 Kobe, and 1999 Chi-Chi earthquakes. The NFGM is composed of high frequencies, representing accelerations, and one or more dominant long-period velocity pulses. It has been further recognized that the large amplitude pulses, primarily related to directivity effect, control the dynamic response of medium- and long-period structures, whereas, the high frequency part of the NFGM plays an important role especially for the response of short-period structures. The impulsive character of NFGM is mainly due to forward-directivity, and fault-normal (FN) component of ground motion is more dominant because of radiation pattern. These aspects of NFGM stimulated researchers to study the characteristics of NFGM and identify its governing parameters that are responsible for observed damages. This study is intended to investigate the near-fault pulse-type characteristics of the three moderate-sized Himalayan earthquakes, characteristics of the extracted near-fault pulses, interpretation of the NFGM response spectra and its comparison with the Indian Seismic (IS) codal spectra, and to analyze and interpret the response of hillslope buildings under the effect of near-fault pulse-type ground motions in the Himalayan region. From seismic safety point of view responses due to NFGMs are compared with the responses obtained from conventional types of seismic inputs.

Strong motion arrays were deployed by the Department of Earthquake Engineering, Indian Institute of Technology, Roorkee, to allow measuring the strong ground motion due to moderate and large earthquakes in the Himalaya. These arrays resulted in recording of strong ground motions due to the 1986 Dharamsala earthquake (M_w 5.5) at nine stations, due to the 1991 Uttarkashi earthquake (M_w 6.8) at thirteen stations, and due to the 1999 Chamoli earthquake (M_w 6.5) at eleven stations. Near-Fault Ground Motion (NFGM) spectral characteristics of these three moderate-sized Himalayan earthquakes have been studied from the 33 available strong ground motion recordings. Pulse characteristics of FN components of ground motions in terms of pulse-periods, spectral pulse-periods and pulse-indicators have been extracted adopting wavelet analysis. To allow for pulse detection, standard methodology proposed by Baker (2007) has been adopted. Seven mother wavelets were used in the analysis, and it was found that db4 and db7 mother wavelets were more efficient in extracting the pulse-type characteristics. However, the spectra of long-period pulses extracted using Daubechies mother wavelet of order seven (db7) are closer to the long-period spectral amplitudes of the FN

components of ground motions at three sites. Comparison of computed pulse-periods of the three earthquakes with the pulse-periods, estimated using available relations between magnitude and pulse-period, showed that computed pulse-periods are on lower side. The estimated pulse-periods by and large conform to the world-wide dataset but are on lower side than the average pulse-periods. It seems that the lower pulse-periods of the Himalayan earthquakes are due to the compressional tectonic environment and thrust-type focal mechanisms. The comparison of peak amplitudes of the velocity pulses estimated using available world-wide relations with the computed amplitudes for the three earthquakes showed lot of variability. NFGM spectra, at Bhatwari and Gopeshwar stations, showed higher spectral amplitudes in the velocity-sensitive and acceleration-sensitive regions compared to Indian codal response spectra. This is attributed to high PGV/PGA ratios. This demonstrated that NFGM leads to widening of acceleration-sensitive region, as a consequence of widening of the acceleration-sensitive region, the structures designed according to IS code as flexible structures shall behave as stiff structures in the near-fault region in the Himalaya.

According to the IS code most of the hilly areas in the Himalaya fall in seismic zone IV and V. The building located on hillslope poses special structural problems. In hilly areas, many multistoreyed r.c. framed buildings rests on hillslope. The floors of these buildings generally step-back towards the hillslope and at the same time the building may have setback also, this stepping back of building towards hillslope result into unequal column heights at the same floor level. The buildings resting on hillslope are highly irregular and asymmetric. These buildings are subjected to severe torsion in addition to lateral shears under the earthquake excitation. In the present study to capture the detailed dynamic response of buildings on hillslope, 3D modeling of the building has been carried out. For this purpose dynamic analysis of two special moment resistant frame (SMRF) 3D configurations consisting of Step-Back (SB) and Step-Back-Set-Back (SBSB) models have been conducted. For both types of building models, the number of storeys has been varied from two to five because most of the residential buildings in the hilly regions are low-rise buildings with number of storeys limited to five storeys in majority of cases. Seismic response has been computed adopting six types of seismic inputs at three sites, namely, the recorded near-fault pulse-type ground motion, near-fault fault-normal (FN) component of ground motion, extracted (EXT) pulse of near-fault fault-normal (FN) component using ‘db7’ mother wavelet, residual (RSD) part of near-fault fault-normal component, estimated site-specific ground motion that include near-fault factor, and the IS codal spectra and its compatible ground motion. For computing dynamic responses of the buildings response spectrum method and modal time history method were adopted.

Response of two types of building models (SB & SBSB) have brought out that as the number of storeys increase from 2 to 5, the response due to extracted (EXT) pulse increases compared to response due to residual (RSD) part of ground motion. This is only true when the seismic excitation is across the slope and direction of floor displacements are observed in the in-plane and out-of-plane on account of the low frequency pulse. However, for all SBSB building models, the response along the slope due to residual (RSD) part is always higher than the response due to extracted (EXT) pulse when the ground motion is applied along the slope because there is no significant variation in the time periods of the models along the slope. At Bhatwari site located in seismic zone IV as per IS code, the responses of all buildings of both types due to codal type ground motion were found to be highly un-conservative compared to pulse type ground motion and estimated site-specific ground motion. At Bhatwari site, for both building forms (SB & SBSB), both response parameters (floor displacements and ground column shear force) due to codal spectra show lowest values compared to those obtained from other seismic inputs. At Gopeshwar site that falls in seismic zone V, for higher storey SB building models, i.e., for 4 and 5 storey building models the response along the slope, and for all the SBSB building models, the response across the slope due to codal type ground motion found highly un-conservative compared to pulse-type ground motion and estimated site-specific ground motion. The same trend was also observed when the response was considered across the slope for 2, 3, and 4 storey SB building models. At Shapur site, because of smaller magnitude of 1986 Dharamsala earthquake, the recorded pulse-type ground motion, extracted (EXT) pulse, and residual (RSD) part of ground motion showed lower response compared to responses obtained due to estimated site-specific ground motion and Indian seismic codal based ground motion for zone V. With the increasing period of buildings, response due to extracted long-period pulse at three sites is in close agreement with responses due to recorded pulse-type ground motions & FN component of ground motions. This illustrates the possibility of representation of NFGM with an appropriate long-period pulse model. The Indian codal spectra needs modification and the effects of pulse-type ground motion due to moderate, large, and great earthquakes could be incorporated for sites located in the vicinity of active faults.

ACKNOWLEDGEMENTS

The research work presented in this thesis was carried out from July 2009 to July 2015 in the Department of Earthquake Engineering, Indian Institute of Technology Roorkee. Many people have put in their contribution towards bringing this research work to the successful completion.

With deep sense of gratitude, I acknowledge the valuable guidance, advice and help rendered to me for this work by my learned supervisors, Dr. Ashwani Kumar, Professor and Shri A.D. Pandey, Assistant Professor, Department of Earthquake Engineering, Indian Institute of Technology Roorkee. Their consistent involvement, inspiration and encouragement to me, bring this thesis into this form without which it was difficult for me to reach its culmination.

I am thankful to Dr. Ashwani Kumar, Professor, and Dr. H.R. Wason, Professor, former Heads of the Department and Dr. M.L. Sharma, Professor, Head of the Department, for providing me all facilities required to complete these studies.

I wish to express my sincere thanks to Dr. V.N. Singh, Professor, Department of Earth Science, and Dr. Pankaj Agrawal, Professor, Department of Earthquake Engineering, Indian Institute of Technology Roorkee, for their constructive comments and inventive suggestions at every step of this work.

Cooperation extended to me by my fellow researchers, Dr. Arjun Kumar and Mr. Nitesh Ahir, in the Department of Earthquake Engineering during various stages of this work is gratefully acknowledged.

It is a pleasure to express my respect, love and gratitude toward my father Shri. Brij Pal and mother Smt. Usha Rani, for their blessings and enormous support.

My heartiest thanks to my wife, Smt. Swati Arya, brother, Mr. Vikas Kumar, and in-laws for their understanding and moral support.

Last but not the least I am thankful to almighty GOD for everything.

(Prabhat Kumar)

CONTENTS

LIST OF TABLES

LIST OF FIGURES

CHAPTER 1

INTRODUCTION

1.1 General

It has now been well recognized that the response of structures and engineering systems subjected to strong ground motion (SGM) due to earthquakes depends on the characteristics of SGM in terms of its amplitudes, frequency content and duration of shaking, and the parameters of structural systems, such as their natural periods and damping values. The 1908 Messina earthquake in Italy (also known as the Reggio earthquake) resulted in the loss of about 83000 lives, and marked the beginning of earthquake engineering in the world. The government of Italy constituted a fourteen members special committee to study this earthquake and make recommendations. The committee was constituted of nine practicing engineers and five professors of engineering (Housner, 1984). The committee's recommendations seems to be first engineering recommendation that structures to resist earthquakes should be designed by equivalent static method. It was recommended that first storey be designed for a horizontal force 1/12 the weight above, and for the design of 2nd and 3rd storey, the horizontal force should be 1/8 of the building weight above. Since then various methods have been developed to compute the response of structures subjected to strong ground shaking. Two most commonly used methods to compute the response of structures are: the response spectrum method and the time history method.

As the knowledge advanced, it was realized that despite incorporating earthquake resistant design, structures suffered significant amount of damages during some of the major earthquakes such as, the 1989 Loma Prieta earthquake (M_w 6.9), the 1994 Northridge earthquake (M_w 6.7), and the 1999 Chi-chi earthquake (M_w 7.6). From the detailed and critical examination of the strong motion time histories, particularly velocity time histories, led to the observation that the time histories contained the pulse-type ground motion that contributed significantly toward such damages during these earthquakes. Studies also demonstrated that structures located within 30 km from the major fault that ruptured and caused these earthquakes, suffered extensive damages despite the incorporation of earthquake resistant design in accordance with the codal provisions. Further, the observed damages were very different than the commonly observed damages, normally expected at far-sites from such earthquakes. This led to the recognition that strong ground motion characteristics at near-fault

sites are very different compared to the strong ground motion characteristics at far-sites. Time histories of the near-fault ground motion (NFGM) contain pulse-like ground motion, rich in low frequency, with large amplitudes and energy concentration at the beginning of the pulse-type shaking, which is dominated by very high energy. The typical seismological and geological parameters that govern the pulse-type ground motion include the forward directivity, the hanging wall, the fling step, and the vertical effect (Huang and Shi, 2000; Kalkan and Kunnath, 2006; Kunnath et al., 2008; Kunnath and Zhao, 2009 and Shuang and Xie, 2007). Studies have shown that these parameters affect the SGM within 20 to 30 km from the source of an earthquake (Huang and Shi, 2000, Shuang and Xie, 2007 and Rathje et al., 2004). In view of these considerations, attention is focused in the recent years to understand the characteristics of the NFGM and incorporate these characteristics in the seismic design procedures so that the structures can be designed to sustain the NFGM.

Pulse characterization of the NFGM and their effects on the response of structures is one of the most promising fields of research in earthquake engineering and structural dynamics. In India, although several seismically active major faults, such as the Main Boundary Thrust (MBT) and the Main Central Thrust (MCT) exist in the Himalaya, with potential of generating moderate and major earthquakes, very little attention has been paid to the study of the NFGM characteristics, and its possible consequences on the damage to buildings and structures. In view of these considerations, the focus of the present work is to study the characteristics of pulse-type NFGM of moderate earthquakes that occurred in the Himalaya and to compute the dynamic response of buildings on the hillslope subjected the NFGM.

1.2 Motivation for the Study

Himalayan region has experienced many moderate, large, and great earthquakes because the region lies on a plate boundary. In the last about 120 years, the region experienced two major and three great earthquakes, namely, the 1897 Assam earthquake (M_w 8.1), the 1905 Kangra earthquake (M_w 7.8), the 1934 Bihar-Nepal earthquake (M_w 8.0), the 1950 Assam earthquake (M_w 8.6), and the 2005 Kashmir earthquake (M_w 7.6). Recently a major earthquake, viz., the Nepal earthquake (M_w 7.8), struck the region around Kathmandu, the capital city of Nepal on 12 May 2015. These earthquakes caused extensive damages and loss of lives. For most of these earthquakes, strong motion records were not available. In India, to collect strong motion data from moderate and major earthquakes, the strong motion programs initiated in mid 60’s, and

the first accelerogram was produced from the 1967 Koyna earthquake (M_w 6.1). In 1983, under a joint Indo-US collaborative research project, the first strong motion (SM) array was deployed in the Himachal Himalaya for systematic collection of the SGM data from the seismically active regions in the Himalaya. This SM array was named as Kangra array. Thereafter, two more SM arrays were deployed in the Shillong region of northeast India (called the Shillong array) and in the Garhwal-Kumaun Himalaya (called the UP array). These SM arrays were equipped with analog type accelerographs (SMA-1 of kinemetrics), and provided valuable strong motion records. The nine strong motion stations of the Kangra array were triggered and provided strong motion recordings of the 1986 Dharamsala earthquake (M_w 5.5) (Chandrasekaran, 1988). The SGM of the 1991 Uttarkashi earthquake (M_w 6.8) was recorded at thirteen stations, and that of the 1999 Chamoli earthquake (M_w 6.5) was recorded at eleven stations of the SM array installed in the Garhwal and Kumaun Himalaya (Chandrasekaran and Das, 1995 and Shrikhande et al., 2000). Several studies related to seismological and strong motion aspects were conducted based on these records (e.g., Rajendran et al., 2000, Shrikhande et al., 2000; Jain and Das, 1993; Jain et al., 1999; Joshi et al., 2001; and Joshi, 2006). However, no effort has been made to study pulse-type characteristics of the NFGM from the records of these earthquakes.

In the Himalaya, major earthquakes have occurred and shall continue to occur in future because of rupturing of major faults/thrusts including the MCT and the MBT. In the vicinity of these major faults, because of urbanization and tourism, many cities have developed and multi-storey buildings have come-up. Further, because of non-availability of flat-land, the prevalent practice in the hilly regions in the Himalaya is to construct buildings/dwelling on hillslopes. Efforts to cut the slopes will be uneconomical, time consuming, and non-environment friendly. Structures designed according to the Indian standard seismic code, IS 1893 (Part 1) : 2002 (IS code) to with stand ground shaking, will be susceptible to extensive damages in case these structures are located in the close proximity of thrusts, because the pulse-type ground motion has been not considered in their design, as this aspect is absent in the IS code.

In India, the design and analysis procedures do not include special factors to take care of pulse-type ground motion in the seismic inputs for near-fault sites as has been adopted by other countries. Recently, Research Design and Standards Organization (RDSO) under the Ministry of Railways drafted the recommendations to increase the spectral values of IS codal spectra by 20% to include the effect of the NFGMs. However, these recommendations are somewhat

arbitrary in character because pulse-type ground-motions are found to exhibit a lot of variability. Therefore, studies are required to address various scientific and engineering aspects associated with the NFGM.

1.3 Objectives of the Study

The purpose of the study is to investigate the near-fault pulse-type characteristics of the moderate Himalayan earthquakes, and to compute and interpret the response of buildings on hillslope subjected to pulse-type ground motion. The strong motion recordings of 1986 Dharamsala earthquake, 1991 Uttarkashi earthquake, and 1999 Chamoli earthquake have been analyzed to study the characteristics of the NFGM. The study has been conducted with the following objectives.

1. To investigate the pulse-type characteristics of SGM in terms of pulse-period, pulse indicator and type of pulse of three moderate Himalayan earthquakes.

2. To estimate the site-specific ground motion at three sites incorporating the near-fault factor.

3. To study the dynamic response of the Step-Back (SB) and Step-Back-Set-Back (SBSB) asymmetric hillslope buildings, subjected to the NFGMs of three Himalayan earthquakes, and site-specific ground motion.

4. To compare the dynamic response of buildings on hillslope computed from pulse-type ground motion with the response computed using codal spectra and site-specific ground motion, and to make appropriate recommendations.

1.4 Plan of the Thesis

The work carried out in the thesis is presented in six chapters. Chapter-1 provides a brief introduction and importance of pulse-type ground motion, and objective of the study. Chapter-2 contains literature review that includes the characteristics of pulse-type ground motion and factors affecting the NFGM, various pulse models used to represent the NFGM, and engineering implication of the NFGM. Chapter-3 describes the methodology used for pulse detection and study of characteristics of extracted pulses for three moderate Himalayan earthquakes. Chapter-4 provides a detailed account of the procedure used to estimate the

ground motion at three selected sites incorporating near-fault factor to represent the pulse-type ground motion in the seismic input. Computation and interpretation of dynamic response of hillslope buildings is described in chapter-5. Summary of results and conclusions drawn from the study along with recommendations made are included in chapter-6.

CHAPTER 2

NEAR-FAULT GROUND MOTION-AN ENGINEERING PERSPECTIVE: A BRIEF REVIEW

2.1 Introduction

The damage potential of the near-fault ground motion (NFGM) have been demonstrated during the damage investigations associated with the 1971 San Fernando, 1979 Imperial Valley, 1989 Loma Prieta, 1992 Landers, 1994 Northridge, 1995 Kobe, and 1999 Chi-Chi earthquakes (e.g., Bertero et al., 1978; Finn et al., 1994; Anderson et al., 1999; Huang and Chen, 2000). This prompted the researchers to study the characteristics of NFGM and identify the governing parameters that are responsible for such damages. The issue of variability of near-fault (NF) and far-field (FF) strong ground motion (SGM) was first addressed during an extensive study of the heavily damaged Olive View Hospital in California, and it was recognized that the damage was caused by the long duration pulse rather than the high frequency acceleration spike (Bertero et al., 1978). It was further emphasized that the enhanced displacement response of long-period structures is primarily attributed to high amplitude of displacement response spectra at long periods. Dominant factors governing the NFGM include forward rupture directivity, fling-step, hanging wall and vertical effect (Huang and Chen, 2000; Kalkan and Kunnath, 2006; Kunnath et al., 2008; Kunnath and Zhao, 2009 and Shuang and Xie, 2007). These factors are responsible for large long-period pulses observed in the NFGM records. For example, near a strike-slip fault, the properties of the extended "double-couple" source tend to dominate the ground motion. Pulse-type ground motions observed in the NFGM are mainly due to seismic source directivity with respect to site due to propagation of the rupture along the fault, and on account of radiation pattern the fault-normal component is more severe than the fault-parallel component. Attempts have been made to modify the design response spectra in seismic design codes (American UBC-1997, Chinese GB50011-2001) to incorporate near-fault influences to protect the structures located in the near fault regions (Xin-le et al., 2007). However, Indian standard code of practice IS1893:2002 is silent about NFGM. This chapter provides a brief review regarding the characteristics and parameters of the NFGM, representation of NFGM using different pulse models and engineering implications of NFGM.

2.2 Characteristics and Parameters of NFGM

The NFGM exhibits large variations and is characterized by its long-period velocity or displacement pulse-like time history. The characteristics of strong ground motions near the source are significantly influenced by the rupture mechanisms that include fault-slip direction and the direction of rupture propagation relative to the site. Hussain and Ramancharla (2013) studied the difference between the NFGMs due to buried and surface faulting earthquakes by adopting 3D applied element method; and observed low frequency component in ground motions due earthquakes associated with buried dip-slip faulting. The acceleration records of NFGM contain high frequency components along with long-period velocity pulses. Integration of NFGM records obtained at close distances to the surface rupture exhibit pulse-like time histories with very large ground velocities and ground displacements. The impulsive characteristics of the NFGM are all the more evident in velocity and displacement time histories. There are four main factors that govern the impulsive characteristics of NFGM namely, forward directivity, fling step, hanging wall, and vertical effect. These factors are described below.

2.2.1 Directivity Effect

Direction of fault rupture towards the sites close to a fault causes large amplitude long-period pulse-motions at sites located in the direction of rupture propagation. This is known as forward rupture directivity, and is responsible for increased low-frequency ground motion at distances within 20 km from the hypocenter (e.g., Shuang and Xie; Rathje et al., 2004). However, it has been observed that the component of ground motion recorded in fault-normal direction is of short duration but more severe than the component of the ground motion in the fault-parallel direction, and this is attributed to the radiation pattern (Somerville, 2000). When the fault rupture velocity is close to the shear wave velocity of the rock near the source, then the wave front arrives as a large pulse-motion. This type of motion is observed at the beginning of the record and polarized in the fault-normal direction. Because of this the fault-normal component is more severe than the fault-parallel component. It has been shown that due to forward directivity there is an increase in the level of spectral response of the strike-normal component for periods above 0.5 sec, however in case of backward directivity the effect is opposite (Finn, 2000)

Somerville et al. (1997) parameterized the conditions that lead to forward and backward directivity in case of a strike-slip fault and a dip-slip fault as shown in **Figure 2.1**. For strike-slip faults, these parameters are based on the length ratio (X) and azimuth angle between the fault plane and ray path to site (θ), and for the dip-slip faults, the parameters depend upon the width ratio (Y) and a zenith angle between the fault plane and ray path to site (φ) (**Figure 2.1)**. Two parameters, $X \cos \theta$ and $Y \cos \varphi$, are used to characterize the rupture directivity. Forward directivity results from smaller angles between the site and fault and for larger fractions of the ruptured fault between the site and hypocenter. Somerville et al (1997) studied geometric conditions leading to forward-directivity from the predicted ratio of fault-normal to fault-parallel spectral accelerations at a period of 3 sec, and concluded that if the ratio is larger than one then the ground motion contains forward-directivity effect.

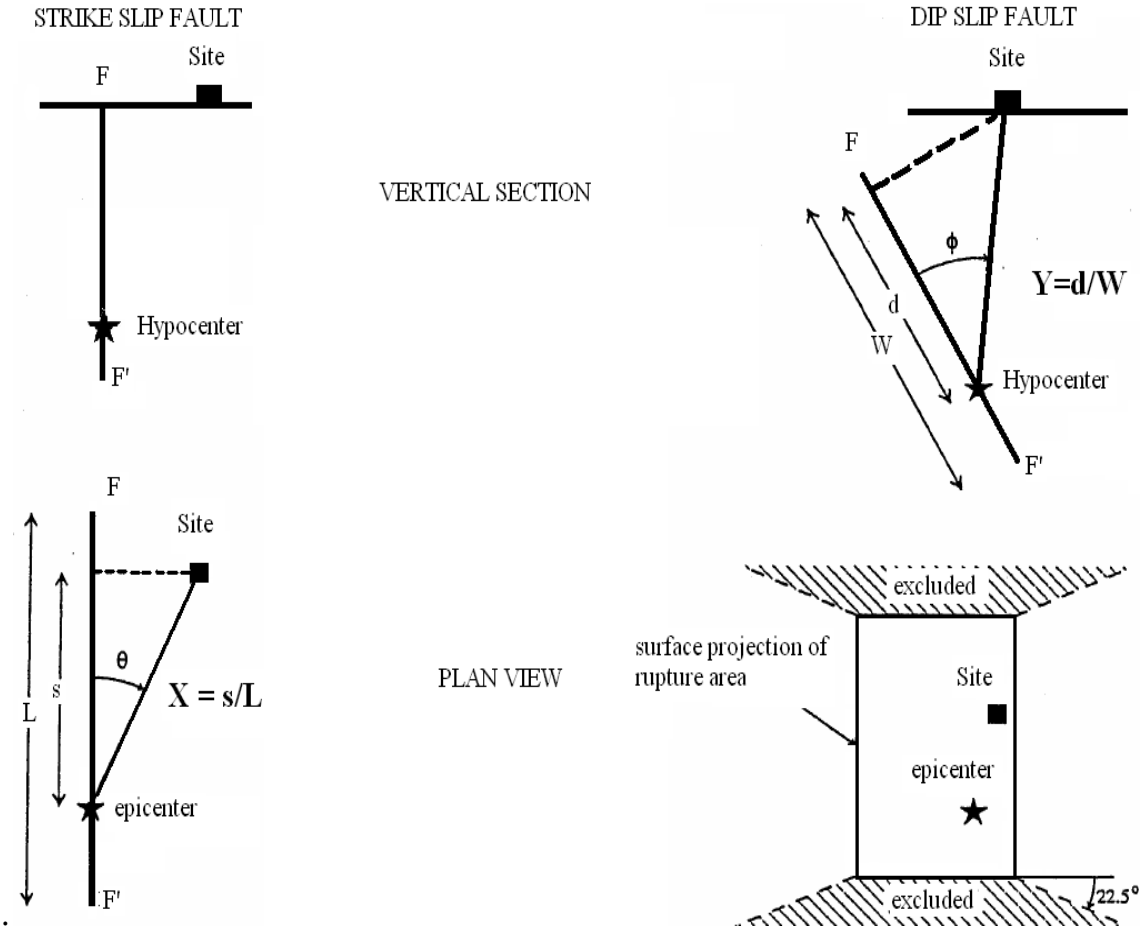

Figure 2.1 Rupture-directivity conditions (after Somerville et al., 1997).

Maniatakis et al. (2008) studied the strong motion records of small to moderate earthquakes ($M_w \leq 6$, seismic intensities MMI≥VIII) obtained from near-fault regions of Greece. He showed that the records contain simple wavelet-pulses of shorter duration and smaller peak ground

velocity (PGV). These pulses represented forward directivity phenomena, and caused severe damages to medium-period structures (periods less than 1 sec) that were located close to the active faults. To decide whether the ground motion records contain pulse due to forward directivity or not, six ground motion parameters, namely, peak ground acceleration (PGA), Cumulative Absolute Velocity (CAV), Peak Ground Velocity (PGV), Arias Intensity (I_A), Root Mean Square Acceleration (a_{rms}), and Damage potential (I) given in **Table 2.1** were computed from the records. If these parameters exceed the prescribed lower bound values, than only the records contain pulse-type ground motion due to forward directivity.

Table 2.1 Ground motion parameters, measured characteristics and lower-bound values (after, Maniatakis et al., 2008).

Ground Motion Parameters	Amplitude	Frequency Content	Duration	Energy	Lower Bound
PGA	√				0.2g
CAV	√			√	0.30g sec
PGV	√			√	20cm/sec
I_A	√		√	√	0.4m/sec
I	√		√		30cm $sec^{-0.75}$
a_{rms}	√	√	√		0.5m/sec^2

These ground motion parameters depend on the characteristics of the strong ground motion in terms of amplitudes, frequency content, duration and energy as shown in the **Table 2.1.**

2.2.2 Fling Step Effect

In the near-fault regions, the permanent ground displacement resulting from tectonic motions is observed as a discrete displacement step in the displacement time history. This step is more prominent in the displacement time history recorded in the direction of fault slip, i.e., parallel to the strike of the fault for the strike-slip earthquake and in the dip direction for the dip-slip earthquake (Somerville et al. 1997). This is called as fling step and leads to pulse like motions. If the rupturing fault moves to the ground surface, will lead to catastrophic damage to the structures due to coseismic deformation in conjunction with the near-fault pulse-type ground motion (Ramancharla and Meguro, 2006). However, pulses from fling-step have different characteristics than forward directivity pulses, and are normally treated separately. **Figure 2.2** shows the orientations of fling step and directivity pulse for strike-slip and dip-slip faulting (Somerville et al. 1997). **Figure 2.3** adopted from Garini et al. (2014) demonstrated the fling step observed due to the 1999 Kocaeli earthquake (M_w 7.4) and the forward directivity

observed from the 1995 Kobe earthquake (M_w 7.0). The figure depicts that in case of strike-slip faulting (shown on the top of the figure) the effect of forward rupture directivity can only be observed in a direction normal to the fault (JMA record during the Kobe earthquake). The filing step that indicated large static offset of 1.7 meter can only be observed in the fault-parallel component (yarimca record of the Kocaeli earthquake). Further, the ground motions that only contain forward directivity pulses indicated no permanent displacement.

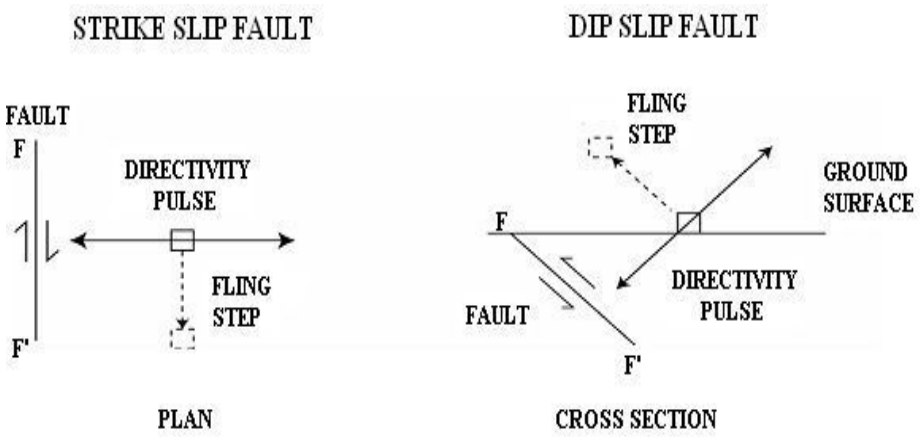

Figure 2.2 Orientations of fling step and directivity pulse for strike-slip and dip-slip faulting (modified from Somerville et al., 1997).

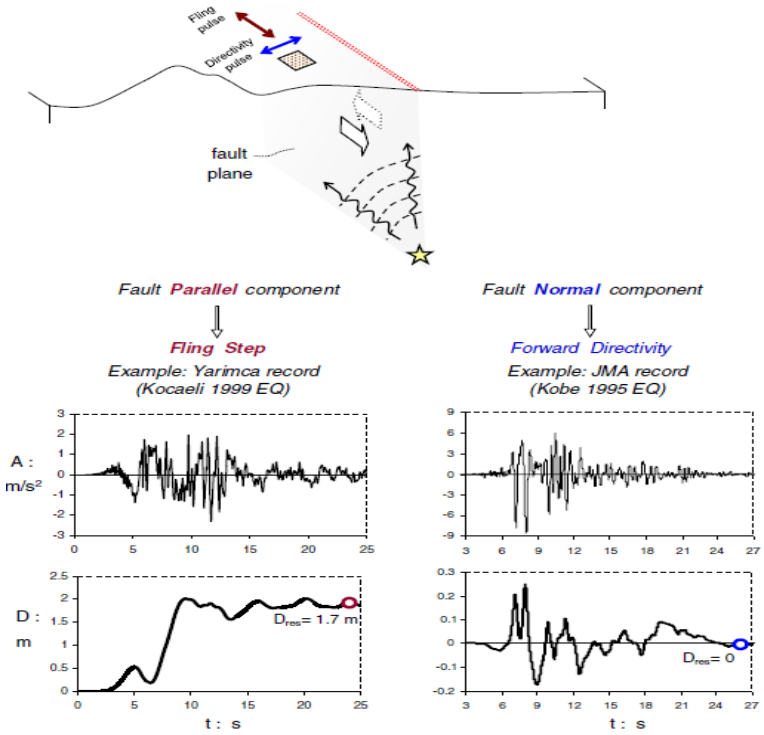

Figure 2.3 The 'fling-step' and 'forward-directivity' phenomena observed in the 1999 Kocaeli earthquake and the 1995 Kobe earthquake. The two sets of acceleration and displacement time histories clearly show these phenomena (after Garini et al., 2014).

2.2.3 Hanging Wall Effect

Systematic differences in the NFGM have been observed on the hanging wall and the footwall. It has been observed that the hanging wall systematically exhibits amplified near-fault ground motion compared to the footwall (Huang and Shi, 2000; Ramancharla et al. 2004). This has been documented during many earthquakes, such as, the 1971 San Fernando earthquake, the 1980 El Asnam earthquake, the 1994 Northridge earthquake, and the 1999 Chi-chi earthquake (Nason, 1973; Ruegg et al., 1982; Oglesby et al., 1998, 2000; Huang and Shi, 2000). Because of this the structures located on the hanging wall suffered most of the damages. During the Chi-Chi earthquake, the sites on the hanging wall recorded larger accelerations compared to the sites located on the footwall. An empirical model incorporating the hanging wall effect for buried faults was developed first time for the Northridge earthquake (Abrahamson and Somerville**,** 1996). This model showed up to about 50% increase in peak horizontal accelerations on the hanging wall over the distance range from 10 to 20 km relative to the median attenuation for the Northridge earthquake. **Figure 2.4** depicts the hanging wall effect because of reverse fault and sites located on the hanging wall side (Site B) will experience higher level of ground motion particularly during reverse faulting.

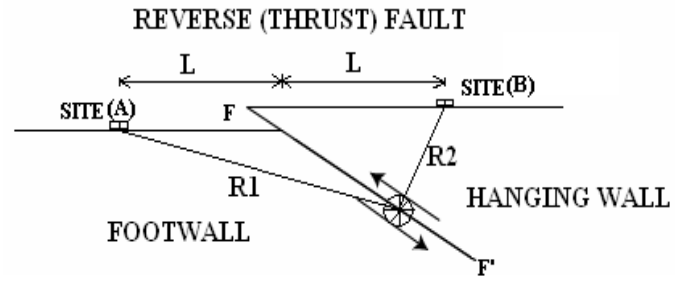

Figure 2.4 Hanging wall effect (after Shuang and XIE, 2007).

2.2.4 Vertical Effect

In the seismic design codes it is a common practice to take vertical acceleration as two third of the horizontal acceleration. However, it is observed in the NFGM records that the ratio of peak vertical acceleration (a_{PV}) to peak horizontal acceleration (a_{PH}) is much higher than 2/3. The ratio of vertical to horizontal response spectra (S_V/S_H) is a function of structural period and distance of sites from the fault. At short periods, the S_V/S_H ratio significantly exceeds the commonly assumed 2/3 for sites close to a fault. At long periods, however, the ratio of 2/3 seems overly conservative for sites close to a fault (e.g., Bozorgnia *et al*, 1995). Egan et al.

(1994) studied ground motion records of moderate to large California earthquakes within about 15 km of the fault ruptures. They found that at periods less 0.2 sec spectral ordinates for vertical components are almost equal to or exceed the horizontal components. The ratios for periods above 0.3 sec were about 1/2 or less and were almost independent of distance. These observations emphasized that vertical accelerations should be considered in design particularly for short period structures in vicinity of major faults. Wang et al. (2002) have shown that the soft soil sites seem to give rise to higher a_{PV}/a_{PH} ratios compared to other types of soil sites.

2.3 Pulse Representation of the NFGM

The NFGM records come in large variety and exhibit complex characteristics due to effects of directivity and fling step. These records are dominated by long-period pulses that contain high peak ground velocity (PGV). This complexity results special type of loading on the structures and make it difficult to evaluate the elastic and inelastic response of structures. To overcome this, attempts have been made to represent the NFGM by equivalent pulse models by simplifying velocity time histories that can reasonably replicate important near-fault response characteristics. Such pulse models have been employed for a systematic design and assessment of dynamic response of structures, and to improve the seismic design code (Alavi and Krawinkler, 2001). The response spectra and displacement reduction factors obtained using the pulse models correlate well with those estimated using recorded ground motions for structural periods close to or longer than the pulse period. However, there is less correlation for short period structures because the high frequency components of the ground motion are excluded in the pulse models. This is a limitation of the simplified pulse models.

Various types of pulse models have been proposed to approximate the NFGM characteristics. These simple pulse models have been used to represent the NFGM to allow studying its dominant kinematic characteristics, and the most prominent frequency component. The guiding criteria for such pulse-model-representations are based on visual inspection of velocity time history records, inspection and evaluation of velocity and displacement response spectra, and evaluation of elastic and inelastic multi degree of freedom system (MDOF) response characteristics (Alavi and Krawinkler, 2001). The fundamental controlling parameters of pulse models are: the type of pulse, pulse period and pulse amplitude. Some of the typical pulse models are described below.

Hall et al. (1995) proposed two types of simple pulses to represent ground displacement showing forward motion (non-reversing type), and forward and backward motion (reversing type). These pulses are shown in **Figure 2.5**. They used these models to compute the response of tall buildings.

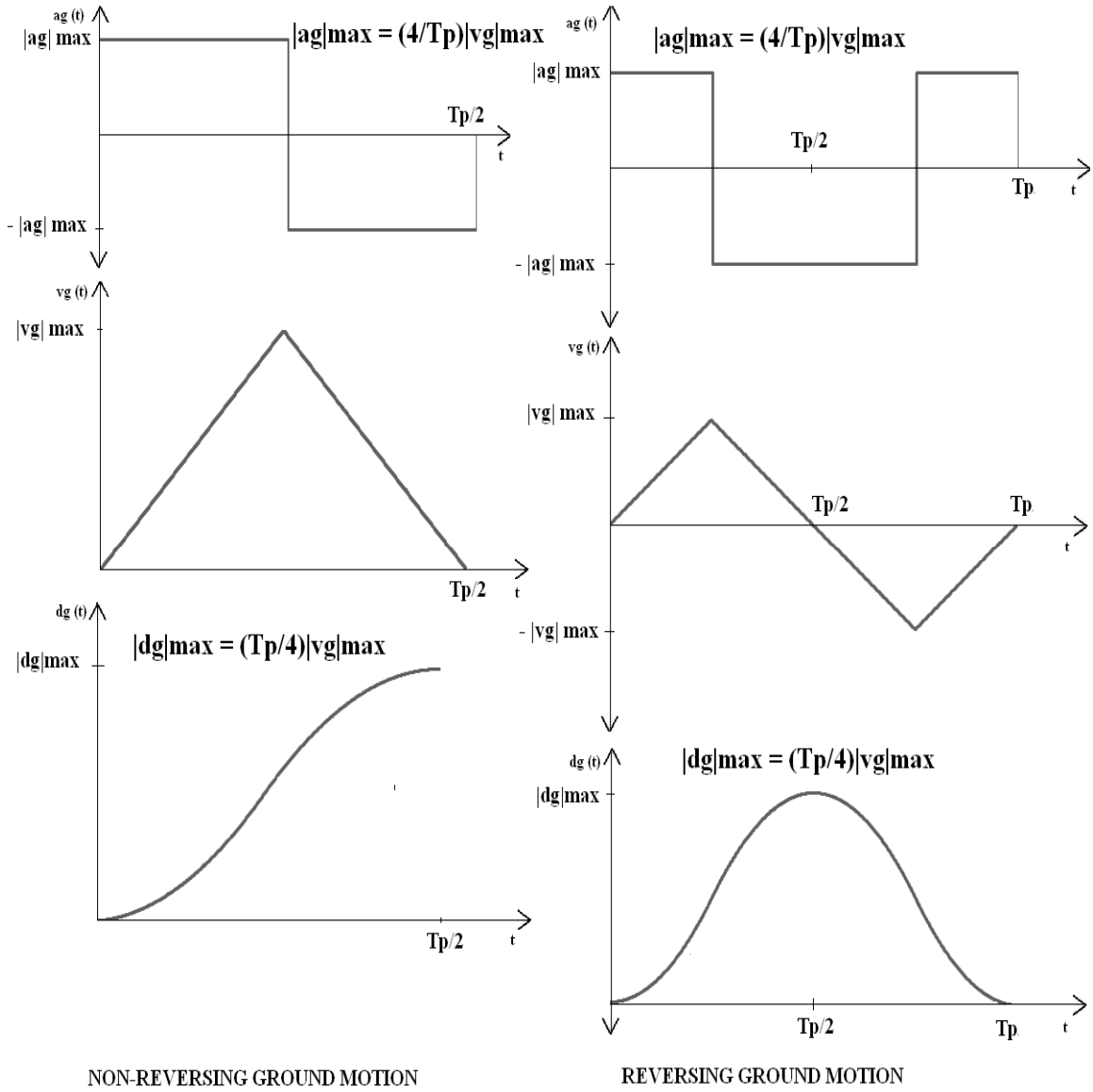

Figure 2.5 Simple pulse-type ground motion (Hall et al., 1995).

Alavi and Krawinkler (2001) proposed three types of Equivalent Pulse Models, namely, half pulse-P1, full pulse-P2, multiple pulse-P3, models. The half pulse-P1 model represented a non-reversing ground displacement history generated through a single square cycle of acceleration input. The full pulse-P2 model represented a reversing ground displacement history generated through a double square cycle of acceleration input. The multiple pulse-P3 model represented repeated pulse sequences generated by the oscillatory type of displacement history.

Makris and Roussos (1998) proposed three types of equivalent velocity pulse (EVP) models. These models were referred as type-A, type-B and type-C, and used to represent earthquake vibrations in terms of sine and cosine waves with different periods. These models are represented by the following expressions.

Type-A $\quad \mathring{u}_g(t) = (V_p/2) - (V_p/2)\cos(\omega_p t), \qquad 0 \le t \le T_p$

Type-B $\quad \mathring{u}_g(t) = V_p \sin(\omega_p t), \qquad 0 \le t \le T_p$

Type-C $\quad \mathring{u}_g(t) = V_p \cos(\omega_p t + \varphi) - V_p \sin\varphi, \qquad 0 \le t \le (n + 0.5 - \varphi/2)T_p$

In the above expressions $\mathring{u}_g(t)$ is the ground velocity, V_p is the pulse velocity, and $\omega_p = 2\pi/T_p$, where, T_p is the pulse period, and φ is the phase angle.

Menun and Fu (2002) after taking into account the existing pulse models, and analyzes of the pulse type records, proposed new EVP models with 5 parameters. They adopted least squares method and non linear regression techniques. The EVP models are represented by the following expressions.

$$\mathring{u}_m(t;\theta) = \begin{cases} V_p \exp[-n_1(0.75T_p - t + t_o)]\sin[(2\pi/T_p)(t - t_o)], & t_o < t \le t_o + 0.75T_p \\ V_p \exp[-n_2(-0.75T_p + t - t_o)]\sin[(2\pi/T_p)(t - t_o)], & t_o + 0.75T_p < t \le t_o + 2T_p \\ 0, & \text{otherwise} \end{cases}$$

Where $\theta = [V_p, T_p, t_0, n_1, n_2]^T$ is the vector representing the model parameters used to define the pulse model. V_p and T_p represent the maximal amplitude and period of velocity pulse respectively, t_0 denotes the starting time of velocity pulse, and n_1 and n_2 are the shape parameters.

Mavroeidis and Papageorgiou (2003) proposed the following analytical model to represent impulsive characteristics of the NFGM.

$$V(t) = \begin{cases} 0.5A\,[1 + \cos(2\pi f_p (t - t_o)/\gamma)]\cos(2\pi f_p (t - t_o) + v), & t_o - \gamma/2f_p \le t \le t_o + \gamma/2f_p \text{ with } \gamma > 1 \\ 0, \text{ otherwise} \end{cases}$$

In this model parameter "A" controls the amplitude of the signal, f_P is the frequency of the amplitude-modulated harmonic (or the prevailing frequency of the signal), υ is the phase of the amplitude-modulated harmonic (i.e., $\upsilon = 0$ and $\upsilon = \pm\pi/2$ define symmetric and antisymmetric signals respectively), γ is a parameter defining the oscillatory character of the signal (i.e., as γ

increases the number of zero crossings increases, for small γ the signal approaches a delta like pulse), and t_0 specifies the epoch of the envelope's peak.

LI and ZHU (2004) based on the work of **Makris and Roussos (1998)** and **Menun and Fu (2002)** on EVP models, proposed the following EVP model.

$$V(t) = \begin{cases} \sum_{i=0}^{N} a_i V_p \sin(\omega_p t), & t\epsilon[0,(N+1)T_p/2] \\ 0, & \text{otherwise} \end{cases}$$

In this equation $\omega_p=2\pi/T_p$, T_p is the pulse period, V_p is the maximum amplitude of velocity pulse, N is the number of half-period cycles, a_i is the contribution ratio of amplitude within the time range from $iT_p/2 \leq T \leq (i+1)T_p/2$ to V_p, and its value is less than 1.0. The number of a_i is equal to N.

TIAN Yu-ji et al. (2007) gave the EVP model, which is the function of pulse period, peak velocity and pulse shape. This model is described by five parameters and has been used to simulate the pulse-type velocity time history. The model is given by the following equation.

$$v(t) = v_p . w(t) . \cos[2\pi f_p (t-t_1)], \qquad 0 \leq t \leq T$$

Where, v_p represents the peak velocity of the pulse, and f_p and T_p are the frequency and period of the pulse ($T_p=1/f_p$), $2\pi f_p t_1$ is the pulse phase angle, and T denotes the duration of the velocity time history. The envelope function of the velocity time history '*w(t)*' is expressed as:

$$w(t) = \exp\{-[2\pi f_p (t-t_o)/\gamma]^2\}$$

Where, t_0 is the time of peak value and γ denotes the rate of peak attenuation. Some shapes of envelope functions are shown in **Figure 2.6.**

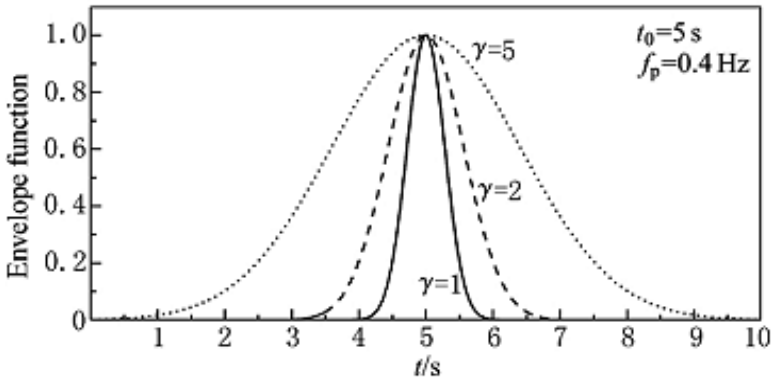

Figure 2.6 Different pulse shapes of envelope function (TIAN Yu-ji et al., 2007).

The maximum peak velocity (V_p) and pulse period (T_p) in the above relations can be determined from the available empirical relations based on earthquake magnitude and closest distances to the ruptured fault (e.g., Somerville, 1998; Alavi and Krawinkler, 2001; Rodriquez-Marek, 2000).

Baker (2007) used wavelet approach, and adopted Daubechies wavelet of order four (db4) as a mother wavelet to extract the largest velocity pulse from a given NFGM. This is shown in **Figure 2.7**. To identify the pulse due to forward directivity, following three criteria are used.

1. The pulse indicator value is greater than 0.85.
2. The pulse arrives early in the time history, as indicated by $t_{20\%,\ orig}$ values that are greater than $t_{10\%,\ pulse.}$
3. The original ground motion has a PGV greater than 30 cm/sec.

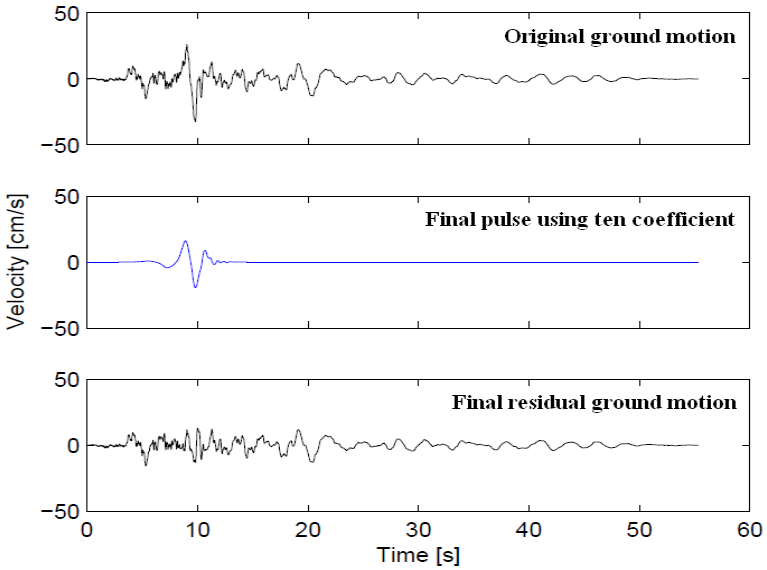

Figure 2.7 Pulse extraction by using wavelet analysis (after, Baker, 2007).

Sabegh (2010) investigated seven different kinds of mother wavelets for pulse extraction. He emphasized that selection of most appropriate mother wavelet plays an important role in effective extraction of ground motion features, and consequently in the estimation of velocity pulse period.

Ghahari et al. (2010) applied moving average filters with appropriate cut-off frequencies to decompose the NFGM into two components having different frequency contents. The first component contains long-period pulses and is called pulse-type record (PTR). The second component contains relatively high-frequency ground motion, and is referred to as back-ground record (BGR). The second component does not include large velocity pulses. This method was applied on 91 records that qualified the above mentioned three criteria (Baker, 2007). The study showed that response spectra computed for PTR and BGR components intersected at a point which is 0.38 of the pulse-period. From this study it was inferred that if the ratio of the structural period to pulse-period is above 0.38 than the structural response will be dominated by PTR type ground motion. Below this period (called the threshold period), the elastic response of the structures is governed by BGR type motion.

2.4 Engineering Implication of the NFGM

The NFGM records are characterized by high frequencies that represent accelerations, along with long-period velocity pulses. The immense damage potential of the NFGM exceeds that of far-field ground motion (FFGM). This has been recognized in many reported studies that have been carried out after the 1971 San Fernando, 1979 Imperial Valley, 1989 Loma Prieta, 1992 Landers, 1994 Northridge, 1995 Kobe, and 1999 Chi-Chi earthquakes. In these studies it has been recognized that the large amplitude pulses, primarily related to the forward directivity and fling effects, control the response of medium and long period structures. The high frequency part of the NFGM also plays an important role especially for short-period structures.

Bertero et al. (1978) first concluded from the observations that large amplitudes at long periods in displacement response spectra are responsible for enlarged displacement response of long period structures. **Hall et al. (1995)** examined the effects of near-source ground motion on flexible buildings, and emphasized that flexible frame and base-isolated buildings designed as per codal provisions undergo severe non-linear deformations. These deformations were attributed to near-source ground motion which was dominated by large rapid displacement

pulses associated with the large long-period velocity pulses. They pointed out that design codes are silent about this type of motion. In the near-fault regions, the base-isolated structures shows maximum bearing displacements in the fault-normal direction, and lead to larger isolator displacement compared to fault-parallel direction (**Deb, 2004**). Experimental and analytical studies of buildings and bridges with fluid viscous dampers showed that fluid viscous dampers with orifice coefficient (α) having value of 0.5 of fluid damper are effective in attenuation high velocity pulses those encountered in the NFGMs (**Deb, 2008**).

Iwan (1997) argued that response spectrum method is not able to capture wave propagation response along the height of the tall structures, and proposed a method of drift spectrum to capture the response of tall structures by using shear beam model. However, **Chopra and Chintanapakdee (1998, 2001)** proved the acceptability of response spectrum method for engineering applications for both elastic and inelastic systems by considering the appropriate values of T_a, T_b and T_c in spectral region of the NFGM. **Malhotra (1999)** demonstrated that pulse-type ground motions lead to narrower velocity sensitive region which is shifted to longer periods. This leads to increase in the base shear and inter-story drift in high-rise buildings with an accompanied increase in ductility demand due to high PGV/PGA ratio.

Krawinkler and Alavi (2001) showed that inelastic response due to the NFGM leads to a significant redistribution of story ductility demands that cannot be captured from an elastic spectral or dynamic analysis. They also demonstrated that simplified representations of the velocity pulse are capable of capturing the salient response features of structures having time periods 'T' subjected to the NFGM in the period range of $0.375 \leq T/T_p \leq 3$, where "T_p" is pulse period. **Mavroeidis et al. (2004)** studied response of elastic and inelastic SDOF systems based on their earlier mathematical model, and concluded that the impulsive character of the near-fault velocity-pulse represented by the parameter (γ) affects the elastic response spectra of the single degree of freedom system (SDOF). The influence of 'γ' on the inelastic response spectra diminishes as the ductility factor (μ) increases. However, the phase parameter (ν) has a minor effect on the elastic and inelastic response spectra of the SDOF system. **Longjun (2006)** proposed seismic design spectra considering four types of EVP models representing different type of the NFGM. Studies have demonstrated that spectral ordinates obtained from simplified pulse models are strongly related to the velocity spectral periods and pulse waveforms.

The NFGM is composed of two components, the long-period large-amplitude velocity pulses with super imposed high frequency component of ground motion. The current design codes are based on far-field records and dynamic response of the structures subjected to the NFGM is expected to be different. Elgohary and Ghobarah, (2003) evaluated the response of structures to the NFGM and compared the same with the standard Canadian and U.S nuclear design spectra used in the nuclear design. This study concluded that the most important parameters to characterize the NFGM are the amplitude of the velocity pulse and its duration. The study suggested that for this purpose, the site-specific seismological studies should be carried out to estimate these parameters. It was further recognized that long-period structures designed according to minimum requirements specified by Canadian and U.S design spectra may suffer damages in the near-fault zone. They recommended that pulse parameters should be taken into account instead of increasing the ordinate of the design spectra.

Ghobarah and Sheikh (2003) compared the response of four building models of 3, 6, 12 and 20 storey-buildings that were designed according to the Canadian codes with response computed using near-fault recordings obtained in the forward directivity zone from moderate and major earthquakes. A set of eight near-fault recordings were used in the study. The major conclusion from the study was that the seismic codes, NBCC (1995) and CSA (1994) codes should consider explicitly the NFGM in the time history analysis instead of simply increasing the amplitudes of the design response spectra. Ghobarah (2004) computed and compared the dynamic response of same structural models by subjecting them to two types of inputs, one from idealized pulses and second from the near-fault recording. Four types of near-fault recordings were used in the study from earthquakes with moment magnitude between 6.7 and 7.4, and the fault distance of these recordings was between 0.7 and 3.0 km. The shape of the pulse was idealized as one full sine cycle or one and a half cycles after filtering the high frequencies from the velocity records of the strong motion recordings. 'f_{max}' that defines the frequency after which the acceleration spectra attenuates vary fast was used as a cut off frequency. In this study the response of long-period structures to idealized pulses was found to be comparable to the response obtained from near-fault recordings. However, the results were not very accurate for short-period structures.

Some of the engineering structures and natural in-situ geological structures such as land slide areas can be modeled as rigid blocks. Such structures can be uplifted and are subjected to rocking motions when excited by earthquake shaking. The behavior of such systems is difficult

to model and is a function of loading and parameters of the rigid block, and the friction at the contact surface. Such systems may overturn when subjected to the NFGM, because of complexity of the ground motion. Gerolymos et al. (2005) computed the overturning response of such systems by subjecting them to five types of pulses which include one cycle sine, and cosine, two types of Ricker wavelets and a rectangular pulse. These pulses are idealized to represent rupture directivity and fling effect. This study introduced "overturning-acceleration amplification" and "rotation-spectra" to explain the overturning response of rigid blocks. Artificial neural network (ANN) modeling was used to develop closed-form expressions to predict whether a rigid block will overturn or survive. One of the important conclusions of the study was that in the absence of knowledge of ground motion, use of simple pulse with the ANN modeling would provide the best engineering solution for design.

Galal and Ghobarah (2006) assessed the safety of nuclear power plants designed according to North American codes, in case such structures are subjected to the NFGM. For this purpose they used 54 fault-normal near-fault recordings that contained forward directivity effect. The study concluded that the US and Canadian design spectra used for design of nuclear plants need modification to reflect the effect of the NFGM. They recommended that the Canadian nuclear-design-spectra (CSA-N289.3 (1992)) for rock sites above 10 Hz be adjusted to accommodate the increased NFGM spectra (mean plus one standard deviation). Further, it was found that the mean plus one standard deviation spectra of the NFGM on rock sites is higher than the US-NUREG spectra (2001) over a wide frequency range for Western United States, and for frequencies less than 30 Hz for Central United States. Therefore, the US-NUREG spectra (2001) need modification to accommodate the increased response due to the NFGM response spectra.

Shakib and Ghasemi (2007) compared the dynamic response of asymmetric single storey models with uni-axial eccentricity subjected to near-fault and far-fault excitations. Such structures with wall elements in both orthogonal directions were subjected to bi-directional excitation and the torsional response was computed for near-fault and far-fault excitation. For the NFGM, considering constant stiffness, the displacement and rotational demand is greater compare to considering variable stiffness. However, for far-field motions the deformation demands are by and large are similar. In the case of NFGM excitation, the minimum rotational response could be obtained considering actual behavior method when the stiffness and strength centre located on the opposite side of the mass center. It is found that displacement ductility

demand increases with the increase in the pulse-period of fault-normal component. Based on the ratio of fundamental period of structure to pulse period, the rotational response was divided into three regions. When this ratio is above one, the rotational demand increases with increasing the stiffness eccentricity, and when this is equal to one the variation in the rotational demand is minimum. For the NFGM excitation, when the stiffness and strength centers are located on the opposite side of the mass center, the stiff side demand would be greater than the soft side. However, when the stiffness and strength centers are located on the same side of the mass center, the soft side demand would be greater than the stiff side.

Ghasemi and Shakib (2008) studied the torsional behavior of multi-storey asymmetric buildings subjected to a set of nine NFGMs and a set of seven FFGMs. The NFGMs were taken in fault-normal and fault-parallel directions. Fault-normal components were also represented by equivalent sine and cosine pulse-forms. Dynamic response of 5 storeys and 10 storeys building models were compared with the response of idealized one-storey building models. From the study it was found that in the NFGMs, the torsional response would be minimized if the locations of stiffness and strength centers are on the opposite side of the center of mass. Further, due to NFGMs the story-drift demand in multi-storey buildings increases from higher storeys to the lower ones. This observation was found to reverse when the buildings were subjected to the FFGMs. It was found that the trend of torsional-demands because of NFGMs is different when compared to that of equivalent sine pulse, and is almost similar when compared with the equivalent cosine pulse. This observation is also found to be valid for the idealized one-storey buildings.

Gazetas et al. (2009) examined the effect of NFGM on sliding systems. To modes the sliding systems they considered rigid blocks placed on horizontal or on inclined plane with frictional contacts in between. The seismic input were imparted in two ways, firstly by taking idealized pulses and secondly taking actual strong ground motion records from four major earthquakes. These records contained the effect of forward directivity and fling step. The study showed that the maximum and residual slippage of such systems depends on the sequence and details of the pulses in the excitation, and on the direction (plus or minus) in which the shaking is imposed on the inclined plane. The slippage is not much affected even by the strongest vertical components of the ground motion. It is found that upper bound sliding displacements from near-fault loading may significantly exceed the values given by some prevalent procedures.

Ventura et al. (2011) explored the effects of near-fault fling-step on the linear and nonlinear-seismic response of six SDOF systems and two existing tall building models. For the analysis they considered the four NFGM recordings that contain fling-step during four different earthquakes. Two types of SGMs were taken for excitation: a) with fling-step, and b) without fling-step. The ground motions "without fling-step" were obtained by filtering the coseismic displacement and velocity pulse that represent fling-step. From the analysis of six SDOF systems subjected to the NFGMs, the analysis showed that the ratio of 'fundamental-period' of the SDOF systems to the 'fling-step rise-time' plays a significant role in controlling the system response. It was found that when the 'fundamental-period' of systems is close to the 'fling-step rise-time', the higher response follows the ground displacements, with its maximum response under the PGD. Dynamic response of the tall buildings showed that there is amplification in the response from the first storey to the middle of the buildings due to the ground motions that contain fling-steps compared the ground motions without fling-steps. This would lead to large damages to structural and non-structural elements of the buildings under stronger shaking.

NFGM is known to impose large demand on structural systems compare to FFGM. Forward directivity pulses that are responsible for large displacements are normally found in the FN component of the NFGM. Ghasemi and Shakib (2011) conducted a study in which they computed maximum velocity direction (MVD) component, from the longitudinal and transverse components of the NFGM and argued that this component has large PGV and PGD values compared to other components of the NFGM. It was found that the spectrum of the MVD component envelope the spectra from all components of ground motion taken in other directions. This showed that for large earthquakes above magnitude (M_w) 7, the UBC near-source factors (N_a, N_v) are more conservative compared to that estimated in this study.

Amirzehni et al. (2013) computed and compared the seismic response of deep basement walls subjected to NFGMs and FFGMs of almost similar intensity. The normal practice for seismic design of these walls in British Columbia, based on the PGA, was found to be conservative, when compared with response of these walls computed using far-fault ground motions (2% exceedance rate in 50 years). For high frequency system (natural frequency about 2.5 Hz), no significant difference in the drift ratio profiles was found due to the NFGMs and FFGMs. However, for both types of ground motions the highest drift ratio occurred at the top of the basement wall. It was found that more drift will occur at the top storey level of the basement

wall. This was attributed to the spectral peaks observed in acceleration and velocity response spectra at the fundamental period of the system.

Garini and Gazetas (2013) investigated the damage potential of NFGM to cause damage to asymmetric strongly-inelastic systems. These systems were idealized as rigid blocks with frictional contact on an inclined base. The inclined base is subjected to NFGMs from 13 earthquakes that contained forward directivity and fling-step. In total 2 x 99 ground motion recordings were used in the study. The total slippage "D" of the block caused by each ground motion was taken as a measure of induced damage. This total slippage "D" was correlated with the various measures of the damage potential of SGM available in the literature, such as PGA, PGV, Housner intensity and Arias intensity. The study showed that most of the acceleration based measures of damage potential are poorly correlated with the slippage. However, the velocity based measures (Housner intensity and velocity spectrum intensity) correlated fairly well with slippage.

Garini et al. (2014) investigated the response of elastic and inelastic systems when subjected to different types of near-fault ground motion excitations. One of the key aspects, which were addressed in this study, was whether only single dominant pulse causes the large displacement or the number of pulses observed in a record control the overall response. The four types of idealized dynamic system studied include: 1) an elastic single-degree-of-freedom (SDOF) system, 2) an elastic-perfectly-plastic (SDOF) system, 3) a rigid block with simple frictional contact on a horizontal base, and 4) a rigid block resting on a inclined plane. Eleven near-fault accelerograms are used and two each accelerograms a single wavelet is "optimally" fitted by the method given by Vassiliou and Makris (2009, 2011). Using this method two types of wavelet were extracted, namely, a Ricker wavelet, and a Mavroeidis and Papageorgiou (2003) wavelet. These wavelets captured broad characteristics of the near-fault pulses and not the details. In total 33 inputs that include eleven near-fault excitations and 22 idealized wavelet pulses, were used to excite the response of four systems. The study showed that NFGM which is primarily composed of forward directivity pulses and fling-step leads to strong response compared to inelastic systems. Sliding systems because of their rigid-plastic behavior may undergo very large slippage which can't be predicted. This is particularly true in case their strength is small (critical yielding acceleration and coefficient of friction). The polarity reversals of excitation have very large effect on the accumulated slip. This may be the reason that we observe very different pattern of damage in similar type of buildings in close proximity.

Elastic response was found to be less sensitive to details of the ground motions, wavelet analysis provided fairly good results, whereas, response of sliding systems were sensitive to the details of pulse characteristics as well as details of sequences of pulses and the number of accelerogram's cycles.

2.5 Concluding Remarks

It has been well recognized that the NFGM has immense damage potential. An absolute lack of mention of NFGM in codal provisions has recently attracted the attention of seismologists and engineers to characterize the parameters of NFGM for engineering applications.

NFGM are normally characterized by intense velocity and displacement pulses of relatively long period that clearly distinguish them from typical FFGM. Further, the NFGM is composed of one or more dominant pulses, whereas, FFGM is ideally represented as a broad frequency band excitation. This impulsive character of NFGM is mainly due to forward directivity and the fault normal component is more dominant due to radiation pattern.

These pulse type motions have caused severe damage to intermediate and long period structures. Due to complex nature of NFGM efforts have been made to represent it by equivalent pulse models, such as half pulse model, full pulse model and multiple pulses model with pulse period (T_p). These pulse models have helped in quantifying seismic demands for structures in terms of controlling parameters of the NFGM, namely, type of pulse, pulse period (T_p), pulse amplitude (V_p), and number of predominant pulses (N) of the models.

Pulse type ground motion representation leads to narrower velocity sensitive region shifted to longer periods. Due to this base shear and inter-story drift increases in high-rise buildings with an accompanied increase in ductility demand. Threshold levels of some of the strong motion parameters can be used to identify the records that contain near-fault effects. Various techniques such as wavelet transformation and moving average filtering have been used to extract the near-fault pulses from the strong motion records.

Efforts have been made to include the effects of NFGM in some of the design codes (e.g., American UBC-1997, Chinese GB50011-2001). However, Indian standard code of practice

IS1893:2002 is silent about NFGM and there is an immediate need to include the NFGM effects that might occur due occurrence of thrust type earthquakes in the Himalaya.

CHAPTER 3

NEAR-FAULT GROUND MOTION CHARACTERISTICS OF THREE MODERATE HIMALAYAN EARTHQUAKES

3.1 Introduction

Three moderate-sized, shallow-focus earthquakes, namely, the 1986 Dharamshala earthquake (M_w 5.5), the 1991 Uttarkashi earthquake (M_w 6.8), and the 1999 Chamoli earthquake (M_w 6.5), occurred in the Himachal Himalaya and the Garhwal Himalaya. Both the Himachal Himalaya and the Garhwal Himalaya form parts of the northwestern Himalaya. Dharamsala earthquake occurred in the Kangra region of the Himachal Lesser Himalaya, at the northwestern edge of the rupture zone of the 1905 great Kangra earthquake. This earthquake was recorded at nine stations of the Kangra strong motion array. This array was deployed in the epicentral track of the Kangra earthquake by the Department of Earthquake Engineering (DEE), Indian Institute of Technology (IIT) Roorkee, in 1983 (Chandrasekeran, 1988). Two moderate-sized earthquakes, at Uttarkashi and Chamoli, occurred in the Garhwal Himalaya. These earthquakes occurred in the central seismic gap postulated between the rupture zones of the 1905 great Kangra earthquake (Mw 7.8; Ms 8.6) and the 1934 great Bihar-Nepal earthquake (Mw 8.0; Ms 8.5) (Khattri and Tyagi, 1983; Khattri, 1987), and caused severe damage in the regions around Uttarkashi and Chamoli. The Uttarkashi earthquake was recorded at thirteen stations, whereas the Chamoli earthquake was recorded at eleven stations of the strong motion array that was deployed in the Garhwal and Kumaon Himalaya by DEE, IIT Roorkee, during 1991-1992 (Chandrasekran and Das, 1995). This array was deployed covering parts of the central seismic gap, so as to measure the strong ground motion (SGM) due to gap-filling earthquakes that could potentially occur in the seismic gap. The strong motion recordings of these three moderate-sized earthquakes have been analyzed for the purpose of identifying near-fault pulses. For pulse detection, standard methodology given by Maniatakis et al. (2008) and Baker (2007) has been adopted. Normally, near fault-pulses are observed in the strong motion records obtained within 20 to 30 km from faults (Rathje et al., 2004). Near-fault pulses are attributed to the forward directivity effect, fling effect, hanging wall effect, and vertical effect (Shuang and Li, 2007). These pulses possess immense damage potential, specifically for long and intermediate period structures. Out of the 33 strong ground-motion recordings that were analyzed, only three recordings have shown pulse-type characteristics. Pulse detection methodology, characteristics of the extracted near-fault pulses, interpretation of

the NFGM response spectra, and its comparison with the Indian Seismic (IS) codal spectra have been described in this chapter.

3.2 Parameters of Earthquakes Studied

Parameters of three moderate earthquakes in terms of their locations, origin times and magnitudes, and fault-plane solutions are listed in **Table 3.1 and Table 3.2**. The epicenter of Dharamshala earthquake was located about 6 km to the north of Dharamshala. The earthquake occurred at a depth of about 7 km. The region surrounding Dharamshala and Kangra exhibits high seismicity and has experienced a great Kangra earthquake in1905 (Ms 8.6). In the seismic zoning of map India, the region falls in seismic zone V, where the maximum expected earthquake intensity is IX or more on MM or MSK scales. The Dharamshala city lies in the vicinity of the Main Boundary Thrust (MBT) and the Main Central Thrust (MCT) falls further to the northeast at a distance of about 25 km. In the last more than 50 years, the region around Dharamshala has witnessed seven -moderate earthquakes with magnitudes between 5.0 and 6.5 (Kumar and Mahajan, 2001). At Dharamshala, the maximum intensity on MM scale was between VI and VIII because of these earthquakes. The focal mechanism solutions of two earthquakes that occurred in the vicinity of Dharamshala in 1968 and 1978, showed thrust faulting with left-lateral strike-slip component (Shrivastava et al., 1987). The 1986 Dharamshala earthquake occurred on a northwest-southeast trending plane that showed right lateral strike-slip motion. The dip angle and dip direction, and slip angle of the plane of movement are 60^{o}, 325^{o}, and 20^{o} respectively. It was interpreted that along this plane lateral mass movement occurred because of up-thrusting of basement blocks of the Indian plate. The occurrence of this earthquake was correlated with the southwest dipping splay between the MCT and the MBT (Kumar and Mahajan, 1991). The 1986 Dharamshala earthquake, with maximum epicentral intensity VIII on MM scale, has oval-shaped isoseismals with longest axis in the northwest-southeast direction. The geometry of isoseismals showed that attenuation of ground motion was fast towards northwest compared to southeast.

The epicenter of the 1991 Uttarkashi earthquake was located in the Garhwal Himalaya, at a distance of about 30 km northeast of Uttarkashi station. The earthquake occurred to the north of the MCT at a shallow depth of about 10 km. The maximum epicentral intensity was IX on MM scale in a region encompassing about 10 sq. km of the epicentral area. This earthquake was recorded on thirteen stations of the strong motion array deployed in the region

(Chandrasekran and Das, 1995). Locations of some of these stations were close to the epicenter of the earthquake. The observed intensity at the Bhatwari and Uttarkashi stations were VIII+ on MM scale. The earthquake occurred because of low angle thrust faulting as revealed from the fault plane solutions given by various investigators (e.g., Kumar et al., 2005, Paul et al., 1998). On the basis of isoseismals, iso-accelerations, aftershock locations, and regional tectonics the most probable causative source of this earthquake has been the Munsiari Thrust (Joshi et al., 2001; Joshi, 2000, 2006). The distribution of aftershocks, meisoseismal area, and the region of maximum recorded peak ground accelerations, all lay from the west to northwest with respect to the probable rupture zone which is associated with the Munsiari Thrust. Most of these effects can be explained in case it is assumed that the rupture associated with the Uttarkashi earthquake propagated in the northwest direction from the hypocenter. From observed PGA, the computed intensity at Bhatwari station is VIII+, whereas, from macroseismic observations, the estimated intensity is IX on MM scale. The computed intensity at Uttarkashi station is VIII+ from the observed PGA and is VIII based on macroseismic observations. The strong ground motion simulated using envelope summation technique shows that the generated resultant envelope follows important strong motion characteristics such as directivity and attenuation affects in case the propagation of rupture is taken toward Bhatwari along the Munsiari Thrust (Joshi et al., 2001; Joshi, 2000, 2006). The Chamoli earthquake occurred 75 km southeast of the Uttarkashi earthquake in the Garhwal Himalaya as a result of thrust faulting at a shallow depth of about 15 km. The maximum observed intensity was VIII on MSK scale in the region that is bound to the north by the MCT and to the south by the Alaknanda fault. The affected region lies in the seismic zone V of the seismic zoning map of India (IS 1893: 2002) and the maximum anticipated intensity is IX or more in the seismic zone V. The Chamoli earthquake was recorded at 11 stations of the strong motion array including the Gopeshwar station which is located in the epicentral region. No expression of surface faulting was observed. However, from the orientation of the elongated isoseismals it appears that the direction of rupture propagation is from east-northeast to west-southwest. As the geometry of the largest intensity isoseismal is governed by the direction and style of rupture, the direction of elongated isoseismal VIII, which is west-southwest to east-northeast, indicates the strike of the fault and slip direction (Shrikhande et al. 2000). The maximum damage was observed in the strike direction at some distance from the epicenter, and less damage was observed near the epicenter normal to strike direction. This observation was interpreted because of the slip on a low angle fault (Shrikhande et al. 2000).

Table 3.1 Parameters of earthquakes studied.

Earthquake	Date	Origin time (IST)			Epicenter		Focal depth (km)	M_w	Agency
		Hr.	Min.	Sec.	Lat.^{O} N	Long.^{O} E			
Dharamshala	April 26,1986	13	05	16.42	32.175	76.287	07	5.3	USGS
Uttarkashi	October 20,1991	2	53	16.45	30.780	78.770	10	6.8	USGS
Chamoli	March 29,1999	0	35	0.00	30.380	79.210	15	6.5	CMT Harvard

Table 3.2 Fault plane solutions of earthquakes studied.

Earthquake	Plane	Strike^o	Dip^o	Slip^o	Source
Dharamshala	NP1	254	16	22	Molnar and Caen (1989)
	NP2	143	84	105	
	NP1	232	60	157	Kumar and Mahajan (1991)
	NP2	131	69	148	
	NP1	299	19	059	CMT Harvard
	NP2	153	74	100	
	NP1	303	28	86	Ram et. al (2005).
	NP2	127	62	92	
Uttarkashi	NP1	18	38	172	PDE Moment Tensor
	NP2	115	85	52	
	NP1	332	19	133	PDE 1ST Motion
	NP2	108	76	77	
	NP1	315	19	55	Kumar et al. (2005)
	NP2	171	74	79	
	NP1	296	5	90	PDE, Monthly
	NP2	116	85	90	
	NP1	317	14	115	CMT Harvard
	NP2	112	78	84	
	NP	315	14	144	Paul et al. (1998)
Chamoli	NP1	282	9	95	USGS
	NP2	97	81	89	
	NP1	280	7	75	CMT Harvard
	NP2	115	83	92	
	NP1	257	10	57	PDE Weekly
	NP2	111	82	95	
	NP1	208	51	16	PDE Monthly
	NP2	108	78	140	
	NP1	200	74	12	Kumar et al. (2006)
	NP2	106	78	164	

3.3 Analysis of Strong Ground Motion Records

The strong motion records obtained from the Dharamshala, Uttarkashi and Chamoli earthquakes have been analyzed for identifying those records that may contain near-fault pulse-type ground motion. For this purpose the criteria based on source to site Distance, peak ground

acceleration, cumulative absolute velocity, peak ground velocity, arias intensity, root mean square acceleration, and damage potential have been adopted. These strong ground motion parameters are related to the important characteristics of ground motion such as amplitude, frequency content, duration and energy of the ground motion.

The Dharamshala earthquake was recorded on nine strong-motion accelerographs, placed at epicentral distances between 5 km and 25 km from the epicenter. **Table 3.3** lists **t**he station names and computed transverse and longitudinal components of peak ground accelerations (PGA) and peak ground velocities (PGV) of Dharamshala earthquake at different strong motion stations. The maximum peak horizontal acceleration was about 243 cm/sec^2 and 204 cm/sec^2 at Shapur station, which was located at distance of about 11 km from epicenter.

Table 3.3 Station names, codes and strong motion parameters of the 1986 Dharamshala earthquake.

S.No	Station Name	Code	Epi.Dst. (km)	COMP (L)	PGA (g)	PGV (cm/sec^2)	COMP (T)	PGA (g)	PGV (cm/sec^2)
1.	Dharamshala	DHAR	6	N76W	0.18	7.1	N14E	0.19	9.5
2.	Kangra	KANG	9	N43W	0.15	4.9	N47E	0.11	9.7
3.	**Shapur**	**SHAH**	**11**	**N75E**	**0.21**	**6.9**	**N15W**	**0.25**	**15.9**
4.	N.Bagwan	NAGB	12	S85W	0.15	8.2	N05W	0.08	4.1
5.	Baroh	BARO	20	N25W	0.06	3.3	N65E	0.06	3.1
6.	Bandlakhas	BAND	23	S27E	0.14	6.6	N63E	0.12	3.9
7.	Sihunta	SIHU	24	N25W	0.05	4.2	N65E	0.04	4.9
8.	Bhawarna	BHAW	24	N82E	0.04	1.5	N08W	0.04	3.2
9.	Jawali	JAWA	25	S86W	0.02	3.3	N04W	0.02	2.1

Thirteen strong-motion accelerographs triggered and recorded the strong ground motion of the Uttarkashi earthquake. These accelerographs were located at distances ranging between 20 and 150 km from the epicenter. The computed transverse and longitudinal components PGA and PGV of the Uttarkashi earthquake at various strong motion stations are tabulated in **Table 3.4.** Two stations were located very close to the surface projection of the Munsiari thrust that is considered as the likely source of this earthquake (Joshi, 2006). The maximum observed intensity of the earthquake was IX on MSK scale in an area of about 20 sq. km in and around the epicenteral zone. Maximum recorded horizontal component of peak acceleration was 304 cm/sec^2 at the Uttarkashi station. This station was located at distance of 40 km from the epicenter. The maximum recorded vertical component of acceleration was 288 cm/sec^2 at Bhatwari station that was located at a distance of 25 km from the epicenter.

Table 3.4 Station names, codes and strong motion parameters of the 1991 Uttarkashi earthquake.

S.No	Station Name	Code	Epi.Dst. (Km)	COMP (L)	PGA (g)	PGV (cm/sec^2)	COMP (T)	PGA (g)	PGV (cm/sec^2)
1.	Almora	ALMO	150	N53W	0.018	1.33	N37E	0.021	12.62
2.	Barkot	BARK	63	N10E	0.095	5.79	N80W	0.082	4.48
3.	**Bhatwari**	**BHAT**	**25**	**N85E**	**0.253**	**17.87**	**N05W**	**0.246**	**29.78**
4.	Ghansiali	GHAN	41	N00E	0.118	8.04	N90E	0.117	7.82
5.	Karnprayag	KARN	67	--	0.062	3.69	--	0.079	3.73
6.	Kosani	KOSA	144	N25W	0.029	1.88	N65E	0.032	1.55
7.	Koteshwar	KOTE	65	N30W	0.101	5.15	N60E	0.066	3.93
8.	Koti	KOTI	116	N10E	0.021	2.34	N80W	0.042	2.86
9.	Purola	PURO	75	N65W	0.075	4.81	N25E	0.093	4.59
10.	Rudraprayag	RUDR	54	--	0.053	2.07	--	0.052	2.71
11.	Srinagar	SRIN	60	--	0.067	1.94	--	0.050	2.02
12.	Tehri	TEHR	54	N63W	0.073	4.21	N27E	0.062	9.23
13.	Uttarkashi	UTTA	40	N15W	0.242	16.96	N75E	0.310	19.47

The strong ground motion due to the Chamoli earthquake was recorded on eleven strong-motion accelerographs. These instruments were placed at distances ranging from 10 km to 120 km from the epicenter. The computed transverse and longitudinal components of the PGA and PGV of this earthquake at different strong motion stations are given in **Table 3.5**. The Gopeshwar station was located at a distance of 13 km from the epicenter and at this station recorded the maximum horizontal component of peak acceleration which was 352 cm/sec^2.

Table 3.5 Station names, codes and strong motion parameters of the 1999 Chamoli earthquake.

S.No	Station Name	Code	Epi.Dst. (Km)	COMP (L)	PGA (g)	PGV (cm/sec^2)	COMP (T)	PGA (g)	PGV (cm/sec^2)
1.	Almora	ALMO	106	N53W	0.027	2.129	N37E	0.028	1.599
2.	Barkot	BARK	118	N10E	0.017	0.981	N80W	0.023	1.413
3.	Chinalisor	CHIN	103	N43E	0.052	3.355	N47W	0.045	3.355
4.	Ghansiali	GHAN	73	N00E	0.073	3.649	N90E	0.083	5.121
5.	**Gopeshwar**	**GOPE**	**13**	**N70W**	**0.199**	**22.440**	**N20E**	**0.359**	**45.890**
6.	Joshimath	JOSH	17	N80E	0.071	4.336	N10W	0.063	9.967
7.	Lansdown	LANS	--	N70E	0.005	0.235	N20W	0.006	0.275
8.	Tehri	TEHR	88	N63W	0.054	4.760	N27E	0.062	6.161
9.	Ukhimath	UKHI	29	N15E	0.091	8.610	N75W	0.096	6.880
10.	Uttarkashi	UTTA	96	N72E	0.054	3.590	N18W	0.064	9.710
11.	Roorkee	ROKE	--	N55W	0.056		N35E	0.047	

Maniatakis et al. (2008) from the study of accelerograms of small and moderate earthquakes (Mw≤6) corresponding to seismic intensities MMI≥VIII obtained from near-fault regions of Greece showed that the records contain simple wavelets characterized by pulses of shorter duration and smaller peak ground velocity (PGV). These pulses represent forward directivity

phenomena and cause severe damages to medium period structures, located close to active faults, with fundamental period less than 1 sec. Several parameters given in **Table 3.6** have been measured to find out whether the ground motion records contain pulse due to forward directivity or not. In case the values of these parameters exceed the prescribed values listed in **Table 3.6**, then the record may show impulsive characteristics indicative of NFGM. The characteristics of strong ground motion parameters are described below:

1) Peak ground acceleration (PGA): it is the most widely used strong ground motion parameter, provides information about the maximum acceleration observed in an earthquake. The most commonly used measure of peak acceleration is the amplitude of peak horizontal acceleration.

2) Cumulative absolute velocity (CAV): defined as the integral of the absolute acceleration time series has been used as an index to indicate the possible onset of structural damage, is represented mathematically by the equation:

$$CAV = \int_0^{t_{max}} |a(t)|\, dt$$

Where $|a(t)|$ is the absolute value of the acceleration time series at time t and t_{max} is the total duration of the time series. CAV has shown good correlation with structural damage potential.

3) Peak ground velocity (PGV): peak horizontal velocity (PHV) is an important parameter that represents the strength of ground motion. It is computed from the integration of acceleration time history and is dominated by intermediate range of frequencies.

4) Arias intensity (I_A): it is estimated by integrating the time history over the entire duration and therefore, is independent of the method used to define duration. It is computed using expression:

$$I_a = \frac{\pi}{2g}\int_0^{\infty} [a(t)]^2 dt$$

5) Root mean square acceleration (a_{rms}): it signifies the level of average acceleration over a specified duration of strong motion.

6) Damage potential (I): The expression $I = PGV.T_D^{0.25}$ is proposed as an instrumental measure of capacity of earthquake ground motion to damage structures having fundamental periods in the medium-period (velocity-controlled) region. Only two fundamental ground motion parameters (i.e., peak ground velocity and the duration of strong shaking) which have been routinely used for predicting ground motion in the design procedures are included in the formula. Expressions to determine the bounds of the medium-period region to apply this formula are also proposed as a function of the basic ground motion parameters.

Table 3.6 Lower-bound values of ground motion parameters (after Maniatakis et al., 2008).

Ground Motion Parameters	Lower–Bound Values
PGA	0.2g
CAV	0.30g sec
PGV	20cm/sec
I_A	0.4m/sec
a_{rms}	0.5m/sec^2
I	30cm sec$^{-0.75}$

The lower-bound values of ground motion parameters listed in **Table 3.6** have been used to identify records (corresponding to seismic intensities MMI≥VIII) that contain near-source effects having strong impulsive character in their velocity traces due to forward directivity.

Applications of above procedures brought out that out of 33 only 2 records contain near fault pulses. There computed strong ground motion parameter are tabulated in **Table 3.7**. These records are from Bhatwari station (1991 Uttarkashi earthquake) and Gopeshwar station (1999 Chamoli earthquake).

Table 3.7 Ground motion parameters of the Uttarkashi and Chamoli earthquakes.

S. No	Ground Motion Parameters	Bhatwari station (Uttarkashi Earthquake)	Gopeshwar station (Chamoli Earthquake)
1.	PGA	0.246g > 0.2g	0.36g > 0.2g
2.	CAV	0.753g sec > 0.30g sec	0.598g sec > 0.30g sec
3.	PGV	28.62cm/sec > 20cm/sec	45.65cm/sec > 20cm/sec
4.	I_A	1.1m/sec > 0.4m/sec	0.800m/sec > 0.4m/sec
5.	a_{rms}	1.07 m/sec^2 > 0.5 m/sec^2	0.71 m/sec^2 > 0.5 m/sec^2
6.	I	44.28cm sec$^{-0.75}$ > 30cm sec$^{-0.75}$	77.7cm sec$^{-0.75}$ > 30 cm sec$^{-0.75}$

From visual inspection it is seen that one of the strong motion record of Dharamsala earthquake of 1986 (obtained at Shapur station) contained near-field velocity pulse because the maximum

peak horizontal acceleration was about 243 cm/sec^2 and peak horizontal velocity was about 15 cm/sec at this station which was located at an epicentral distance of 11 km. Although, this record only satisfy one criterion given in **Table 3.6**, but has been included for further analysis. The epicenter of these three earthquakes and respective selected location of stations are shown in **Figure 3.1**.

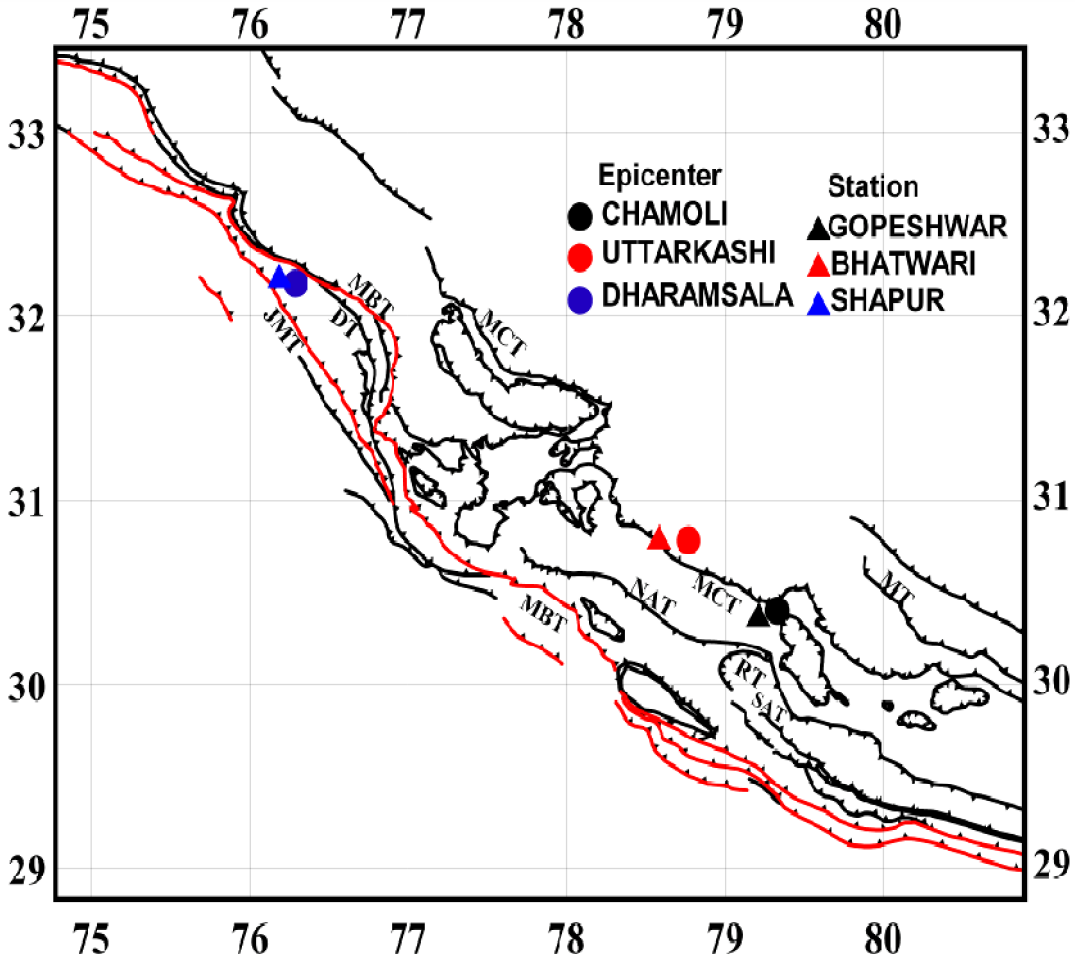

Figure 3.1 Epicenters of three earthquakes and locations of stations that contain near-fault pulses.

3.4 Pulse Detection Methodology

Several models have been developed by various researchers to represent near-field pulses. These models are known as Equivalent Velocity Pulse (EVP) Models (Alavi and Krawinkler, 2000; Mavoeidis et al., 2004; Mavoeidis, 2004; Mavoeidis and Papageorgiou, 2003; Hall et al., 1995; Li and Zhu, 2004, Agrawal et al., 2002; Menun and Fu, 2002; Lili et al., 2005). Mainly three parameters have been used to describe these models, namely, the amplitude of the velocity pulse, time period of the velocity pulse, and shape of the pulse. In these models,

various pulse shapes have been used to represent the observed pulses in the velocity time history. Several mathematical techniques, including some signal processing techniques, have been adopted to represent the complex character of the velocity pulses. In recent years, the Wavelet technique has been employed to extract pulse waveforms and the periods of velocity pulses from velocity time histories (Baker, 2007; Maniatakis et al., 2008; Mavroeidis and Papageorgiou, 2003). In the present work, the methodology proposed by Baker (2007) based on wavelet theory has been applied on three selected strong ground motion records that were produced due to rupturing of buried faults in the Himalaya. These possibly contain near-fault effects. Wavelet analysis is a new mathematical tool widely applied in signal processing, which is much more suitable for the study of non-stationary processes, compared to Fourier transform technique (Chik and other, 2009). Earthquake ground motion in the time-domain can be characterized as a non-stationary signal. Fourier transform is a powerful tool to extract information about the frequency content of the signal; however, it fails to provide the frequency localization of the signal in the time domain (Gurley and Kareem, 1999). Hence, there is a loss of time-frequency representation in Fourier transform. This limitation of Fourier transform can be overcome by Wavelet transform, which allows for full time-frequency representation of the time series by decomposing a signal into wavelets that are localized in time and represent a narrow range of frequencies (Haigh et al., 2002). Wavelets are ideal tools to identify various phases in a signal with different frequency contents, and with a localized time distribution (Rezai and Ventura, 2002). These wavelets are the basis functions that satisfy a certain set of mathematical requirements. Wavelet transformation decomposes the signals into its wavelets, which are scaled and shifted versions of the so-called mother wavelets. The Wavelet transform of the signal x(t), is represent as follows (Gurley and Kareem, 1999),

$$\mathrm{WT}(s, l) = \int_{-\infty}^{\infty} x(t).\omega_{s,l}(t)dt$$

Where,

$$\omega_{s,l}(t) = \frac{1}{\sqrt{s}} w\left(\frac{t-l}{s}\right) = \frac{1}{\sqrt{s}} w(t)$$

$\omega_{s,l}(t)$ = Wavelet Basis Function.

$w(t)$ = Mother Wavelet.

The above expression shows that any signal x(t) can be represented as a linear combination of basis function and the transformation is separately computed for different parts of the time

domain signal. WT(s, l) represents the correlation between the wavelet and a localized part of the signal in terms of the time-scale functions. All the basis functions are generated by scaling and shifting of functions called mother wavelets w(t), which are oscillatory and have amplitudes that quickly decay to zero in both the positive and negative directions. The coefficient associated with the wavelet having scale "s" and position "l" provide useful signal information. At high frequencies good time resolution is achieved, whereas at low frequencies good frequency resolution is obtained. If the signal has a major component of a frequency corresponding to a given scale, then the wavelet at this scale is close to the given signal at a particular location. The corresponding wavelet transform coefficient determined at this location has a relatively large value that describes the signal energy on the adopted variable time-scale in the time domain. Parameters used to characterize wavelet (s and l) are dimensionless. The wavelet dilates if s>1 and contracts if s<1; therefore, s is the scaling parameter that captures the local frequency content. For a small value of "s" the basis function becomes a stretched wavelet, corresponding to a low frequency function. However, for a large value of "s" the basis function becomes a contracted version of the prototype wavelet, corresponding to a high frequency function. The time scale distribution of time-domain functions can be used to extract different features hidden inside the function. As the resolution changes and "s" takes different values, the wavelet changes, in both its width and oscillating frequency inside the domain of the function to match all possible sizes of components in the function. In case a significant portion of ground motion time history is described by one or a few wavelets with large coefficients, then this will be used to indicate the presence of a pulse as in the case of near-fault ground motion in velocity time history.

Baker (2007), having adopted the wavelet approach and using Daubechies wavelet of order four as a mother wavelet, extracted the largest velocity pulse from a given ground motion. For the purpose of finding the period and location of the pulse, the continuous wavelet transform of the velocity time history is computed, and the coefficient with the largest absolute value is identified. The wavelet associated with this largest coefficient is useful to identify the period and location of the pulse. The extracted pulse using this procedure clearly captures the velocity pulse while ignoring the high frequency motion of the original ground motion, and can be used to extract pulse from any type of ground motion, regardless of the existence of a directed velocity pulse. However, for non-pulse like ground motion, it has been observed the extracted pulse does not normally represent the dominant component of the ground motion, and the residual ground motion is nearly identical with original ground motion. Therefore, the

significance of pulse type ground motion depends on the difference between residual and original time history. Two predictor variables, i.e., PGV ratio of the residual record to the original record, and the energy ratio of the residual record to original record, has been used as a Pulse Indicator (PI) to predict the likelihood that a given record is pulse like or non-pulse like (Baker, 2007). If the value of PI is above 0.85 the record contains pulse type ground motion, and if the value is below 0.15 the record is non-pulse type, respectively. The following expression is used to compute PI:

$$PI = \frac{1}{1+\exp(-23.3+14.6(PGVratio)+20.5(Energyratio))}$$

Adopting the above procedure, the three selected ground motion velocity time histories, as well as their fault normal components, have been analyzed to extract the largest velocity pulse using various mother wavelets. For computing fault-normal component, each ground motion time history has been rotated to fault normal orientation invoking the method given by Somerville (1997b). All the three selected ground motion records, obtained at Shapur, Bhatwari and Gopeshwar stations located in the epicentral region, are found to be rich in low frequency near-field motions and energy is concentrated in a narrow band. Several mother wavelets, namely, Daubechies (db4 and db7), Haar (haar), Symlet (sym4), Coiflets (coif2), Reverse biorthogonal (rbio2.4) and Biorspline (bior1.3) have been used to extract the pulse from the velocity time history and predict the value of pulse period, which is the most important characteristic associated with ground motion. The selected mother wavelets used for pulse detection fall in two categories. Haar (haar), Daubechies (db4 and db7), Symlet (sym4) and Coiflet (coif2) are orthogonal wavelets, whereas, Reverse bioorthogonal (rbio2.4) and Biorspline (bior1.3) wavelets are bi-orthogonal wavelets (Sabegh, 2010). Different mother wavelets because of their variability give different values of pulse indicator and pulse period of the extracted long period velocity pulse. The original ground motion records along with their extracted pulses using different mother wavelets are shown in **Figures 3.2, 3.3, 3.4, 3.5 and 3.6**. Associated pulse indicators and pulse periods are tabulated in **Table 3.8, 3.9 and 3.10**. The selected time domain windows for strong ground motion at Bhatwari and Gopeshwar stations is up to 10 sec and 8 sec respectively, whereas, for Shapur station it is up to 5 sec because captured pulse is located in these time domain windows in the selected ground motion. No fling step effect has been considered in pulse detection because the wavelet basis functions used for pulse extraction have zero residual displacement, so fling effect will not be detected.

.**Table 3.8 Pulse indicators and pulse-periods using different mother wavelets for transverse/FN components of strong ground motion at Shapur station.**

Mother Wavelet	Shapur (Transverse/Fault-Normal Component)	
	Pulse Indicator (PI)	Pulse Time-Period (Tp)
db4	0.9051	0.53 sec
db7	0.9431	0.52 sec
haar	0.7631	0.40 sec
sym4	0.4241	0.59 sec
coif2	0.5692	0.55 sec
rbio2.4	0.6431	0.50 sec
bior1.3	0.8223	0.47 sec

Table 3.9 Pulse indicators and pulse-periods using different mother wavelets for transverse and FN components of strong ground motion at Bhatwari station

Mother Wavelet	Bhatwari (Transverse Component)		Bhatwari (Fault-Normal Component)	
	Pulse Indicator (PI)	Pulse Time-Period (Tp)	Pulse Indicator (PI)	Pulse Time-Period (Tp)
db4	0.9450	1.12 sec	0.9112	1.09 sec
db7	0.9459	1.33 sec	0.9280	1.30 sec
haar	0.6319	0.80 sec	0.5111	0.78 sec
sym4	0.6675	1.04 sec	0.5353	1.04 sec
coif2	0.8147	1.00 sec	0.4941	1.02 sec
rbio2.4	0.7261	1.19 sec	0.5307	1.15 sec
bior1.3	0.6861	0.92 sec	0.3633	0.90 sec

Table 3.10 Pulse indicators and pulse-periods using different mother wavelets for transverse and FN components of strong ground motion at Gopeshwar station.

Mother Wavelet	Gopeshwar (Transverse Component)		Gopeshwar (Fault-Normal Component)	
	Pulse Indicator (PI)	Pulse Time-Period (Tp)	Pulse Indicator (PI)	Pulse Time-Period (Tp)
db4	0.9939	1.37 sec	0.9813	1.40 sec
db7	0.9505	1.39 sec	0.9019	1.39 sec
haar	0.9999	1.04 sec	0.9996	1.08 sec
sym4	0.9989	1.34 sec	0.9886	0.37 sec
coif2	0.9975	1.43 sec	0.9624	1.54 sec
rbio2.4	0.9985	1.55 sec	0.9893	1.84 sec
bior1.3	0.9998	1.22 sec	0.9990	1.22 sec

The orientation of the recorded transverse component of time history at Shapur station during Dharamsala earthquake of 1986 demonstrated that it is in the fault normal direction, provided the fault plane solution given by Molner et al. (1989) is considered as the focal mechanism of this earthquake. The analysis of this record has been carried out using seven mother wavelets and the results obtained are listed in **Table 3.8**. It is evident from the values given in **Table 3.8** that both Daubechies wavelets db4 and db7 are capable of extracting the pulse form from the

velocity time history efficiently as both have pulse indicators (PI) above 0.85 and pulse periods of 0.532 sec and 0.520 sec respectively. However, the other wavelets are unable to extract the pulse form efficiently from the recorded ground motion as the values of pulse indicators (PI) are below 0.85.

On similar lines, the transverse component of recorded time history at Bhatwari station during the Uttarkashi earthquake of 1991 and its fault normal component obtained considering the fault plane solution given by Paul et al. (1998) have been analyzed using seven mother wavelets. The extracted pulse indicators and pulse periods from the velocity time history are listed in **Table 3.9**. It has been revealed that from the seven mother wavelets, Daubechies wavelets, db4 and db7, allowed the extraction of the pulse form from the recorded ground motion and its fault normal component as the values of pulse indicators (PI) are above 0.85. The extracted pulse period using both the components falls in the range between 1.09 sec and 1.33 sec.

The recorded transverse component of ground motion during Chamoli earthquake of 1999 at Gopeshwar station and its fault normal component oriented on the basis of fault plane solution given by Kumar et al. (2006) have been analyzed for near fault pulse detection in velocity time history adopting the selected seven mother wavelets. All the seven mother wavelets were capable of extracting the near fault pulse from the ground motion, and it has been found that all mother wavelets gave values of pulse indicator (PI) above 0.85 at Gopeshwar station without much variation. However, a large variation in pulse time period that vary between 1.04 sec to 1.55 sec in transverse component and 1.08 sec to 1.84 sec in fault normal component has been brought out. The results are listed in **Table 3.10**.

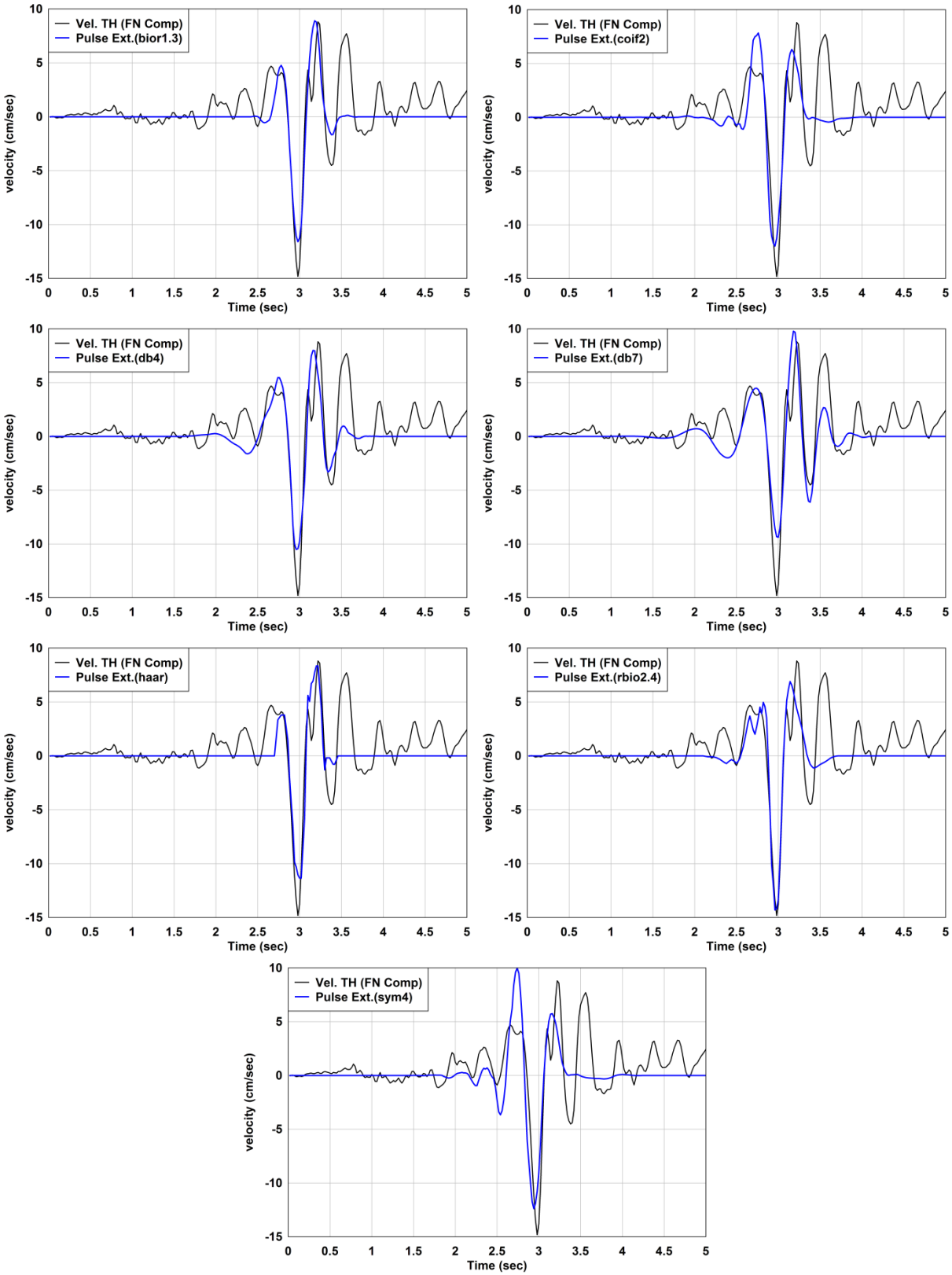

Figure 3.2 Original ground motion/FN component and extracted pulses at Shapur station.

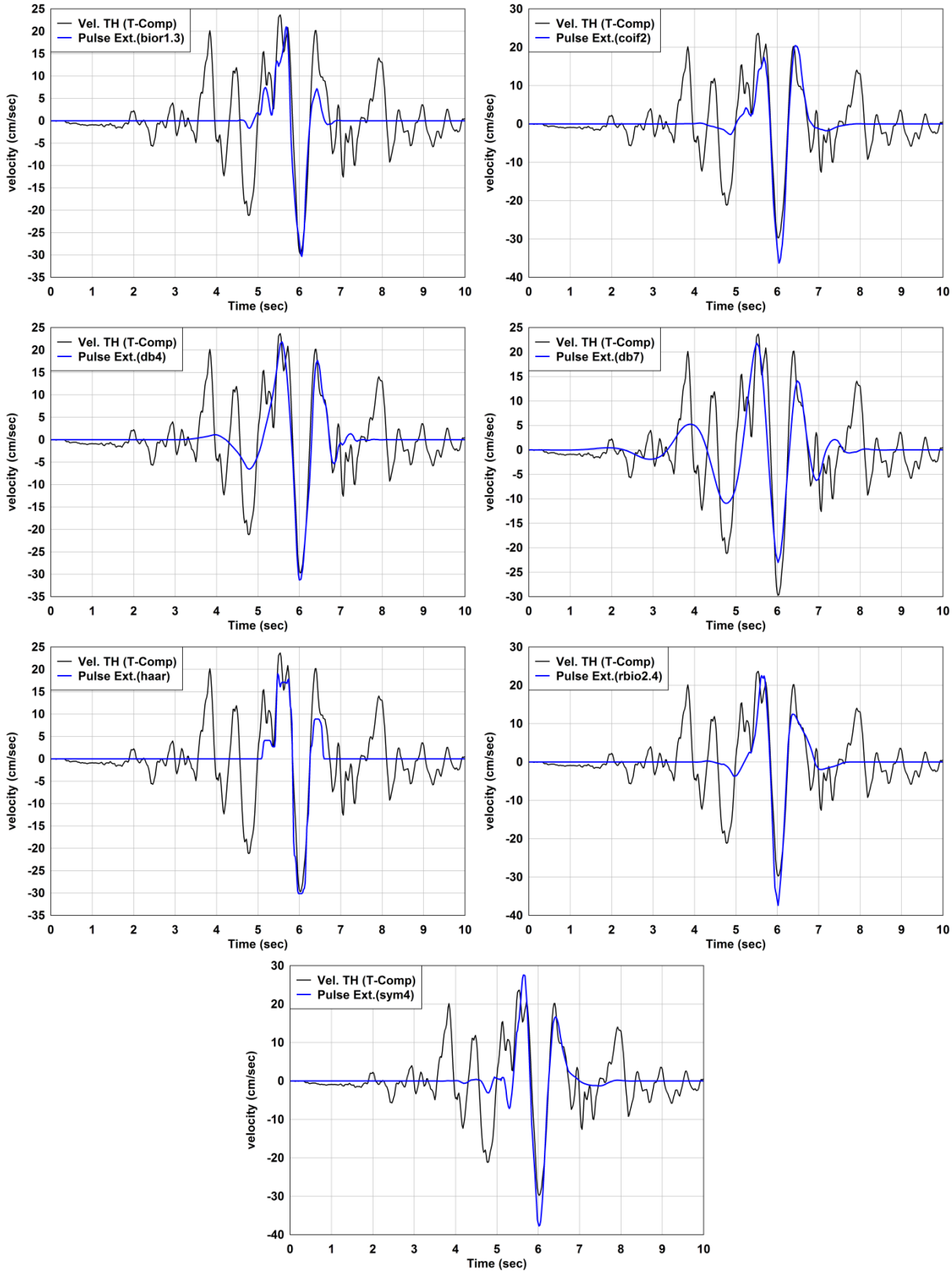

Figure 3.3 Original recorded ground motion and extracted pulses at Bhatwari station.

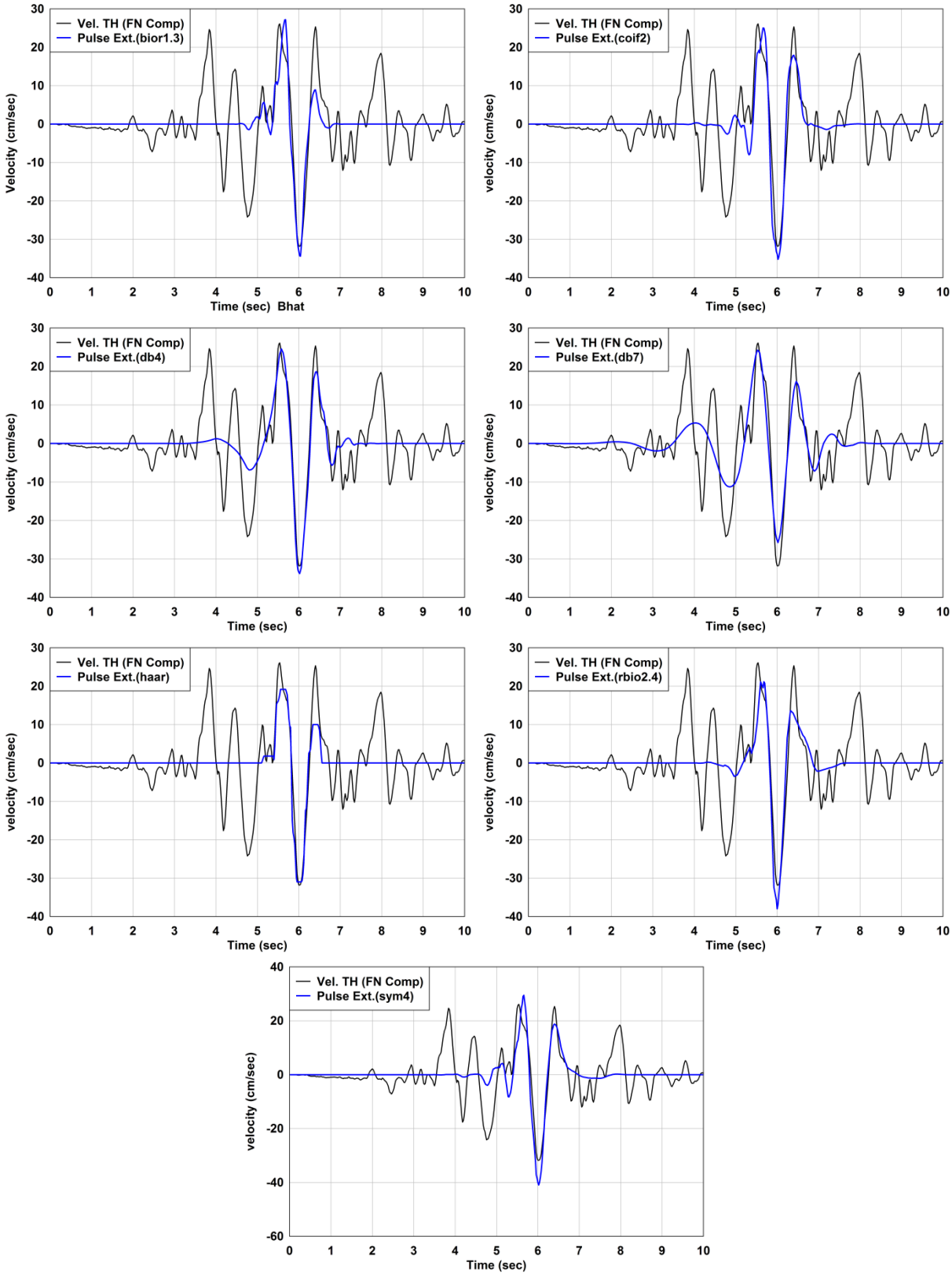

Figure 3.4 Fault-normal component and extracted pulses at Bhatwari station.

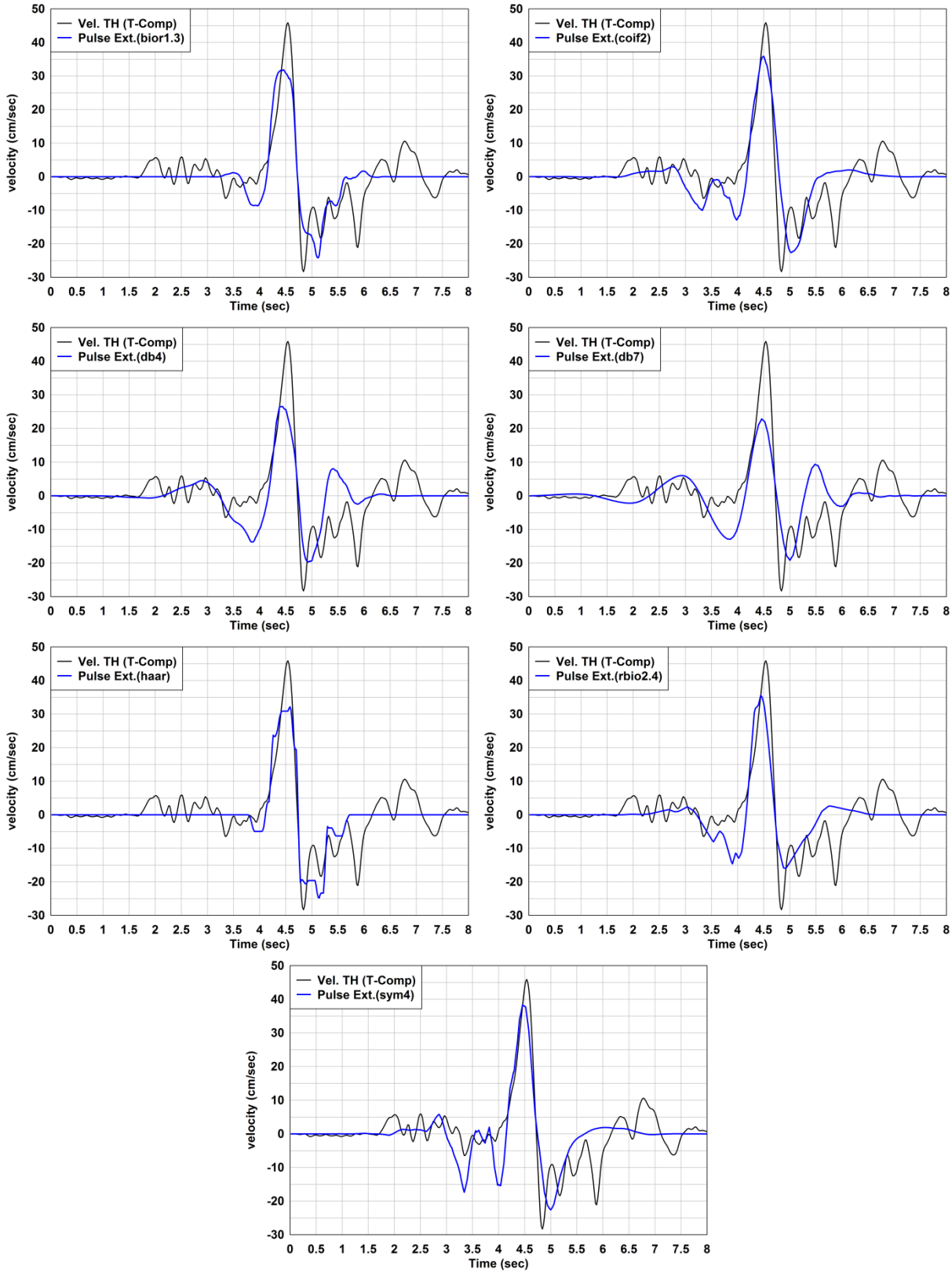

Figure 3.5 Original recorded ground motion and extracted pulses at Gopeshwar station.

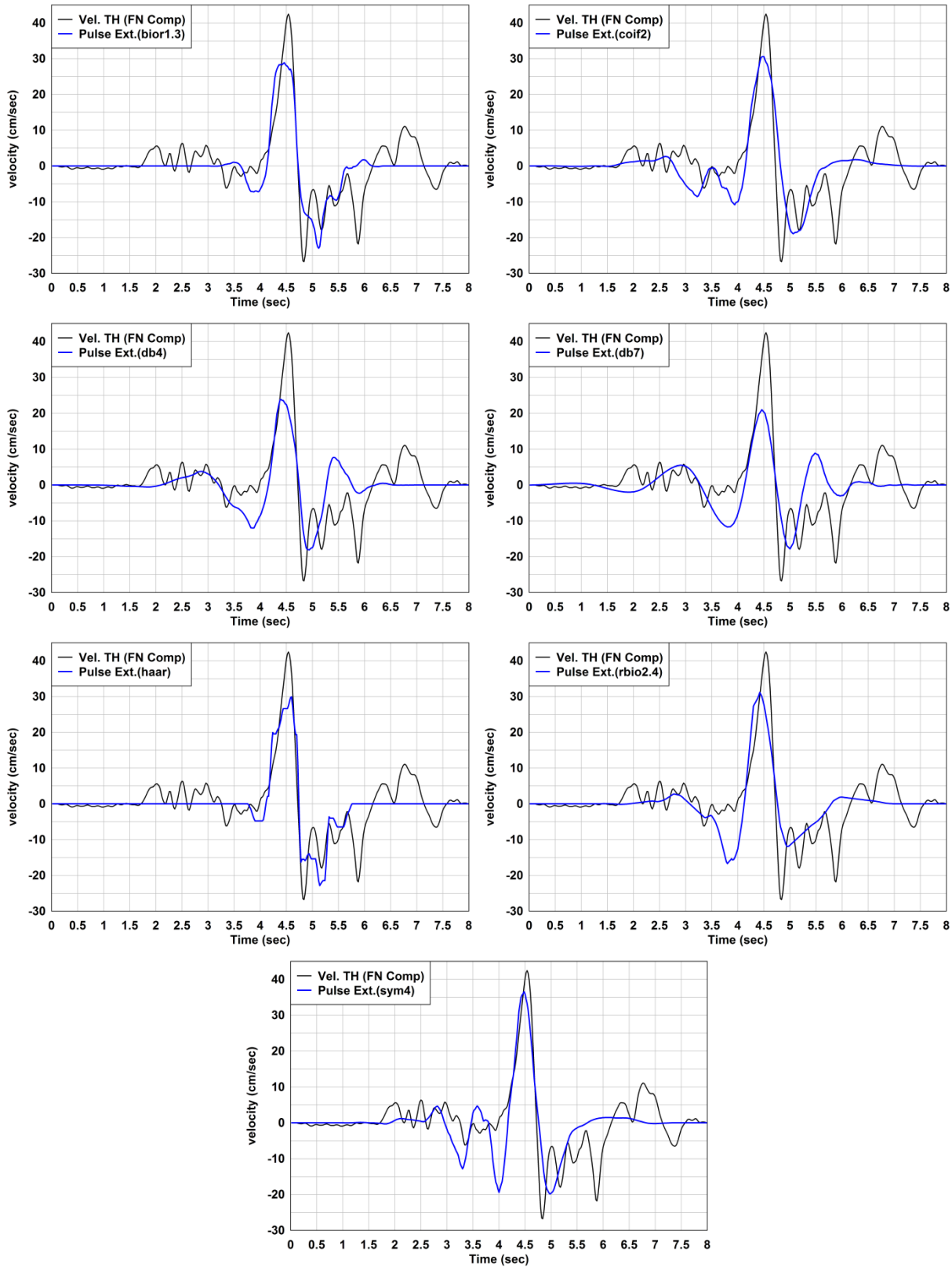

Figure 3.6 FN-component and extracted pulses at Gopeshwar station.

3.5 Interpretation of Results

Structural response is governed by the pulse period of the dominant pulse when energy is primarily concentrated in it. Therefore, the pulse period forms a key parameter for structural engineers, because the structural response due to pulse waveform or pulse type motion depends on the ratio of fundamental period of the structure to the pulse period (Anderson and Bertero, 1987; Mahin et al., 1976; Alavi and Kriawinkler, 2001; Mavreoidis et al, 2004).

The period associated with the maximum Fourier amplitude of a wavelet can be used to define a pseudo period (Tp) of the largest associated wavelet coefficient (Baker, 2007). The pulse periods (pseudo-periods) of the estimated ground motion are different for extracted pulses which are associated with different type of mother wavelets. On account of this, a variation is observed in the pulse periods of the estimated ground motion. However, the appropriate estimation of this key parameter (pulse period) is a necessary requirement for structural engineers to study the response of structures located in the near-field environment.

Various methods have been suggested by researchers to define the pulse-period of a velocity pulse. Rodriguez-Marek (2000) used the method of counting zero crossings above a prescribed threshold level of amplitude, or, the number of half-cycle pulses in the velocity-time history with amplitudes at least 50% of the peak ground velocity of the record. Methods have been developed based on fitting a truncated harmonic wave to the pulse using techniques of nonlinear optimization (e.g., Menun and Fu, 2002; Mavreoidis and Papageorgiou, 2003; Makris and Roussos, 1998; Agrawal et al, 2002). Krawinklar and Alavi (2001) estimated the pulse period of the velocity pulse by identifying a clear and global peak in the velocity response spectrum of the ground motion. This allowed for the estimation of pulse period or equivalent pulse period (Tv-p) in a relatively unambiguous manner. Bray and Radriguez-Marek (2004) found slightly higher value of pulse period (Tp) compared to the value of pulse period (Tv-p) estimated from spectral-velocity response spectra, which used the method of zero crossing time or the time at which velocity is equal to 10% of the peak velocity of the pulse. Further, wavelet analysis indicates that the estimated pulse period (Tp) is generally larger than the pulse period (Tv-p) estimated from spectral velocity response spectra (Baker, 2007). Therefore, it has been concluded that in case of a significant difference between wavelet based pulse period and pulse period obtained by velocity spectral method, it would be appropriate to use wavelet based pulse period because its identification is free from user judgment and provides best pulse period

along with its occurrence in space and time (Baker, 2007). Based on these ideas, the following interpretation has resulted from the observed near-fault ground motions of the three chosen Himalayan earthquakes.

3.5.1 Dharamshala Earthquake-Recorded Transverse (FN) Component at Shapur Station

Recorded transverse-component/fault-normal component of ground motion at Shapur station has been analyzed using seven mother wavelets. However, only two mother wavelets, namely db4 and db7 were able to successfully extract the near fault pulse from the ground motion. The values of pulse indicator (PI) estimated from these two mother wavelets are above 0.85 and pulse periods (Tp) are 0.53 sec and 0.52 sec respectively. The spectral velocity curves of recorded ground motion and pulses identified using the two mother wavelets (db4 and db7) are plotted in **Figure 3.7**. The Figure shows that pulse period associated with spectral velocity of ground motion is 0.4 sec. By examining the shapes of the spectral velocity curves shown in **Figure 3.7** it is observed that the pulse obtained using db7 wavelet is close to the pulse hidden in the ground motion, because the spectral velocity curve of db7 wavelet is well matched with, and also shows a trend very similar to, the spectral velocity curve of the recorded original ground motion in the intermediate-period-range compared to the pulse shape obtained using db4 wavelet. Hence, the db7 wavelet is more efficient in extracting the pulse having pulse period (Tp) 0.52 sec and pulse indicator (PI) 0.94 than the other wavelets at this station. Furthermore, the value of pulse indicator using db7 is larger than the value of pulse indicator obtained from db4 which is 0.90.

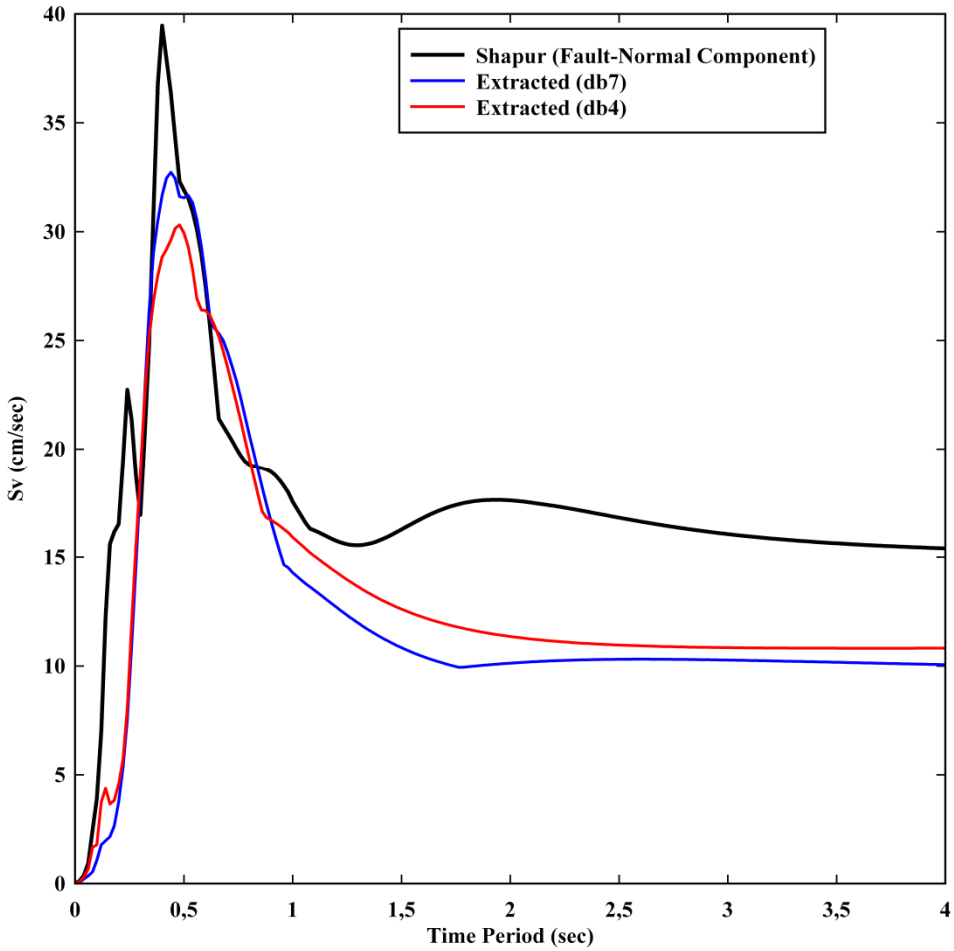

Figure 3.7 Velocity spectra of FN component and extracted pulses at Shapur Station.

3.5.2 Uttarkashi Earthquake-Recorded Transverse Component and Computed Fault-Normal Component at Bhatwari Station.

Transverse component of the recorded ground motion has first been analyzed for pulse detection adopting seven mother wavelets to allow for detection of near-fault pulse type characteristics i.e., significant long period velocity pulse. These mother wavelets were then applied on the computed fault normal component at Bhatwari station to detect the near-fault pulse. The computed spectral velocity curves of recorded transverse component and computed fault normal component are displayed in **Figure 3.8**. As is evident from this figure, the fault normal component is more severe compared to the recorded transverse component. However, both the curves follow similar trends. Analysis of both the components have brought out that out of seven mother wavelets only two mother wavelets i.e., db4 and db7 enabled pulse extraction from the ground motion with values of pulse indicators (PI) above 0.85. The variation in values of pulse indicators obtained using other five mother wavelets along with wavelets db4 and db7 lies between 0.63 to 0.95 and 0.36 to 0.93 for both the components. All

the computed values of pulse indicators are above 0.15 and show varying pulsivity along with varying pulse periods between 0.8 sec to 1.33 sec and 0.78 sec to 1.30 sec as tabulated in **Table 3.9**. Considering these variations in pulse periods and trends of the spectral velocity curves of recorded transverse component and computed fault normal component plotted in **Figure 3.8**, it can be concluded that pulse period (Tv-p) associated with spectral velocity of ground motion for the transverse component is 1.28 sec and for the fault-normal component is 1.3 sec. Computed spectral velocity curves of the recorded ground motion and the fault normal component, along with the pulses extracted by db4 and db7, are shown in **Figures 3.9 and 3.10** respectively. It is observed from the comparison of these spectral velocity curves that pulse obtained by db7 wavelet is close to the pulse hidden in both the ground motions. This can be inferred from the fact that the spectral velocity curve of the db7 wavelet is well matched with, and shows a trend analogous to, the spectral velocity curves of the recorded original transverse component and fault normal component of ground motion, when compared with the db4 wavelet. In case of transverse component of recorded ground motion, pulse period (Tp) computed using wavelet db7 is 1.33 sec which is closer to the spectral pulse period (Tv-p) 1.28 sec having the value of pulse indicator (PI) 0.95. Hence, the db7 wavelet is more efficient than other wavelets, and the value of pulse indicator is also greater than that obtained using db4 wavelet. For the case of computed fault normal component of ground motion, it is found that the db7 wavelet is once again more efficient than other wavelets in extracting the long period pulse. In this case, the estimated pulse period (Tp) is 1.30 sec which is equal to spectral pulse period (Tv-p) of 1.30 sec with value of pulse indicator (PI) as 0.93. This value of pulse indicator is greater than that obtained using wavelet db4.

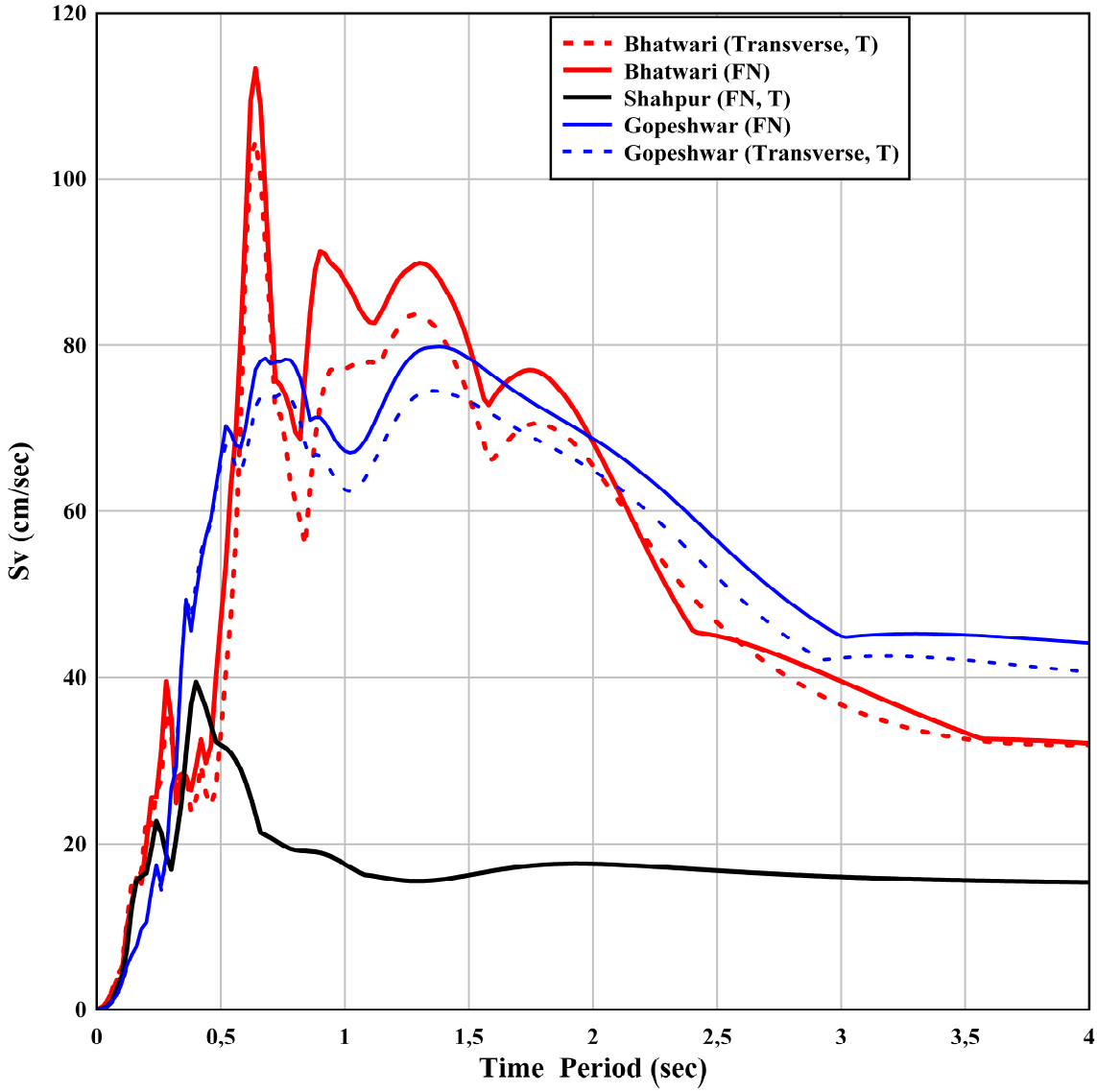

Figure 3.8 Velocity spectra of FN and recorded transverse components at Shapur, Bhatwari, and Gopeshwar stations.

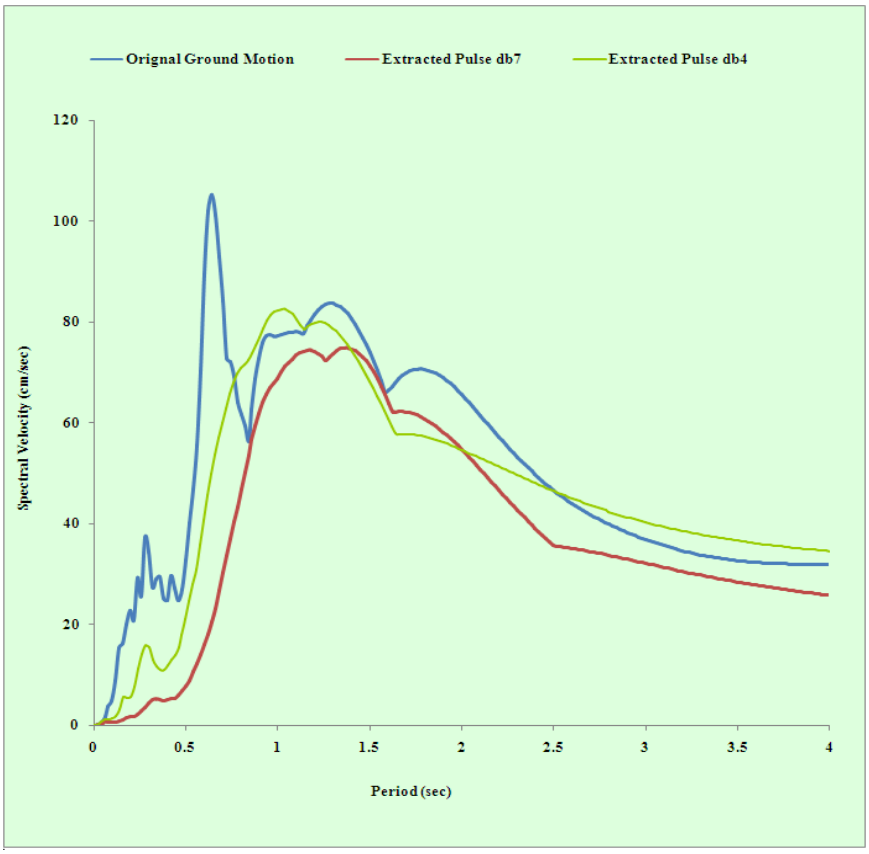

Figure 3.9 Velocity spectra of transverse component and extracted pulses at Bhatwari station.

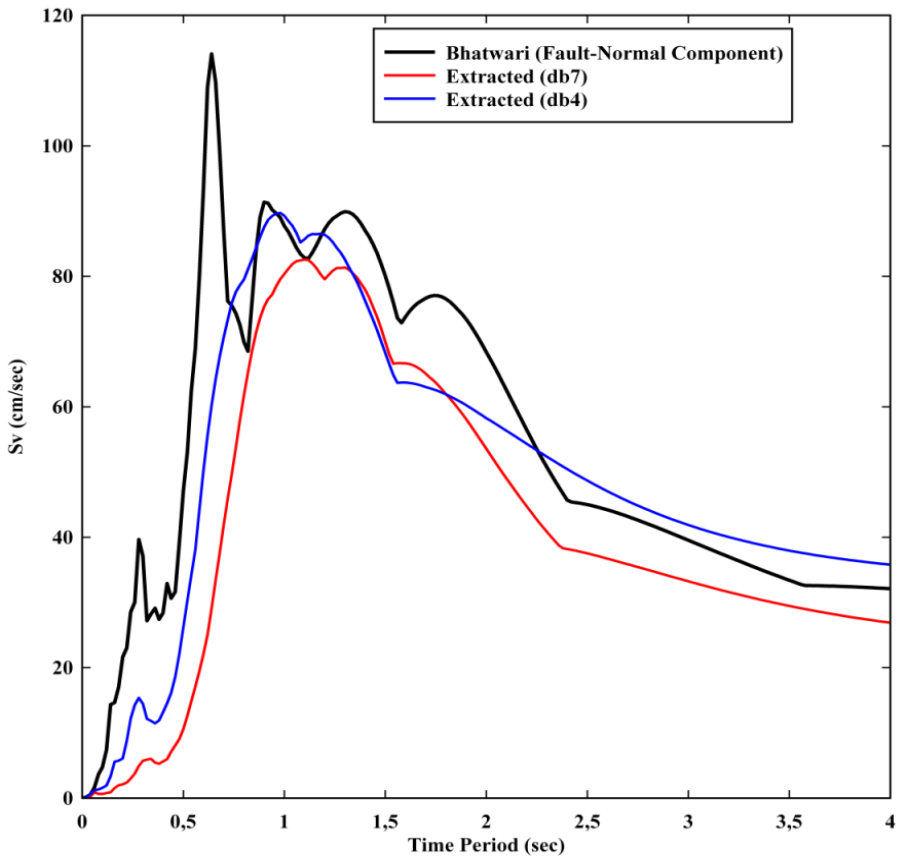

Figure 3.10 Velocity spectra of FN component and extracted pulses at Bhatwari station.

3.5.3 Chamoli Earthquake-Recorded Transverse Component and Computed Fault-Normal Component at Gopeshwar Station

The recorded transverse component of ground motion at Gopeshwar station, located in the epicentral region, is found to be rich in low frequencies due to near-fault ground motion. The energy is concentrated in a narrow band. The near-fault pulse type characteristics of ground motion that exhibit significant long period velocity pulse has been detected using seven mother wavelets. The same mother wavelets have been applied on the computed fault normal component at Gopeshwar station to allow for detection of the near-fault pulse. The computed spectral velocity curves of recorded transverse component and computed fault normal component are plotted in **Figure 3.8**. The figure shows that the fault normal component is more pronounced then the recorded transverse component. Analysis of both the components by employing the seven wavelets has brought out that all the wavelet-forms are capable of extracting the pulse type characteristics from both the components of ground motion. In all the cases, the values of pulse indicators (PI) are above 0.85. For transverse component of the recorded ground motion, the values of pulse indicators vary between 0.95 and 1.00 and the pulse periods vary from 1.04 sec to 1.55 sec, whereas for computed fault normal component the values of pulse indicators (PI) lie in the range 0.90 to 1.00, and the pulse periods vary from 1.08 sec to 1.84 sec. The values of pulse indicators (PI) and pulse periods are tabulated in **Table 3.10**. Taking into account these variations in pulse periods, and also the shapes of spectral velocity curves of the recorded transverse component and the computed fault normal component as plotted in **Figure 3.8**, it can be concluded that pulse period (Tv-p) associated with spectral velocity of ground motion in transverse component is 1.38 sec and in fault-normal component is 1.28 sec. All the seven wavelets have pulse indicators (PI) above 0.85 and show good efficiency in extracting pulse characteristics from the ground motion. However, it is important to decide that which wavelet amongst the seven is best for extraction of the near-fault pulse. This decision can be made on the basis of a comparative study on pulse periods (Tp) obtained using different wavelets and the spectral pulse periods (Tv-p) of the ground motions, and comparing the spectral shapes of extracted pulse-forms using seven wavelets with the spectral shapes of the ground motions as shown in **Figure 3.11 and 3.12.**

3.5.3.1 Interpretation of Transverse Component of Recorded Ground Motion at Gopeshwar Station

It has been observed in reported studies that pulse periods (Tp) are similar or slightly higher than the periods obtained from the velocity response spectra of the ground motion (Baker, 2007; Bray and Marek, 2004). In the present study, the pulse periods obtained using haar, sym4 and bior1.3 wavelets are smaller, and those obtained by coif2 and rbio2.4 are higher than the spectral pulse period (Tv-p) estimated from the recorded ground motion (**Figure 3.11**). On the other hand, the pulse periods obtained by **db4 and db7** wavelets are close to the spectral pulse period (Tv-p) of the ground motion. Comparison of the spectral velocity curves of extracted seven pulses with the spectral velocity curve obtained from recorded transverse component of ground motion shows that peaks associated with haar, sym4, bior1.3, coif2 and rbio2.4 occur before the long period peak of the recorded transverse component, whereas the trend of the peaks associated with **db4 and db7** pulses match with the long period peak of recorded transverse component of ground motion (**Figure 3.11**).

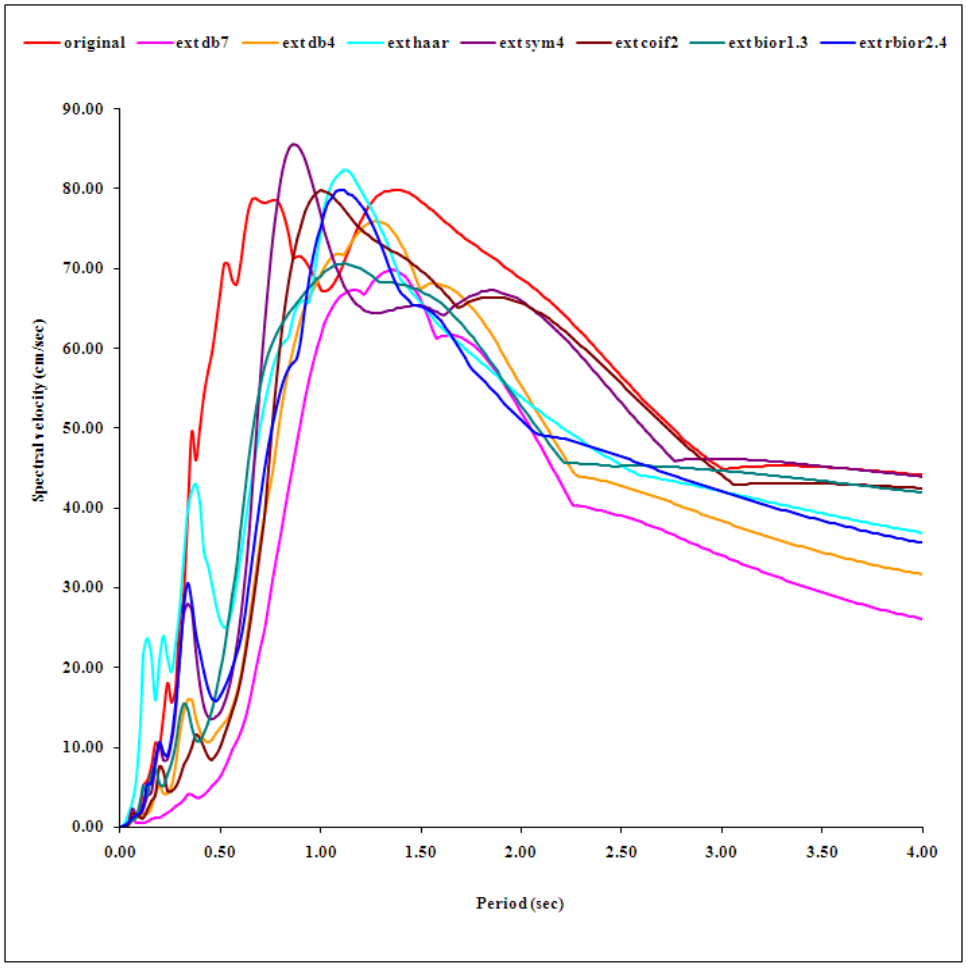

Figure 3.11 Velocity spectra of original recorded ground motion (transverse component) and extracted pulses at Gopeshwar station.

3.5.3.2 Interpretation of Computed Fault-Normal Component of Recorded Ground Motion at Gopeshwar Station

Considering the variations in pulse periods of the extracted pulses, and the time period associated with the peaks of the spectral velocity curve of the computed fault normal component, a long period peak at (Tv-p) 1.28 sec in spectral velocity curve of computed fault normal component has been observed (**Figure 3.12**). The period of this peak which is above 1 sec is interpreted as spectral pulse period (Tv-p). The pulse periods of the extracted pulses for computed fault normal component are found to be less than the Tv-p (1.28sec) using haar and bior1.3 wavelets, whereas pulse periods obtained using coif2 and rbio2.4 wavelets are higher. However, pulse periods obtained by adopting the db4, db7 and sym4 wavelets are slightly higher but closer to the spectral pulse period (Tv-p) of the computed fault normal component compared to those obtained using other wavelets. Comparison of the spectral velocity curves of extracted pulses using db4, db7 and sym4 wavelets with spectral velocity curve of computed fault normal component of ground motion has revealed that spectral peak of sym4 extracted pulse occurs before the long period peak of computed fault normal component of ground motion. Further, the trend of the spectral curve obtained using **db4 and db7** wavelets are very well correlated with the trend of spectral curve of computed fault normal component. The match in trend of the curves seems to be more consistent above one sec period (**Figure 3.12**).

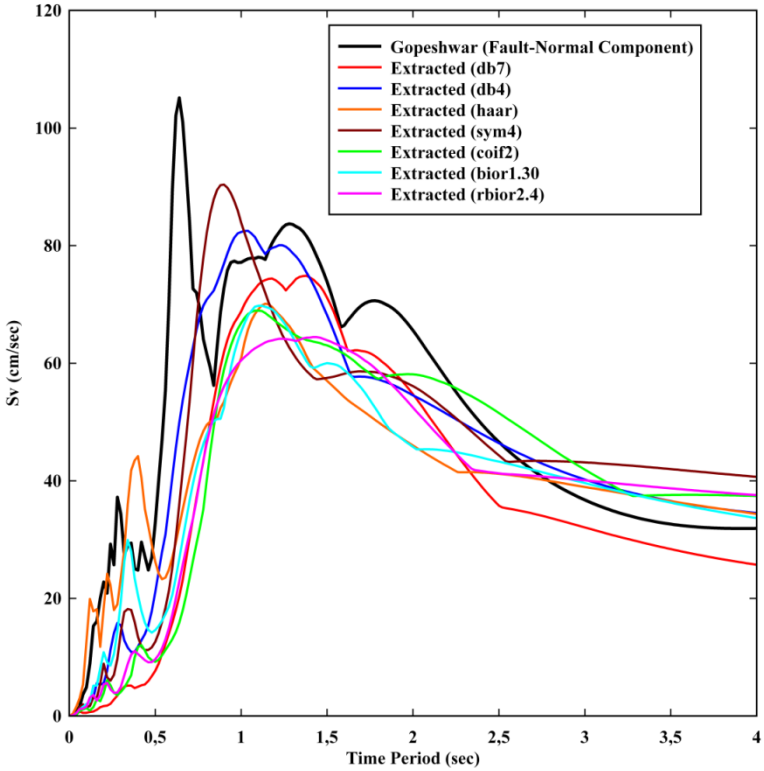

Figure 3.12 Velocity spectra of FN-component and extracted pulses at Gopeshwar station.

3.6 Comparison of Estimated and Computed Pulse-Periods and Amplitudes

Various researchers have developed relationships between magnitude and pulse period using different data sets. These relationships can be adopted to estimate pulse period from the magnitude (Alavi and Krawinkler 2001; Baker 2007; Bray and Marek 2004; Ghahari et al. 2010; Mavroeidis and Papageorgiou 2003; Somerville 2000; Somerville et al. 1999; Somerville 2003). Applicability of these relationships for the Himalayan region has been examined, and for this purpose, the pulse periods obtained in the present study have been compared with those estimated using available relationships. The results are presented in **Table 3.11** and show that no single relationship given by various investigators can be applied to the Himalayan region. Pulse-periods estimated using various relationships are generally on higher side compared to the computed pulse period. However, the closest match seems to be with the three relationships given by Alavi and Krawinkler (2001), Somerville (2003) and Bray and Marek (2004). The variability in the pulse periods estimated using different relationships with those estimated in the present study can be attributed to several factors, such as the relationships being based on different types of data sets, use of different methodologies for pulse period estimation, types of source mechanisms, and site characteristics below the recording stations, to name few. For the three Himalayan earthquakes, the estimated pulse periods are plotted in **Figure 3.13** along with the world-wide dataset of 91 pulse type ground motions, which shows that the limited data set for the Himalayan earthquakes conforms with the world-wide data set given by Baker (2007)**.** It has been observed that for Himalayan earthquakes, the pulse periods are short, and this might be due to compressional tectonic environment and thrust type focal mechanism. This particular aspect needs further study when more near-fault strong motion data becomes available.

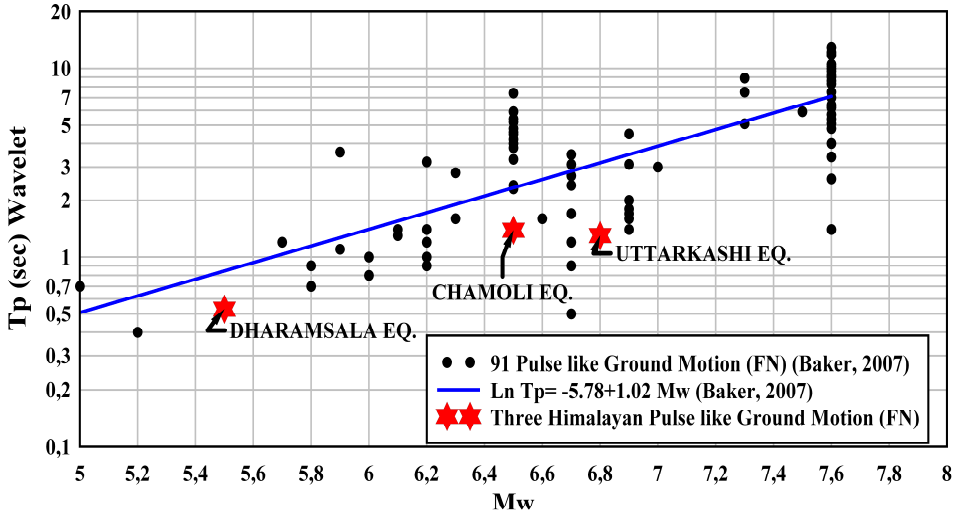

Fig. 3.13 Pulse periods verses earthquake magnitude for pulse like ground motions.

Table 3.11 Pulse period comparison of three Himalayan earthquakes at three sites, estimated using wavelet analysis and various relationships.

Earthquakes	Station Code	Mw	WA (sec)	Tv-p (sec)	SOM (1998) (sec)	MOD (1999) (sec)	ALAVI (2000) (sec)	SOM(R) (2003) (sec)	SOM (S) (2003) (sec)	BRAY (2004) (sec)	BAKR (2007) (sec)	SFG (2010) (sec)
Dharamsala	**SHAH**	5.5	0.53	0.40	0.69	0.56	0.88	0.38	0.76	0.49	0.84	0.86
Uttarkashi	**BHAT**	6.8	1.30	1.30	2.45	2.51	2.23	1.7	2.15	1.89	3.18	3.16
Chamoli	**GOPE**	6.5	1.39	1.28	1.83	1.78	1.8	1.2	1.69	1.38	2.34	2.34

The velocity time history of the near fault ground motion contains large amplitude, long period velocity pulses. The peak amplitudes of theses pulses depend on the magnitude, distance, and site conditions. Relationships between logarithm of peak horizontal velocity, magnitude, and the logarithm of distance have been developed adopting different data sets (Somerville,1998; Alavi and Krawinkler, 2000; Rodrigues-Marek, 2000; and, Bray and Marek, 2004). The comparison of computed fault-normal peak horizontal velocity due to three Himalayan earthquakes at three sites, with those estimated using these relationships, are shown in **Table 3.12**. No relationship seems to be applicable for the Himalayan region to predict the peak amplitudes of the velocity pulses.

Table 3.12 Comparison of computed fault-normal peak horizontal velocity due to three Himalayan earthquakes at three sites with those estimated using various relationships.

Earthquakes	Station Code	Mw	R (km)	Marek (2000) cm/sec	Somer. (1998) cm/sec	Alavi (2000) cm/sec	Bray & Marek (2004) cm/sec	Velocity (FN) cm/sec
Dharamsala	SHAH	5.5	11	23.91	16.71	9.43	31.58	15.9
Uttarkashi	BHAT	6.8	22	29.02	55.26	52.69	28.25	31.7
Chamoli	GOPE	6.5	13	34.84	48.55	41.99	38.51	42.2

3.7 Comparison of Near-Fault Response Spectra with Indian Seismic Codal Spectra (IS 1893: 2002, Part 1)

Figure 3.14 shows a comparison of the accleration response spectra obtained from three near-fault, fault-normal components, due to three moderate-sized Himalayan earthquakes, with the response spectra estimated from IS 1893: 2002. It is evident from the figure that spectral amplitudes are increasing at all the periods with increasing magnitudes, and show peaks in their elastic response spectra due to near-fault pulses in the time history. The comparison of the spectra of the three near-fault ground motions have brought out that spectral amplitude for smaller earthquakes may become more pronounced at smaller and intermediate periods as observed at Shapur station during the 1986 Dharamsala earthquake (Mw=5.5). The spectral-amplitudes of near-fault ground motion recorded at Shapur station are by and large compatibile with IS code spectra in the period range of 0.1 sec to 0.5 sec, barring one peak at 0.16 sec with

a spectral value of 2.91. However, as the period increases beyond 0.5 sec, the spectral values are low compared to the codal spectral values.

The spectral values of fault-normal component at Bhatwari station due to the Uttarkashi earthquake, are much higher than the codal spectral values at intermediate and long periods upto 2 sec. As a consequence of this, the response of structures designed in the elastic range using IS code may not remain in the elastic range. Therefore, the structures are likely to experience non-linear deformations and resulting damages. The spectral values of fault-normal component at Gopeshwar station due to Chamoli earthquake are lower than the codal values upto 0.4 sec and there after the spectral values increase upto 1.7 sec, with a hump at 0.8 sec which shows the effect of the long period component in the time history.

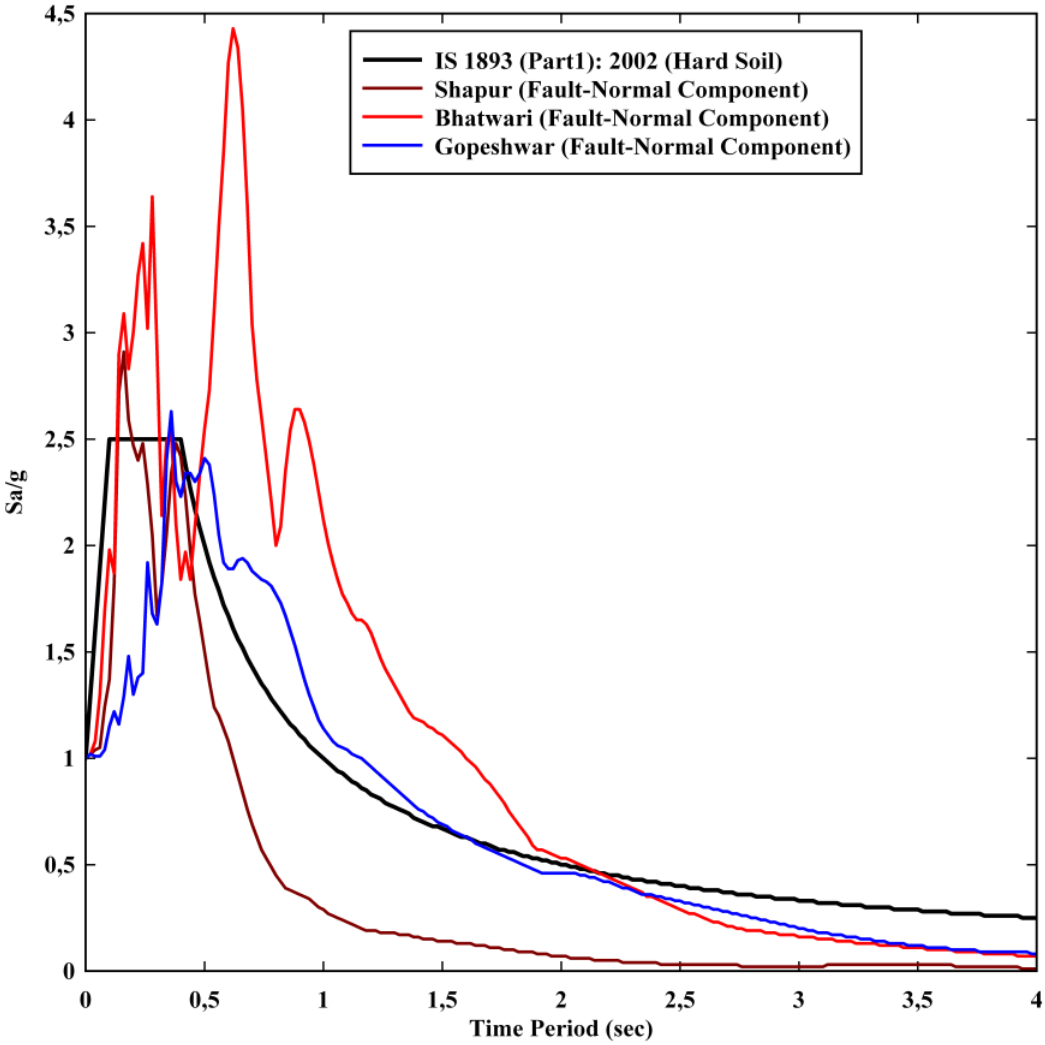

Figure 3.14 Acceleration spectra for three near-fault fault-normal components and IS codal spectra.

The characteristics of the near-fault ground motion have been more clearly revealed in the velocity spectra as shown in **Figures 3.15 and 3.16**. **Figure 3.15** shows the comparison of velocity spectra of the fault-normal components of ground motion at Shapur and Gopeshwar stations with codal velocity spectra, whereas, the comparison of velocity spectra of fault-normal component at Bhatwari station with codal velocity spectra is shown in **Figure 3.16**. According to Indian code (IS 1893: 2002) the Shapur and Gopeshwar stations are located in zone V, whereas Bhatwari station falls in zone IV; all three stations are on hard soil.

A comparison of velocity spectra at Shapur station with codal spectra has demonstrated that the buildings designed according to Indian seismic code are much safer than the threshold minimum, and near-fault pulse type ground motion produced due to small earthquakes (Mw~5.5) is of little consequence. The comparison of the velocity spectra of fault-normal component at Gopeshwar station with codal spectra has brought out that spectral values are on much higher side than the codal spectral values in the long period ranging from 0.6 sec to 2.3 sec. This contrasting observation is due to higher PGA/PGV ratio at Gopeshwar station compared to Shapur station and is related to the size of the earthquake. Velocity spectra of fault-normal component at Bhatwari station show higher spectral values at long periods from 0.5 sec to 3.1 sec compared to codal spectral values. This finding is in agreement with the one at Gopeshwar station and can be attributed to the presence of a long period pulse in the velocity time history.

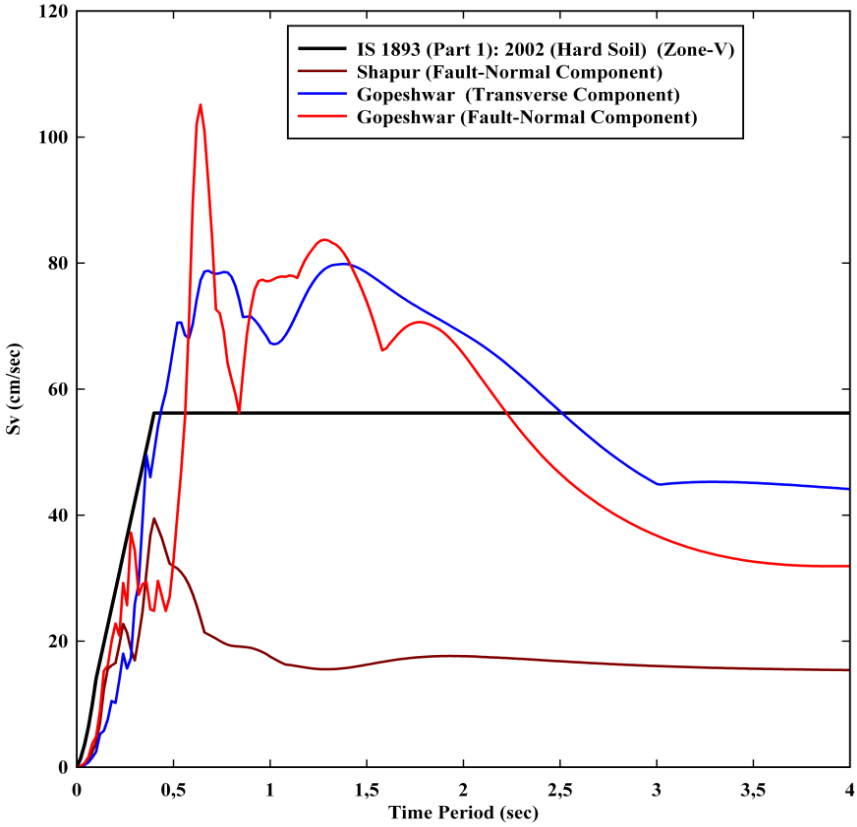

Figure 3.15 Velocity spectra for FN-components and recorded transverse components at Shapur and Gopeshwar stations with IS codal spectra.

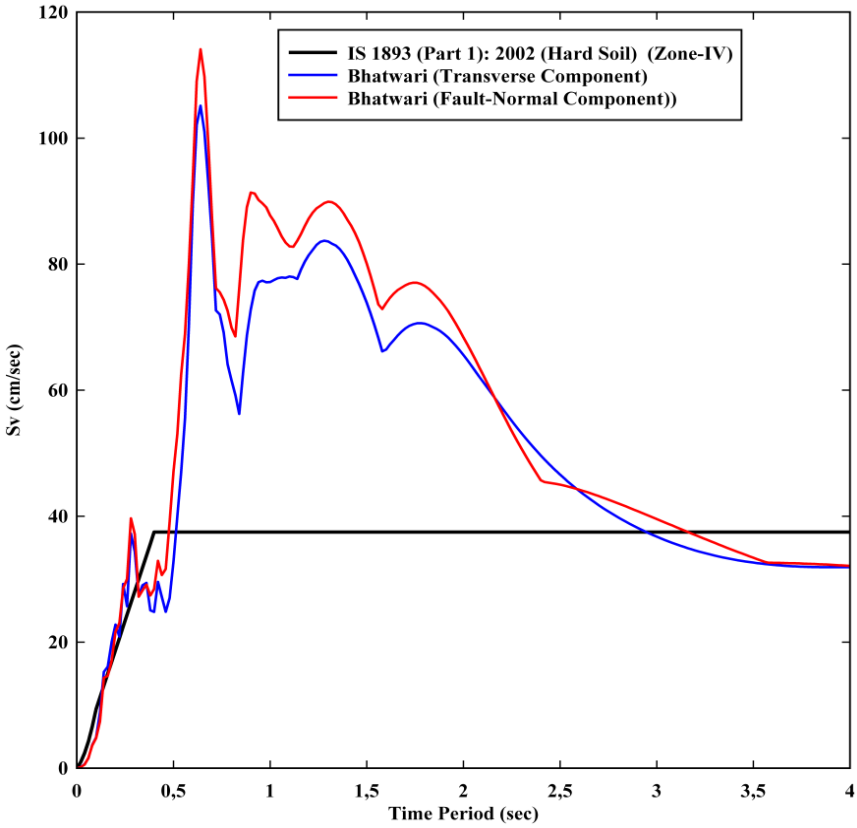

Figure 3.16 Velocity spectra for FN-components and recorded transverse component at Bhatwari station with IS codal spectra.

Malhotra (1999) emphasized that for both ordinary ground motion and pulse-like ground motions, the peak values of ground acceleration, velocity and displacement are the most important response parameters. However, he demonstrated that for near-fault pulse type ground motion the width of acceleration sensitive region increases in a tripartite plot due to high PGV/PGA ratio. To verify this observation, the tripartite plots of the 5% damped elastic response spectra of recorded fault-normal components of ground motions at Shapur and Gopeshwar stations have been compared with codal response spectra for zone V (Hard Soil) as shown in **Figure 3.17**. Similarly, the fault-normal component at Bhatwari station has been compared with codal response spectra for zone IV (Hard Soil) as depicted in **Figure 3.17**. In these plots, the natural period T is along the horizontal axis, pseudo-spectral velocity along the vertical axis, pseudo spectral acceleration along the -45^{o} axis, and the spectral displacement along the +45^{o} axis.

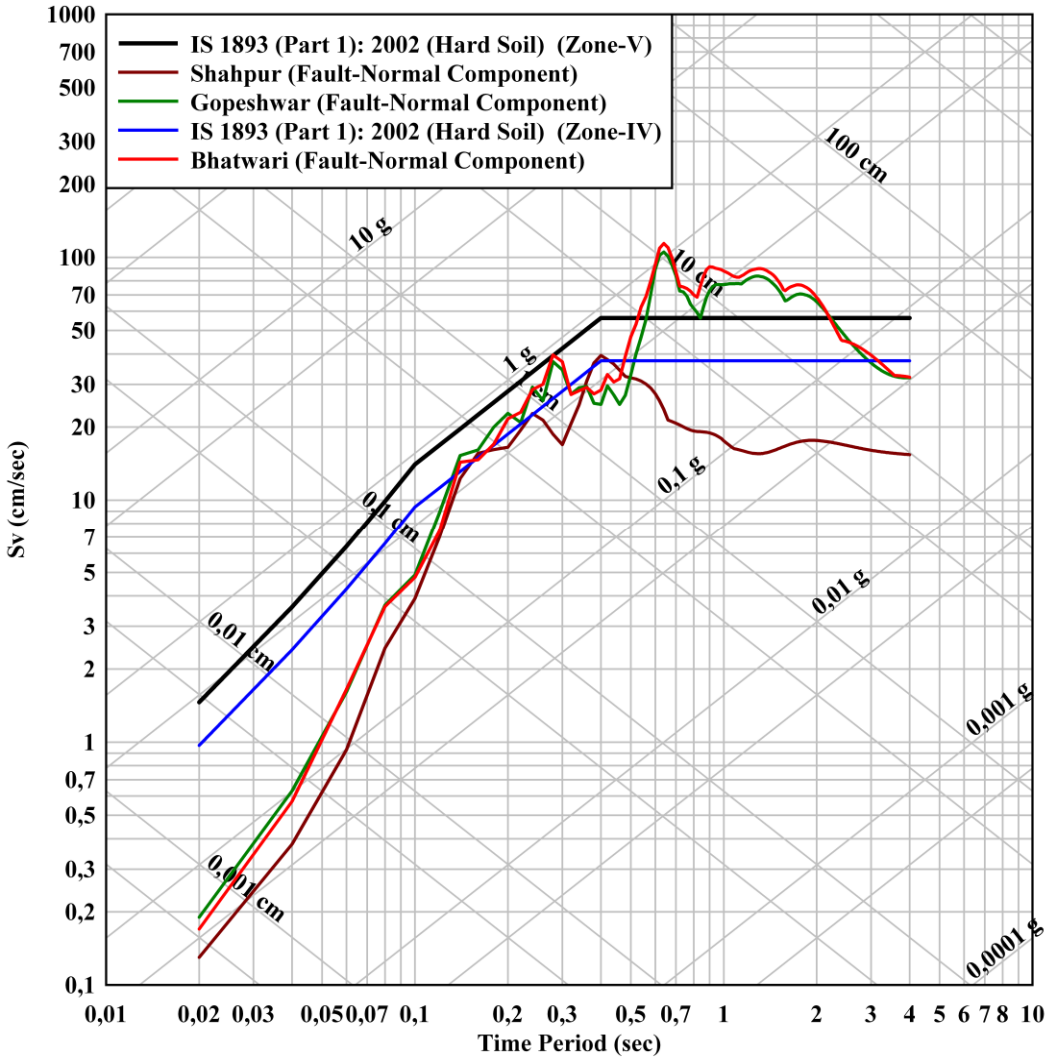

Figure 3.17 Tripartite plot of 5 % damped for fault-normal components at Shapur, Gopeshwar and Bhatwari stations along with IS codal spectra.

It is well known that the spectral amplitudes at short periods are sensitive to the values of PGA, whereas, those at long periods are sensitive to the values of PGD. In the intermediate range of periods, the spectra amplitudes are sensitive to the values of PGV. Further, high frequencies in the ground motion control the values of PGA, as well as the response of short-period systems; low frequencies on the other hand, control the values of PGD and the response of long-period structures. The frequencies confined to the intermediate range control the value of PGV and govern the response of structures falling in this period range.

In the tripartite plot, the middle region having constant pseudo spectral velocity signifies the velocity-sensitive region, whereas, the regions to the left and right of this are known as the acceleration-sensitive and displacement-sensitive regions, respectively. The values of PGA, PGV, and PGD control the spectral amplitudes in these three regions, while the widths of these regions depend on the ratios between PGA, PGV, and PGD. A higher value of the PGV/PGA ratio leads to a wider acceleration-sensitive region, whereas a lower PGD/PGV ratio leads to a wider displacement-sensitive region. **Table 3.13** shows the comparison of widths of the acceleration sensitive regions obtained from plotting of PGA and PGV of three near-fault ground motions on tripartite graph with those obtained from codal values for hard soil (IS 1893: 2002, Part 1).

Table 3.13 Acceleration-sensitive region width of three near-fault FN-components.

Earthquakes	Station	Mw	PGA (g)	PGV (cm/sec)	PGV/PGA (sec)	Width of acceleration sensitive region (sec)
Dharamsala	Shapur	5.5	0.248	14.3	0.06	0.35
Uttarkashi	Bhatwari	6.8	0.253	31.8	0.13	0.65
Chamoli	Gopeshwar	6.5	0.343	43.3	0.13	0.53

The values listed in **Table 3.13** show that for ground motion at Shapur station due to the Dharamsala earthquake, the acceleration-sensitive region extends up to 0.35 sec which is slightly lower than that the codal value of 0.40 sec. Considering the FN components, the acceleration-sensetive regions for the Uttarkashi and Chamoli earthquakes at Bhatwari and Gopeshwar stations extend up to 0.65 sec and 0.53 sec, respectively. These values are higher than the codal value of 0.40 sec. These widenings of acceleration-sensitive regions for the Uttarkashi and Chamoli earthquakes are due to the higher PGV/PGA ratios for these two ground motions. Examination of the velocity-sensitive regions in the tripartite plots indicates that at the Bhatwari and Gopeshwar stations, the spectral amplitudes are higher than the codal spectral amplitudes as shown in **Figure 3.17**. However, at Shapur station, the spectral

amplitudes are lower compared to the codal spectral amplitudes. In a nutshell, the acceleration-sensitive regions of NFGMs for the Uttarkashi and Chamoli earthquakes are wider than the acceleration-sensitive region given by the IS code. Current IS code does not have a provision to include the effect of NFGMs. In view of this, there is a need to revise the design spectra given in the IS code to incorporate the effect of NFGMs for sites located in the vicinity of seismically active faults.

3.7 Concluding Remarks

For the three Himalayan earthquakes, Daubechies mother wavelets of order four (db4) and seven (db7) are found to be more efficient in extracting the pulse-type characteristics from the near-fault strong ground motion recordings. However, the spectra of long-period pulses extracted using Daubechies mother wavelet of order seven (db7) are closer to the long-period spectral amplitudes of the FN components of ground motions at three sites. For the Dharamshala earthquake, FN component of ground motion at Shapur station showed pulse-type ground motion with the pulse-period (Tp) 0.52 sec and pulse-indicator (PI) 0.94. For the Uttarkashi and Chamoli earthquakes, computed FN components at Bhatwari and Gopeshwar stations showed pulse-type ground motion in their velocity time-histories. At Bhatwari and Gopeshwar stations the pulse-periods of FN components are 1.30 sec and 1.39 sec respectively.

A comparison of velocity spectra at Shapur station with codal spectra has demonstrated that the buildings designed according to the IS code are safe, and that the near-fault pulse-type ground motion produced due to small earthquakes (M_w~5.5) is of little consequence. The spectral values of FN component at Bhatwari station due to the Uttarkashi earthquake are much higher than the codal spectral values at intermediate and long periods. The spectral values of FN component at Gopeshwar station due to the Chamoli earthquake are lower than the codal values by upto 0.4 sec, and then the spectral values increase upto 1.7 sec, with a hump at 0.8 sec which shows the effect of long-period component in the time-history. As a consequence of this, the response of structures and buildings with fundamental period above 0.4 sec designed using the IS code may not remain in the elastic range, and are likely to experience non-linear deformations and resulting damages.

At Shapur station the width of the acceleration-sensitive region is slightly less compared to the IS code and the spectral amplitudes are lower compared to the codal spectral amplitudes. This is attributed to small size of the Dharamshala earthquake compared to the Uttarkashi and

Chamoli earthquakes. In a nutshell, the acceleration-sensitive regions due to near-fault ground motions of the Uttarkashi and Chamoli earthquakes have higher width than that given by the IS code. Because of this, the structures designed to be flexible in the intermediate-period and long-period range will behave as stiff structures, and subjected to increased base shear. Current IS code (IS: 1893 (Part1): 2002) does not account for this widening of the acceleration-sensitive region which occurs due to the effect of NFGM. This aspect should be incorporated in the IS code for designing structures located in the vicinity of seismically active faults in the Himalayan region.

Spectral characteristics of near-fault pulse-type ground motions due to the Uttarkashi and Chamoli earthquakes have illustrated that the IS code is deficient in addressing the long-period near-fault ground motions, particulary for the Himalayan regions. Therefore, the IS code needs modification, and the effect of NFGM in terms of increasing spectral amplitudes towards long-periods should be incorporated in the design spectrum. Because of lack of sufficient number of near-fault recordings, the present study is unable to recommmend a specific design spectra for near-fault sites. In the future when sufficient data shall be available, it may be possible to arrive at a specific NFGM design spectra.

For the three Himalayan earthquakes, the comparison of estimated pulse-periods with the world-wide data set (Baker 2007) of ninety-one pulse-type ground motions show that the limited data set for the Himalayan earthquakes conforms with the world-wide data set. The estimated pulse-periods (Tp and Tv-p) of these three earthquakes fall within the range of computed pulse-periods obtained adopting various available worldwide relations of NFGM velocity pulse. An important outcome of the study for the Himalayan earthquakes is that the observed pulse-periods are short and this might be ascribed to compressional tectonic environment and thrust type focal mechanism. The computed values of the peak horizontal velocity (FN component) from the available relationships showed lots of variance with those observed in the present study. These aspects needs further study when more near-fault strong motion data become available.

CHAPTER 4

ESTIMATION OF GROUND MOTION INCLUDING NEAR-FAULT FACTOR FOR SHAPUR, BHATWARI AND GOPESHWAR SITES

4.1 Introduction

In chapter 3 the pulse-type ground motion characteristics of three moderate Himalayan earthquakes that occurred in the states of Uttarakhand and Himachal Pradesh have been described. The IS code (IS 1893: 2001 (Part 1)) is silent on the aspect of pulse-type ground motion in the dynamic analysis of structures. Further, the IS code suggests that based on the study of regional and local geology, tectonics around the site, and seismotectonic setup of the area, the site-specific design acceleration spectra should be developed and used in place of the standard design response spectra according to IS code. It is suggested by Division of Engineering Services Geotechnical Services, Caltrans, 2012 that the site-specific spectra should be modified for the near-fault sites. Based on these considerations, in this chapter, the site-specific design acceleration spectra at three sites incorporating the NFGM factor is developed adopting deterministic approach. This effort includes the computation of peak ground accelerations, and spectral accelerations (5% damping) at spectral periods between 0.01 sec and 4.0 sec with the inclusion of near-fault factor in the spectral shapes. From the estimated site-specific spectra the compatible time histories for the three sites are generated. The estimated response spectra and generated time histories have been used in the dynamic analysis of hillslope buildings.

4.2 Geology and Seismotectonics around the Three Sites

The broad geological framework and tectonic features mapped in the region around three sites are given in the **Figure 4.1** (GSI, 2000). The 1986 Dharamshala earthquake with epicenter at 32.15^{O} Lat. and 76.40^{O} Long., was a moderate shallow-focus earthquake (mb = 5.5; Focal depth = 7 km). The reported epicenter of the earthquake falls in the Sub Himalaya to the south of the Main Boundary Thrust (MBT). The Shapur site is located almost in the southern fringe of the Himalayan belt. The geological formations around this site can be broadly divided into two types: a) to the northeast the rocks mainly belong to the Himalayan orogenic belt, and b) to the southwest, the area is covered by the Quaternary alluvial deposits (stiff soil) of the Indo-Gangetic plains. In the immediate vicinity of the site the rock-types primarily belong to Siwalik

sequence. These rocks are sedimentary in character and mainly composed of sandstones, shales and limestones. On the local scale the geology and tectonics of the area has been studied by many investigators (e.g., Thakur, 1998; Naresh et al. 2013). Recently, Naresh et al (2013) has examined the characteristics of local seismicity of the Kangra-Chamba region which encompasses the site. One of the distinctive characteristic of this area is the presence of Chamba nappe. To the northeast between the MBT and the MCT, the part of the Himalaya is designated as the Lesser Himalaya. The rocks types of the Lesser Himalaya are poorly metamorphosed and are composed of phyllites, slates and lime-stone called the Panjal Imbricate Zone (PIZ). To the northeast of the Lesser Himalaya is the Higher Himalaya which is mainly composed of crystalline rocks. Further, to the northeast of the Higher Himalaya is the Tethys Himalaya. The boundary between the Higher Himalaya and Tethys Himalaya is called Southern Tibet Detachment (STD). The boundary between the Lesser Himalaya and the Higher Himalaya is known as MCT. It is found that the weakly metamorphosed rocks of Chamba nappe are similar to rocks of Tethys Himalaya sequence (e.g. Thakur, 1998) and these are resting on the rocks of Higher Himalaya. Because of southward transgression, the Lesser Himalayan belt pinches out in this part, and the MCT is identified with the Panjal thrust. Extension of Chamba nappe to the south is a matter of debate. One school of thought says that Chamba thrust marks the southern boundary of Chamba nappe whereas Rautela and Thakur (1992) postulated that Chamba nappe extends upto Panjal thrust/MBT.

The focal mechanism of the 1986 Dharamshala earthquake was mainly thrust faulting and faulting had occurred on a shallow dipping low-angle thrust fault striking at an angle of 299^{O} with dip $N60^{O}W$. The plunge and azimuth of the P-axis was 28^{O} and 35^{O} respectively.

The epicenter of the 1905 Kangra earthquake (Ms = 8.6) lies about 25 km northwest to the epicenter of the 1986 Dharamshala earthquake. Naresh et al (2013) investigated the seismicity pattern from the distribution of hypocenters of 159 local earthquakes, and mapped 3 different source regions in the source zone of the 1905 Kangra earthquake. The local seismicity occurring at different depth-levels shows different types of focal mechanism. The events associated with the low magnitude seismicity, occurring in the upper 8-10 km of the crust, show both reverse faulting and normal faulting. The reverse faulting occurs along Chamba/Panjal/MCT and because of this Chamba nappe slides towards southwest. Whereas, the normal faulting events occuring along the Chamba normal fault. At intermediate depths from 8 to 15 km the seismicity shows thrust faulting which results because of slip along the

detachment or lower part of the MBT. Below the plane of detachment, the earthquakes show normal faulting that occurred because of complex interplay of regional stresses with secondary stresses in local northeast-southwest trending structures.

The Bhatwari site falls in the crystalline complex just to the north of the MCT. The rocks of the crystalline complex are mainly composed of gneisses and granites. To the southwest of the site are the rocks that comprise Inner Lesser Himalaya (ILH). The ILH lies between the North Almora Thrust (NAT) and the MCT. The rocks of ILH are of low and high grade metamorphic rocks which primarily constitutes schist, phyllities, quartzites and limestones. These rocks are affected by compressive tectonic forces because of Himalaya orogeny. From the seismological considerations the site falls in a zone of moderate earthquakes. This zone is 50 km wide which has been identified in the vicinity of MCT. The zone is called as Main Himalayan seismic belt (Ni and Barazangi, 1984; Mukhopadhaya and Kayal, 2003). Most of the moderate earthquakes in this zone are confined to shallow depths between 10 and 20 km. The Indian plate is under-thrusting the Eurasian plate along a low angle thrust plane, known as detachment surface. This is also called the Main Himalayan Thrust (MHT). The depth of the MHT has been estimated between 17 and 20 km near the MCT (Ni and Barazangi, 1981; P.Mahesh, 2012). It is suggested that below the MCT lies the basement thrust zone. The transition zone between the plane of detachment and basement thrust acts as a geometrical asperity (Pandey et al. 1995). Recently, Caldwell et al. (2013) mapped the geometry of the MHT in the Garhwal Himalaya adopting common conversion point (CCP) stacking technique. The seismic images brought out that the MHT has a flat-ramp-flat type structure. The upper flat is located at a depth of 10 km below the sea level and dip 2^{O} toward north, and this connects to a mid crustal ramp and the ramp dips at 16^{O}. The lower flat is 20-25 km below sea level and dips at 4^{O} toward north. For the 1991 Uttarkashi earthquake, two fault plane solutions are given (Atlas, 2000). According to the HRV solution the earthquake occurred at a shallow dipping 14^{O} and striking 317^{O}. The P-Axis has 207^{O} azimuth and plunge 32^{O}. According to second solution, the earthquake occurred on a shallow dipping fault with 26^{O} dip and 349^{O} striking. The azimuth and plunge of P-Axis is 210^{O} and 30^{O} respectively. The direction of pressure axis is almost same in both the solutions. The compressional forces are acting $N30^{O}E$ which is in the direction of the tectonic motion of the Indian plate. Gopeshwar station is located to the south of the MCT, and the 1999 Chamoli earthquake epicenter lies very close and about 13 km to the east of Gopeshwar station. The site is located in the ILH and comprises of low and high grade metamorphic rocks.

4.3 Identification and Estimation of Seismotectonic Sources around the Sites

Seismotectonic sources are those seismically active geological structures which can produce earthquakes of different sizes and types. From the point of view of mathematical modeling these sources can be modeled as point, line, area or volumes, depending upon the type of source chosen and our ability to define it in the geological space (**Reiter, 1990**). For the estimation of ground motion parameters, at a particular site or for region, the first step is to identify the seismotectonic sources. Based on regional seismicity and tectonic setting around the sites under study, seismotectonic sources in terms of active faults (linear) have been identified, which are within a radius of 30 km from the three selected sites. For this purpose the seismotectonic maps of the study region given in the seismotectonic atlas are utilized (GSI 2000). The identified seismotectonic sources (active faults) at three sites are listed in **Table 4.1** and are shown in **Figure 4.1.**

Table 4.1 Identified seismotectonic sources within a radius of 30 km from each site.

Site	Seismotectonic Source	Type of Seismotectonic source
Shapur	Main Boundary Thrust (MBT)	Neotectonic Thrust Fault
	Drang Thrust (DT)	Thrust Fault
	Jwala Mukhi Thrust (JMT)	Neotectonic Thrust Fault
	Vaikrita Thrust (VT)	Thrust Fault
Bhatwari	Main Central Thrust (MCT)	Thrust Fault
Gopeshwar	Main Central Thrust (MCT)	Thrust Fault
	Alaknanda Fault (AF)	Neotectonic Fault
	Thrust Fault-1 (TF1)	Thrust Fault
	Ramgarh Thrust (RT)	Thrust Fault
	North Almora Thrust (NAT)	Thrust Fault

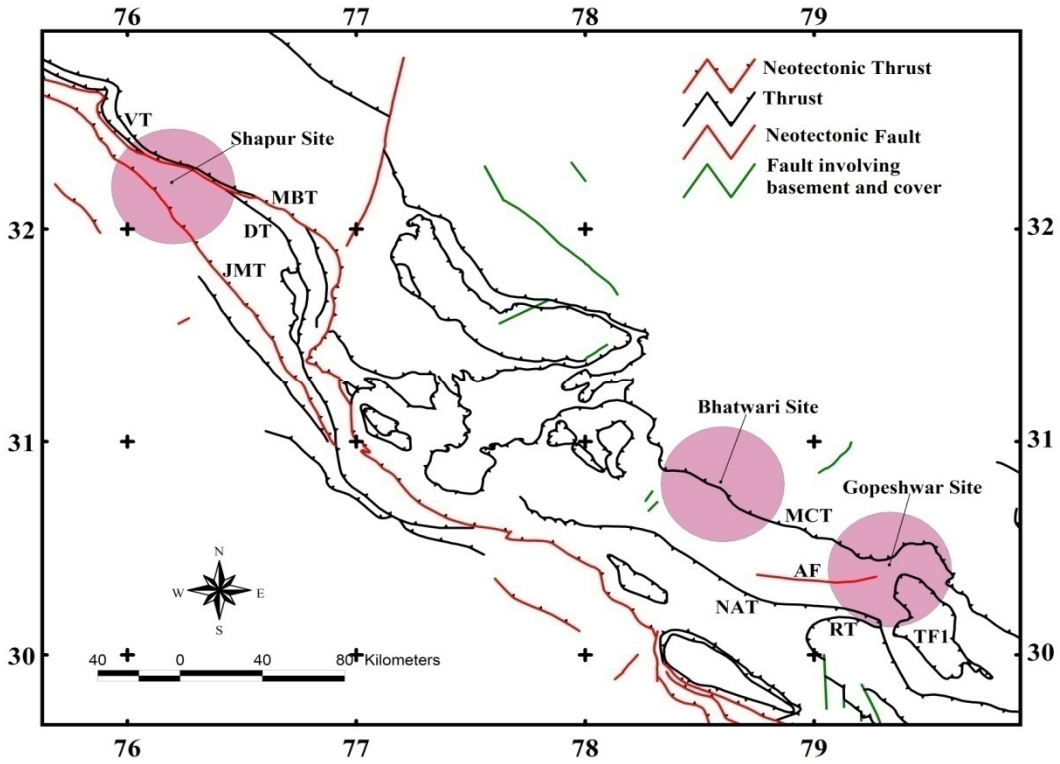

Figure 4.1 Identified seismotectonic sources (active faults) within a radius of 30 km from the Shapur, Bhatwari, and Gopeshwar sites.

4.3.1 Estimation of Maximum Magnitude of Sources and Rupture Width

First step in deterministic approach is to estimate the seismic potential of a seismotectonic source. The seismic potential normally estimated in terms of maximum magnitude (M_{max}) that an active fault or seismotectonic source can produce. The commonly accepted procedures for determining this maximum magnitude are either to assign the observed maximum magnitude of a seismotectonic source from the earthquake catalog or to determine it using empirical correlations between key fault parameters, namely, fault rupture length, fault displacement and fault area, and magnitude. In this study for determining the maximum magnitude for each active fault, the concept of fault surface rupture length has been utilized, because it is a reasonable approach adopted by many investigators. To apply the method, the fault lengths of the faults (**Table 4.1**) are measured from the seismotectonic atlas. The measurements were accomplished by digitizing the identified faults using **Arc Info GIS** software. The measured lengths are given in the **Table 4.2**.

On the empirical basis using world wide data it is suggested that 1/3 to 1/2 of the total length of fault would rupture producing the maximum earthquake (Mark, 1977). Using the criteria of 1/3 of the length of the fault likely to rupture is estimated (**Table 4.2**). Adopting the following

relations (equations 4.1, 4.2 and 4.3) between the surface rupture length (L) and moment magnitude (M_w) for earthquake with strike slip, reverse, and normal fault type focal mechanism (**Wells and Coppersmith, 1994**.), Mw for each seismotectonic source is computed.

$M_w = 5.16 + 1.12\log L$ - (4.1)

$M_w = 5.00 + 1.22\log L$ - (4.2)

$M_w = 4.86 + 1.32\log L$ - (4.3)

From the estimated M_w, the rupture width (RW) for each seismotectonic source is computed from the following relation (equation 4.4) given by **Wells and Coppersmith, 1994.**

$\text{Log (RW)} = -1.01 + 0.32M_w$ - (4.4)

Because most of the recent moderate-sized earthquakes in the Himalaya have occurred at shallow-depths with low angle reverse-faulting, the dip angle (α) is taken as 15° for thrust type seismotectonic sources. Adopting the above relationships, the maximum magnitude and rupture width for various seismotectonic sources have been computed and are listed in **Table 4.2.**

Table 4.2 Fault lengths, rupture length, maximum moment magnitude (M_w), and rupture widths of seismotectonic sources.

Seismotectonic Source	Fault Length (Lo) (km)	Rupture Length (L) (km)	M_w	Rupture Width (RW) (km)
Alaknanada Fault (AF)	51	17	6.5	12
Drang Thrust (DT)	231	77	7.3	21
Jwala Mukhi Thrust (JMT)	289	96	7.4	23
Main Boundary Thrust (MBT)	525	175	7.7	29
Main Central Thrust (MCT)	645	215	7.8	32
Ramgarh Thrust (RT)	192	64	7.2	20
Thrust Fault-1 (TF1)	172	57	7.1	19
Vaikrita Thrust (VT)	215	72	7.3	21
North Almora Thrust (NAT)	230	77	7.3	21

As is evident from the **Table 4.2**, the estimated maximum moment magnitude (M_w) for various seismotectonic sources ranges from 6.5 to 7.8.

4.4 Attenuation Model Used

The ground-motion characteristics are a function of the earthquake source, properties of the medium through which waves propagate (attenuation), and site characteristics (site effects). The most commonly used method to represent the ground motion is through attenuation relations also called ground-motion models (Bolt and Abrahanson, 2003). In these models the effects of the earthquake source, wave propagation, and site response are represented by the magnitude (size of an earthquake), and fault-type or focal mechanism (e.g., strike-slip, reverse, thrust, and normal fault); source-to-site distance (e.g., point-source or finite-source distances), and site conditions (e.g., rock, stiff-soil, and soft-soil). Recently, additional parameters (e.g., tectonic environments, direction of rupture propagation, focal depth, hanging-wall effect, and soil depth.) are also used to parameterize the strong ground motion (Bolt and Abrahanson, 2003).

In the language of mathematics the attenuation model represent a relation between strong ground motion parameter (e.g., PGA, PGV, PGD, and PSA) to parameters of earthquake, path, and site. General attenuation model is represented as (Cambell, 2003).

$$Y = c_1 e^{c2M} R^{-c3} e^{-c4r} e^{c5F} e^{c6S} e^{\varepsilon} \quad \text{or} \quad \ln(Y) = c_1 + c_2 M - c_3 \ln R - c_4 r + c_5 F + c_6 S + \varepsilon \qquad -(4.5)$$

In the above equation 4.2, **Y** is the strong motion parameter of interest, **M** is magnitude of earthquake, **r** is the source to site distance, **F** is a parameter characterizing the type of faulting, **S** is a parameter characterizing the type of local site conditions, **ε** is a random error term with zero mean and standard deviation equal to standard errors of estimate in ln(Y). **R** is a distance term normally expressed using following relation (equation 4.6):

$$R = r + c_7 \exp(c_8 M) \qquad \text{or} \qquad R = (r^2 + [c_7 + \exp(c_8 M)]^2)^{0.5} \qquad -(4.6)$$

Coefficients c_3, c_7, c_8 are the functions of R and M. (Campbell, 2003).

In last more than fifty years a large number of attenuation relations have been developed and used in the engineering practice. The earlier relations were simple in character, but with time as the knowledge advanced and more data from strong recordings became available, more and more parameters were included in representing the strong ground motion.

Since early 1960s, the most widely used parameter to represent strong ground motion (SGM) was the peak horizontal ground acceleration. As the knowledge progresses, it was realized that response of the structure is better represented by a response spectrum. In view of this most of the modern attenuation relations include relations for response spectral accelerations as well as for peak acceleration. The selection of an attenuation model to be fitted to a specific strong motion data set is guided by the quality and quantity of the data set. Large numbers of attenuation relations are available in the literature and a comprehensive review has been given by Cambell (1985), Boore at al. (1997) and Douglas (2011).

4.4.1 New Generation Attenuation (NGA) Relationships

The NGA models currently in use for seismic hazard assessments, and are based on very large database of thousands of strong-motion records. These records were compiled from crustal earthquakes occurring at shallow depths in active tectonic environments. These NGA relations have been incorporated into most of the recent national seismic hazard maps published by the U.S. Geological Survey (Petersen and others, 2008). Comprehensive description on various aspects of NGA models is given by Power et al (2008) and Kaklamanos et al (2011). The project was coordinated by the Lifelines Program of the Pacific Earthquake Engineering Research Center (PEER), in partnership with the U.S. Geological Survey and the Southern California Earthquake Center. Five ground-motion prediction equations (GMPEs) developed during the NGA project, include: Abrahamson and Silva (2008), Boore and Atkinson (2008), Campbell and Bozorgnia (2008), Chiou and Youngs (2008a), and Idriss (2008). Because the model of Idriss (2008) does not explicitly include site response, and because the other four models include site response; using the same variable to describe the site condition (V_{S30}); the model given by Idriss (2008) could not be implemented. A summary of the input parameters used in the four GMPEs is presented in **Table 4.3**.

Table 4.3 Input parameters of the NGA models (Kaklamanos and Baise, 2011).

	Model			
Parameter	**AS08**	**BA08**	**CB08**	**CY08**
Source Parameters:				
Moment magnitude, M_W	*	*	*	*
Depth to top of rupture, Z_{TOR}	*		*	*
Down-dip rupture width, RW	*			
Fault dip, δ	*		*	*
Style-of-faulting flag (function of rake angle, λ)	*	*	*	*
Aftershock flag	*			*
Path Parameters:				
Closest distance to the rupture plane (rupture distance), R_{RUP}	*		*	*
Horizontal distance to the surface projection of the rupture (Joyner-Boore distance), R_{JB}	*	*	*	*
Horizontal distance to top edge of rupture measured perpendicular to the strike (site coordinate), R_X	*			*
Hanging wall flag	*			*
Site Parameters:				
Time-averaged shear wave velocity over the top 30 meters of the subsurface, V_{S30}	*	*	*	*
Depth to V_S = 1.0 km/s ($Z_{1.0}$)	*			*
Depth to V_S = 2.5 km/s ($Z_{2.5}$)			*	
PGA (or Sa) on rock, as baseline for nonlinear site response	*	*	*	*

Ground-motion prediction (NGA) relation given by Boore and Atkinson (2008) allows the estimation of average horizontal-component ground motion as a function of four main parameters, viz., earthquake magnitude, distance from source to site, local average shear-wave velocity, and fault type. The equations are given to obtain PGA, PGV, and PSA (5%) at periods between 0.01 s and 10 s. In terms of parameters involved the Boore and Atkinson (2008) model is simple compared to other NGA models, and is easier to implement in many applications (Sinha and others, 2012, 2014). In view of these considerations, this attenuation model has been adopted in the present study to estimate the ground motion. The equation governing the model is given as:

$$\ln(Y) = F_{\mathbf{M}}(M_{\mathbf{W}}) + F_{\mathbf{D}}(R_{\mathbf{JB}}, M_{\mathbf{W}}) + F_{\mathbf{S}}(V_{\mathbf{S30}}, R_{\mathbf{JB}}, M_{\mathbf{W}}) \qquad -(4.7)$$

In the above equation 4.7, Y represents the strong motion parameter (response variable) and F_M, F_D, and F_S functions that represent the magnitude scaling, distance scaling, and site

amplification, respectively. M_W is moment magnitude, R_{JB} is the Joyner-Boore distance, and V_{S30} is the average shear-wave velocity from the surface up to a depth of 30 m.

The ground-motion prediction equations developed by Boore and Atkinson (2008) are based on a data-set of 1574 records from 58 earthquakes. These earthquakes fall in magnitude (Mw), ranging between 5 and 8, and $R_{JB} \leq 200$ km and focal depths between 2 and 31km with most of the earthquakes has depth less than 20km. these equations are believed to be applicable for shear wave velocity (V_{S30}) between 180 and 1300m/s. Three earthquakes namely, 1987 Whittier Narrows, 1994 Northridge, and 1999 Chi-Chi, contributed 7%, 10% and 24% of the strong motion recordings. The authors excluded the aftershock recordings because the spectral scaling of strong motion due to aftershocks is thought to be different than the main shocks. Further, earthquakes with single recording were also excluded from the data-set. For small earthquakes, the data-set lacked recordings at close distances from source. This model did not include some of the factors of strong ground motion, such as: depth-to-top of rupture, hanging wall/footwall or basin depth because residual analysis did not improve the predictive capabilities of model on an average.

4.4.2 Source to Site Distance

Several types of source to site distances are taken into account to characterize the decrease in ground motion as it propagates from the earthquake source to the site. Distance measures can be grouped into two broad categories depending upon whether they treat earthquake source as point source (point source measure) or as a finite source (finite sources measures) (Cambell, 2003). A brief account of distance measures commonly used in attenuation modeling is as follows:

i) Point Source Distance Measures: Two types of point source distance measures are adopted in strong motion prediction models. These are: distance from the epicenter to the site (epicentral distance, r_{epi}) and distance from the hypocenter to the site (hypocentral distance, rhypo). These distances are mainly used for small earthquakes because small earthquakes can be represented by point sources. For large earthquakes r_{epi} and r_{hypo} are poor measure of distance. Point-source distance measures can be only used for large earthquakes when fault rupture plane cannot be identified for past or future earthquakes. It is suggested that

attenuation relations developed using point source distances should not be used to estimate the strong ground motion parameters for large earthquakes (Campbell, 2003).

ii) Finite Source Distance Measures: Three types of distance measures have been used as finite source distance measures. These are shown in **Figure 4.2** (Abrahamson and Shedlock, 1997). The first distance measure, given by Joyner and Boore (1981), represents the closest horizontal distance to the vertical projection of the rupture plane from the site (normally referred as r_{jb}). Second distance measure is the closest distance to the rupture plane (r_{rup}) and third one (r_{seis}) is the closest distance to the seismogenic part of the rupture plane (Cambell, 2003). The width of the rupture plane (W) can be calculated from the magnitude (Mw) adopting the equation: $Log(W) = -1.01 + 0.32M_w$, (Wells and Coppersmith, 1994), where, "W" is in km and the standard deviation of log(W) is 0.15. Campbell (1997) recommended that average depth to the top of the inferred plane should be taken as 3 km or more, even when fault ruptures the Earth's surface.

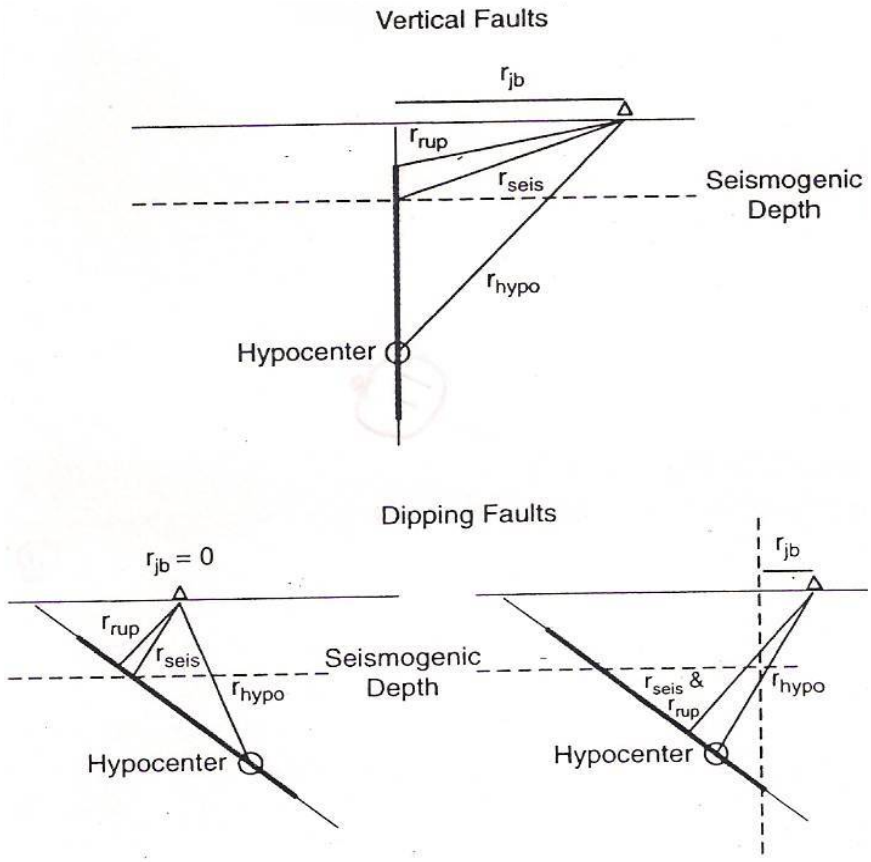

Figure 4.2 Source to site distance measure used in ground motion attenuation models (Abrahamson and Shedlock, 1997).

4.5 Estimation of Maximum Considered Earthquake (MCE) and Development of Spectral Acceleration (PSA 5%) Incorporating Near-Fault Factor

For the estimation of maximum considered earthquake at the three selected sites (Shahpur, Bhatwari, and Gopeshwar), respective potential seismotectonic sources are identified. For this purpose the major tectonic features mapped around these sites are taken into account (**Figure 4.1**). Observed seismicity patterns are also considered, but because of short-sample of seismicity no specific source could be mapped. The major parts of the two states (Uttarakhand and Himachal Pradesh) lie in the frontal part of the Himalayan arc that extends from the Hazara arc in the west to the Burme arc in the east. Major interplate seismicity observed in these two states is due to the continental collision between India and Eurasia tectonic plates and subsequent under-thrusting of the India plate below the Eurasia plate. This convergence process of two plates leads to the crustal shortening along the longitudinal thrusts and transverse faults in Himalaya and gives rise to earthquake activity.

The New Generation Attenuation (NGA) relation developed by Boore and Atkinson (2008) has been adopted to compute peak horizontal acceleration (PHA) and spectral accelerations (S_a) at 5% damping. Both PHA and S_a are computed with mean plus one standard deviation because Bhatwari, Gopeshwar, and Shapur sites lie in the regions of high seismicity. This relation has been adopted because it is applicable for seismically active, shallow-crustal earthquakes. The adopted NGA-relation (Boore and Atkinson, 2008) has been implemented using "R" software in the nga-package, developed by Kaklamanos et al. 2010. "R" is statistical computing software which performs batch calculations, and is well-known in the statistical and scientific community. The spectral accelerations were estimated at spectral-periods between 0.01 sec and 4.0 sec with the inclusion of near-fault factor in the spectral shapes. To allow the inclusion of near-fault effect, the spectral accelerations are increased by 20% (sites within 15 km of a causative fault) for periods longer than 1 sec and tapers linearly to zero at a period of 0.5-second (**Figure 4.3**). This approach has been adopted from Division of Engineering Services Geotechnical Services, who's used this approach for Developing Deterministic Acceleration Response Spectrum including near-fault factor (Caltrans, 2012). Jain and Das (1993) studied the characteristics of SGM recordings obtained during the 1991 Uttarkashi earthquake (M_w 6.8). In this study, they evaluated the comparative consistency of codal provisions (IS 1893: 1984) with respect to the recorded ground motions and considering that the recording instruments were located at rock-sites. Mittal et al. (2012) classified the site characteristics of

300 sites of the strong motion network installed in seismic zone III, IV and V along Himalayan belt and adjoining Indo-gangatic plains. For site classification the site geology given in seismotectonic atlas of India and its environs, and information from other relevant sources was taken into account. This study showed that the Bhatwari and Gopeshwar sites lie on quartzite/dolomites and quartzite/slates respectively, whereas, the Shapur site lies on the firm-rock. For all the seismotectonic sources within 30 km from each site **(Figure 4.1)**, peak horizontal ground accelerations (zero period acceleration) and pseudo-spectral acceleration (5%-damping) at each site have been computed adopting the prescribed attenuation relationship.

The computed values of peak horizontal accelerations (PHAs) at each site for rock site/stiff soil conditions along with sources are listed in **Table 4.4.** The highest value among the computed values is taken to represent the acceleration (MCE) at each site.

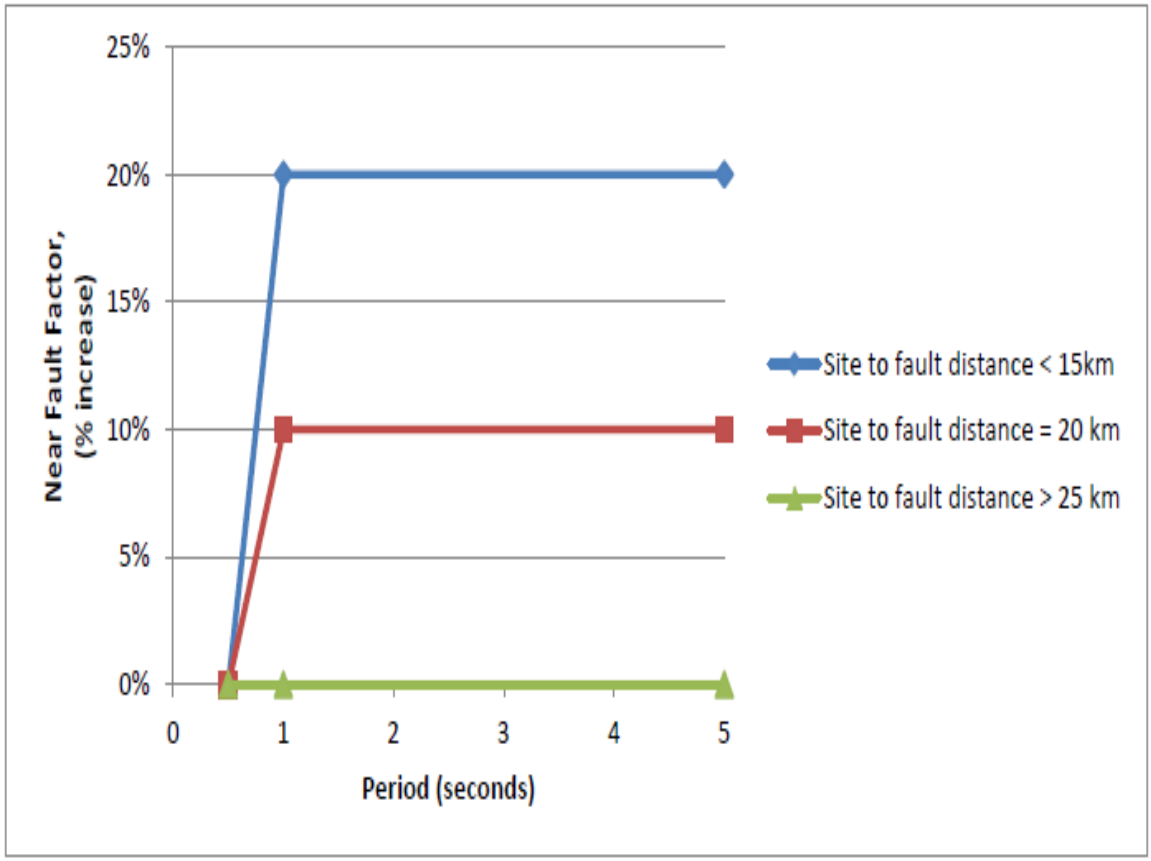

Figure 4.3 Near-fault factors recommended for developing deterministic acceleration response spectrum (Caltrans, 2012).

Table 4.4 Computed peak horizontal accelerations (A_h (g)) at three selected sites

Site	A_h (g)	Source
Shapur	**0.50**	Jwala Mukhi Thrust (JMT)
	0.47	Main Boundary Thrust (MBT)
	0.36	Vaikrita Thrust (VT)
	0.28	Drang Thrust (DT)
Gopeshwar	**0.51**	Main Central Thrust (MCT)
	0.50	Thrust Fault-1 (TF1)
	0.46	North Almora Thrust (NAT)
	0.42	Ramgarh Thrust (RT)
	0.36	Alaknanda Fault (AF)
Bhatwari	**0.58**	Main Central Thrust (MCT)

For the **Gopeshwar** and **Shapur sites** that fall in Zone V according to IS code, five response spectra have been estimated for each site (**Figure 4.4 and 4.5**). The response spectra include: i) Site-specific response spectra including near-fault factor, ii) Spectra due to transverse component of recorded ground motion that have pulse-type ground motion, iii) Spectra due to fault-normal (FN) component of recorded ground motions, iv) Spectra due to extracted pulse ground motion, and v) Spectra due to residual (RSD)/high frequency part of fault-normal (FN) component. For the purpose of comparison of these spectra with the codal spectra for zone V (IS 1893:2002) is also shown in the **Figure 4.4 and 4.5**.

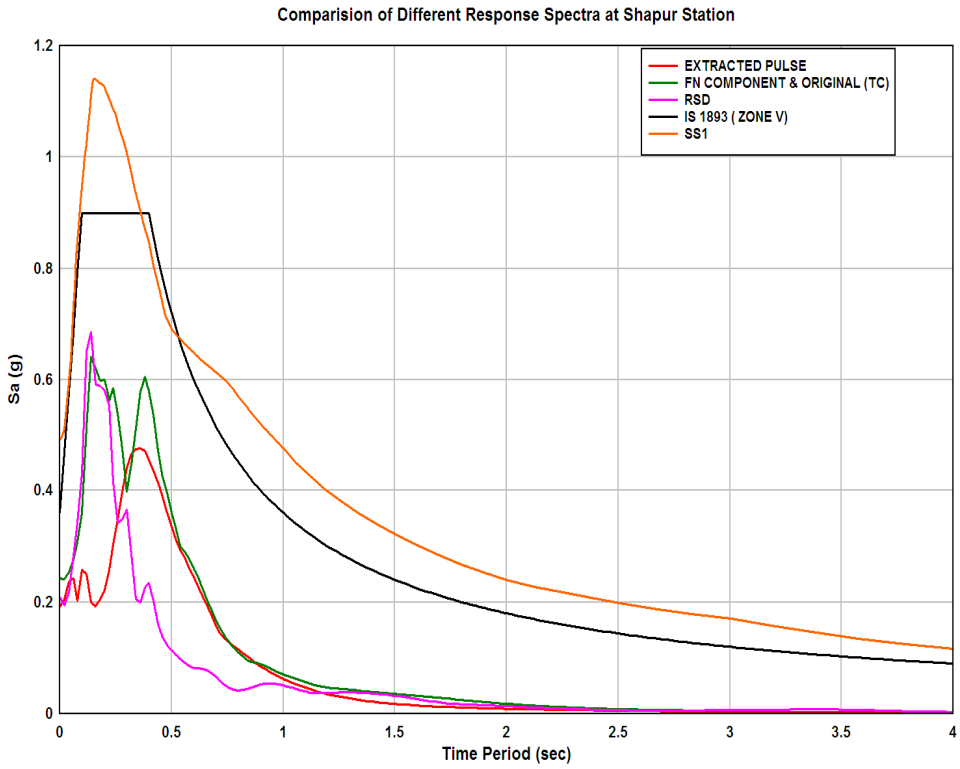

Figure 4.4 Response spectra(s) of SSGM, TC component, FN Component, extracted pulse, and residual at Shapur site and IS Codal spectra.

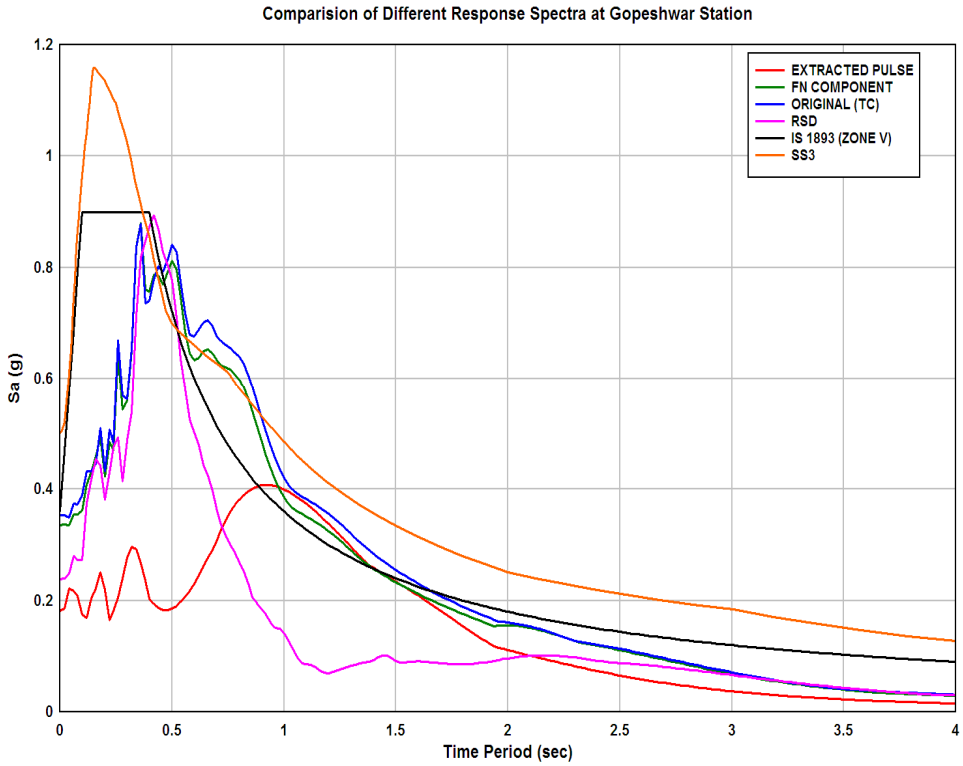

Figure 4.5 Response spectra(s) of SSGM, TC component, FN component, extracted pulse, and residual at Gopeshwar site and IS Codal spectra.

At the **Gopeshwar and Shapur** sites the spectral shapes of estimated ground motion show higher values at time periods ranging from 0.1 to 0.35 sec and 0.55 to 4.0 sec compared to codal spectral values. At Gopeshwar site, transverse component (TC) and FN component of recorded ground motion show higher spectral values between 0.40 and 0.90 sec compared to estimated site-specific (SS3) spectra including near-fault factor. At Shapur site, the spectral values of transverse component/FN component, extracted (EXT) pulse, and residual (RSD) component of recorded ground motion are below the spectral envelop of estimated site-specific (SS1) and codal spectral amplitudes. This is because of smaller magnitude of Dharamsala earthquake (M_w 5.5) compared to Uttarkashi and Chamoli earthquakes.

At the **Bhatwari** site which falls in Zone IV as per IS code, similar five response spectra (5% damping) as stated above have been estimated (**Figure 4.6**). For the purpose of comparison of these spectra with the codal spectra for zone IV (IS 1893:2002) is also shown in the **Figure 4.6**.

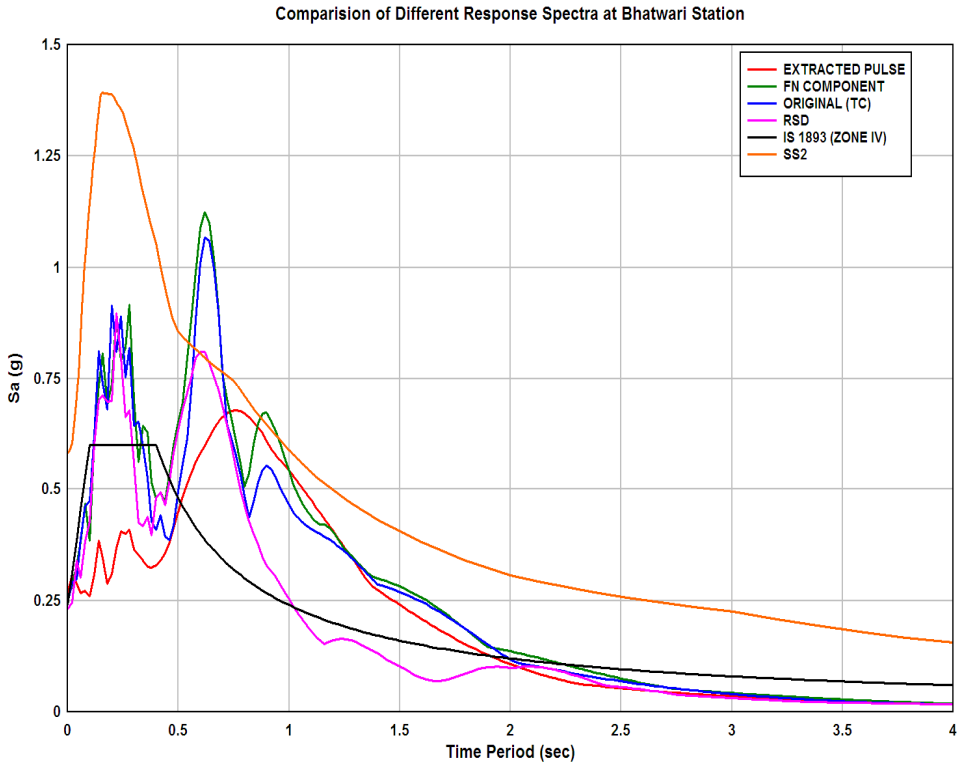

Figure 4.6 Response spectra(s) of SSGM, TC component, FN component, extracted pulse, and residual at Bhatwari site and IS codal spectra.

At **Bhatwari** site due to the Uttarkashi earthquake, the spectral amplitudes of recorded transeverse component (TC) and fault-normal (FN) component are much higher than the codal spectral amplitudes at periods ranging from 0.1 to 0.35 sec and from 0.45 to 2.0 sec. The spectral amplitudes due to residual (RSD) part of FN ground motion are much higher than the codal spectral amplitudes at periods ranging from 0.1 to 0.25 sec and from 0.45 to 1.0 sec. Whereas, spectral amplitudes due to extracted (EXT) pulse that represents low-frequency ground motion showed higher amplitudes than the codal spectral amplitudes at periods ranging from 0.5 to 2.0 sec. At **Bhatwari** site, the acceleration spectral values of estimated site-specific ground motion (SSGM) significantly exceeds the codal spectral values at all the time-periods because the Bhatwari site lie in Zone IV with zone factor 0.24 (zero-period acceleration). Whereas, this type of variation found much less at **Gopeshwar and Shapur sites** because these sites lie in Zone V with zone factor 0.36 (zero-period acceleration). However, spectral shapes of transverse-component (TC), FN component and residual (RSD) part of fault-normal (FN) component of recorded ground motion showed higher values between 0.5 and 1 sec compared to site-specific ground motion (SSGM) spectra (SS2) that include near-fault factor at the Bhatwari site.

4.6 Generation of Compatible Time Histories

In the previous section the site-specific spectra that include near-fault factor have been estimated. The next step is to generate ground-motion time-histories compatible with these spectra (target-spectra) over the period range of significance for the structures. For the generation of time-histories, two methods are normally suggested. First method involves selecting the acceleration time-histories from the available recorded time-histories of earthquakes having similar characteristics, and the second method involves the computing synthetic time-histories or modifying the recorded time-histories (USACE, 1999). It is suggested that while selecting the recorded ground motions, at least four time-histories should be selected. Further, the valleys and peaks of individual spectra should not match at particular time-period, and peaks of spectra of selected time-histories should not exceed the design spectrum excessively. In this method, scaling of individual time-histories is done by a constant factor to allow matching the spectral fit. However, no changes are made in the spectral amplitudes and relative frequency content of the accelerograms (USACE, 1999). Several methods have been developed and based on these methods computer codes are written to generate synthetic time-histories. The programs either allow computing complete time-history or modifying a recorded time-history so that the response spectrum of the resulting accelerogram closely matches the design or target spectrum. Techniques that are based on modifying recorded time-history are preferred because they preserve time-domain characteristics of actual ground motions. Two techniques that have been widely used for this purpose are the frequency-domain RASCAL computer code developed by Silva and Lee (1987) and the time-domain technique developed by Lilhanand and Tseng (1988). These techniques found to preserve the basic time-domain character of the generated accelerogram and a good fit to a smooth target spectrum (USACE, 1999).

Synthetic techniques adopted for developing time-histories have several merits, namely, a single time-history allows good fit to the design spectrum; duration of strong shaking and of accelerogram natural appearance can be achieved; and three components of ground motion, each providing a good spectral match can be developed (USACE, 1999). In case the approach of selecting the time histories from the suite of recorded motions is adopted, this approach suffers from many shortcomings such as: multiple dynamic analyses are required for the accelerograms selected from the sample of selected time-histories; individual spectrum peaks of some of the accelerograms may exceed the smooth design spectrum. Further, it has been

seen that a reasonably good spectral fit may be achieved for one horizontal component, but when same scaling factors are applied to the other horizontal and vertical components for the same recorded time-history, the spectral fit is usually not as good (USACE, 1999). Several time histories can be generated to match the same target response spectrum, and each generated time-history would be equally acceptable from the point of view seismic analysis (USACE, 1999).

Based on the discussion given above, in the present study, the compatible time histories are generated at each site for target acceleration response spectra estimated in the previous section, using wavelet-based algorithm given by Mukherjee and Gupta (2002). This algorithm decomposes given accelerogram (taken as input accelerogram) into a desired number of time-histories with non-overlapping frequency contents. Then each of the time-histories is suitably scaled for matching the response spectrum of the revised accelerogram with a prescribed design target spectrum. This method is based on an iterative procedure that modifies a recorded accelerogram such that the temporal variations in its frequency content are retained in the synthesized accelerogram. The proposed procedure is more realistic than other procedures that use the phase characteristics of a recorded accelerogram. The method does not use the Fourier spectrum or power spectral density function. The success of method depends on how judiciously a recorded accelerogram is selected to simulate the desired non-stationary features. Because the recorded accelerograms were available at Shapur, Bhatwari and Gopeshwar sites, these accelerograms were selected as input for modification. Their recorded transverse components (TC) have been taken for generating the time-histories to match the estimated site-specific (SS) response spectra at the selected three sites to obtain the compatible time histories.

At Bhatwari site **Figure 4.7 and 4.8** shows the recorded transverse-component (TC) of acceleration time-history and the time-history obtained after spectral matching. The generated accelerogram in **Figure 4.8** shows normalized peak horizontal ground acceleration. These normalized values have to be multiplied by 0.58 g and 0.27 g to obtain MCE and DBE time history for dynamic analysis at the site. **Figure 4.9** shows the very close spectral match of modified time-history with respect to target spectra at the Bhatwari site.

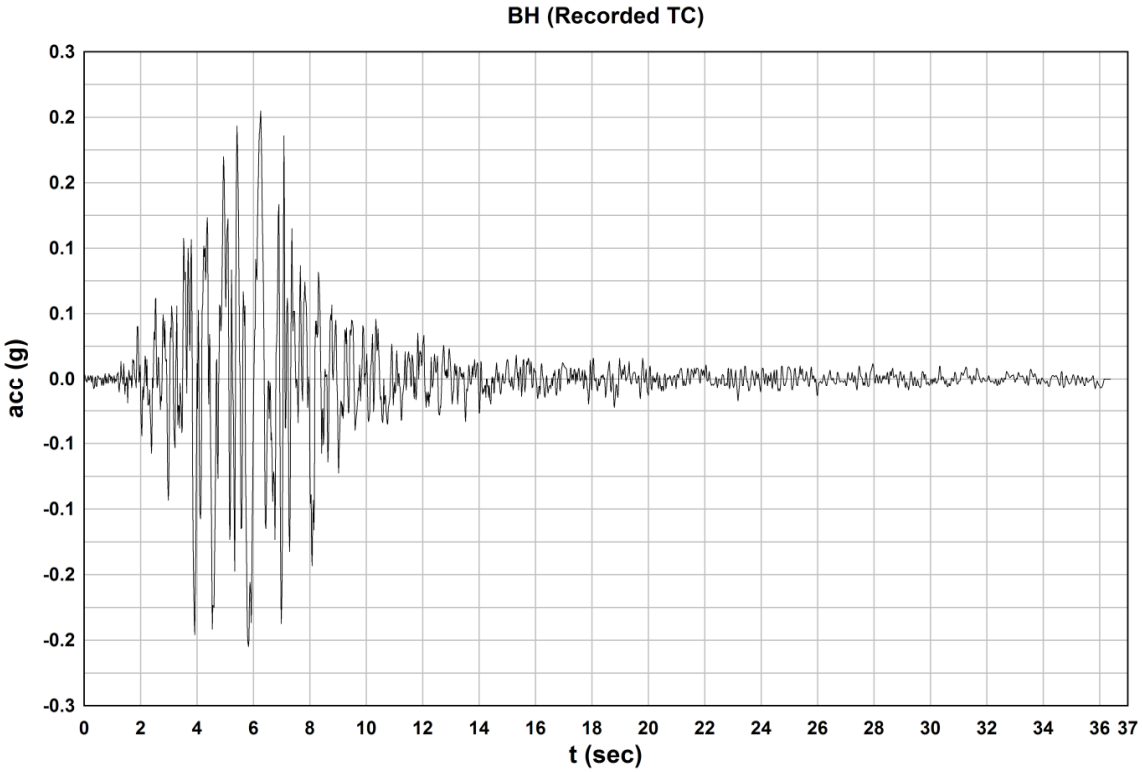

Figure 4.7 Recorded TC of the acceleration time-history at Bhatwari site.

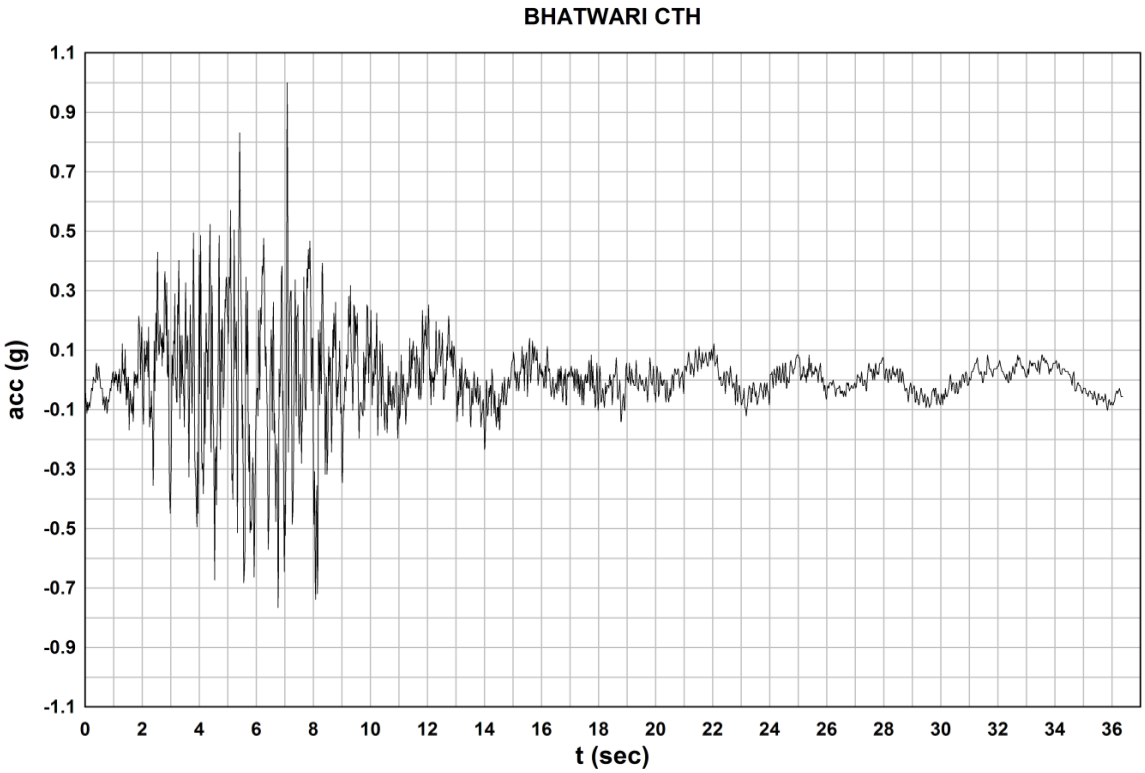

Figure 4.8 Compatible acceleration time-history (normalized) with respect to estimated ground motion response-spectra at Bhatwari site.

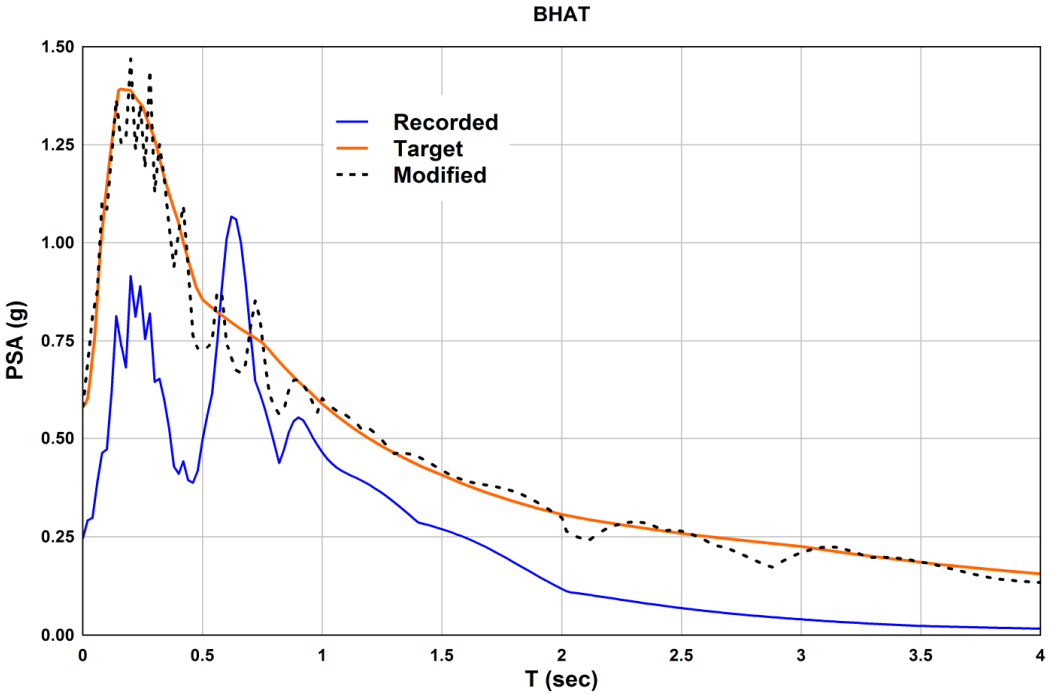

Figure 4.9 Comparison of the PSA spectra for recorded (blue-line) and generated compatible time-history (dotted black-line) with the target spectrum (orange-line) at Bhatwari site.

Figure 4.10 and 4.11 shows the recorded TC acceleration time-history and the time-history after spectral matching process at Gopeshwar site. The **Figure 4.11** shows the accelerogram with normalized peak horizontal ground acceleration of 1.0 g. The ordinates of **Figure 4.11** will have to be multiplied by 0.51 g and 0.26 g to obtain MCE and DBE time history to carry out the dynamic analysis at the site. **Figure 4.12** shows the very close spectral match of modified time-history with respect to target spectra at the site.

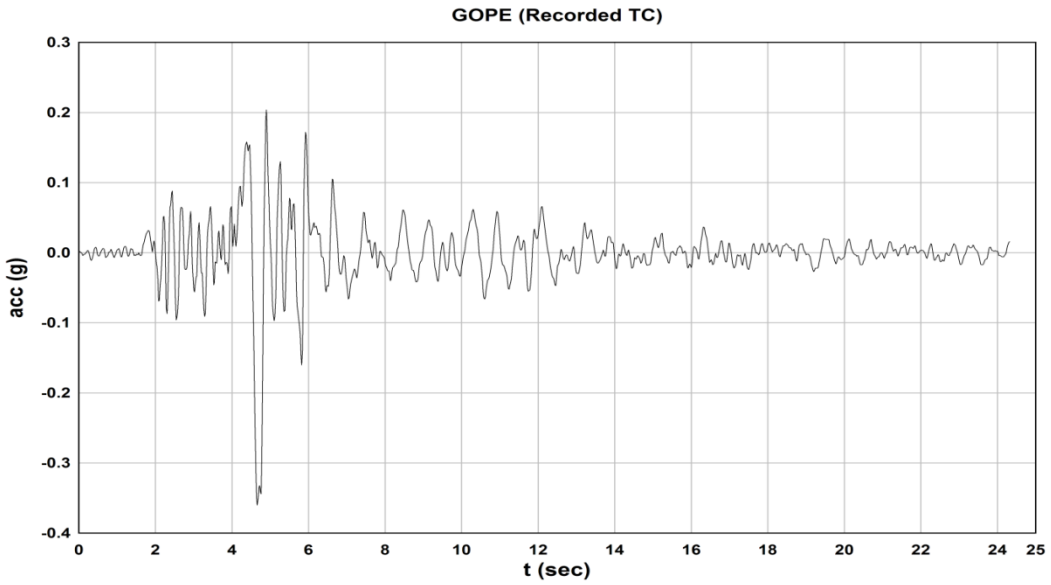

Figure 4.10 Recorded TC acceleration time-history at Gopeshwar site.

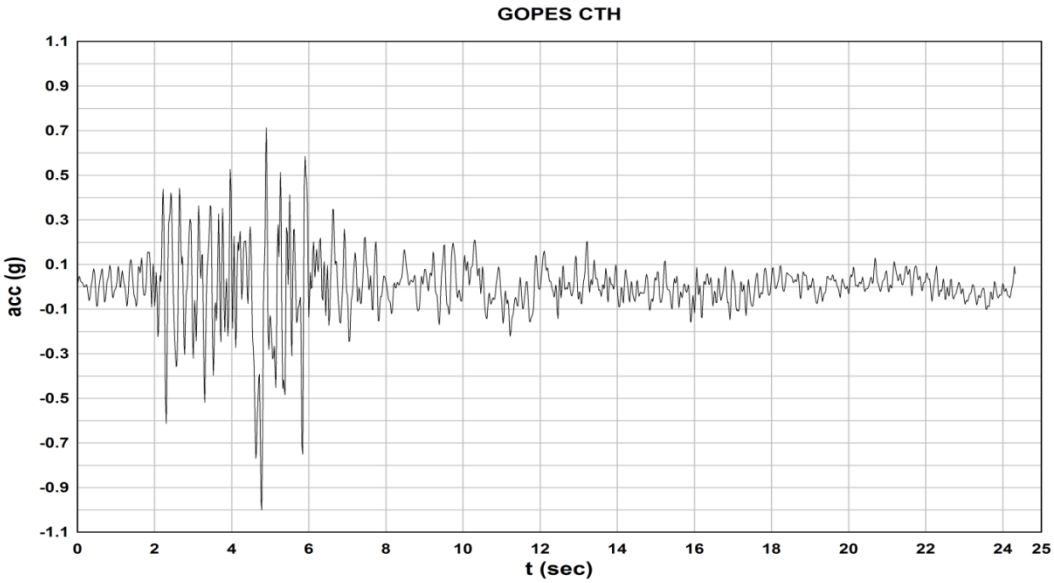

Figure 4.11 Compatible acceleration time-history (normalized) with respect to estimated ground motion response-spectra at Gopeshwar site.

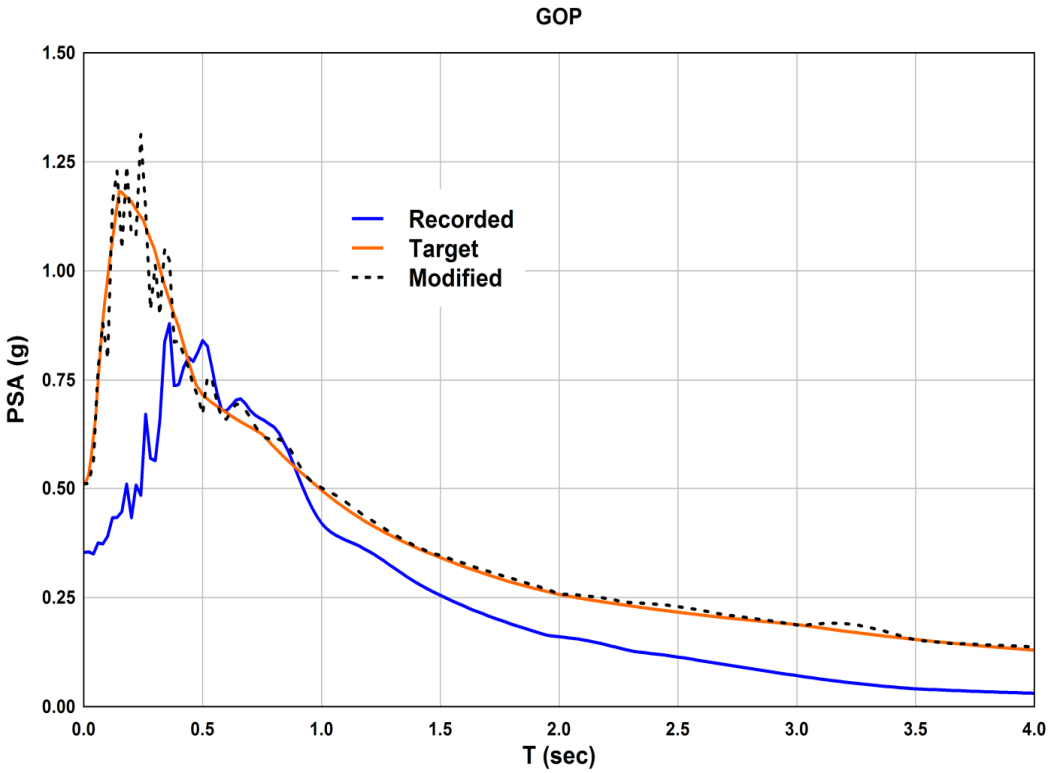

Figure 4.12 Comparison of the PSA spectra for recorded (blue-line) and generated compatible time-history (black-line) with the target spectrum (orange-line) at Gopeshwar site.

Figure 4.13 and 4.14 shows the recorded (transverse-component) acceleration time-history and the time-history after spectral matching process at Shahpur site. The **Figure 4.14** shows the accelerogram with normalized peak horizontal ground acceleration of 1.0 g. The ordinates of **Figure 4.14** will have to be multiplied by 0.50 g and 0.25 g to obtain MCE and DBE time

history. **Figure 4.15** shows the very close spectral match of modified time-history with respect to target spectra at the site.

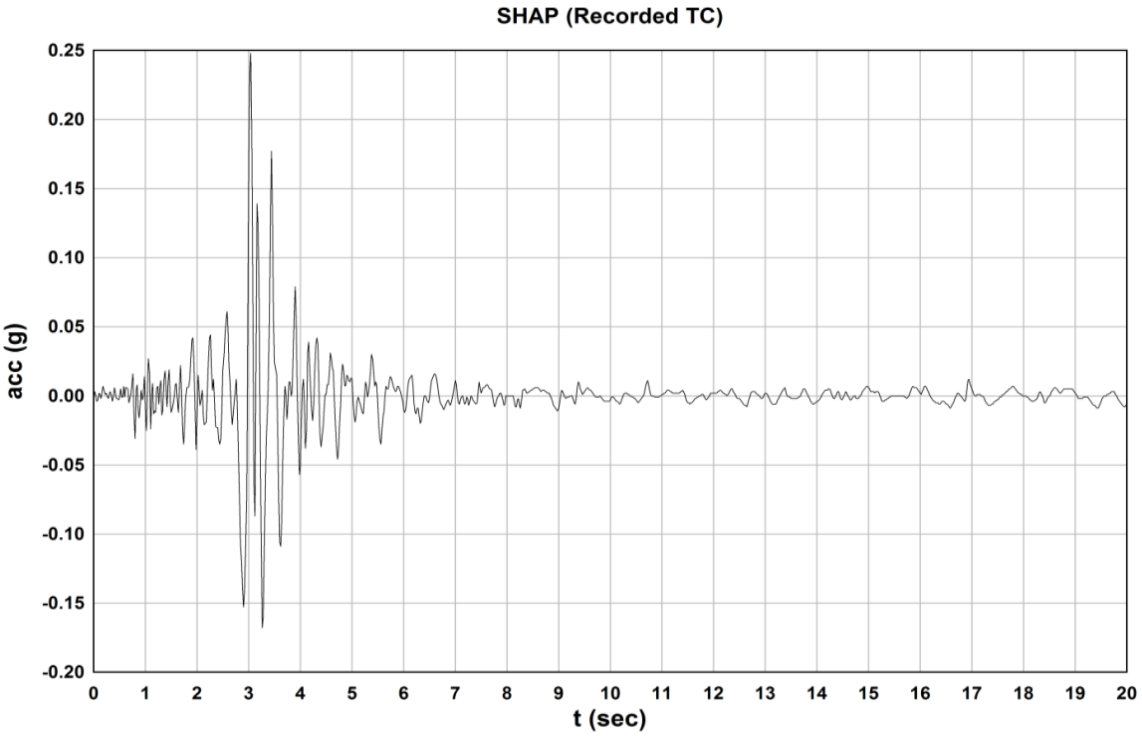

Figure 4.13 Recorded TC acceleration time-history at Shapur site.

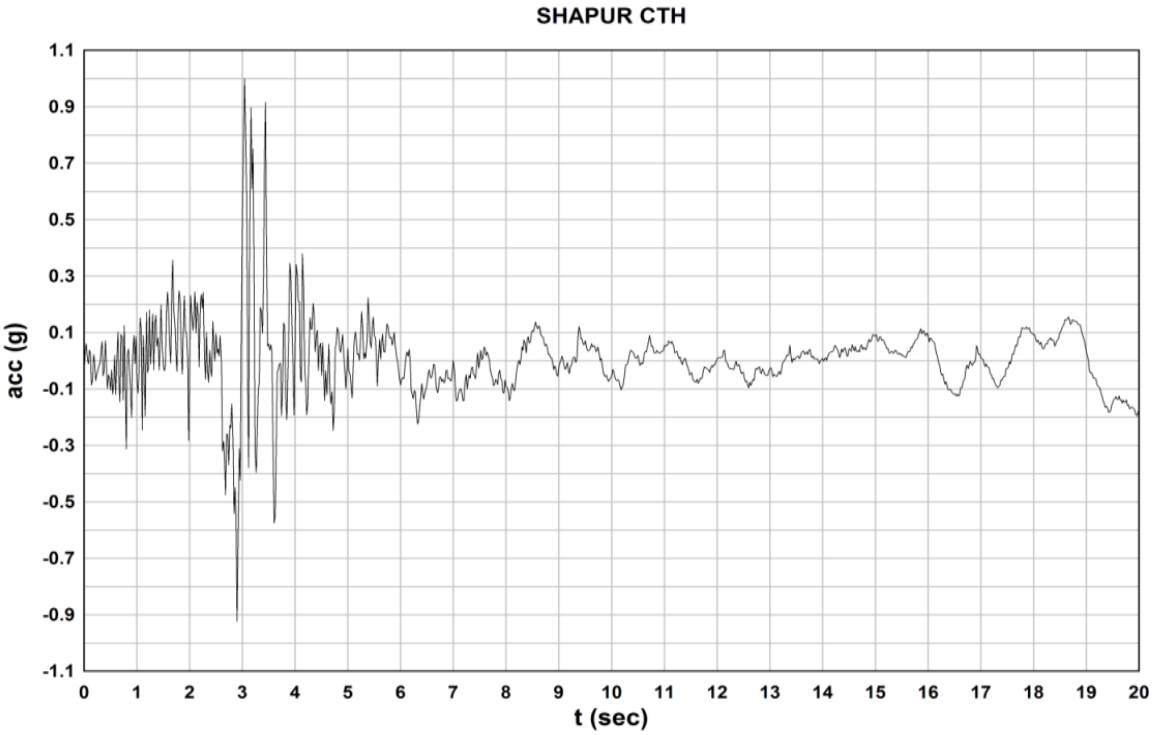

Figure 4.14 Compatible acceleration time-history (normalized) with respect to estimated ground motion response-spectra at Shapur site.

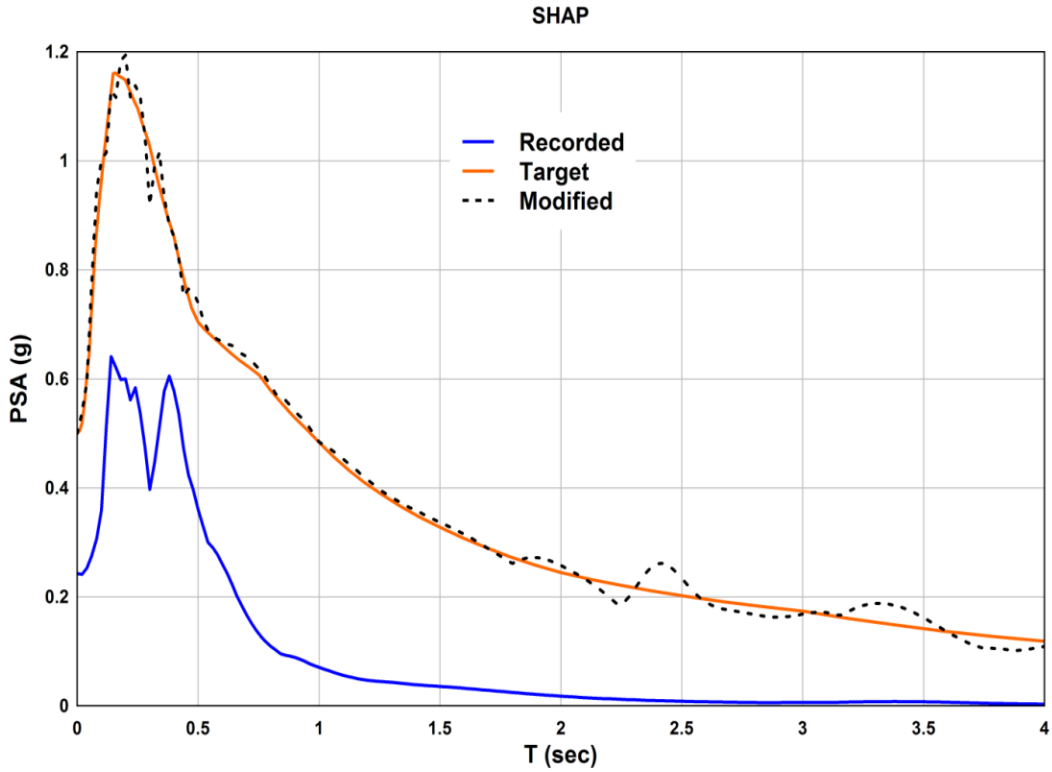

Figure 4.15 Comparison of the PSA spectra for recorded (blue-line) and generated compatible time-history (black-line) with the target spectrum (orange-line) at Shapur site.

4.7 Concluding Remarks

At three sites, the ground motion is estimated by incorporating the near-fault factor, showed much higher Peak Horizontal Accelerations (PHA) compared to NFGM recordings at these sites. This is because of adopted deterministic approach considering the worst scenario earthquakes at these sites. At **Bhatwari** site the spectral shapes of estimated ground motion exceeds the codal spectral values at all time periods. However, spectral shapes of transverse-component, FN component and extracted pulse component of recorded ground motion showed higher values between 0.5 and 1 sec compared to estimated ground motion spectra. At **Gopeshwar and Shapur** sites the spectral shapes of estimated ground motion show higher values at time periods ranging from 0.1 to 0.35 sec and 0.55 to 4.0 sec compared to codal spectral values. At Gopeshwar site, transverse component and FN component of recorded ground motion show higher spectral values between 0.40 and 0.90 sec compared to estimated spectra. At Shapur site, the spectral values of transverse component, FN component, extracted pulse, and residual component of recorded ground motion are below the spectral envelop of estimated and codal spectral amplitude. This is because of smaller magnitude of the Dharamshala earthquake (M_w 5.5) compared to the Uttarkashi and Chamoli earthquakes.

CHAPTER 5

DYNAMIC ANALYSIS OF HILLSLOPE BUILDINGS

5.1 Introduction

Most of the hilly regions in the Himalaya are getting urbanized because of increase in population and economic development. To accommodate this growing population there is an increase in demand of houses; and multistoried buildings is one of the possible options. Further, because of economic growth, there is a significant increase in the flow of tourists to the hill-stations located in the hilly regions. To allow tourism industry to flourish and to attract tourists, a large number of hotels of different structural forms consistent with local topography (e.g., step-back (SB) or step back-set back (SBSB)) have come up in the hilly areas. One of the major constraints in the construction of buildings in the hilly regions is the scarcity of plain land resulting in buildings being constructed on hillslopes. In hilly regions, the orientation of hillslope buildings is an important issue and it was observed during part earthquakes that the downhill buildings suffered more damages compared to the uphill buildings (Meena and others, 2013). To accommodate the ground slope, the buildings on hillslope often have less number of storeys toward hillside and more toward valley side (Jain et al., 1999). The undulating terrain provides a unique opportunity to experiment with aesthetic architectural configurations of buildings within domain of the space available. The buildings on the hillslopes are generally irregular in shape, due to which the distribution of mass and stiffness of such buildings vary along the horizontal and vertical planes (Verma, 1989; Pachuau, 1992; Kumar and Paul, 1997; Kumar and Paul, 1999, Pandey et al., 2011). Hence, the eccentricity of these buildings varies floor-wise. An asymmetric building will have both translational and torsional displacements, i.e., coupled displacement during earthquake excitation (Shakib and Datta, 1993; Jangid and Datta, 1995; Shakib and Ghasemi, 2007; Shakib and Tohidi, 2002**;** Ghasemi and Shakib, 2008). The torsional response of asymmetric buildings can be resisted either by providing additional strength or by increasing the energy absorbing capacity (Jangid and Datta, 1995). The Indian seismic code (IS 1893: 2002) recommends modal analysis to obtain the dynamic response of the irregular/unsymmetrical frame buildings, especially those with height above 12 meter, located in seismic zones IV and V. In this chapter, commonly adopted configurations of R.C. framed buildings, as adopted on hillslope, are studied from seismic considerations under the effect of NFGM.

5.2 Structural Models adopted for Analysis

The buildings resting on sloping ground, generally existing in hilly areas, usually have a step-back (SB) configuration or a combination of step-back and set-back (SBSB) configuration as shown in figures 5.1 and 5.2. Both these configurations experience coupled translational and rotational motions during earthquakes, making them susceptible to greater damage. Therefore, a three dimensional (3D) modeling with 6-dof at each node of such buildings is recommended to capture the detailed dynamic responses of the buildings (Kumar and Paul, 1994; Kumar, 1996; Kumar et al., 2012). Two, special moment resistant frame (**SMRF**) 3D configurations consisting of SB and SBSB models are considered for dynamic analysis (Figures 5.1 and 5.2). These models are selected because most of the residential buildings in the hilly regions are low-rise buildings with number of storeys limited to five storeys in majority of cases. For both types of building models, the number of storeys has been varied from two to five. The representative step-back building models are shown in Figure 5.1. These models are represented with only one bay in Y-direction and from two to three bays in X-direction depending on the number of storeys.

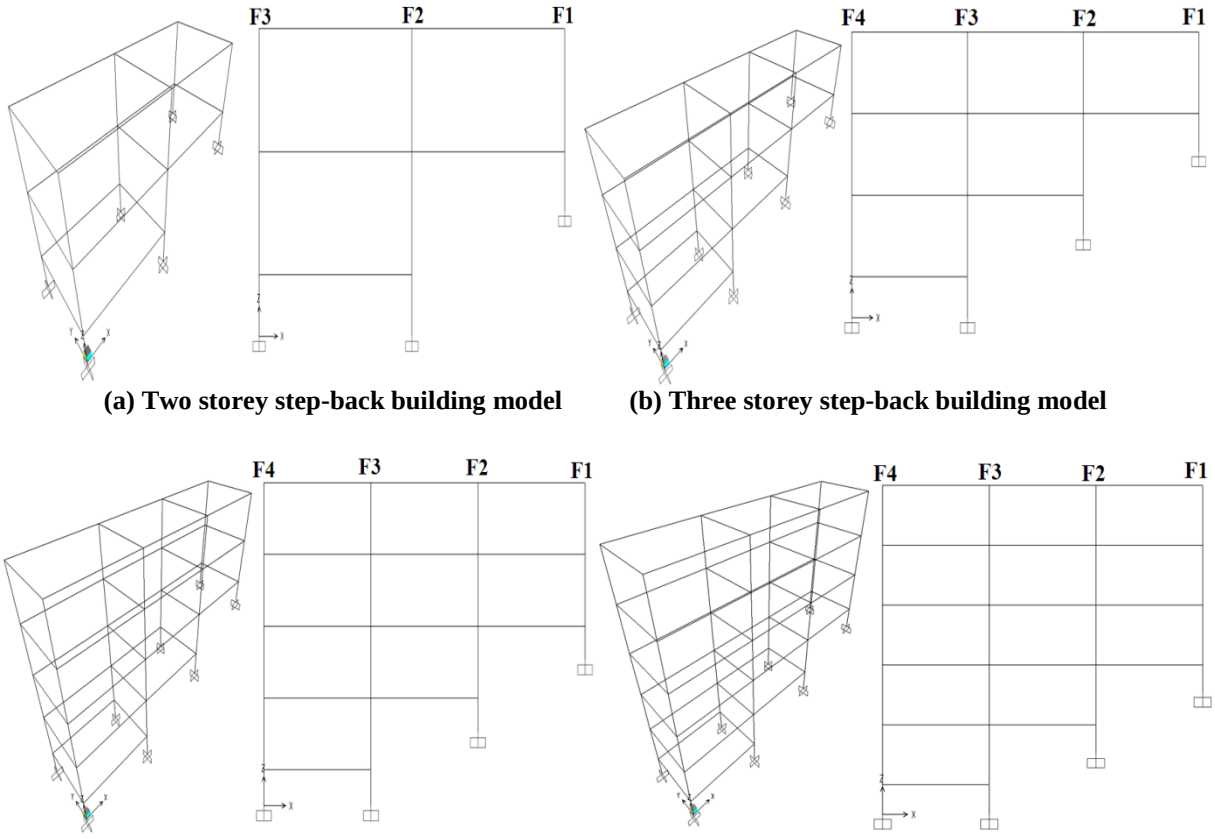

(a) Two storey step-back building model **(b) Three storey step-back building model**

(c) Four storey step-back building model **(d) Five storey step-back building model**

Figure 5.1 Step-Back (SB) building models

The step-back-set-back building models are depicted in Figure 5.2. These SBSB models also have one bay in Y-direction and two to five bays in X-direction according to the number of storeys.

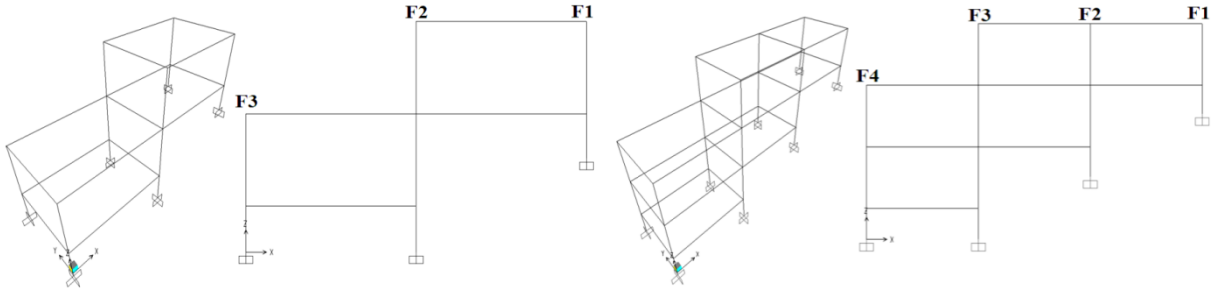

(a) Two storey step-back-set-back building model (b) Three storey step-back-set-back building model

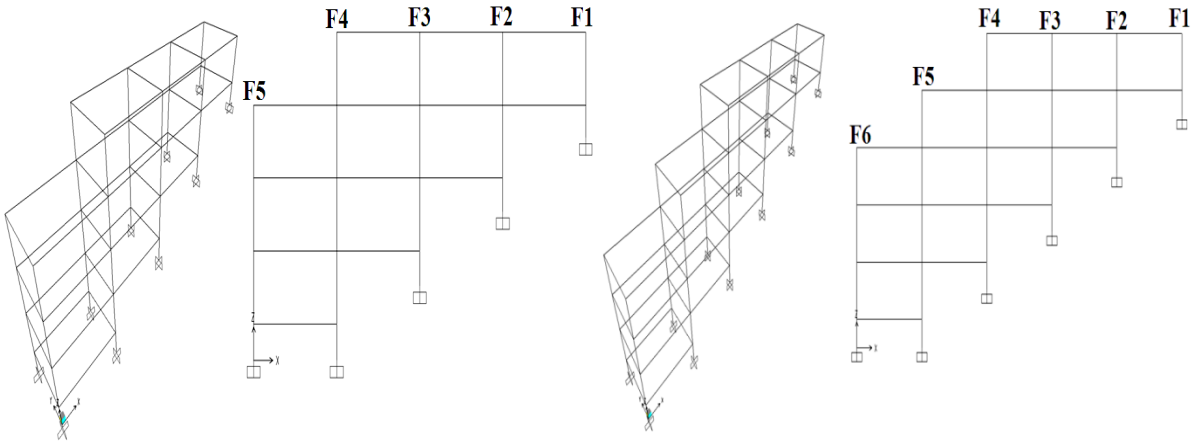

(c) Four storey step-back-set-back building model (d) Five storey step-back-set-back building model

Figure 5.2 Step-Back-Set-Back (SBSB) building models

The slope of the ground for both types of structures has been taken as 27 degree with horizontal which has been adopted earlier by Birajdar et al. (2004). The structural material is assumed to be isotropic and homogenous. The sectional properties of the models and load imposed on the models are listed in Table 5.1 and Table 5.2. The floors have been modeled as rigid diaphragms. Damping considered for all structural modes of vibration is five percent (5%).

Table 5.1 Properties of the considered building models

Height of each floor: 3.5 m
Plan dimension of each storey block: 7 m x 5 m
Slab thickness: 0.15 m
Wall thickness: 230 mm
Parapet wall thickness: 230 mm
Density of concrete: 25 KN/m^3
Poisson's Ratio: 0.2
Damping: 0.05
Size of column: 230mm x 500mm
Size of beams: 230mm x 500mm
Material properties, M 25 & Fe 415

Table 5.2 Load intensity imposed on considered building models

Slab dead	3.75 KN/m^2
Floor Live load	3 KN/m^2
Roof Live load	1.5 KN/m^2
Floor Finish	1 KN/m^2
Roof Finish	1.5 KN/m^2
Exterior Wall Load	16.15 KN/m
Interior Wall Load	10.5 KN/m
Parapet wall load	6.9 KN/m

5.3 Seismic Inputs

Seismic inputs are the earthquake data that are necessary to perform different types of seismic analysis. In the context of seismic analysis and design of structures, various earthquake data may be required depending upon the nature of analysis being carried out. Seismic inputs for structural analysis are provided either in the time domain or in the frequency domain, or in both time and frequency domains (Datta, 2010). The most common way to describe a ground motion is with a time history record. The motion parameters may be acceleration, velocity, or displacement, or all the three combined together. Further, available data for the study are in an analogue form, which are digitized before they are used as seismic inputs. Time histories of ground motions are used directly for the time domain analysis of structures subjected to deterministic seismic inputs. Another type of seismic input which is in frequently used for design is the response spectrum. In fact, the response spectrum is the most favored seismic input for earthquake engineers from design consideration. There are a number of response spectra that are defined for representing the ground motion, such as, displacement response spectrum, pseudo velocity response spectrum, and absolute acceleration response spectrum. These spectra also exhibit the frequency characteristics of the ground motions. The absolute acceleration response spectrum is commonly used as an input for the response spectrum methods of analysis of structures.

To perform seismic analysis, six types of seismic inputs are considered in the study at each selected site from both the design and analytical perspectives, listed below.

1. Recorded near-fault pulse-type ground motion.
2. Near-fault fault-normal (FN) component of ground motion.
3. Extracted (EXT) pulse of near-fault fault-normal (FN) component using ‘db7’ mother wavelet.
4. Residual (RSD) part of near-fault fault-normal component.

5. Estimated site-specific (SS) ground motion that include near-fault factor.
6. Indian seismic codal spectra and its compatible ground motion.

Brief details about the pulse extraction and their characteristics are presented in Chapter 3, and the estimation of site-specific ground motions including near-fault factor along with comparison with other seismic inputs are studied in Chapter 4.

5.3.1 Response Spectra

Figures 5.3, 5.4, and 5.5 illustrate acceleration spectra of the above listed seismic inputs at each site. The Gopeshwar and Shapur sites that fall in Zone V, and the Bhatwari site falls in Zone IV according to Indian Seismic code (IS 1893: 2002).

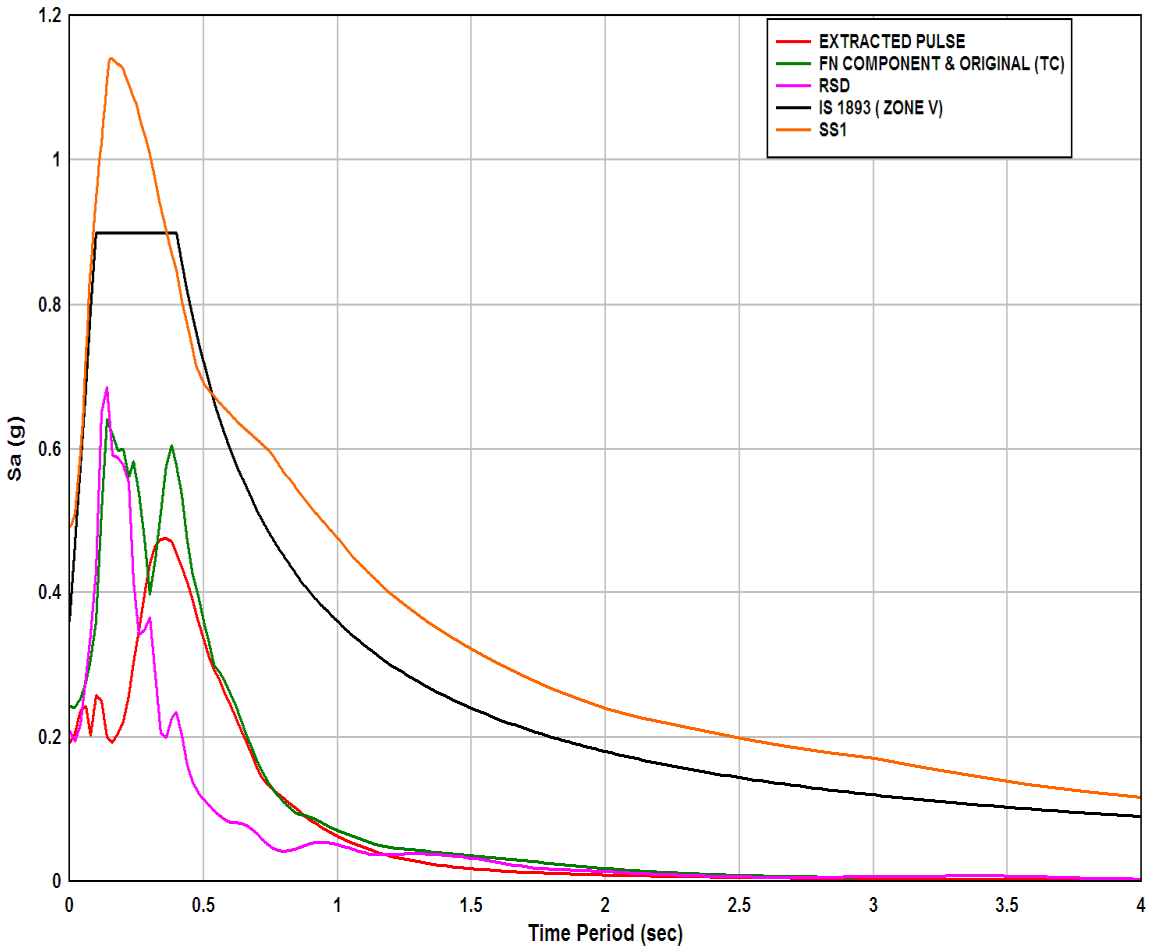

Figure 5.3 Response spectra of various seismic inputs Shapur site.

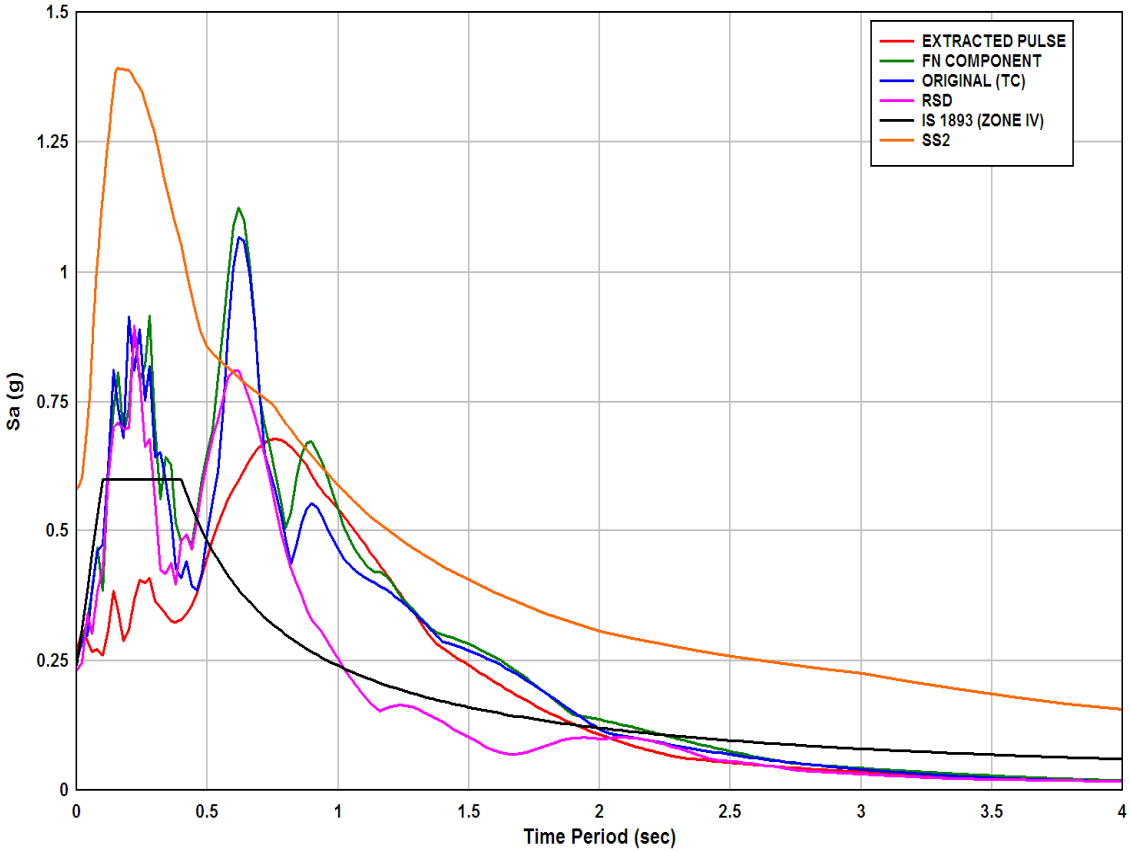

Figure 5.4 Response spectra of various seismic inputs Bhatwari Site.

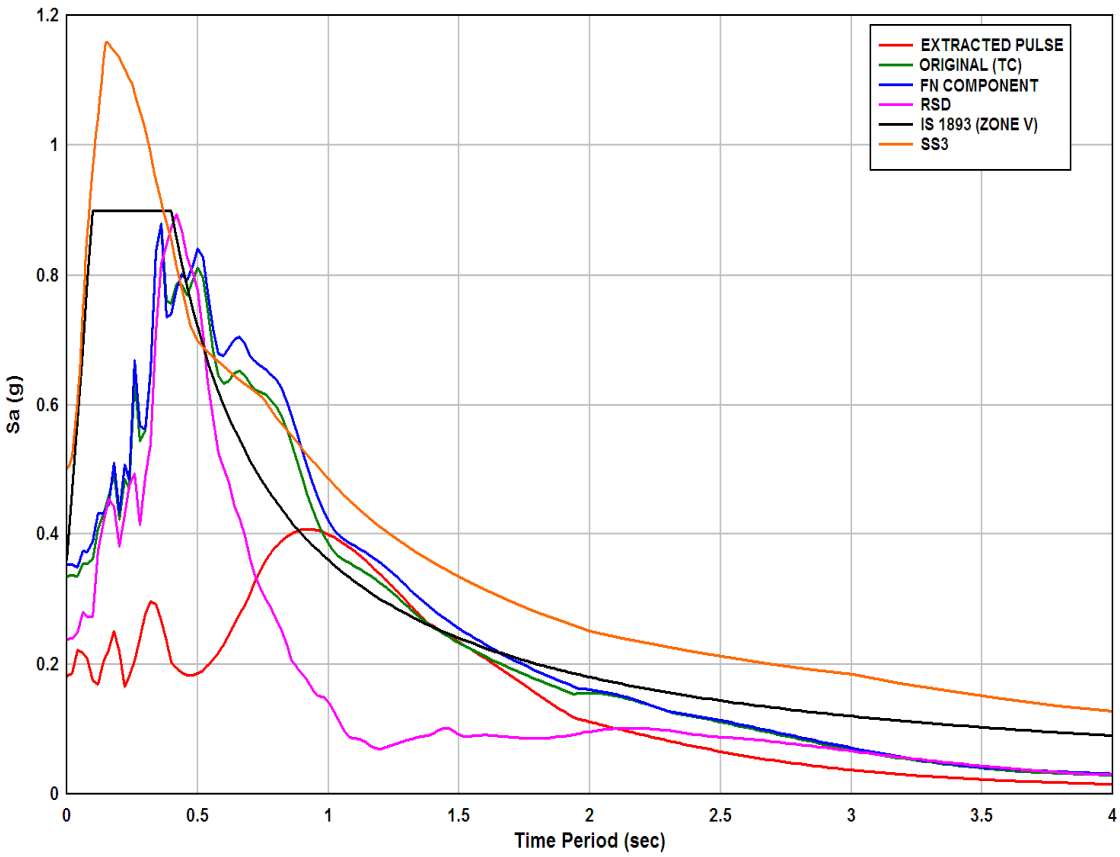

Figure 5.5 Response spectra of various seismic inputs Gopeshwar Site.

5.3.2 Time History

Acceleration time histories at each site considered as seismic inputs are shown in Figures 5.6 to 5.20. Figures 5.6 to 5.9, 5.10 to 5.14 and 5.15 to 5.19 show the time histories at Shapur, Bhatwari and Gopeshwar sites respectively. Whereas, Figure 5.20 shows IS codal compatible time history for hard rock/stiff soil. The recorded transverse component at each site exhibits pulse-type characteristics. As the pulse-type ground motion due to directivity effect is more dominant in the FN direction (Somerville, 1997b), the recorded time-histories at Shapur, Bhatwari and Gopeshwar stations were oriented in FN direction for pulse extraction. For this purpose the fault plane solutions given by Molner et al., 1989, Paul et al., 1998, and Kumar et al., 2006 have been adopted respectively, and the method suggested by Somerville, (1997b) has been used. The orientation of recorded transverse component of time history at Shapur station during Dharamsala earthquake of 1986 demonstrated that it is in the fault-normal direction (Kumar et al., 2012). Ghobarah and Sheikh (2003) recommended that the seismic codes should consider explicitly the NFGM in the time history analysis instead of simply increasing the amplitudes of the design response spectra by defining the pulse parameter such as, pulse magnitude, pulse shape, and its duration in a time history form.

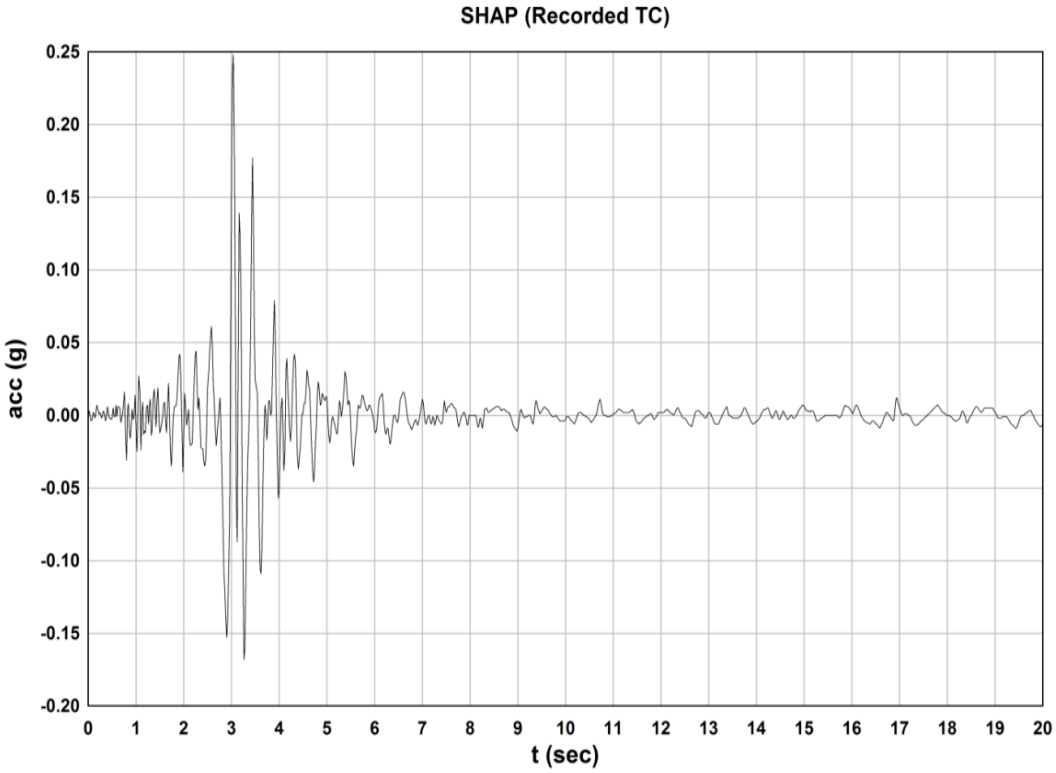

Figure 5.6 Recorded transverse component acceleration time-history at Shapur site

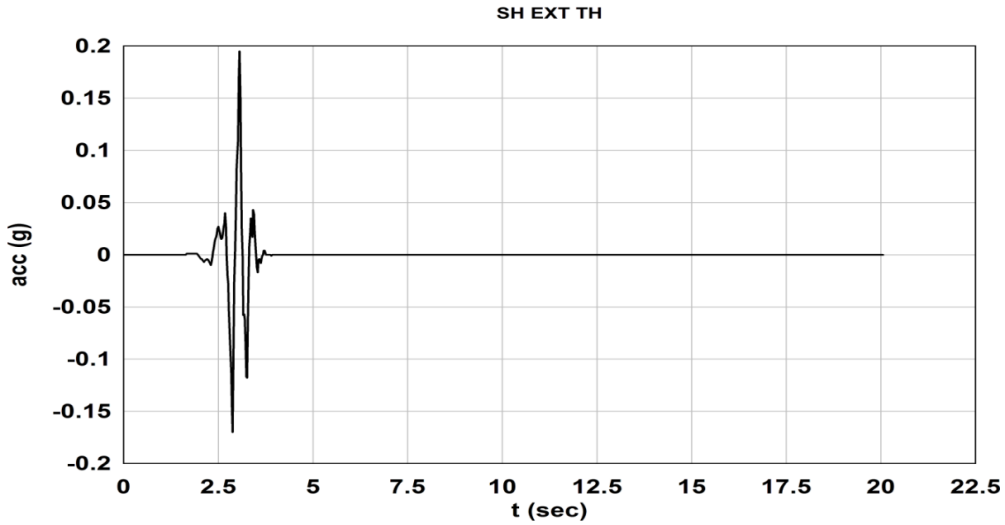

Figure 5.7 Extracted Pulse of the acceleration time-history at Shapur site

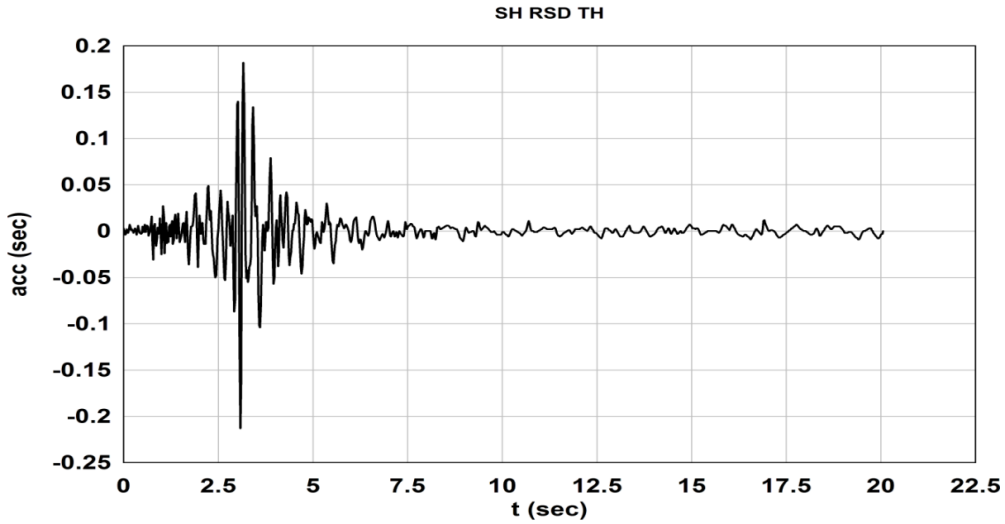

Figure 5.8 Residual part of the acceleration time-history at Shapur site

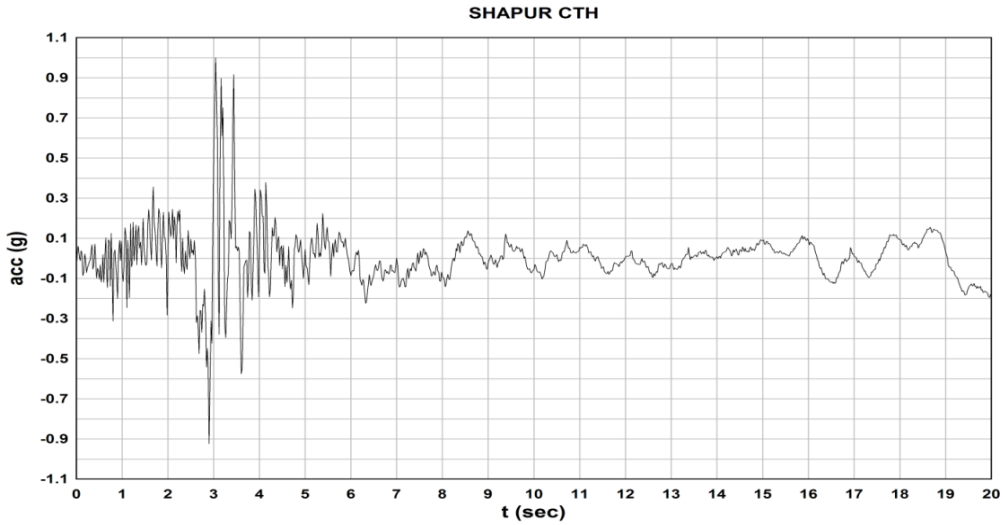

Figure 5.9 Compatible acceleration time-history (normalized) with respect to estimated ground motion response-spectra at Shapur site

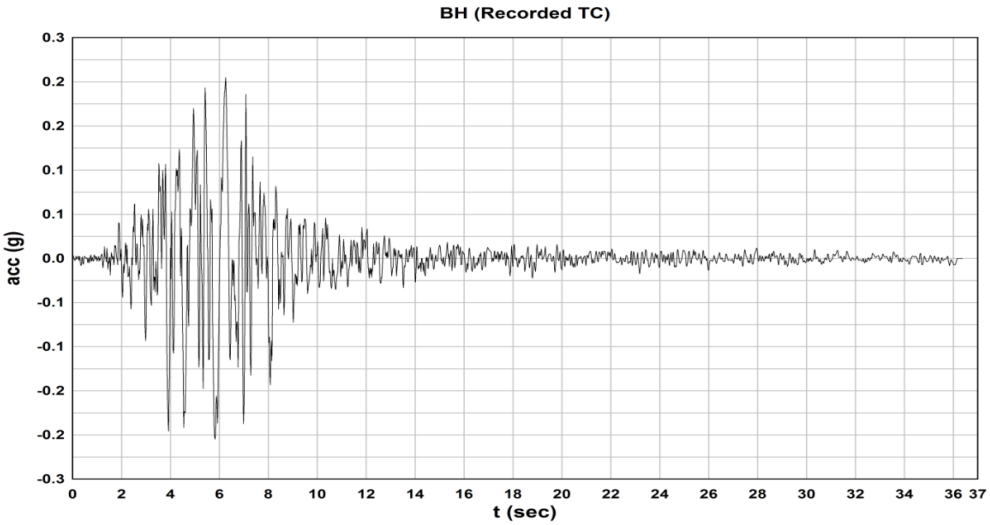

Figure 5.10 Recorded transverse component of the acceleration time-history at Bhatwari site

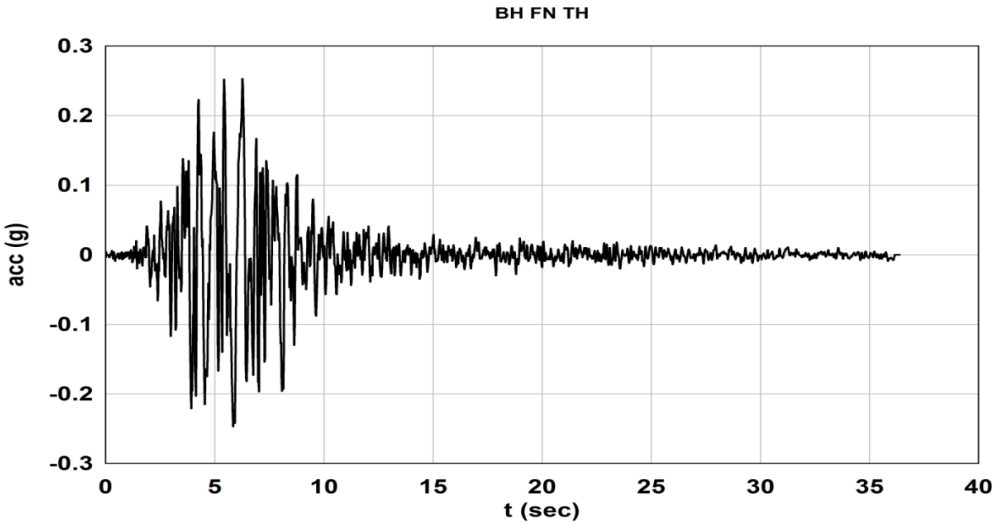

Figure 5.11 Fault-Normal component of the acceleration time-history at Bhatwari site

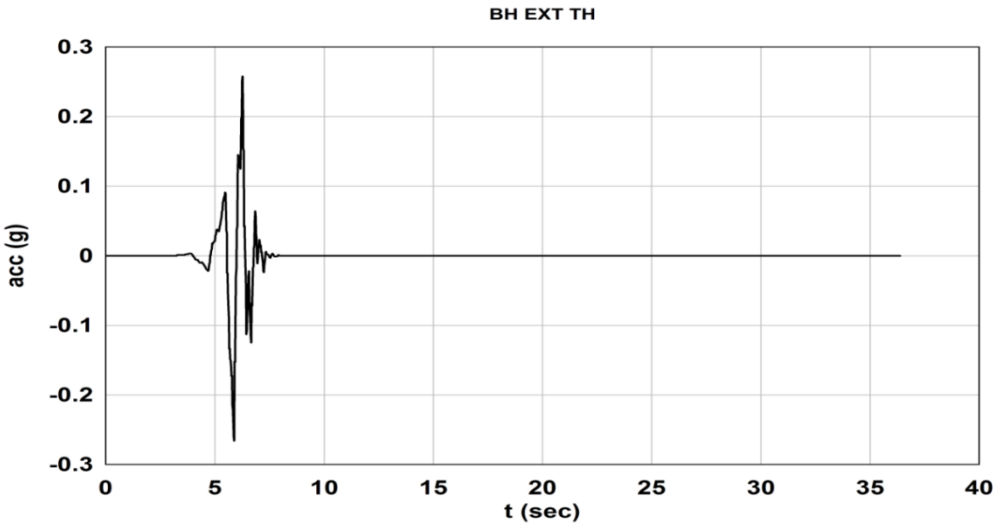

Figure 5.12 Extracted Pulse of the acceleration time-history at Bhatwari site

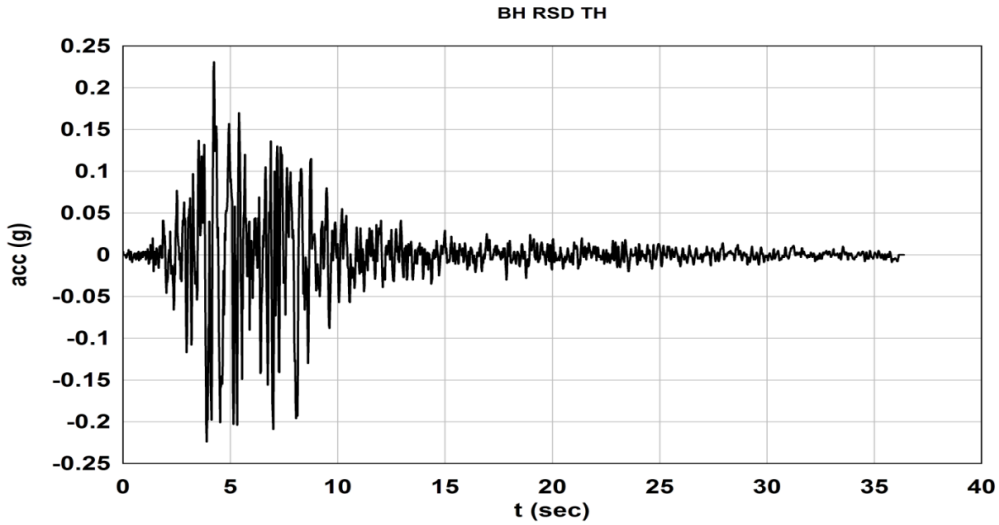

Figure 5.13 Residual part of the acceleration time-history at Bhatwari site

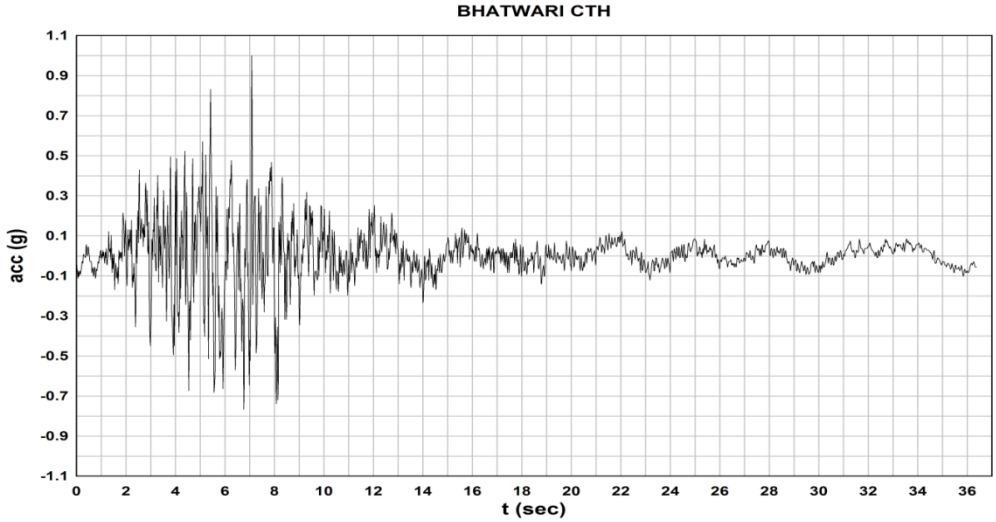

Figure 5.14 Compatible acceleration time-history (normalized) with respect to estimated ground motion response-spectra at Bhatwari site

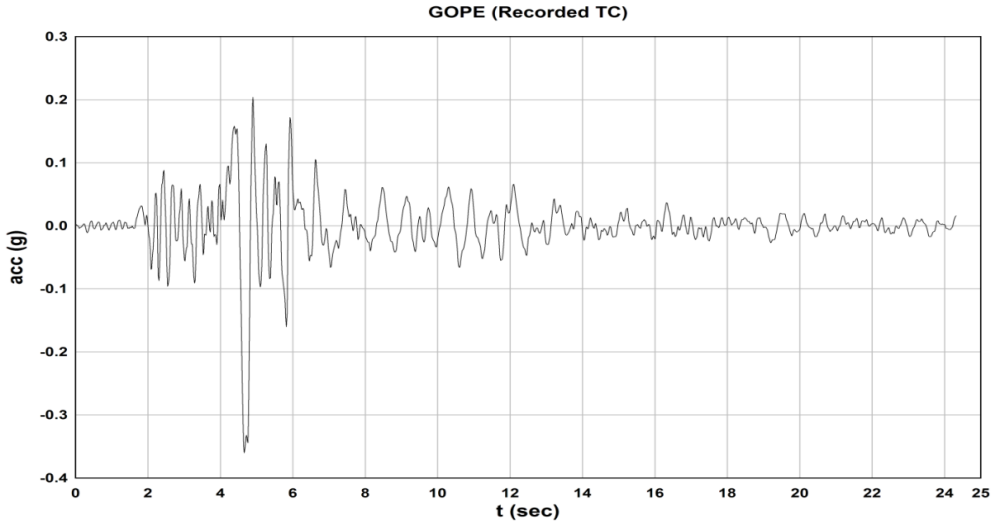

Figure 5.15 Recorded transverse component acceleration time-history at Gopeshwar site.

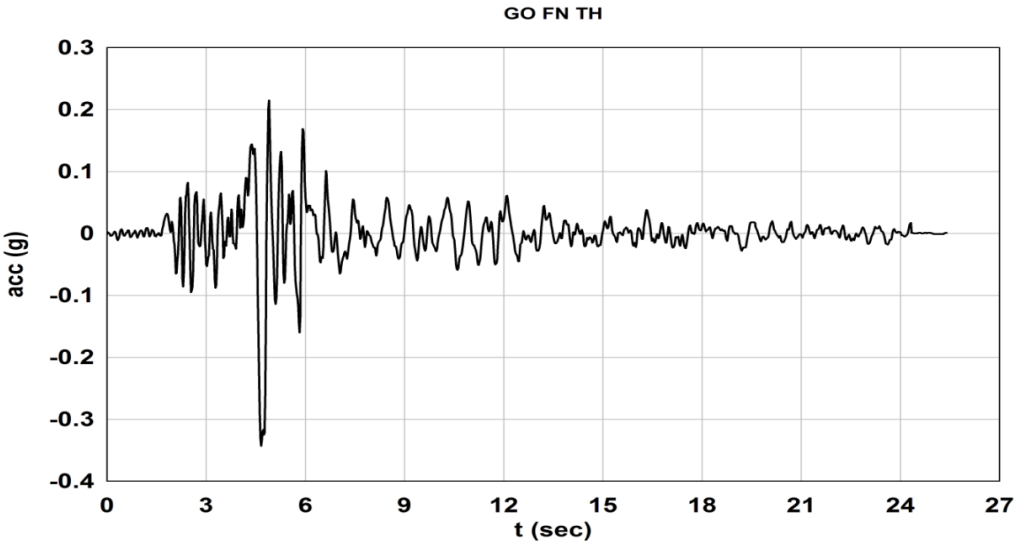

Figure 5.16 FN-component of the acceleration time-history at Gopeshwar site.

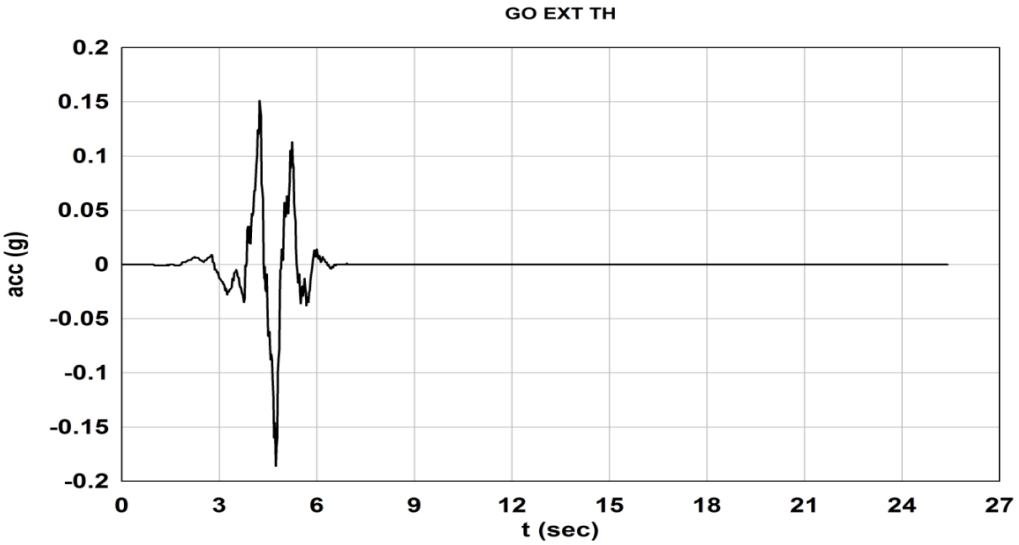

Figure 5.17 Extracted Pulse of the acceleration time-history at Gopeshwar site.

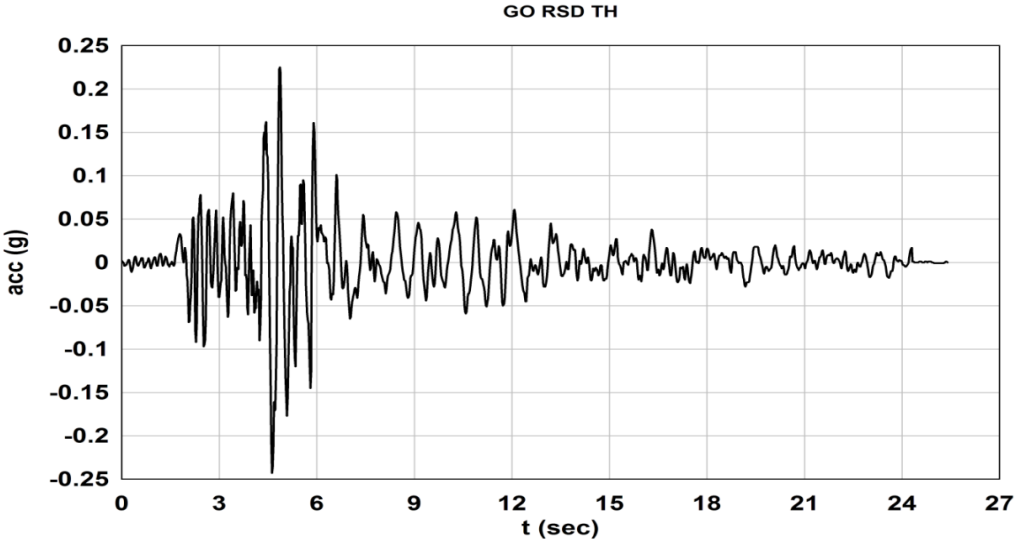

Figure 5.18 Residual part of the acceleration time-history at Gopeshwar site.

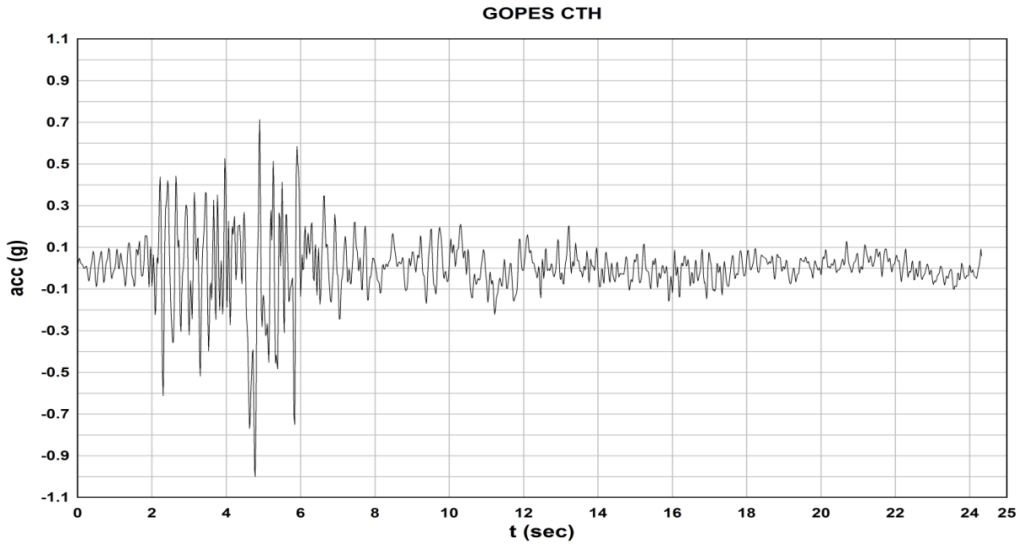

Figure 5.19 Compatible acceleration time-history (normalized) with respect to estimated ground motion response-spectra at Gopeshwar site.

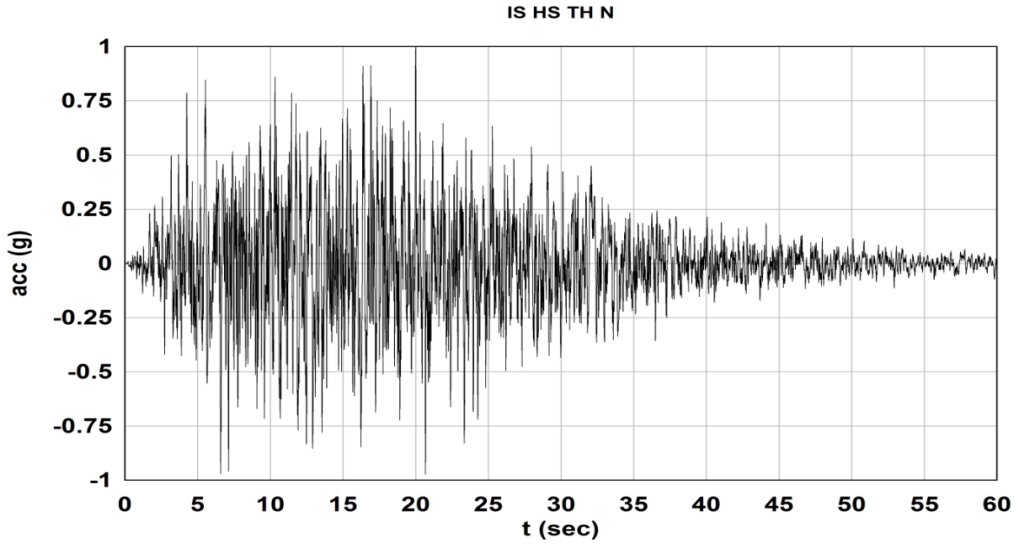

Figure 5.20 Compatible acceleration time-history (normalized) with respect to IS codal response-spectra at stiff soil/rock.

5.4 Dynamic Analysis of Building Models

The two types of building frame models having step-back (Fig. 5.1), and a combination of step-back and set-back configuration (Fig. 5.2) are taken for studying the dynamic analysis, i.e., free vibration analysis and seismic response analysis which includes response spectrum analysis (RSA) and modal time history analysis (MTHA).

5.4.1 Free Vibration Analysis of Building Models

The natural time periods of vibration of studied step-back and step-back-set-back building models are listed in **Table 5.3**. The number of modes selected for performing dynamic analysis

is limited to ensure that the modal mass participation is more than 90 percent. Mode shapes for the first six modes of each type of model have been plotted in **Figures 5.21 to 5.24** for step-back building models (SB), and in **Figures 5.25 to 5.28** for step-back-set-back building models (SBSB).

Table 5.3 Natural time periods of SB and SBSB building models

212SB		**313SB**		**413SB**		**513SB**	
Mode	Period (sec)	Mode	Period (sec)	Mode	Period (sec)	Mode	Period (sec)
1	0.694958	1	0.932731	1	1.320758	1	1.729388
2	0.442638	2	0.470397	2	0.822945	2	1.190086
3	0.362654	3	0.379641	3	0.650819	3	0.940206
4	0.274022	4	0.368618	4	0.475625	4	0.593671
5	0.161264	5	0.260395	5	0.325980	5	0.416563
6	0.157328	6	0.179437	6	0.282216	6	0.361191
7	0.134577	7	0.165569	7	0.249374	7	0.297548
8	0.113887	8	0.158508	8	0.214774	8	0.297237
9	0.082048	9	0.156666	9	0.178496	9	0.261340
10	0.061043	10	0.120502	10	0.158359	10	0.233519
11	0.060568	11	0.113868	11	0.156503	11	0.178557
12	0.049405	12	0.084294	12	0.154499	12	0.178311
-------		13	0.083085	13	0.117249	13	0.158340
		14	0.081841	-------		14	0.156480
		-------				15	0.146595
212SBSB		**313SBSB**		**414SBSB**		**515SBSB**	
Mode	Period (sec)	Mode	Period (sec)	Mode	Period (sec)	Mode	Period (sec)
1	0.521410	1	0.753973	1	1.005135	1	1.032126
2	0.404029	2	0.458362	2	0.498878	2	0.585801
3	0.325986	3	0.356000	3	0.433382	3	0.457991
4	0.272654	4	0.352995	4	0.369800	4	0.375879
5	0.158288	5	0.264507	5	0.323824	5	0.362852
6	0.156433	6	0.177520	6	0.257844	6	0.302095
7	0.129857	7	0.163696	7	0.191679	7	0.257107
8	0.114773	8	0.158427	8	0.188015	8	0.202766
9	0.083310	9	0.156510	9	0.172388	9	0.196513
-------		10	0.121518	10	0.158248	10	0.178446
		11	0.113927	11	0.156387	11	0.166918
		12	0.081997	12	0.144558	12	0.161669
		-------		13	0.116550	13	0.158171
				-------		14	0.156295
						15	0.132320

a) Modal Analysis of Step-Back Building Models

Mode shapes for the first six modes of vibrations have been plotted in **Figures 5.21 to 5.24** for Step-Back (SB) building models. Free vibration analysis of these SB building models shows that the **first** and **fourth** modes of vibration are across the slope, **second** mode of vibration is a combination of vibration across the slope and torsional vibration, and **third** mode of vibration is along the slope for all the SB building models. Whereas, the **fifth** mode of vibration, for 212SB building model is a combination of vibration across the slope and torsional vibration, and for 313SB, 413SB and 513SB building models is across the slope. Further, the **sixth** mode of vibration, for 212SB building model is across the slope, and for 313SB, 413SB and 513SB building models is a combination of vibration across the slope and torsional vibration. It is observed that as the number of storeys increases, the **first-mode** time periods, i.e., across the slope, increases significantly. Whereas, there is not much variation in the time period along the slope, i.e., **third-mode**, for 212SB and 313SB building models, however, the 413SB and 513SB building models show increase in time period compared to 212SB and 313SB building models.

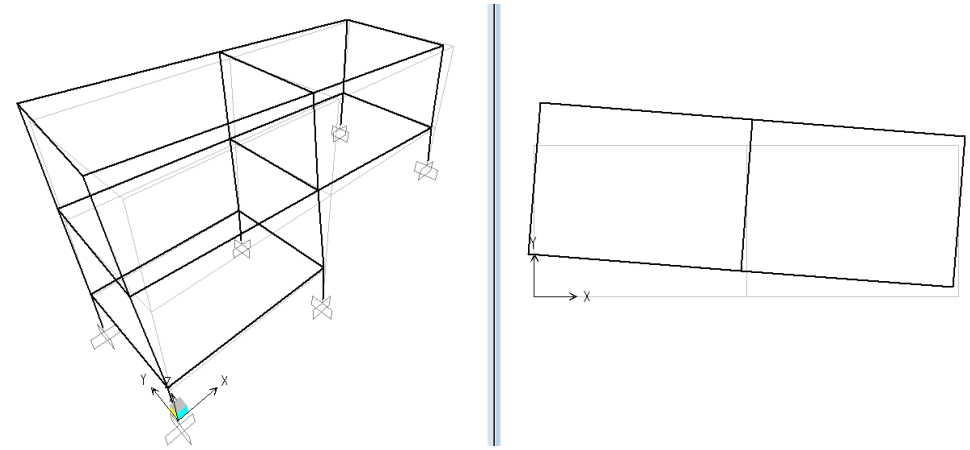

First Mode Shape, T = 0.694958 second

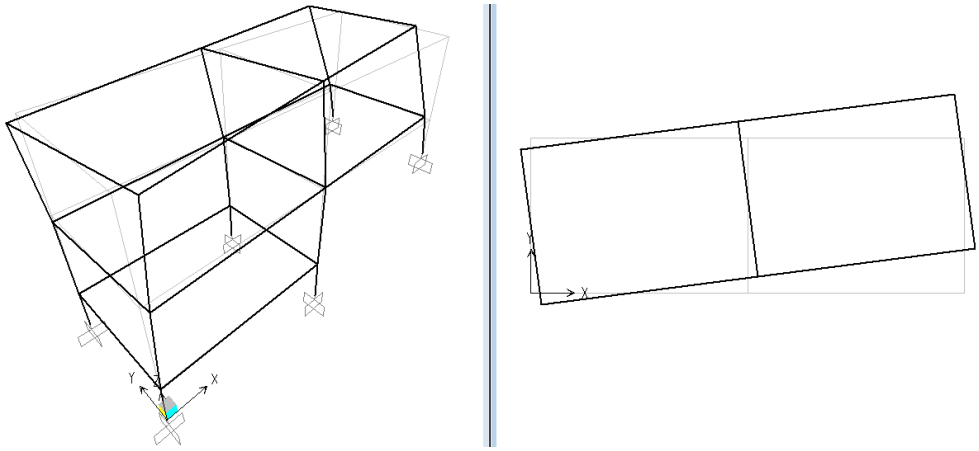

Second Mode Shape, T = 0.442638 second

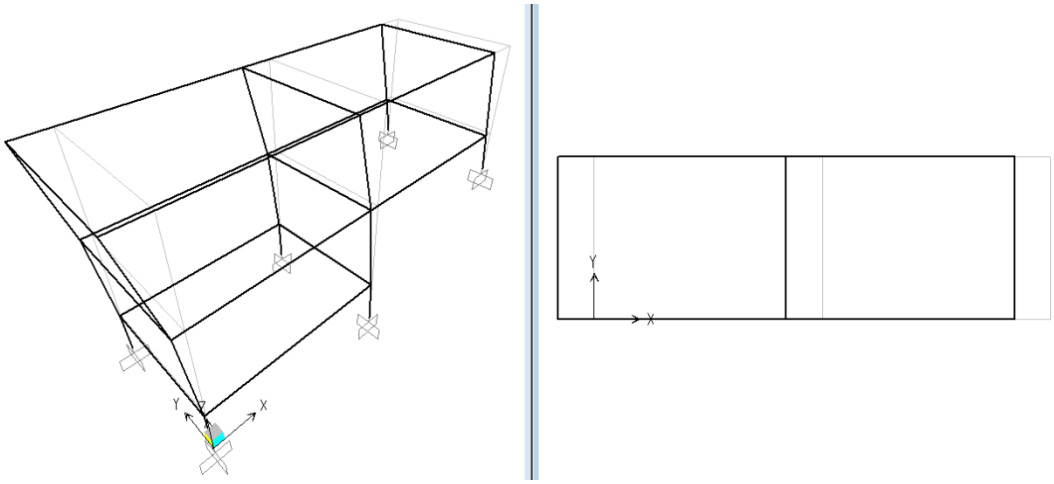

Third Mode Shape, T = 0.362654 second

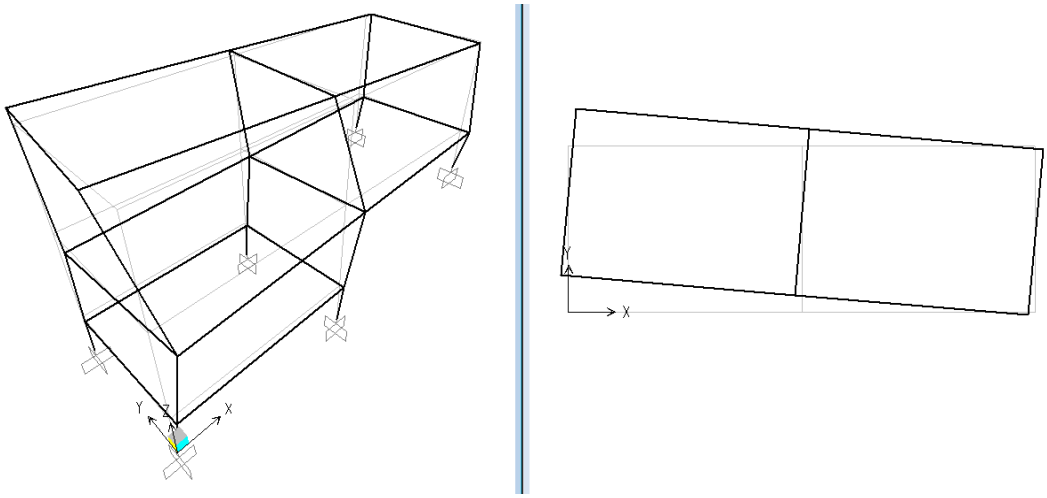

Fourth Mode Shape, T = 0.274022 second

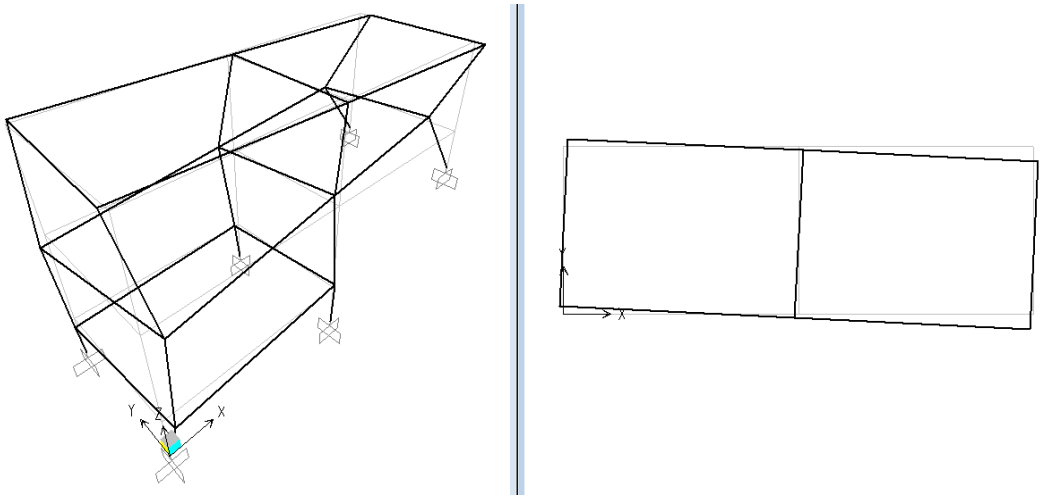

Fifth Mode Shape, T = 0.161264 second

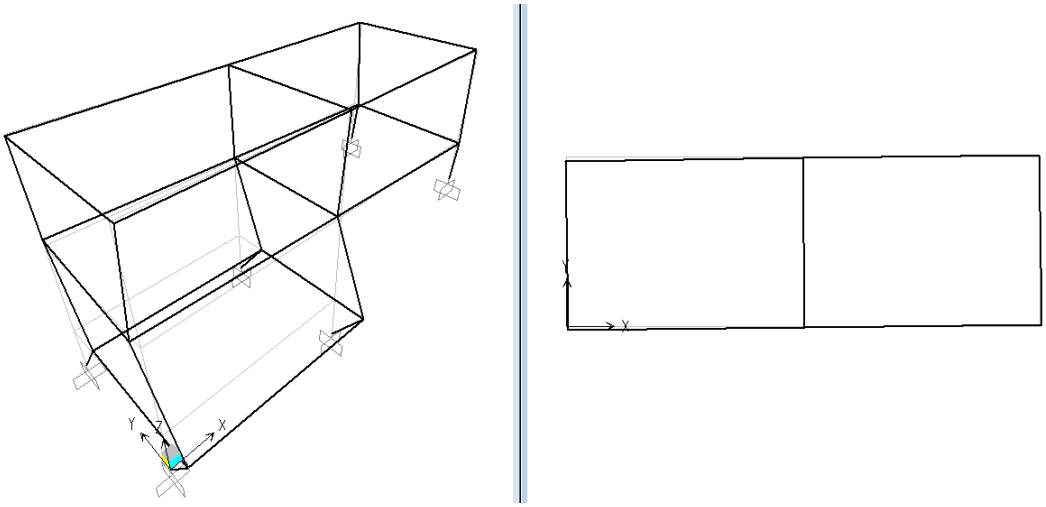

Sixth Mode Shape, T = 0.157328 second

Figure 5.21 First six mode shapes of two storey step-back building model.

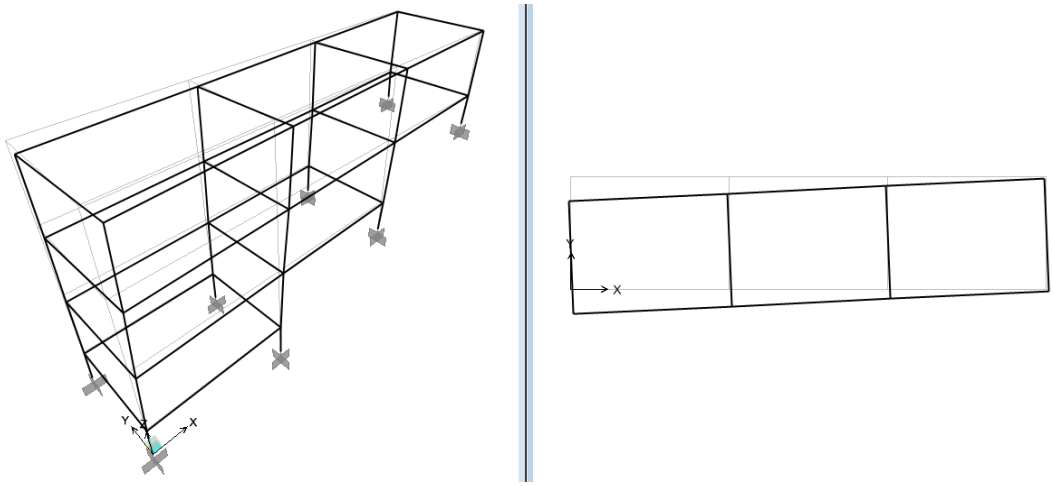

First Mode Shape, T = 0.932731 second

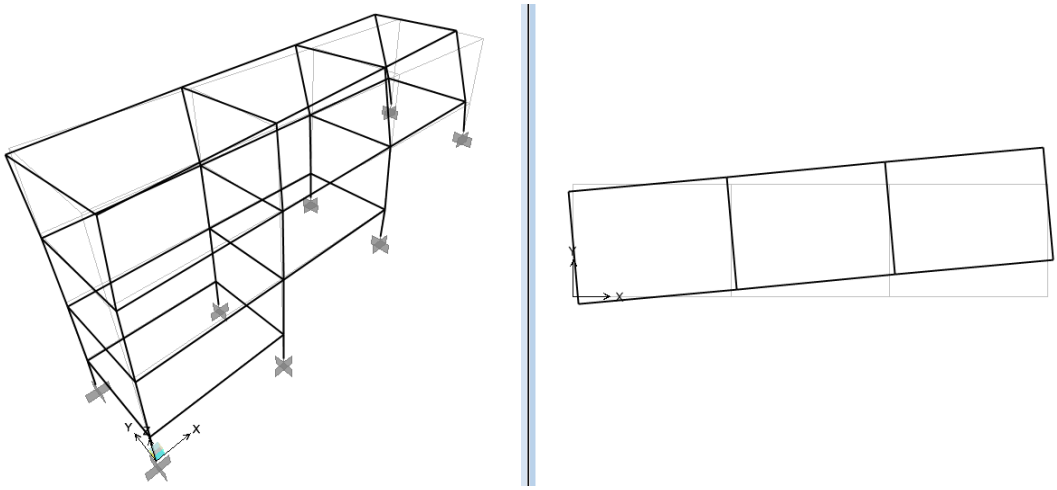

Second Mode Shape, T = 0.470397 second

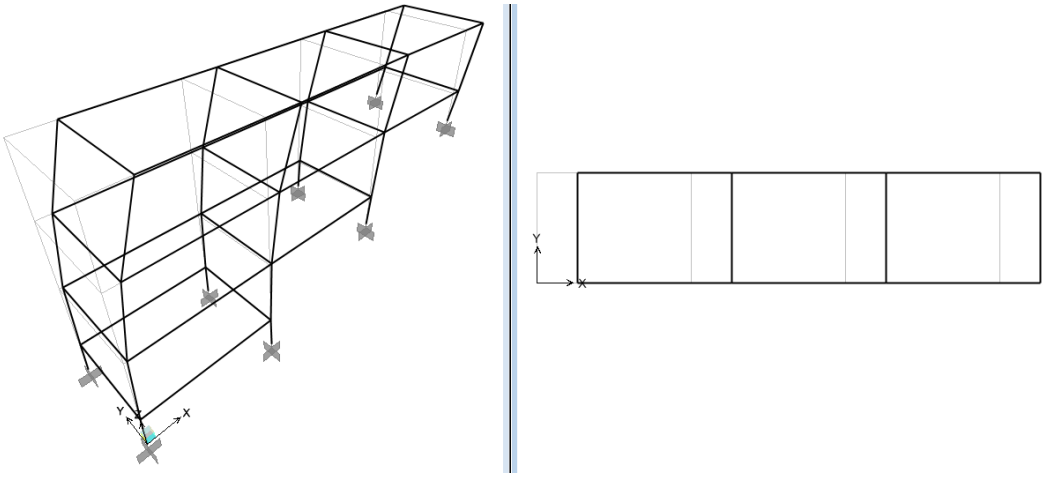

Third Mode Shape, T = 0.379641 second

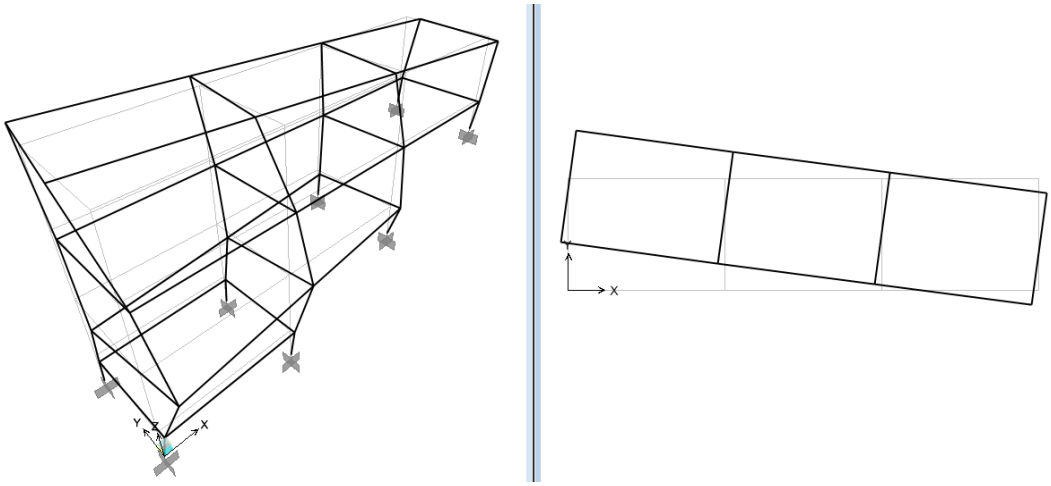

Fourth Mode Shape, T = 0.368618 second

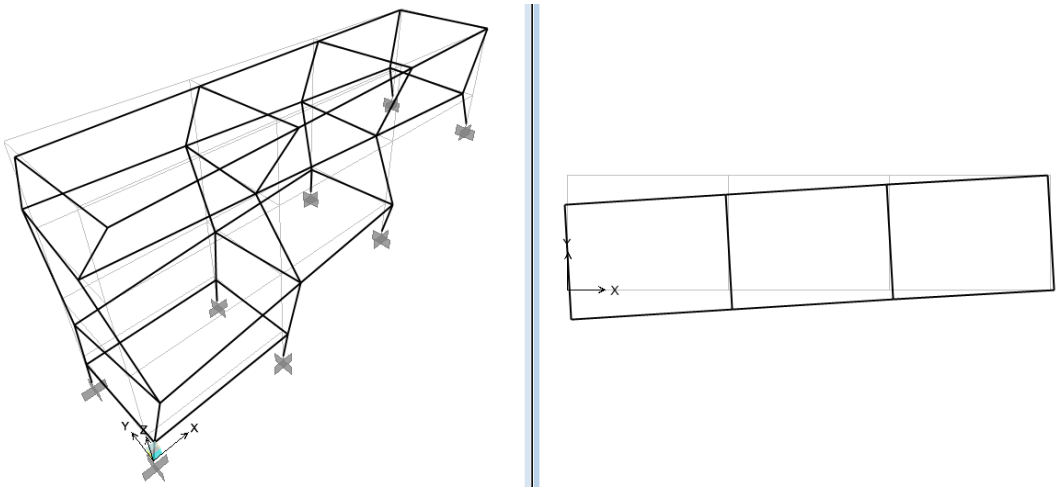

Fifth Mode Shape, T = 0.260395 second

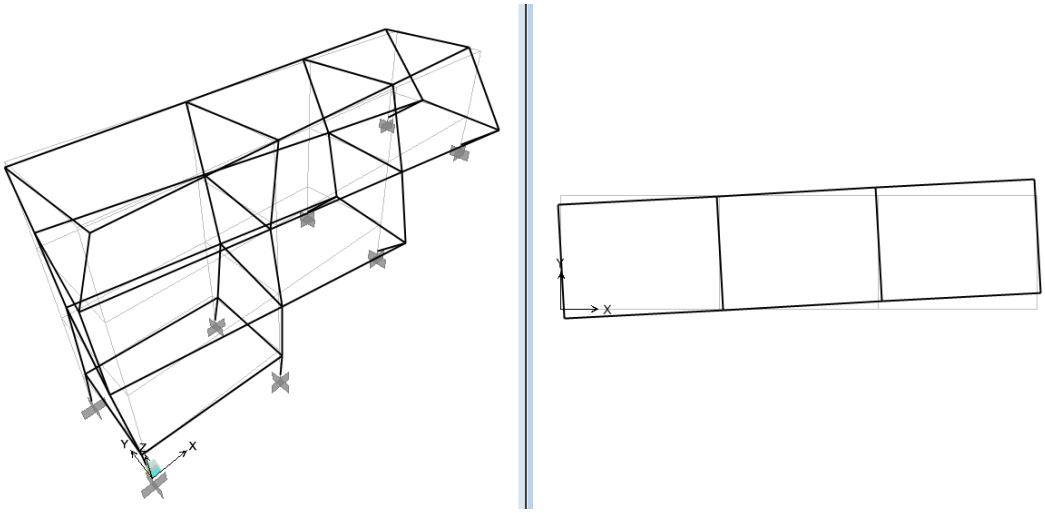

Sixth Mode Shape, T = 0.179437 second

Figure 5.22 First six mode shapes of three storey step-back building model.

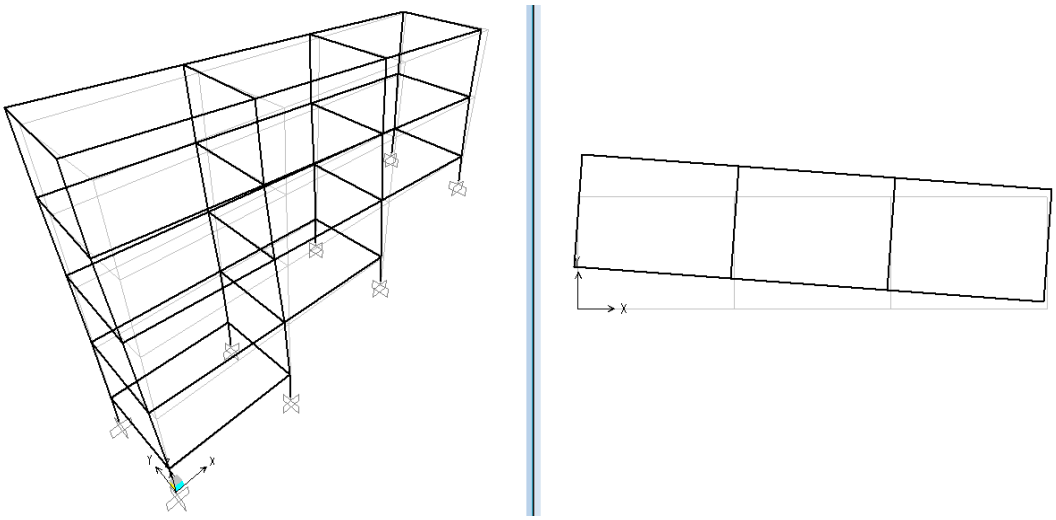

First Mode Shape, T = 1.320758 second

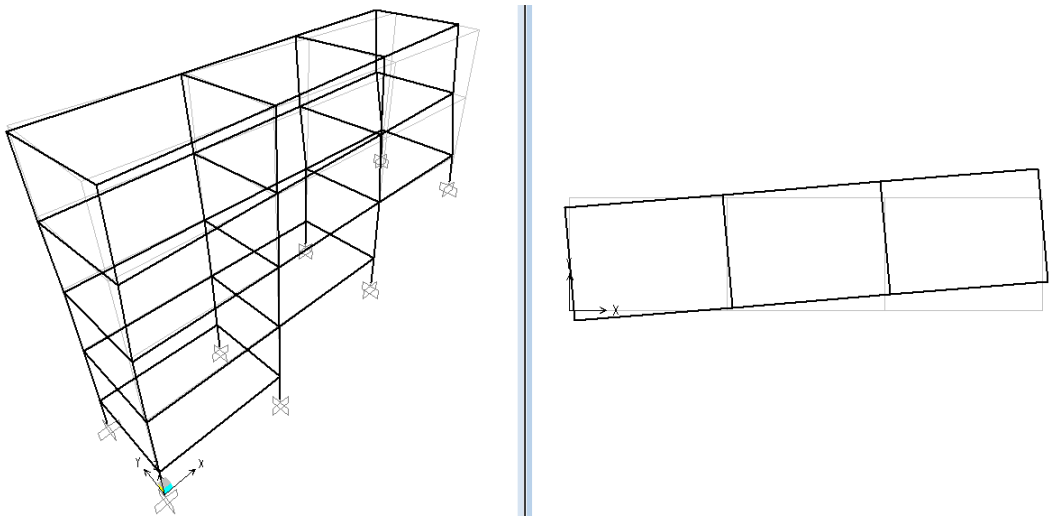

Second Mode Shape, T = 0.822945 second

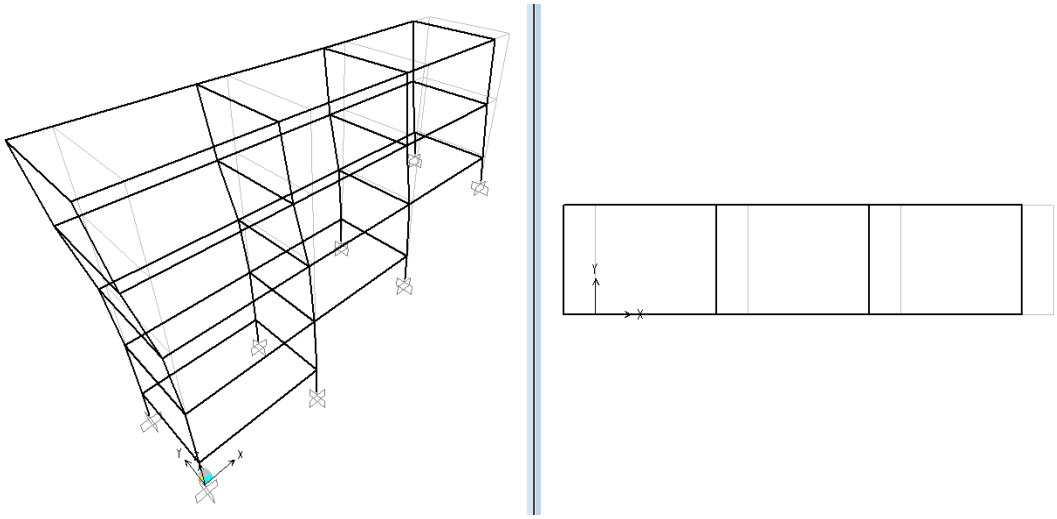

Third Mode Shape, T = 0.650819 second

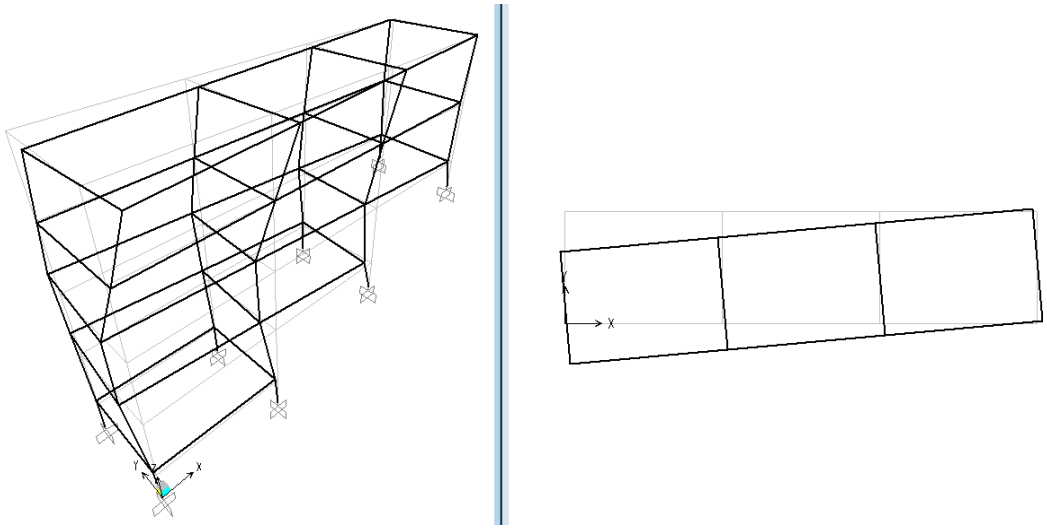

Fourth Mode Shape, T = 0.475625 second

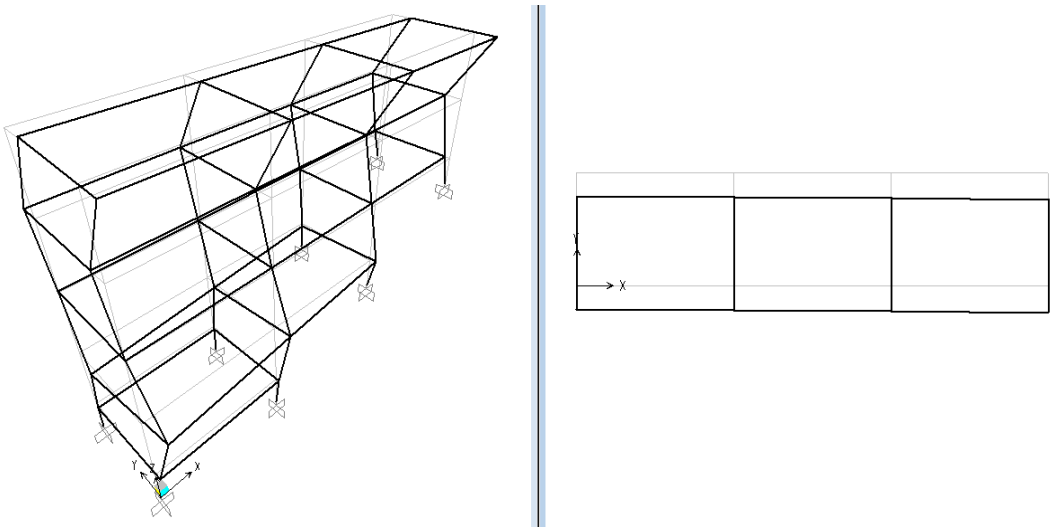

Fifth Mode Shape, T = 0.325980 second

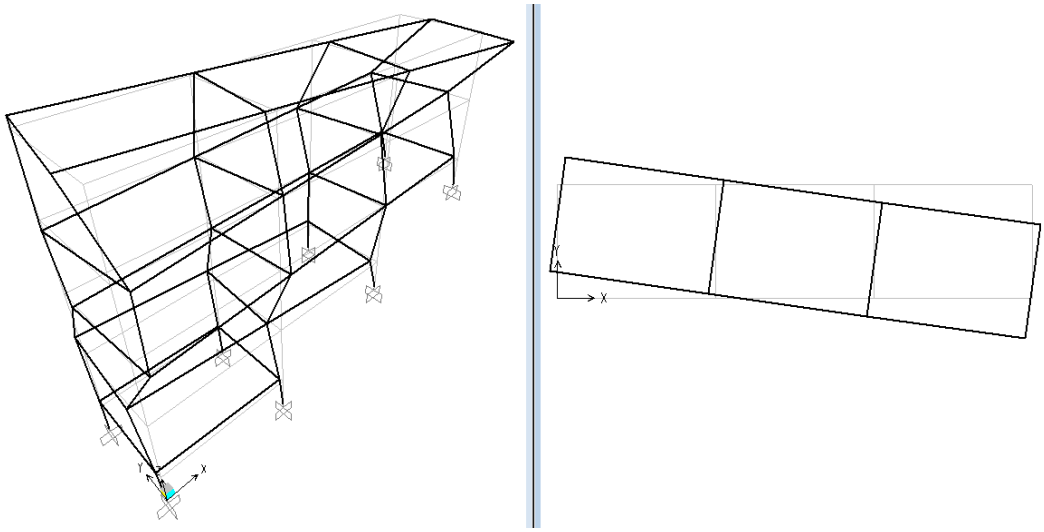

Sixth Mode Shape, T = 282216 second

Figure 5.23 First six mode shapes of four storey step-back building model.

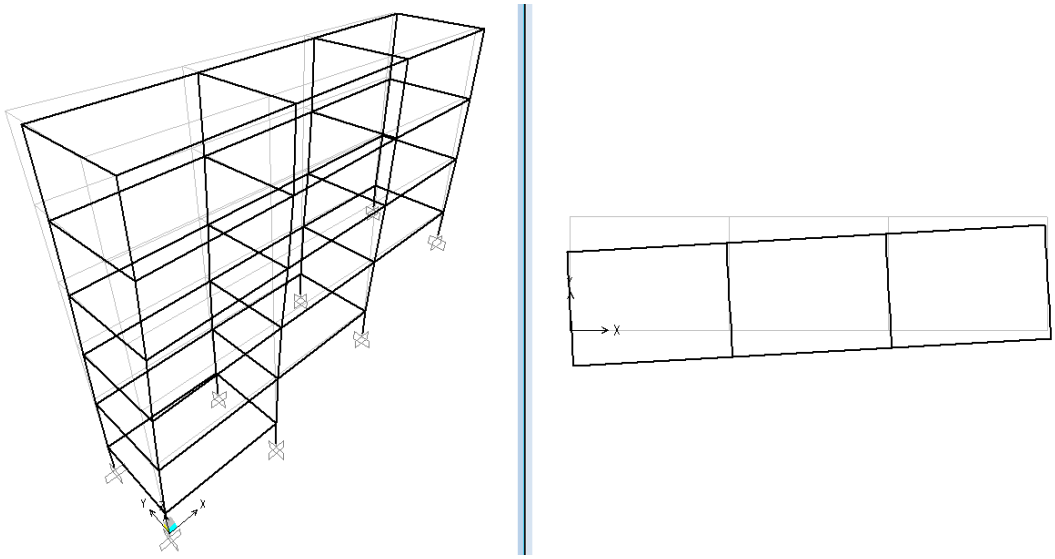

First Mode Shape, T = 1.729388 second

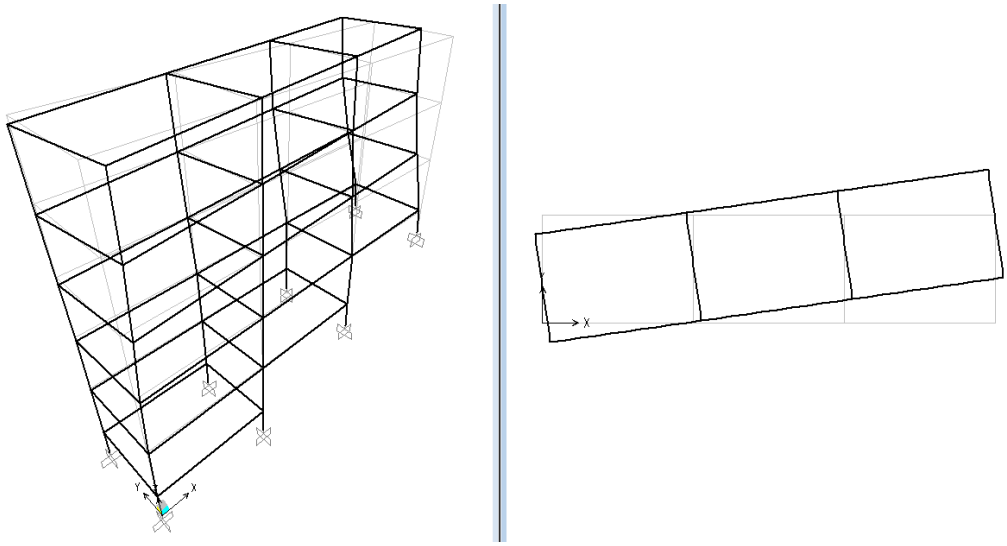

Second Mode Shape, T = 1.190086 second

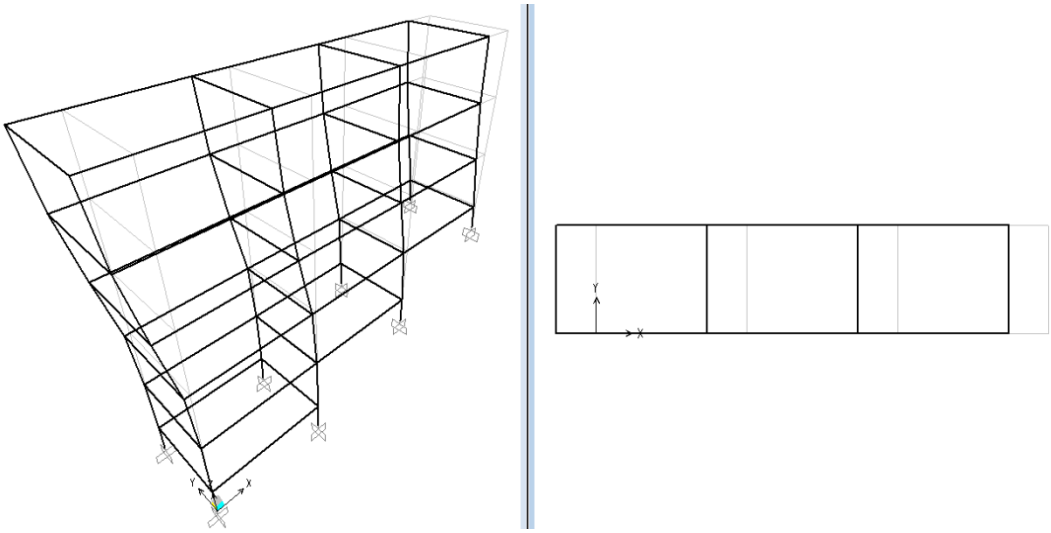

Third Mode Shape, T = 0.940206 second

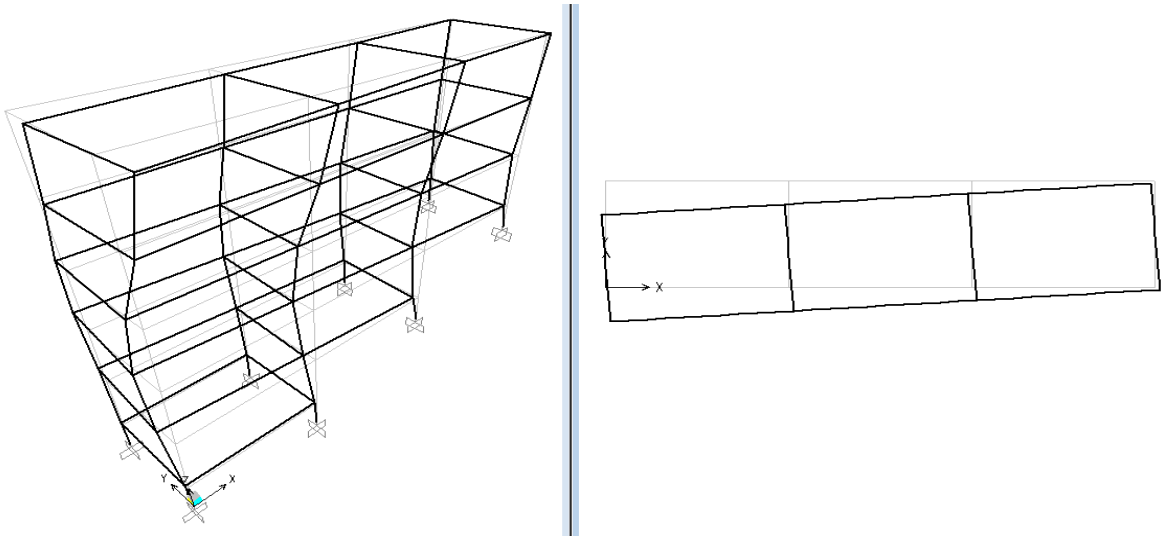

Fourth Mode Shape, T = 0.593671 second

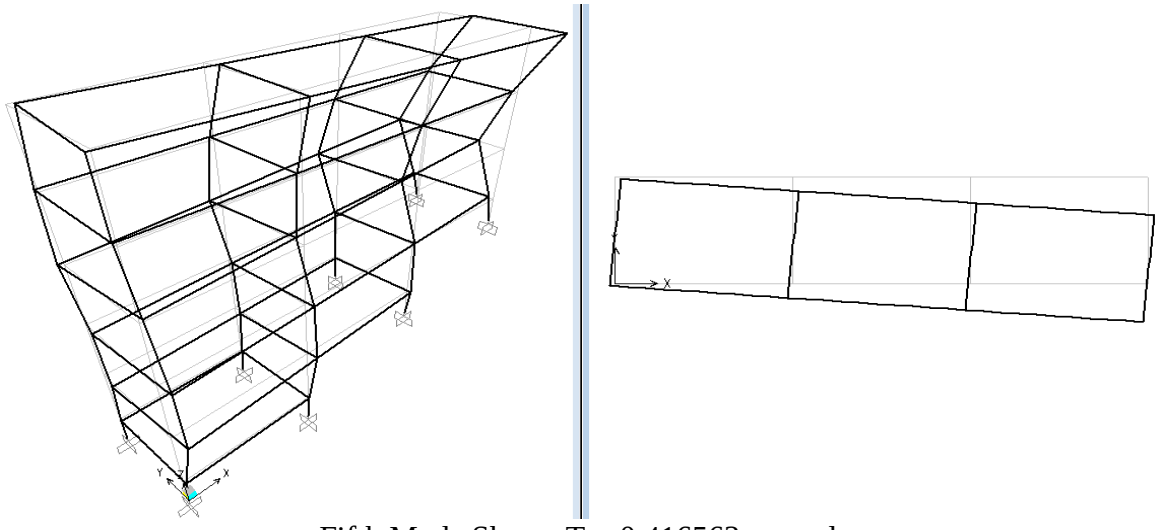

Fifth Mode Shape, T = 0.416563 second

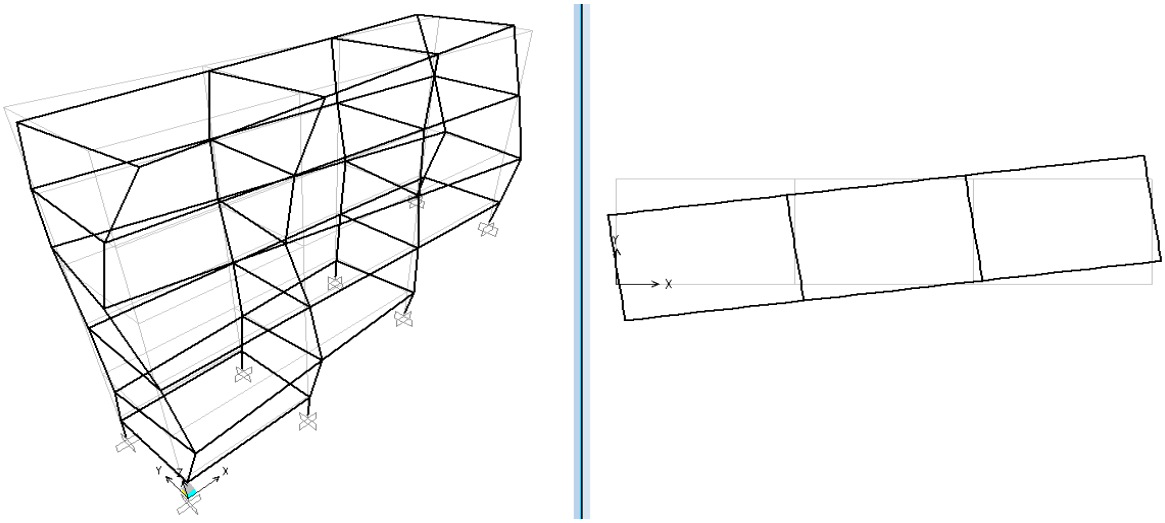

Sixth Mode Shape, T = 0.361191 second

Figure 5.24 First six mode shapes of five storey step-back building model.

b) Modal Analysis of Step-Back-Set-Back Building Models

Mode shapes for the first six modes of vibrations have been plotted in **Figures 5.25 to 5.28** for Step-Back-Set-Back (SBSB) building models. Free vibration analysis of these SBSB building models shows that the **first** mode of vibration is across the slope for all the SBSB building models. The **second** and **sixth** modes of vibration, for 212SBSB, 313SBSB building models is a combination of vibration across the slope and torsional vibration, and for 414SBSB, 515SBSB building models is across the slope. The **third** mode of vibration, for 212SBSB building model is along the slope, and for 313SBSB, 414SBSB, 515SBSB building models is a combination of vibration across the slope and torsional vibration. The **fourth** mode of vibration, for 313SBSB, 414SBSB building models is along the slope, and for 212SBSB, 515SBSB building models is a combination of vibration across the slope and torsional vibration. The **fifth** mode of vibration, for 515SBSB building model is along the slope, for 212SBSB building model is a combination of vibration across the slope and torsional vibration, and for 313SBSB, 414SBSB building models is across the slope. It is observed that as the number of storeys increases, the **first-mode** time periods, i.e., fundamental time period across the slope, increases significantly, but not much variation have been found in 414SBSB and 515SBSB building models. Whereas, there is not much variation in the fundamental time periods along the slope, i.e., **third-mode**, for 212SBSB building model, **fourth-mode** for 313SBSB and 414SBSB building models, and **fifth-mode** for 515SBSB building model.

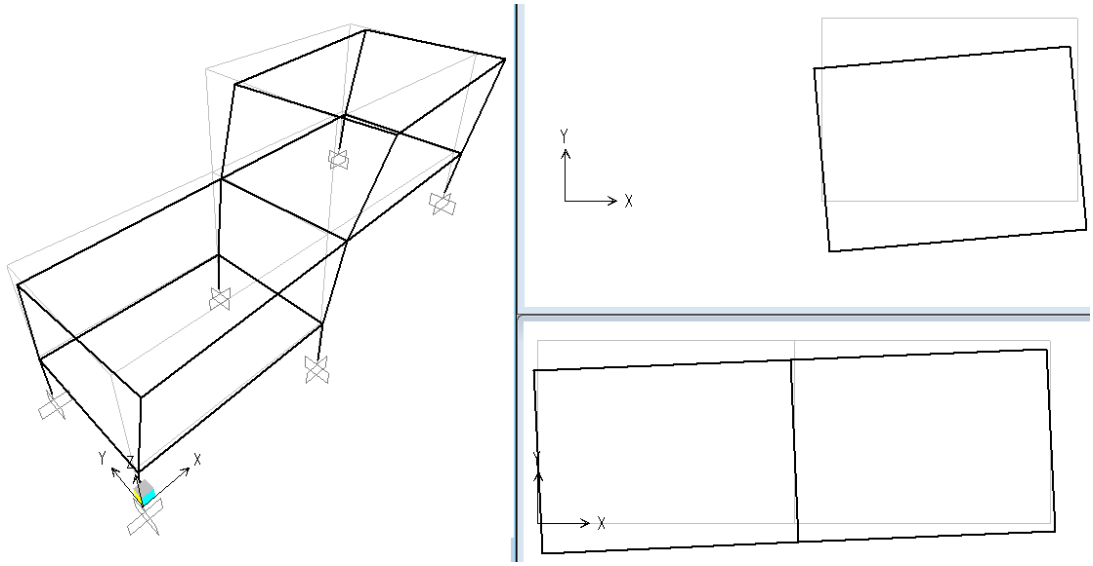

First Mode Shape, T = 0.521410 second

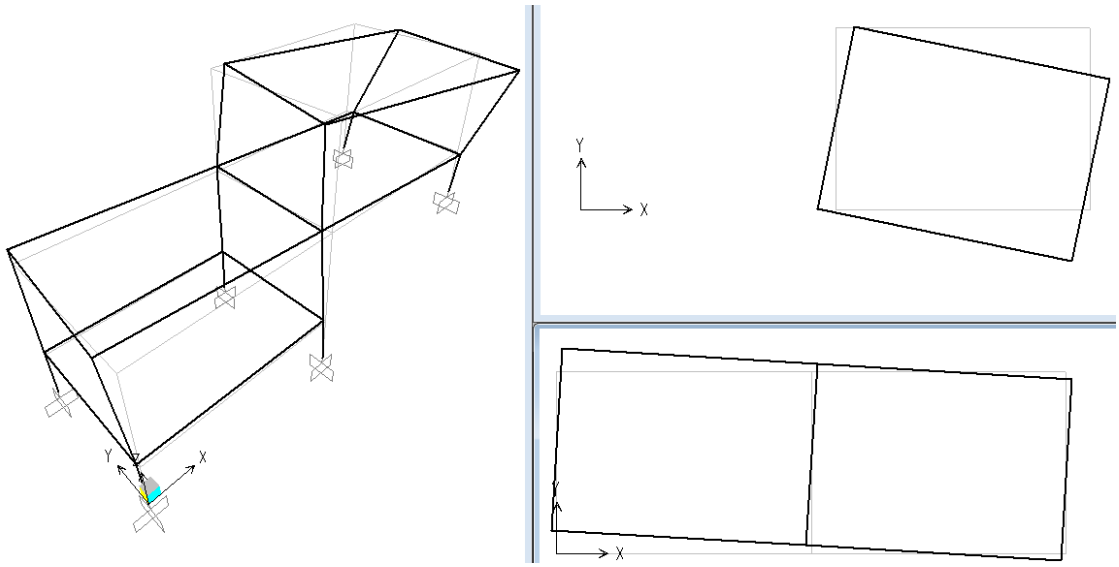

Second Mode Shape, T = 0.404029 second

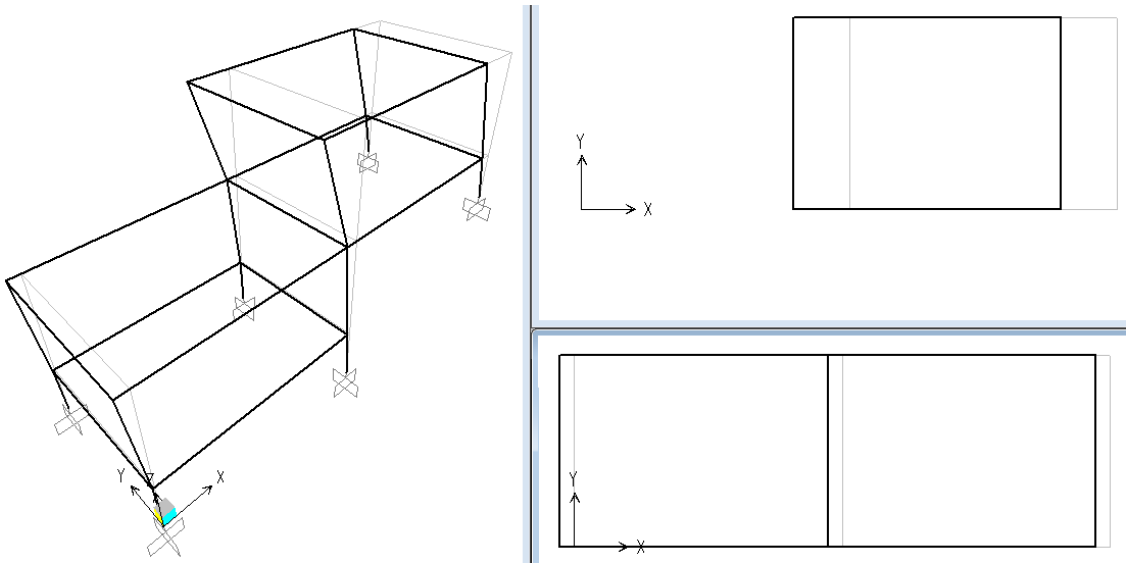

Third Mode Shape, T = 0.325986 second

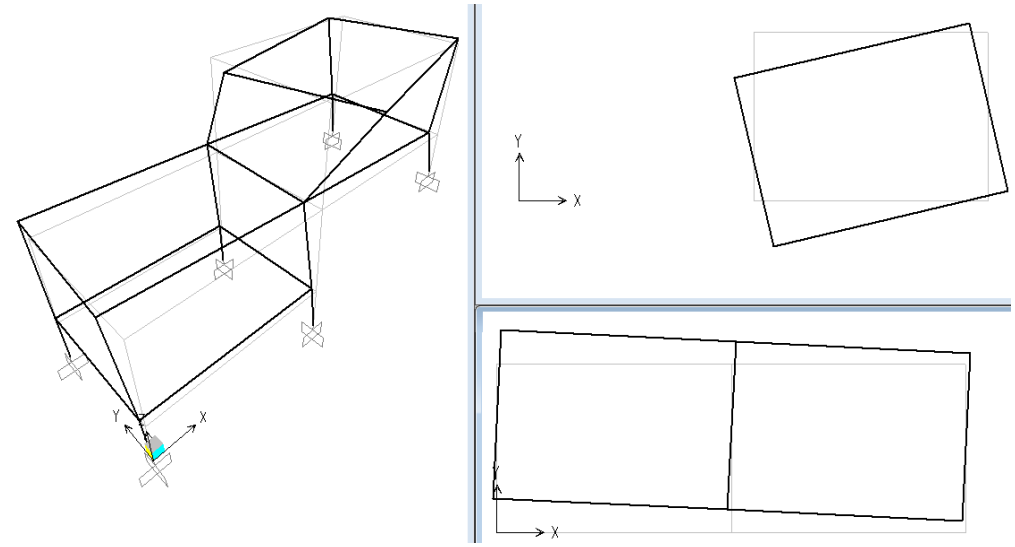

Fourth Mode Shape, T = 0.272654 second

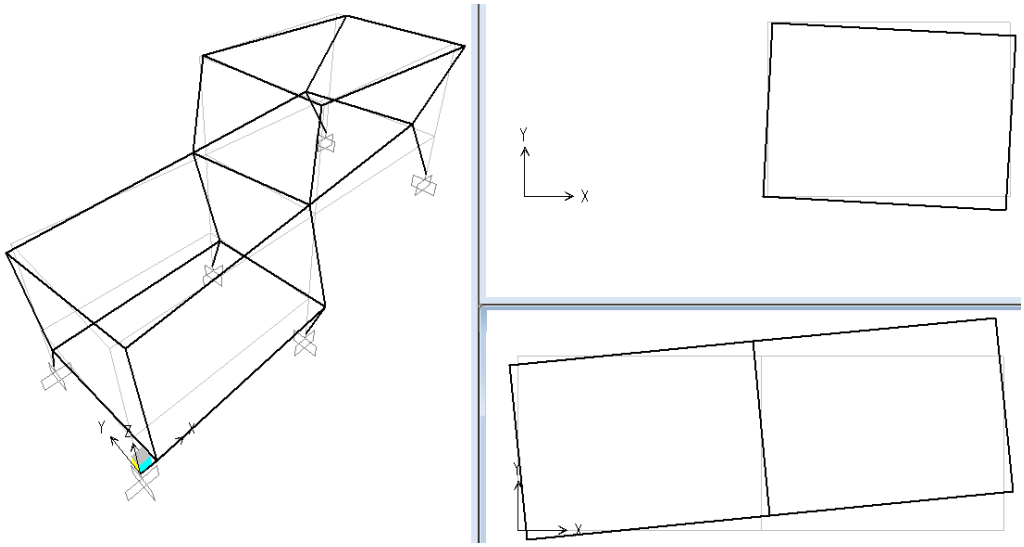

Fifth Mode Shape, T = 0.158288 second

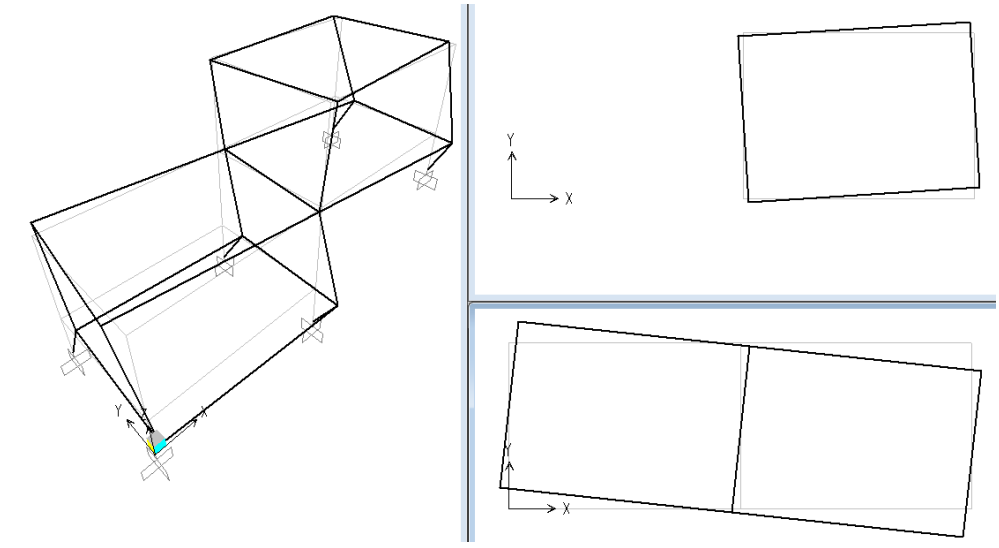

Sixth Mode Shape, T = 0.156433 second

Figure 5.25 First six mode shapes of two storey step-back-set-back building model.

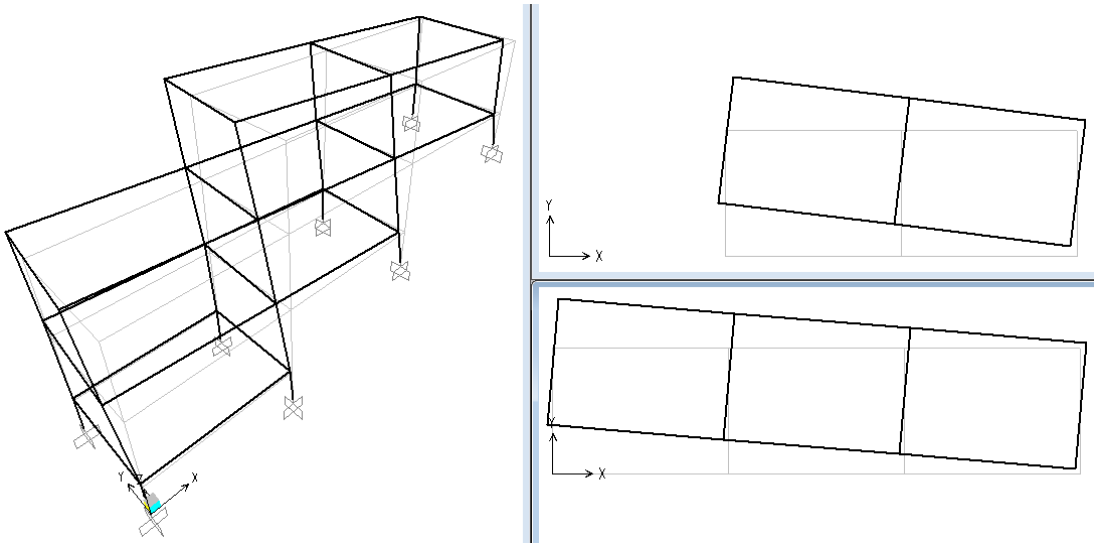

First Mode Shape, T = 0.753973 second

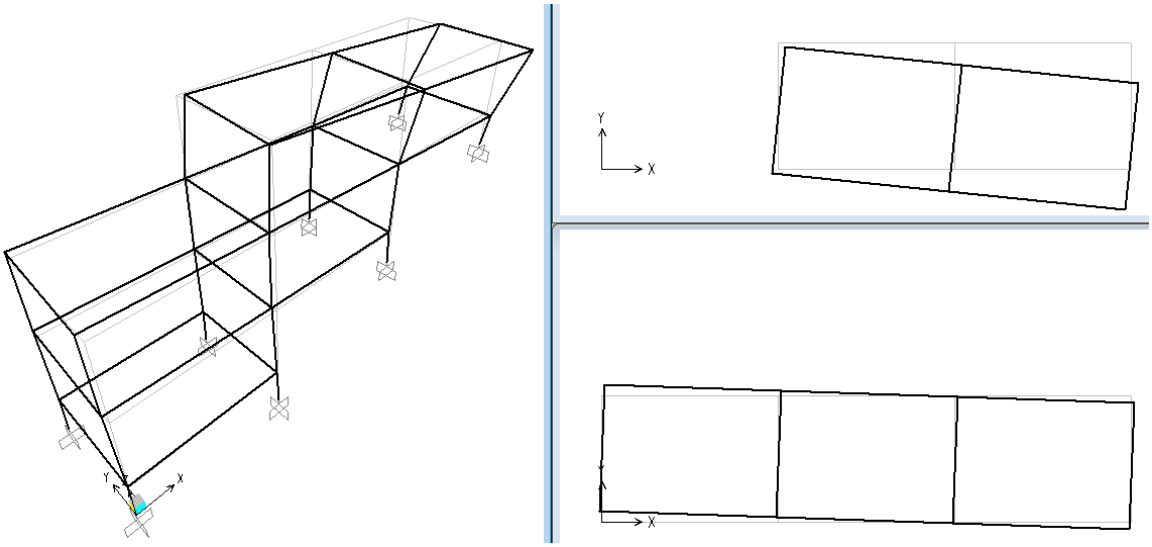

Second Mode Shape, T = 0.458362 second

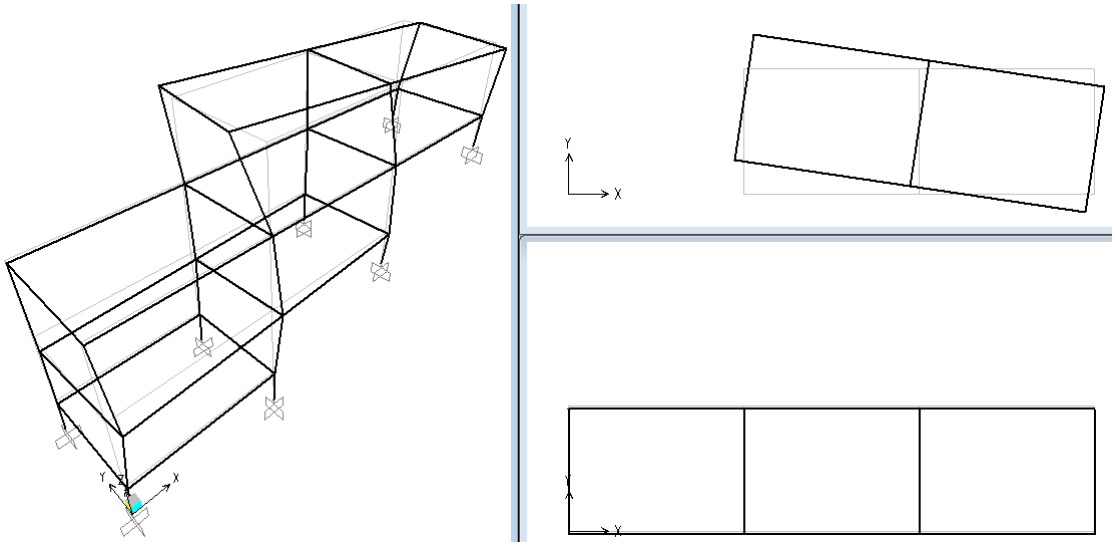

Third Mode Shape, T = 0.356000 second

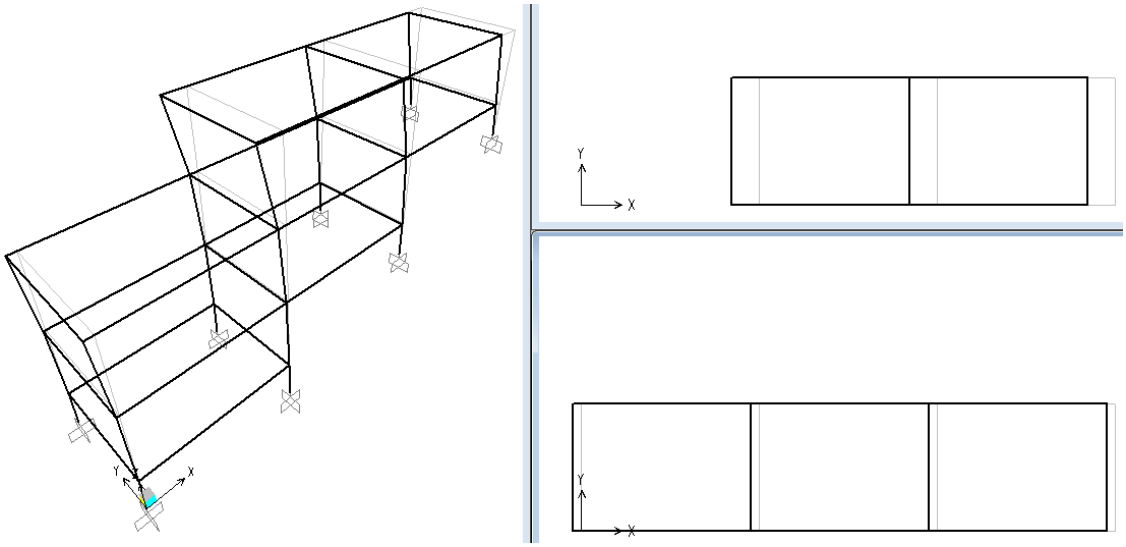

Fourth Mode Shape, T = 0.352995 second

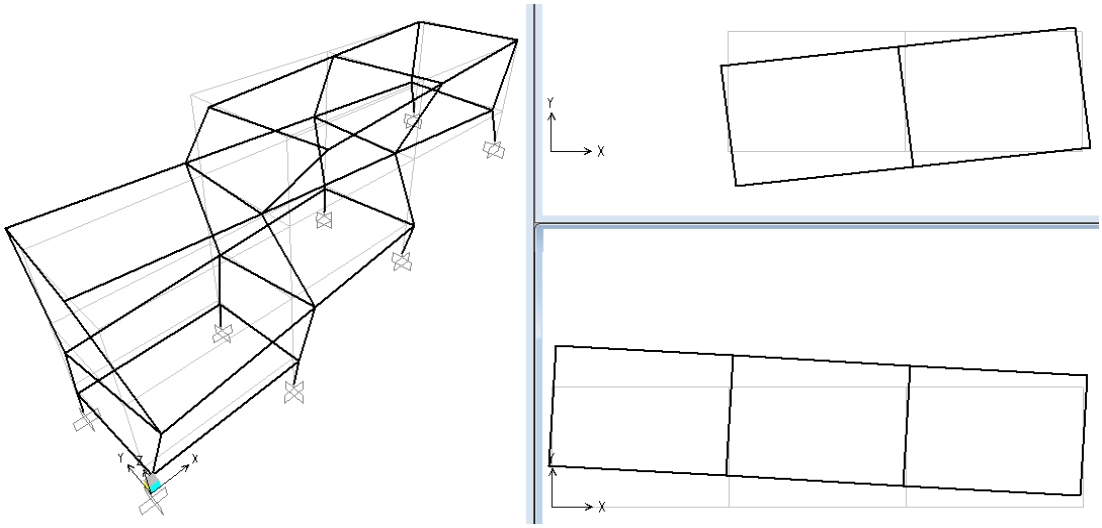

Fifth Mode Shape, T = 0.264507 second

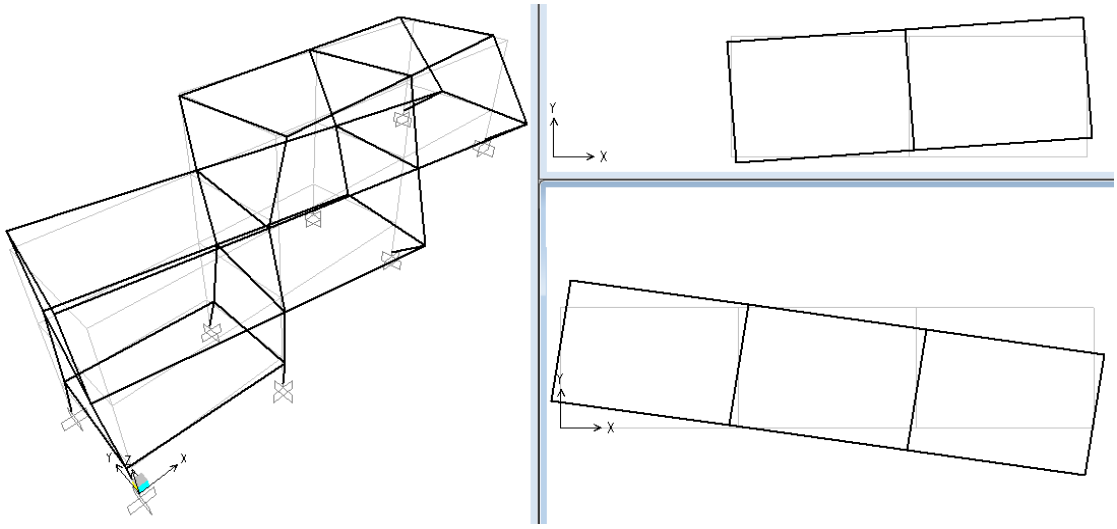

Sixth Mode Shape, T = 0.177520 second

Figure 5.26 First six mode shapes of three storey step-back-set-back building model.

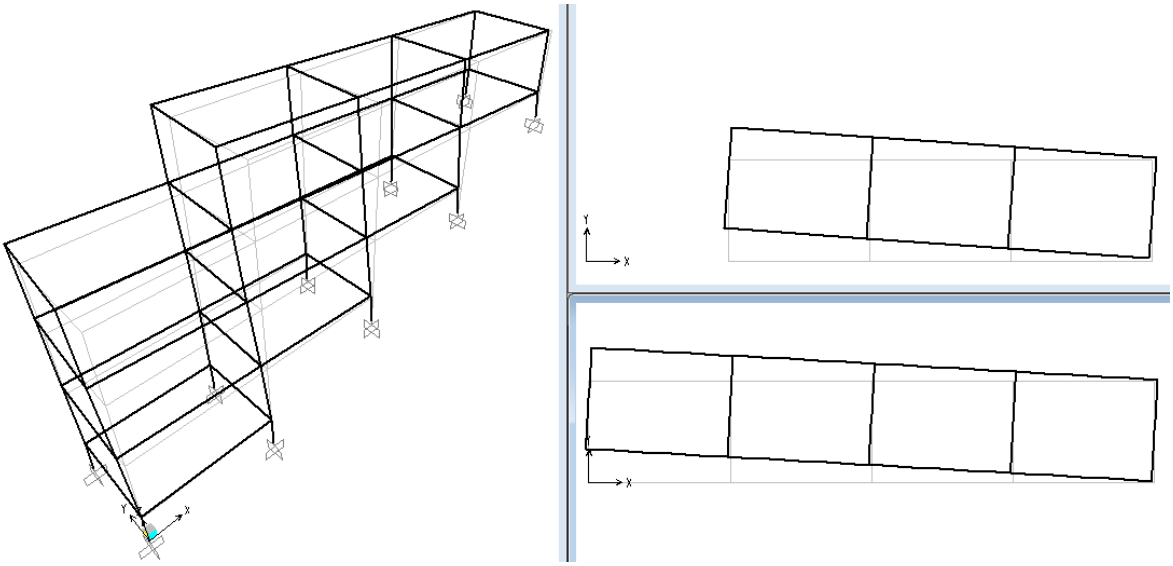

First Mode Shape, T = 1.005135 second

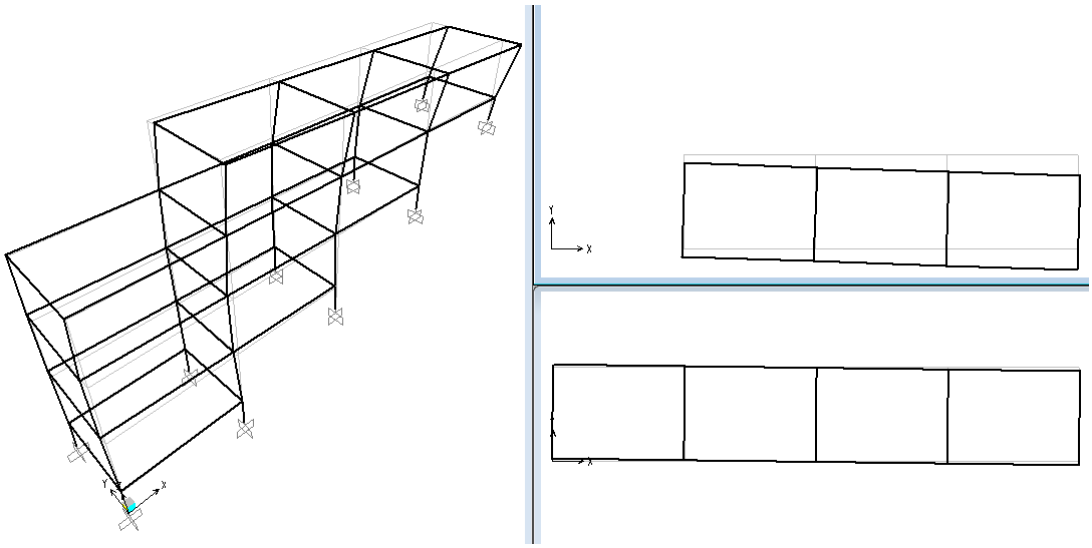

Second Mode Shape, T = 0.498878 second

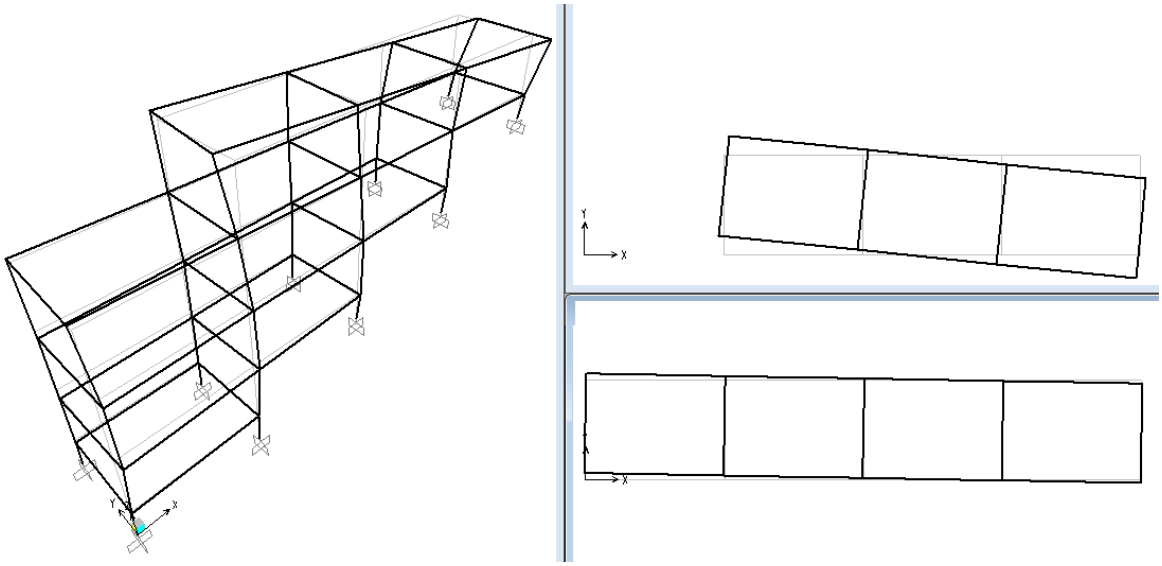

Third Mode Shape, T = 0.433382 second

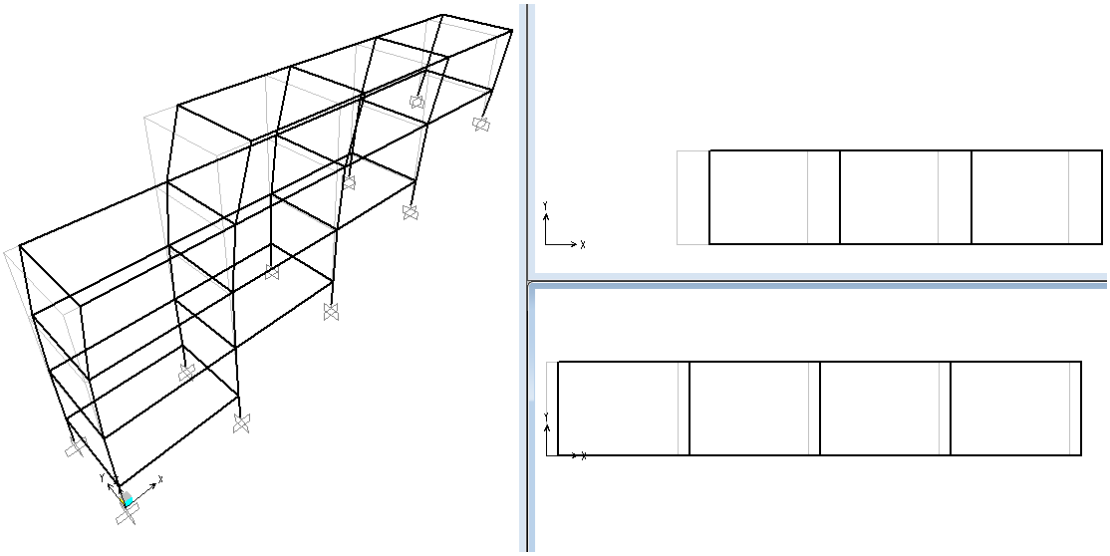

Fourth Mode Shape, T = 0.369800 second

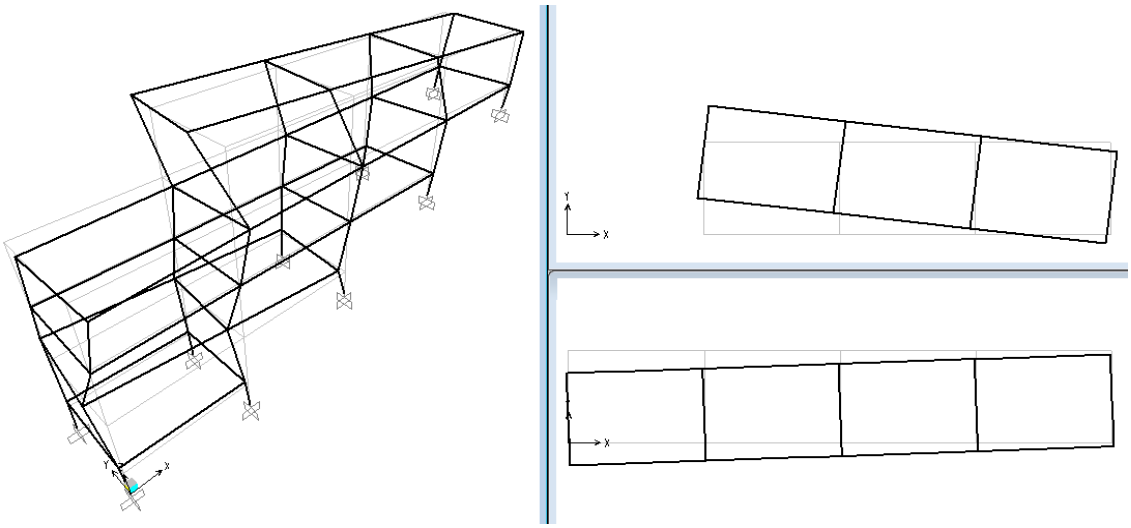

Fifth Mode Shape, T = 0.323824 second

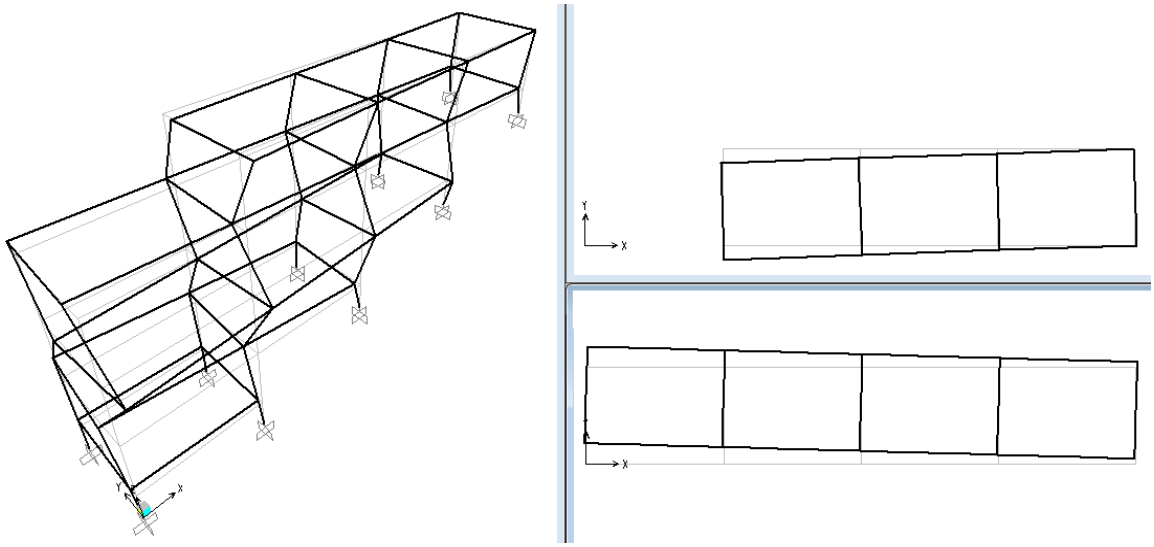

Sixth Mode Shape, T = 0.257844 second

Figure 5.27 First six mode shapes of four storey step-back-set-back building model.

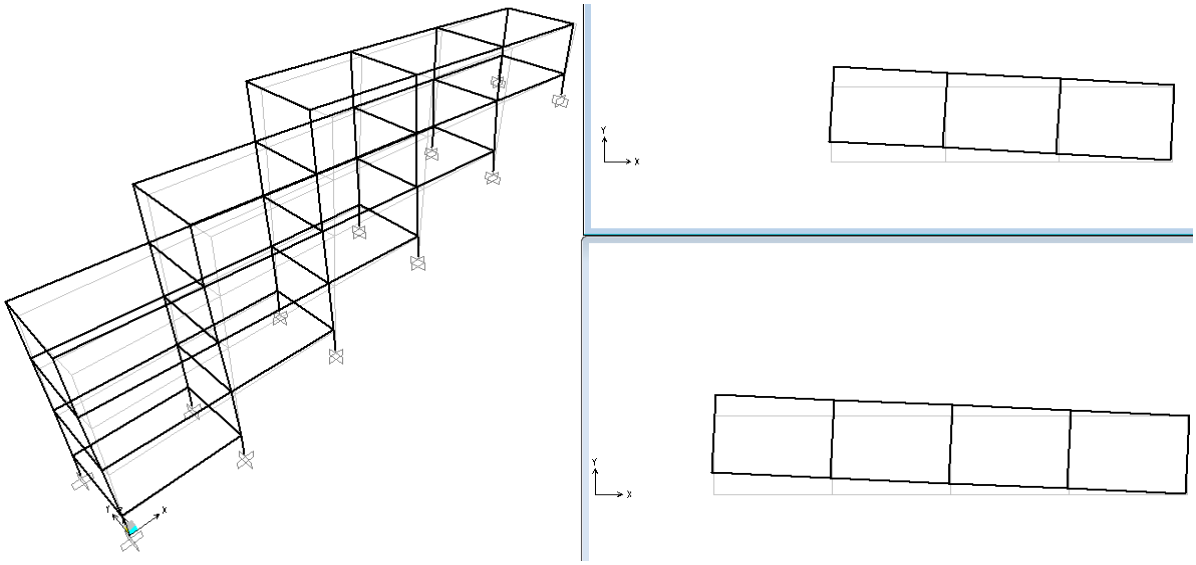

First Mode Shape, T = 1.032126 second

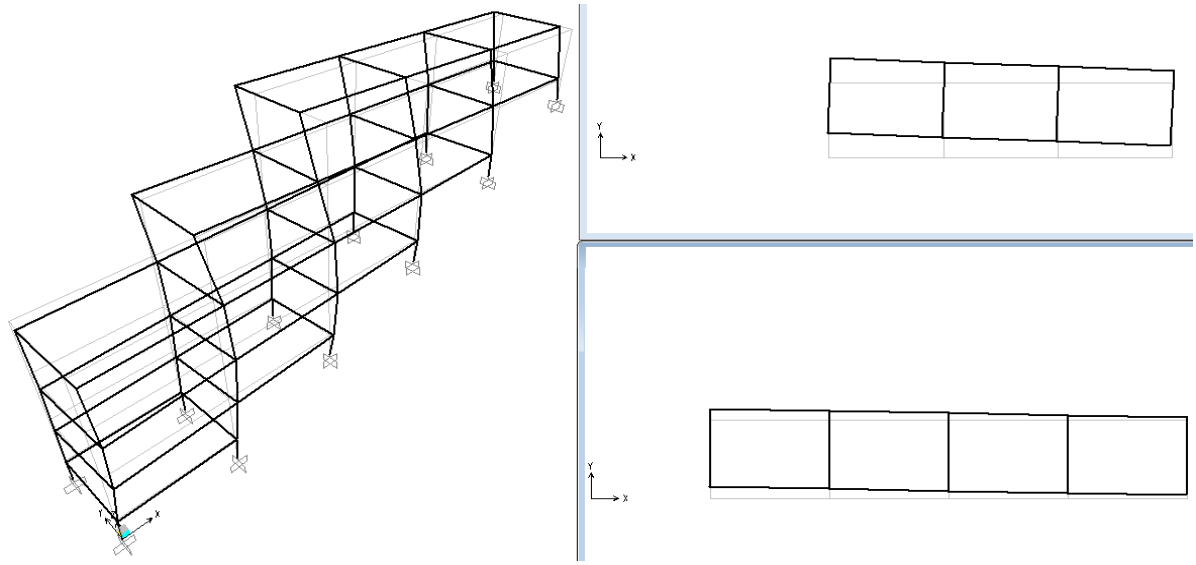

Second Mode Shape, T = 0.585801 second

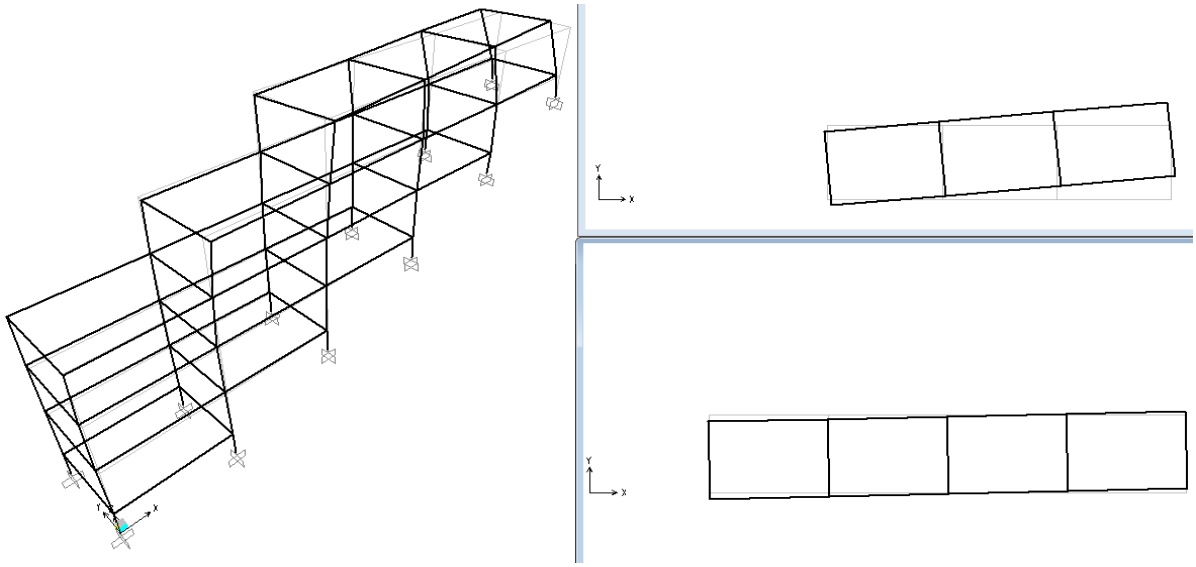

Third Mode Shape, T = 0.457991 second

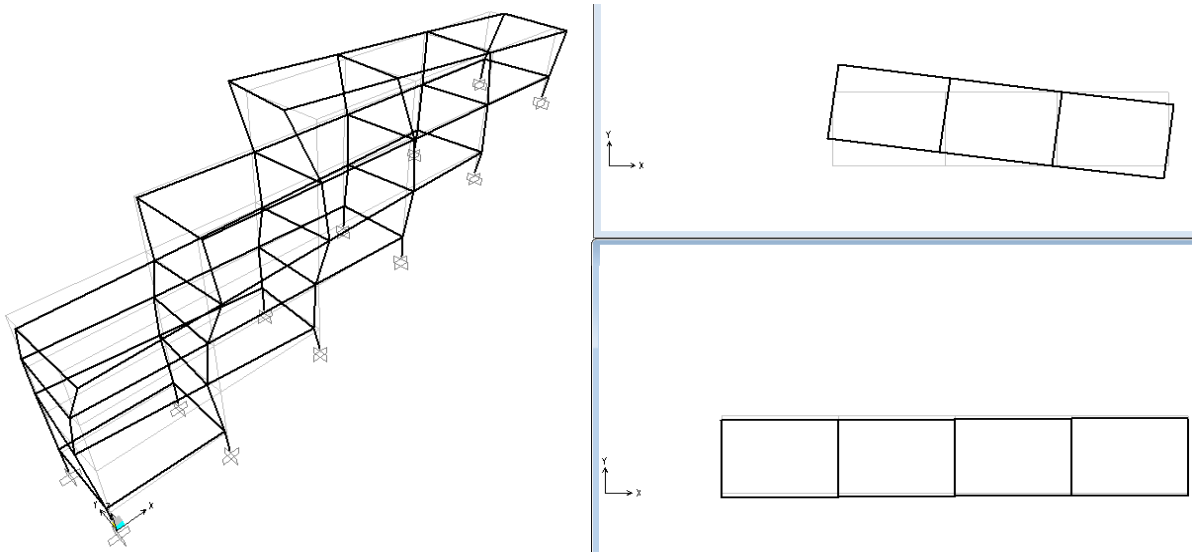

Fourth Mode Shape, T = 0.375879 second

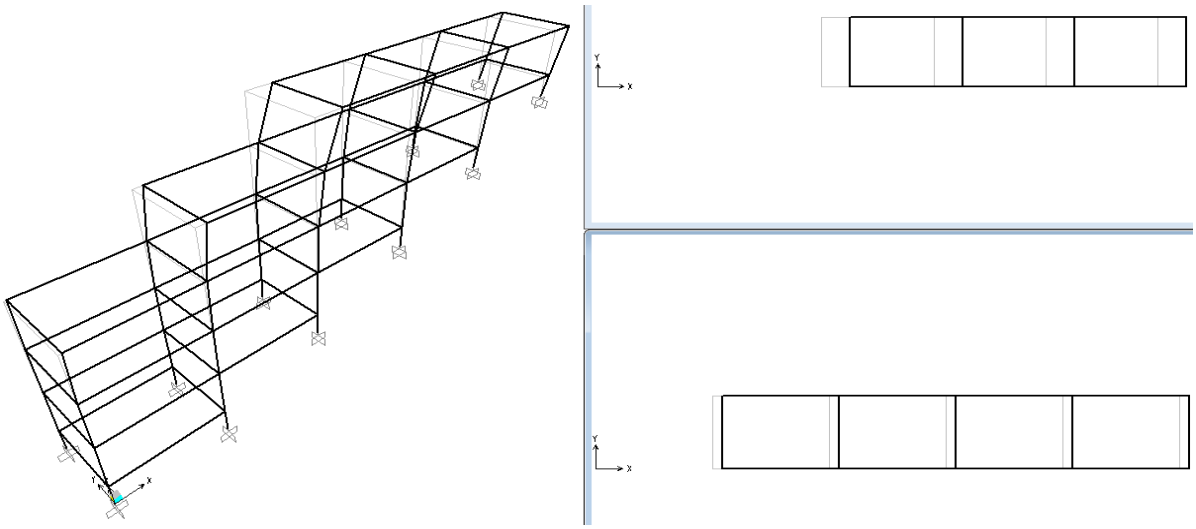

Fifth Mode Shape, T = 0.362852 second

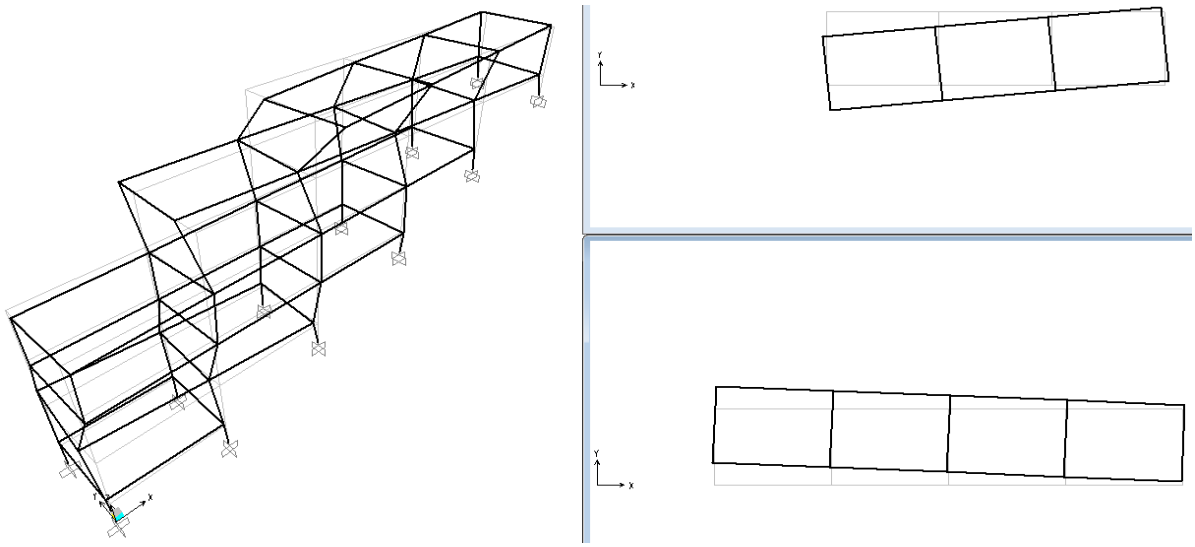

Sixth Mode Shape, T = 0.302095 second

Figure 5.28 First six mode shapes of five storey step-back-set-back building model.

5.4.2 Seismic Analysis

Responses of buildings on hillslope subjected to NFGMs are analyzed. From seismic safety point of view responses due to NFGMs are compared with the responses obtained from conventional types of seismic inputs.

The seismic analysis (Response Spectrum Analysis and Modal Time History Analysis) of buildings is carried out for rigid base (fixed-base) laid on rock site conditions in longitudinal (along the slope, X) and transverse direction (across the slope, Y). The dynamic analysis of all buildings has been carried out adopting:

i) Response spectrum method (according to IS: 1893 (Part 1): 2002).
ii) Response spectra obtained by NFGMs along with their extracted pulses and residual components.
iii) Response spectra obtained by site-specific ground motion (SSGM) at three sites.

The dynamic responses of the buildings were also computed adopting modal time history method, when the base is subjected to different types of ground motion time histories.

a) Response Spectrum Analysis

The seismic analysis of structures cannot be carried out simply based on the peak value of the ground acceleration as the response of the structure depend upon the frequency content of ground motion and its own dynamic properties. To overcome the above difficulties, earthquake response spectrum is the most popular tool in the seismic analysis of structures. There are computational advantages in using the response spectrum method of seismic analysis for prediction of displacements and member forces in structural systems. The method involves the calculation of only the maximum values of the displacements and member forces in each mode of vibration using smooth design spectra that are the average of several earthquake motions.

The analysis consists in determining response in each mode of vibration using response spectrum and then superimposing the responses in various modes to obtain the total response. To estimate the total response of the structure, the contribution of significant modes of vibration is required. The number of modes selected for performing dynamic analysis is limited to ensure that the modal mass participation is more than 90 percent. To obtain the peak response quantity, the method of square root of sum of squares (SRSS) is used. The SRSS

method of combining maximum modal responses is valid where the modal time periods of the structure are well separated. However, this method yields poor results where the time periods of major contributing modes are very close together. **Figures 5.3, 5.4, and 5.5** illustrate acceleration spectra used as seismic inputs at each site to carry out the response spectrum analysis of the considered building models. In the analysis no load combinations are considered and the seismic inputs are applied in one direction at a time to obtain the response quantity.

b) Modal Time History Analysis

A modal dynamic analysis is used to analyze transient linear dynamic problems using modal superposition, since it bases the structure's response on the modes of the system. The modal dynamic procedure provides time history analysis of linear systems. The excitation is given as a function of time and it is assumed that the amplitude curve is specified so that the magnitude of the excitation varies linearly within each increment.

In the linear modal time history analysis of the considered building models, the time histories that are used as seismic inputs at each site are shown in **Figures 5.6 to 5.20**. The maximum response parameters are obtained by considering the significant modes of vibrations of each building models, listed in **Table 5.3** assuming constant damping of 5% for all modes of vibration. The output time-step size for analysis considered as 0.01 sec for codal compatible time history (CCTH) analysis, because the time interval of CCTH amplitude values is 0.01 sec. However, for other seismic inputs the output time step size for analysis is 0.02 sec. The analysis performed in both across the slope and along the slope to capture the torsion effect on response parameters in 3D building models, considering zero initial condition that starts from unstressed state.

5.4.3 Results and Discussion of Response Spectrum Analysis

At selected sites, the results obtained on the dynamic structural response (seismic analysis) of considered buildings (SB and SBSB) are discussed on the trend basis considering various types of ground motions (seismic inputs). The computed results are expressed in terms of two parameters: floor displacements (horizontal) and shear forces in the ground columns. In the figures, symbols XX, YX and YY stands for, seismic input in X, Y, Y directions and computed response parameters in X, X, Y directions, respectively.

a) Floor Displacements of Step-Back Building Models along and across the Slope.

XX: Response along the slope (X-Dir) when seismic excitation along the slope (X-Dir).

Floor displacements (FDs) in the X-direction, for all the considered step-back (SB) building models subjected to estimated site-specific ground motion (SSGM) at **Shapur site** (SS1), is higher than other seismic inputs, and much closer to the response due to codal spectra for two and three storey (212SB and 313SB) building models (**Figure 5.29**). At **Bhatwari site**, the FDs of two and three storey building models due to estimated SSGM (SS2) found to be much higher than other seismic inputs (**Figure 5.31**). As the number of storey increased to four storey, the response due to estimated SSGM (SS2) found lower than the responses due to recorded and fault-normal (FN) component of ground motion, and closely match with FN-component in case of five storey building model. At **Gopeshwar site**, the comparable FDs observed (**Figure 5.33**) due to estimated SSGM (SS3) and codal spectra, and are in similar trend as obtained at Shapur site for all the SB building models.

In two, three and four storey SB building models, the FDs due to residual part (RSD) of ground motion (FN-component) is higher compared to the FDs due to extracted (EXT) pulse of ground motion (FN-component) at **Bhatwari and Gopeshwar sites** (**Figures 5.31 and 5.33**). Further, at **Gopeshwar site**, this variation is much higher for two and three storey building models, and the response due to residual (RSD) part of ground motion (FN-component) is very close to the responses due to the estimated SSGM (SS3), codal spectra, FN-component, and recorded ground motion (GOP P). In case of 513SB building model, the FDs due to extracted (EXT) pulse of ground motion shows significantly higher values compared to residual (RSD) part of ground motion at **Bhatwari and Gopeshwar sites** (**Figures 5.31 and 5.33**) because of low frequency nature of the extracted (EXT) pulse and comparatively longer-period of structure. However, **at Shapur site**, for all SB building models, the response due to extracted (EXT) pulse of ground motion is higher compared to residual (RSD) part of ground motion. Whereas, the response of the building models due to recorded ground motion (SHAP P) and residual (RSD) part becoming closer with the increasing number of storeys (**Figure 5.29**).

YX: Response along the slope (X-Dir) when seismic excitation across the slope (Y-Dir).

In two and three storey building models, the effect of asymmetry is more clearly seen compared to four and five storey building models (**Figures 5.29, 5.31 and 5.33**), when the seismic inputs are applied in “Y- direction” and observed floor displacements (FDs) in “X-

direction". It is observed that the floor-displacements (X-direction) due to all the considered seismic inputs have comparatively higher values of FDs (YX) at intermediate-floors compare to respective "XX" displacements in 313SB building model at **Bhatwari and Gopeshwar sites (Figures 5.31 and 5.33)**. Whereas, in 212SB building model this response observation is not seen in case of SSGM (SS2) and codal spectra at **Bhatwari site,** and only be seen in case of extracted (EXT) pulse of ground motion at **Gopeshwar site**. However, for 413SB and 513SB building models, the effect of torsion (YX-FDs) is seen to be very less at all floor levels at three selected sites.

YY: Response across the slope (Y-Dir) when seismic excitation across the slope (Y-Dir).

For 313SB, 413SB and 513SB building models, the FDs in Y-direction due to application of extracted (EXT) pulse of ground motion in Y-direction is much higher than residual (RSD) part of ground motion at **Bhatwari and Gopeshwar sites** (**Figures 5.32 and 5.34**), and have almost closely comparable values at **Shapur site** (**Figure 5.30**). However, the floor displacements at all floor-levels due to SSGMs (SS1, SS2 and SS3) is much higher, and due to residual (RSD) part of ground motion is much lower compared to other seismic inputs, except in 2 storey building model at **Bhatwari and Gopeshwar sites.** Whereas, at these two sites, response due to FN-components and recorded ground motions (BHAT O, GOP P) are little higher than the response due to SSGMs (SS2, SS3) in 212SB building model.

It is observed that as the number of building storey increases from two to four at **Bhatwari site**, the response (FDs) due to extracted (EXT) pulse of ground motion becoming closer to that computed from recorded ground motion (BHAT O) and FN-component (**Figure 5.32**). Whereas, at **Gopeshwar site,** the above observation seen for all the building models (**Figure 5.34).** At **Shapur site** the response due to both type of ground motions, i.e., extracted pulse (EXT) and recorded ground motion (SHAP P/FN) well match (closely) for all the building models and getting closer to the response due to residual (RES) part of ground motion (**Figure 5.30)**.

At **Bhatwari site**, the response of all SB building models due to codal spectra found much lower than the response due to other seismic inputs; and it is also found that as the number of storeys increases, the response due to the residual (RSD) part of ground motion becoming closer to that of codal spectra. However, at **Gopeshwar site,** the response due to the residual (RSD) part of ground motion found much lower than that of codal spectra. Whereas, the response due to codal spectra found almost comparable; to that computed from original

recorded ground motion (GOP P), FN-component, and extracted (EXT) pulse of ground motion for 513SB building model, and to that computed from FN-component for 413SB building model**.**

b) Floor Displacements of Step-Back-Set-Back Building Models along and across the Slope.

XX: Response along the slope (X-Dir) when seismic excitation along the slope (X-Dir).

For all the four SBSB building models, the maximum FDs (XX) is obtained due to SSGM (SS1, SS2 and SS3) compared to other seismic inputs at three sites (**Figures 5.35, 5.37 and 5.39**). At **Shapur and Gopeshwar sites,** this response (FD-XX), i.e., due to SSGM (SS1 and SS2) found closer to that computed from codal spectra at all floor-levels of the building models (**Figures 5.35 and 5.39**). However, at **Bhatwari site**, the response due to SSGM (SS2) is significantly higher than that of codal spectra (**Figure 5.37**).

For all the four models, the FD (XX) due to residual (RSD) part of ground motion is higher than that computed from extracted (EXT) pulse of ground motion (FN) at **Bhatwari and Gopeshwar sites** (**Figures 5.37 and 5.39**), and found comparable with the responses due to FN-component of ground motions, original recorded ground motions (BHAT P and GOP P) and codal spectra. However, at **Shapur site,** the response due to extracted (EXT) pulse of ground motion (FN) found higher than that computed from residual (RSD) part in all the building models; and also match with the response due to FN-component, but very close match seen in 212SBSB model (**Figure 5.35**). It is also observed that as the storey height increases, the response due to residual (RSD) part of ground motion (FN) shows close matching with the response due to FN-component at intermediate floors of the models compared to that of extracted (EXT) pulse ground motion (FN).

The above discussed results are in X-direction when the seismic inputs are applied in the X-direction (**XX**).

YX: **Response along the slope (X-Dir) when seismic excitation across the slope (Y-Dir).**

At **Bhatwari and Gopeshwar sites,** as the building storeys increases from three to five, FDs-YX due to torsional effect found more significant than the FDs-XX (non-torsional displacements) at all the intermediate floor levels for all types of seismic inputs (**Figures 5.37 and 5.39**); except due codal spectra and residual (RSD) part response at **Bhatwari site**, and

residual (RSD) part response at **Gopeshwar site**. However, at **Shapur site,** higher FDs-YX observed compared to FDs-XX (non-torsional displacements) at all the intermediate floors only due to SSGM (SS1) and codal spectra in 3, 4, and 5 storey building models (**Figure 5.35**).

At **Bhatwari site,** the FDs (YX) of 3, 4 and 5 storey building models due to extracted (EXT) pulse ground motion (FN) is higher than the responses due to residual (RSD) part of ground motion (FN) and codal spectra. However, the response due to the extracted (EXT) pulse is closer to the response due to FN-component of ground motion, and have comparable values to that computed from SSGM (SS2) at all floor levels of SBSB building models (**Figure 5.37**).

At **Gopeshwar site**, the FDs (YX) of 4 and 5 storey building models due to extracted (EXT) pulse of ground motion is higher than the responses due to residual (RSD) part of ground motion and codal spectra; and the response due to the extracted (EXT) pulse is closer to the response due to original recorded ground motion (GOP P) and have comparable values to that computed from SSGM (SS3) at all floor levels of SBSB building models (**Figure 5.39**). However, for 2 storey building model, responses (FDs-YX) due to FN-component of ground motion, recorded ground motion (GOP P), estimated SSGM (SS3), codal spectra, and residual (RSD) part of ground motion are higher than the response due to extracted (EXT) pulse ground motion, and have comparable values at all floor levels. Whereas, in 3 storey building model, the response due to extracted (EXT) pulse of ground motion is higher than residual (RSD) part of ground motion, and lower than that of codal spectra; but the response due to SSGM (SS3) is highest and comparable with FN-component and recorded pulse-type ground motion (GOP P).

At **Shapur site**, the FDs (YX) in all SBSB building models due to extracted (EXT) pulse ground motion is higher than that of residual (RSD) part of ground motion; and but in 4 and 5 storey building models, the responses due to extracted pulse (EXT) and residual (RSD) part found closer. Further, the SSGM (SS1) and codal spectra show significantly higher responses than other seismic inputs in all the SBSB building models (**Figure 5.35**).

YY: Response across the slope (Y-Dir) when seismic excitation across the slope (Y-Dir).

At **Bhatwari site**, as the building height exceeds from 2 to 3, 4 and 5 storeys, the floor displacements (FD-YY) due to extracted (EXT) pulse overshoot the responses due to residual (RSD) part, original recorded pulse-type ground motion (BHAT O), and FN-component of ground motion (**Figure 5.38**). For 212SBSB building model, FDs-YY due to residual (RSD) part seen to be much closer to that of FN-component, and higher than the responses due to

extracted (EXT) pulse and codal spectra. Further, as the building height increasing from 3 to 5 storeys, the response due to residual (RSD) part getting lower and lower compared to other seismic inputs, and comes closer and closer to the response due to the codal spectra. Furthermore, for all building models, the response due to SSGM (SS2) is highest, and the response due to codal spectra is lowest.

At Gopeshwar site, for 212SBSB and 313SBSB building models, floor displacements in the Y-direction due to originally recorded pulse-type ground motion (GOP P) and FN-component are seen higher compared to other seismic inputs; and in case of 414SBSB and 515SBSB building models, the responses due to 'GOP P' and FN-component are only higher than the codal spectra and residual (RSD) part ground motion responses (**Figure 5.40**). However, for 212SBSB building model, FDs-YY due to residual (RSD) part seen to be much closer to displacements due to SSGM (GOP P) and codal spectra, and much higher compared to extracted (EXT) pulse of ground motion. As the building height goes over 2 storey, i.e., for 3, 4 and 5 storey, the FDs-YY due to extracted (EXT) pulse shows higher response that that of residual (RSD) part of the ground motion. Further, for 414SBSB and 515SBSB building models the response due to extracted (EXT) pulse even over reaches the responses due to codal spectra, FN-component and original recorded ground motion (GOP P), and becoming closer to the response due to SSGM (SS3).

At Shapur site, for all the SBSB building models, the responses (FD-YY) due to SSGM (SS1) and codal spectra are higher than the other seismic inputs. For 212SBSB building model the response due to codal spectra is very close to the response due to SSGM (SS1). For all the SBSB building models, the response due to extracted (EXT) pulse is higher than the response obtained due to residual (RES) part of ground motion, and has closer response to that computed from original recorded (FN/SHAP P) ground motion (**Figure 5.36**). However, with the increasing storey of the building models, the responses due to FN-component and extracted (EXT) pulse becoming closer to the response due to residual (RSD) part.

c) Ground Column Shear Force in Step-Back Building Models along and across the Slope.

XX: Response along the slope (X-Dir) when seismic excitation along the slope (X-Dir).

For Step-Back building models, the shear force in columns at ground level in frame "F1" attracts much higher force compared to other frames, because of short column effect. At **Bhatwari and Gopeshwar sites**, the ground column shear force **(**GCSF) in frame "F1" due to

residual (RSD) part of ground motion is higher than that obtained from extracted (EXT) pulse of ground motion for 2, 3 and 4 storey building models (**Figures 5.43 and 5.45**). Further, **at Gopeshwar site (Figure 5.45)**, this variation is much higher for 2 and 3 storey building models, and also that the response due to residual (RSD) part of ground motion is not in much difference with the response due to SSGM (SS3), codal spectra, FN-component of ground motion, and recorded ground motion (GOP P). **At Bhatwari site**, the variation found to be comparable between the responses due to residual (RSD) part, extracted (EXT) pulse, FN-component, and originally recorded ground motion (BHAT O/BHAT P), and remains almost same for 2, 3 and 4 storey building models (**Figure 5.43**). This variation remain closely below the response due to codal spectra for 2 and 3 storey building models; but for 4 storey building model, the variation become much higher than the response due to codal spectra along with close matching of the response due to SSGM (SS2) and residual (RSD) part of ground motion. Whereas, for 513SB building model, the GCSF in frame "F1" due to extracted (EXT) pulse of ground motion shows significantly higher response compared to residual (RSD) part of ground motion at **Bhatwari and Gopeshwar site** because of low frequency nature of extracted (EXT) pulse and comparatively longer-period of structure (**Figures 5.43 and 5.45**). **At Bhatwari site**, the response of 513SB building model due to codal spectra is much lower than that computed from original recorded ground motion (BHAT O), FN-component, and residual (RSD) part of ground motion (**Figure 5.43**). Whereas, at **Gopeshwar site**, the variation between the responses computed from codal spectra, original recorded ground motion (GOP P), FN-component, and extracted (EXT) pulse of ground motion is less; and much higher than that of residual (RSD) part (**Figure 5.45**).

At **Shapur site**, for all SB building models, the response due to extracted (EXT) pulse of ground motion is higher compared to residual (RSD) part of ground motion, and also closer to the response due to recorded fault-normal (FN) component of ground motion. For 4 and 5 storey building models at Shapur station, the variation of responses due to codal spectra and SSGM (SS1) with respect to FN-component, extracted (EXT) pulse, and residual (RSD) part is much higher compared to 2 and 3 storey building models (**Figure 5.41**). GCSF in frame "F1" for all the considered "SB" building models subjected to SSGM (SS1) at **Shapur site**, is higher than other seismic inputs, and has much closer to the response due to codal spectra for 2 and 3 storey building models compared to 4 and 5 storey building models (**Figure 5.41**).

At **Bhatwari site**, the GCSF in frame "F1" of 2 and 3 storey building models due to SSGM (SS2) found to be much higher than other seismic inputs. As the number of storey increased to

4, the response due to SSGM (SS2) found lower than the response due to originally recorded (BHAT P) and FN-component ground motions, and again the SSGM (SS2) response is higher than other seismic inputs but have a close response value with FN-component of ground motion in case of 513SB building model (**Figure 5.43**). **At Gopeshwar site**, the variation of GCSF in frame "F1" of building models due to SSGM (SS3) and codal spectra are found in similar trend as that of at **Shapur site**.

YX: Response along the slope (X-Dir) when seismic excitation across the slope (Y-Dir).

At Gopeshwar site, the application of seismic inputs in the Y- direction (across the slope) have showed that shear force in ground column in X- direction (along the slope) due to torsional effect are equally important as they exceed non-torsional response (XX) for some seismic inputs in 212SB and 313SB building models (**Figure 5.45**). However, for 413SB and 513SB building models, the torsional (YX) and non-torsional (XX) responses are comparable in frame "F1", and in frame "F2" the torsional response (YX) exceeds non-torsional (XX) response. The torsional response (YX) due to the extracted (EXT) pulse in 3, 4 and 5 storey SB building models significantly exceeds the residual (RSD) response, and much closer to the response due to FN-component and original ground motion (GOP P) in frames "F1" and "F2". However, the response due residual (RSD) part is higher than extracted (EXT) pulse in frame "F1" of 212SB model, but the variation between them is too low. The responses due to these two seismic inputs show much lower value than the responses due to FN-component, original recorded ground motion (GOP P), codal spectra, and SSGM (SS3). As the number of storey increases the response (YX) due to SSGM (SS3) becomes relatively higher with respect to other seismic inputs.

At Bhatwari site, the response (GCSF-YX) due to torsional effect is of great consequence as they exceed non-torsional response (XX) for all ground motions in frame "F1" of 212SB and 313SB, and in frame "F2" of 313SB, 413SB and 513SB building models (**Figure 5.43**). The response due to codal spectra is found least in frame "F1" and "F2" of 212SB and 313SB compared to other ground motions. However, in 413SB and 513SB the response due to codal spectra has only little higher value than that of residual (RSD) part of ground motion. The torsional response (YX) due to extracted (EXT) pulse in 3, 4 and 5 storey building models exceeds the residual (RSD) part response, and found closer to the response due to FN-component and original recorded ground motion (BHAT O/BHAT P) in frame "F1" of 3 and 4 storey building models. Further, in all the SB building models, the response due to codal

spectra found to be lower than the responses due to original recorded ground motion (BHAT O/BHAT P), FN-component, SSGM (SS2), and extracted (EXT) pulse. It can be seen that the response due to residual (RSD) part is higher than extracted (EXT) pulse in "F1" of 212SB building model, but the variation between them is too low. The responses due to these two seismic inputs show little lower values than the responses due to original recorded pulse-type ground motion (BHAT O), FN-component, and SSGM (SS2). Moreover, as the number of storey increases the response (YX) due to SSGM (SS2) becomes relatively higher with respect to other seismic inputs.

At Shapur site, it is clearly seen that the effect of torsional response (YX) only be significant due to codal spectra and SSGM (SS1) (**Figure 5.41**). In all the SB building models (2 to 5 storey), the response due to extracted (EXT) pulse, is higher than the residual (RSD) part of ground motion, and closer to the response due to the FN-component of ground motion.

YY: Response across the slope (Y-Dir) when seismic excitation across the slope (Y-Dir).

At Gopeshwar site, the application of seismic inputs across the slope (Y-direction) has brought out that the shear force across the slope (Y-direction) due to SSGM (SS3) is higher in ground columns in all frames for all the building models, and becoming more higher compared to other seismic inputs as the number of storeys increases (**Figure 5.46**). The response due to residual (RSD) part of ground motion, is more than the extracted (EXT) pulse in all the frames (F1, F2 and F3) of 212SB building model, and lower than the response due to extracted (EXT) pulse in all frames of 313SB, 413SB and 513SB building models. Further, as the building storeys increases, the relative variation between the responses due to codal spectra, FN-component, original recorded ground motion (GOP P), and extracted (EXT) pulse getting narrower.

At Bhatwari site, the shear force (YY) due to SSGM (SS2) is highest and due to codal spectra is lowest in ground columns in all the frames for all the building modals. The variation between the responses due to SSGM (SS2) and other seismic inputs goes on increasing with the increasing number building storeys (**Figure 5.44**). The response due to residual (RSD) part of ground motion, is more than the extracted (EXT) pulse of ground motion in all the frames (F1, F2 and F3) of 212SB building model, and lower than the response due to extracted (EXT) pulse in frames 'F1, F2 and F4' of 313SB, 413SB and 513SB building models. Further, for 3 and 4 storey building models, the relative variation between the responses due to FN-component,

original recorded ground motion (SS2), and extracted (EXT) pulse is lower than that of 2 and 5 storey building models.

At Shapur site, the response (YY) due to SSGM (SS1) is highest in ground columns in all frames for all the building models, and the response due to SSGM (SS1) and codal spectra is significantly higher compared to the FN-component, extracted (EXT) pulse and residual (RSD) part of ground motion (**Figure 5.42**). For all the building models in all the frames, the GCSF (YY) due to residual (RSD) part of ground motion and FN-component of ground motion are higher than the extracted (EXT) pulse; except in 'F1' of 212SB building model.

d) Ground Column Shear Force in Step-Back-Set-Back Building Models along and across the Slope.

XX: Response along the slope (X-Dir) when seismic excitation along the slope (X-Dir).

At Gopeshwar site, for all step-back-set-back (SBSB) building models, "XX" component of shear force shows higher response due to residual (RSD) part of ground motion compared to the extracted (EXT) pulse in all building frames (**Figure 5.51**). Further, the response due to residual (RSD) part of ground motion, found to be closer to the responses due to recorded ground motion (GOP P) and FN-component of ground motion for all the building models, but lower than the response due to the codal spectra. However, the response due to SSGM (SS3) is highest.

At Bhatwari site, for all step-back-set-back (SBSB) building models, "XX" component of shear force shows higher response due to residual (RSD) part of ground motion compared to the extracted (EXT) pulse of ground motion in all building frames (**Figure 5.49**). Further, the responses due to recorded ground motion (BHAT O/BHAT P) and FN-component of ground motion for all the building models in frame "F1" are closer to the response due to the codal spectra, and the responses due to these three ground motions are higher than that of response due to the residual (RSD) part of ground motion. Furthermore, in other frames of all SBSB building models, the response due to residual (RSD) part of ground motion is closer to the response due to FN-component, and the response due to recorded ground motion (BHAT O/BHAT P), FN-component of ground motion, and residual (RSD) part of ground motion are higher than the response due to the codal spectra. However, the response due to SSGM found to be highest.

At Shapur site, the responses due to SSGM (SS1) and codal spectra, are much higher than other seismic inputs, with little difference in them (**Figure 5.47**). The response due to extracted (EXT) pulse is more than the response due to the residual (RSD) part of ground motion in frame 'F1' of 3, 4 and 5 storey building models, and have almost same response in 2 storey building model. Further, for other frames, the response due to residual (RSD) part of ground motion, is more than the response due to extracted (EXT) pulse and closer to the response due to the FN-component.

YX: Response along the slope (X-Dir) when seismic excitation across the slope (Y-Dir).

At Gopeshwar site, it is brought out that the effect of torsion is more significant in 3, 4 and 5 storey SBSB building models as GCSF (YX-response) due to all types of seismic inputs exceeds respective XX-response (GCSF due to non-torsional effect) in all building frames, except response due to residual (RSD) part of ground motion in frame 'F1' **(Figure 5.51).** In the above three models, i.e., 3, 4 and 5 storey building models, the YX-response due to extracted (EXT) pulse has exceeded significantly the response due to residual (RSD) part of ground motion in all frames. Further, the response due to extracted (EXT) pulse also exceeds the responses due to codal spectra, recorded pulse-type ground motion (GOP P) and FN-component; and closer to the response due to SSGM (SS3) in all frames of 4 and 5 storey building models. However, in all SBSB building models, the responses due to FN-component of ground motion and original recorded ground motion (GOP P) are higher than that of codal spectra. Further, it is observed that the torsional effect is significant in frame 'F1' compared to other frames in 212SBSB building model; and the response due to residual (RSD) part of ground motion, exceeds the response due to extracted (EXT) pulse and is closer to the responses due to other ground motions at the selected site.

At Bhatwari site, it is brought out that the torsional effect is significant in all building models as YX-response due to all types of seismic inputs exceeds respective XX-response (non-torsional response) in all building frames except response due to SSGM (SS2) in frame "F1" of 212SBSB building model **(Figure 5.49)**. In other three SBSB models, i.e., 3, 4 and 5 storey building models, the response (YX) due to torsional effect of extracted (EXT) pulse has exceeded significantly the response due to residual (RSD) part of ground motion in all the frames. Further, the response due to extracted (EXT) pulse, exceeds the responses due to the codal spectra, FN-component and recorded pulse-type ground motion (BHAT P/BHAT O), and closer to the response due SSGM (SS2) in all frames of 3, 4, and 5 storey building models.

However, the responses due to FN-component and recorded pulse-type ground motion (BHAT O/BHAT P) show much higher values than that of codal spectra in all the building models. In 212SBSB building model, the response due to residual (RSD) part of ground motion, exceeds the responses due to extracted (EXT) pulse, recorded pulse-type ground motion (BHAT P/BHAT O) and codal spectra; and closer to the response due to FN-component of ground motion. The response due to the SSGM is highest in all frames of all the SBSB building models.

At Shapur site, it is found that the YX-response because of torsional effect is significant in all the frames of 3, 4 and 5 storey building models due to the codal spectra and SSGM at the site **(Figure 5.47)**. The response due to the extracted (EXT) pulse is found higher than that of residual (RSD) part of ground motion in all the frames in all the building models; and closer to the response due to FN-component of ground motion. However, the observed response due to the SSGM is the highest in all the frames of the SBSB building models.

YY: Response across the slope (Y-Dir) when seismic excitation across the slope (Y-Dir).

At Gopeshwar site, when the seismic inputs or excitations are in Y-direction, much higher response (Y-direction) is observed due to residual (RSD) part of ground motion than the response due to extracted (EXT) pulse of ground motion in all building frames of the 212SBSB building model **(Figure 5.52)**. The 313SBSB building model shows almost comparable responses due to extracted (EXT) pulse and residual (RES) part of ground motion in all the building frames. However, the response due to extracted (EXT) pulse shows much higher response compared to residual (RES) part of ground motion in all the frames of 4 and 5 storey building models; except in frame “F1”, where these responses are comparable. Further, in 4 and 5 storey building models, the response due to the extracted (EXT) pulse is almost comparable with the responses due to codal spectra, FN-component and recorded pulse-type ground motion (GOP P) in all the frames (except in “F1”), with highest response due to the SSGM (SS3) in all the frames. However, in frame “F1” of 212SBSB building model and in frames “F1 and F2” of 313SBSB building model, the responses due to FN-component and recorded pulse-type ground motion (GOP P) are higher than that of codal spectra, extracted (EXT) pulse and residual (RES) part of ground motion; and closely comparable to the response due to the SSGM (GOP P).

At **Bhatwari site,** when the seismic inputs or excitations are in Y-direction, higher response in Y-direction is observed due to residual (RSD) part of ground motion than the response due to extracted (EXT) pulse in all the frames of 212SBSB building model, and close to the response due to FN-component **(Figure 5.50)**. The 313SBSB building model shows little higher response value due to extracted (EXT) pulse compared to residual (RES) part of ground motion in all frames. However, the response due to extracted (EXT) pulse shows much higher response compared to residual (RES) part of ground motion in all the frames of 4 and 5 storey building models. Further, the response due to extracted (EXT) pulse is almost comparable with the responses due to FN-component and recorded pulse-type ground motion (BHAT P/BHAT O) in all the frames of 3, 4 and 5 storey building models. All the frames of all the building models show highest response due to SSGM (SS2) compare to other seismic inputs. However, 3 storey building model shows lowest response due to codal spectra, whereas, the 4 and 5 storey building models show comparable responses due to codal spectra and residual (RSD) part of ground motion and lowest too, and 2 storey building model shows lowest response due to codal spectra and extracted (EXT) pulse, and lowest too.

At Shapur site, the 212SBSB building model shows higher response due to extracted (EXT) pulse compare to residual (RES) part of ground motion in frame 'F1', and vice-versa in other frames of the building **(Figure 5.48)**. However, the 3, 4 and 5 storey building models show higher response due to residual (RES) part of ground motion in all the frames of the building models. All the building models show much higher response due to SSGM (SS1) and codal spectra compared to other seismic inputs, and response due to SSGM (SS1) is the highest amongst all.

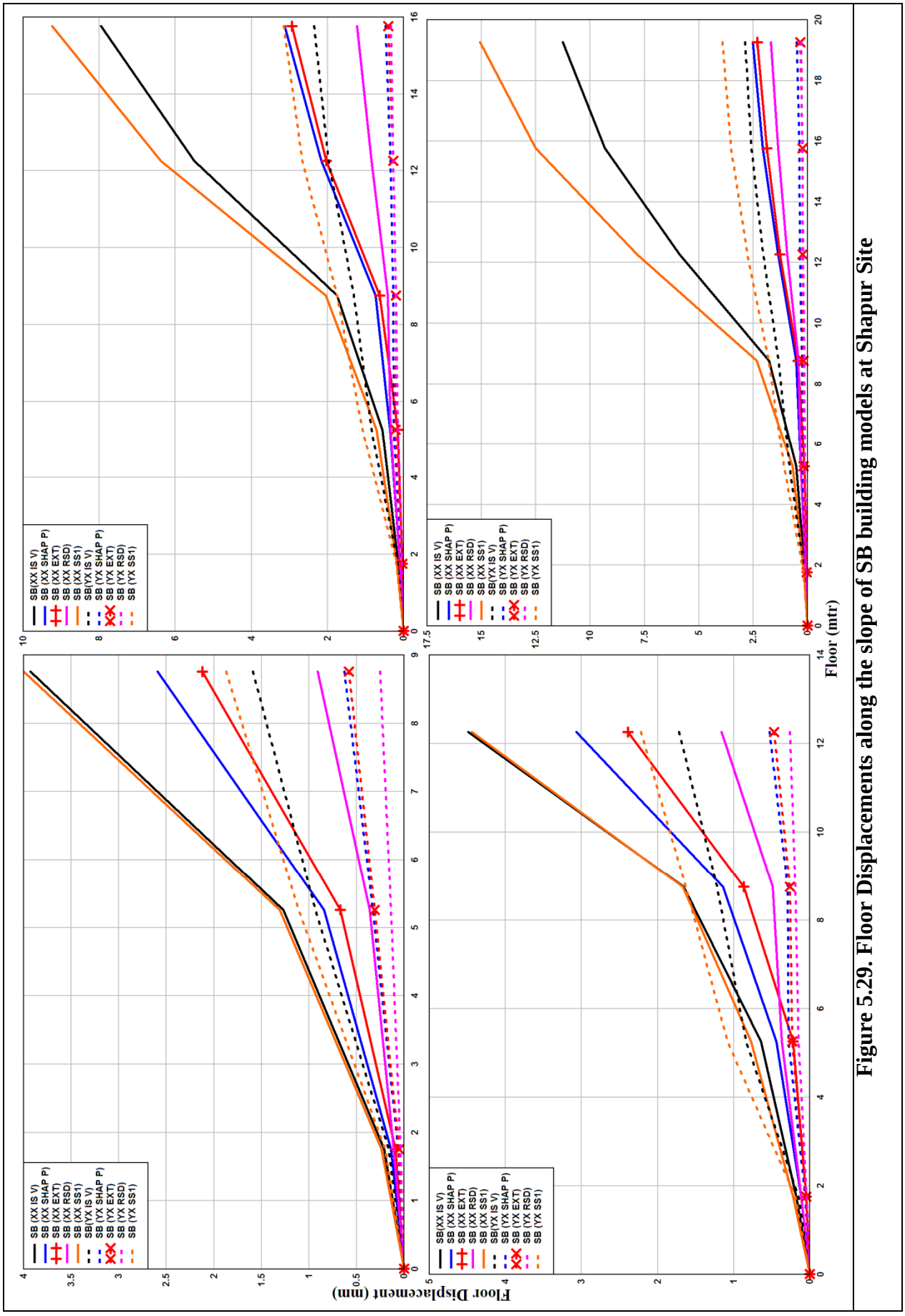

Figure 5.29. Floor Displacements along the slope of SB building models at Shapur Site

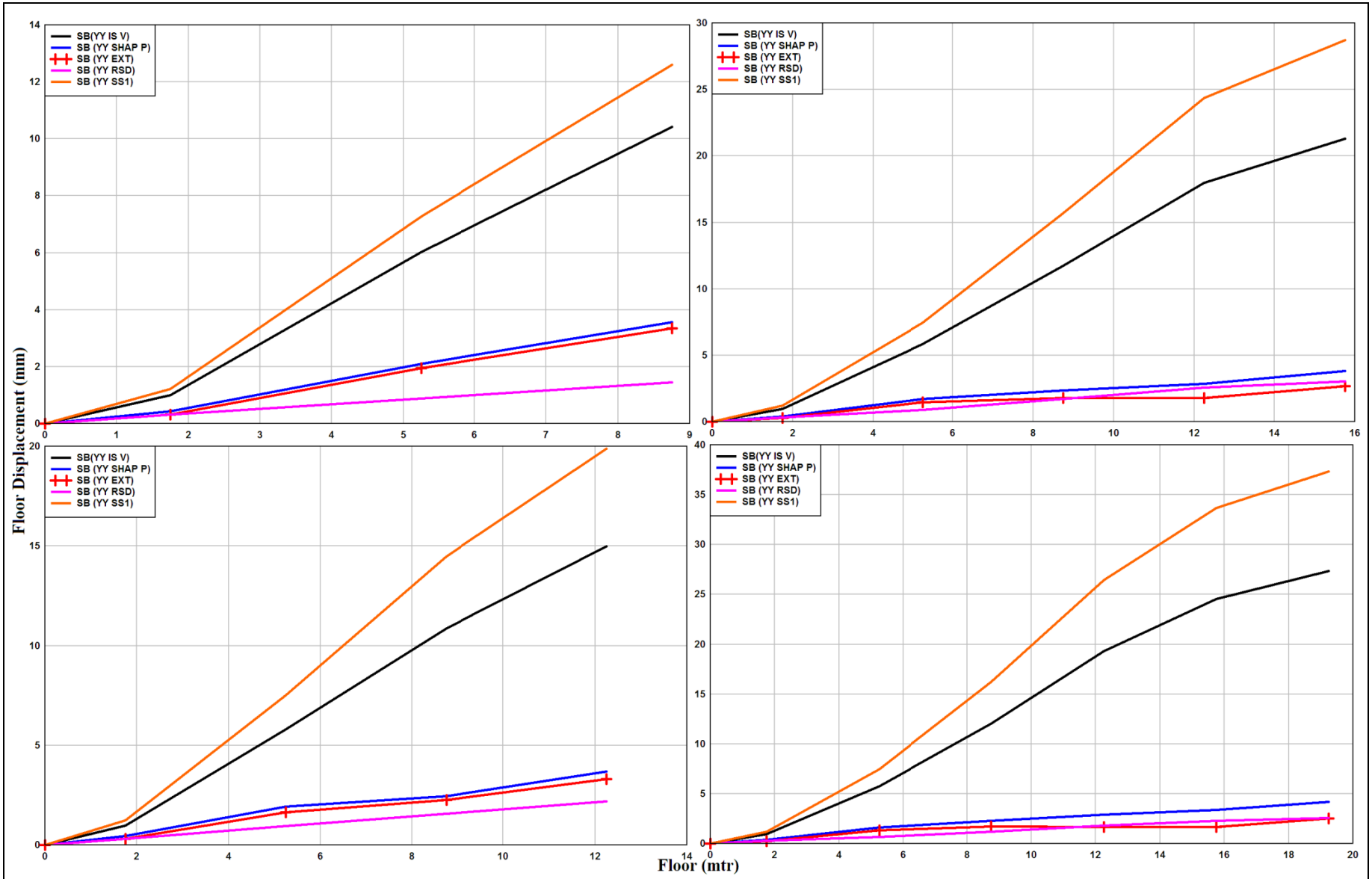

Figure 5.30. Floor Displacements across the slope of SB building models at Shapur Site

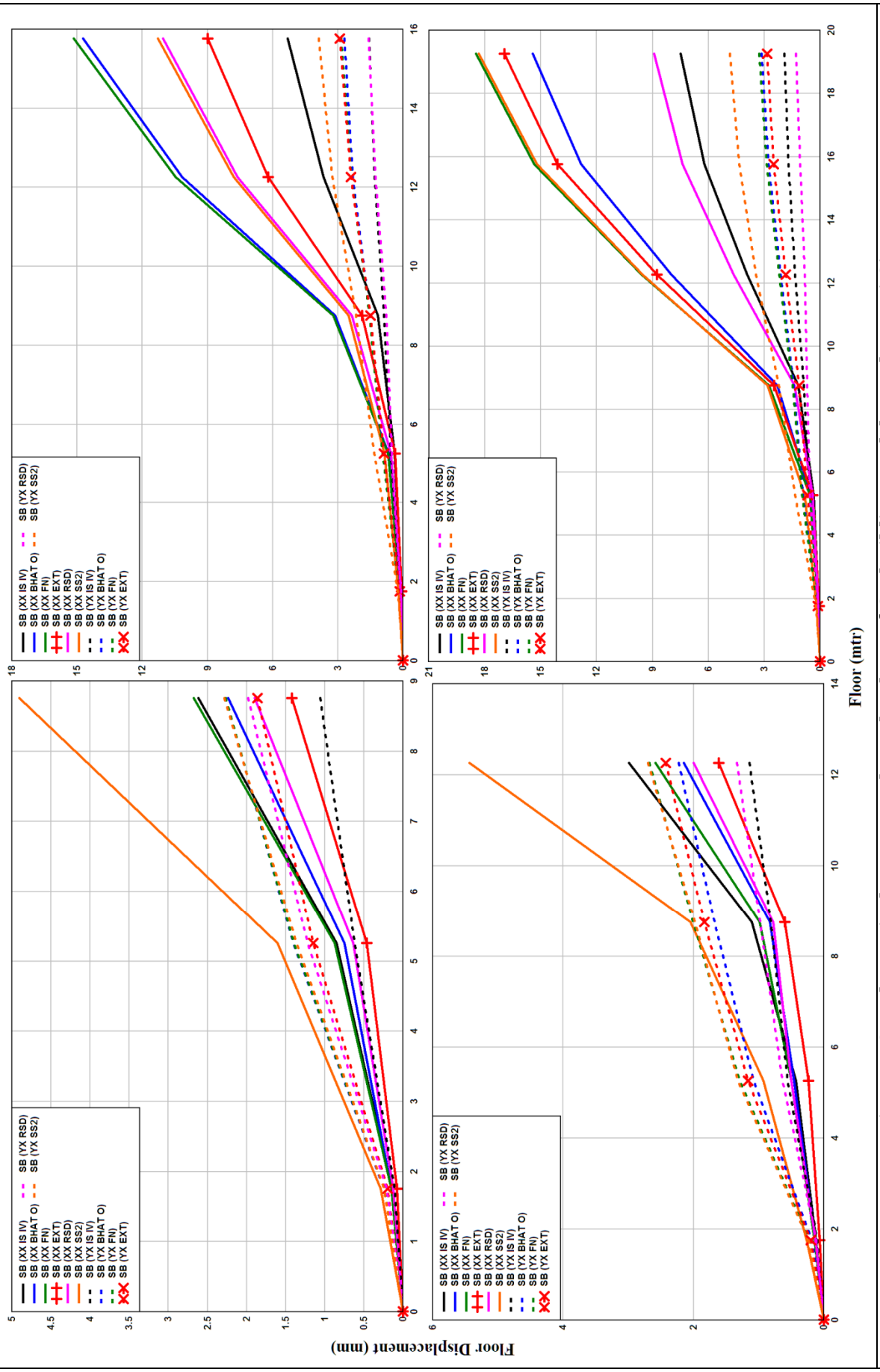

Figure 5.31. Floor Displacements along the slope of SB building models at Bhatwari Site

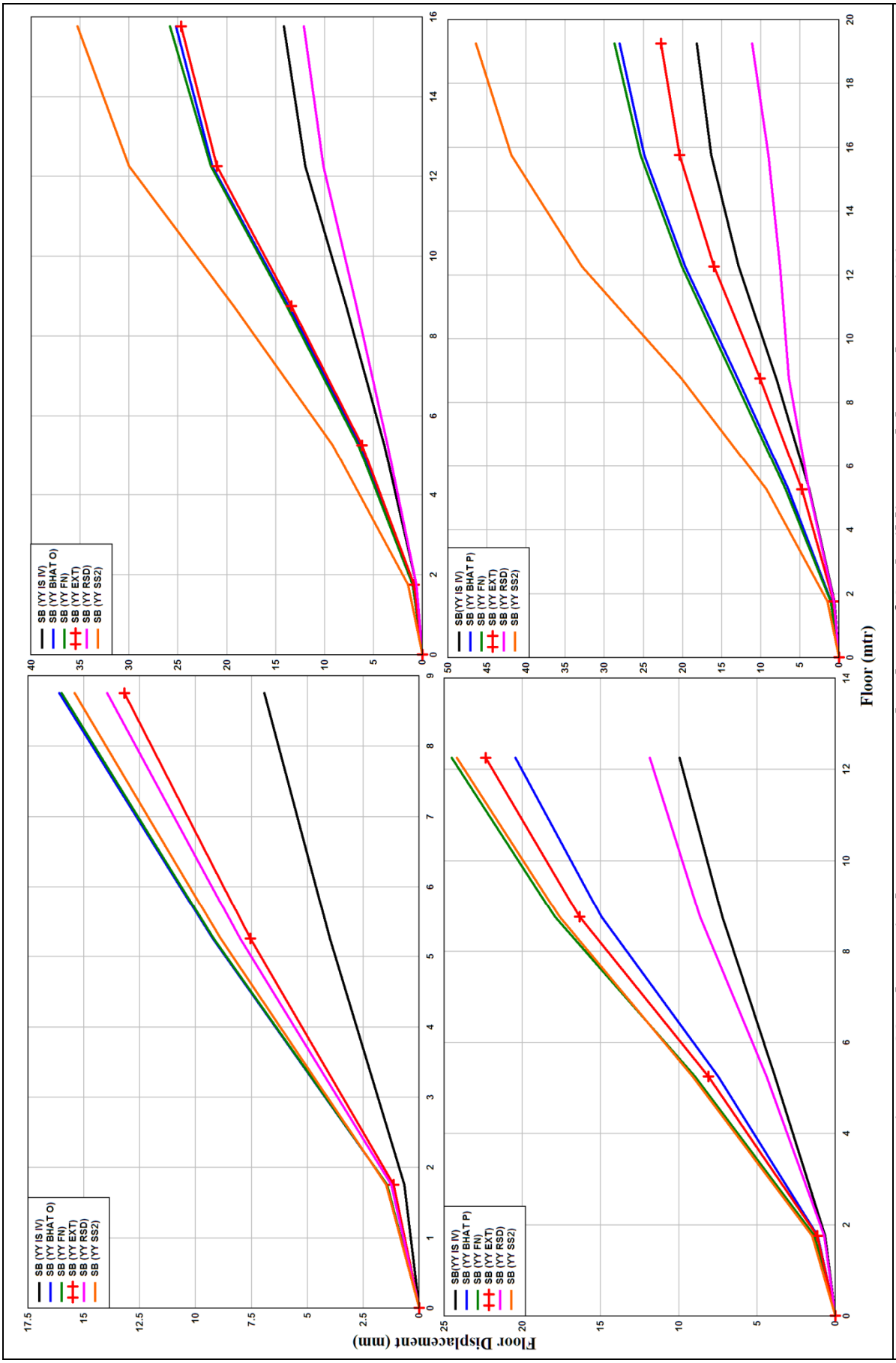

Figure 5.32. Floor Displacements across the slope of SB building models at Bhatwari Site

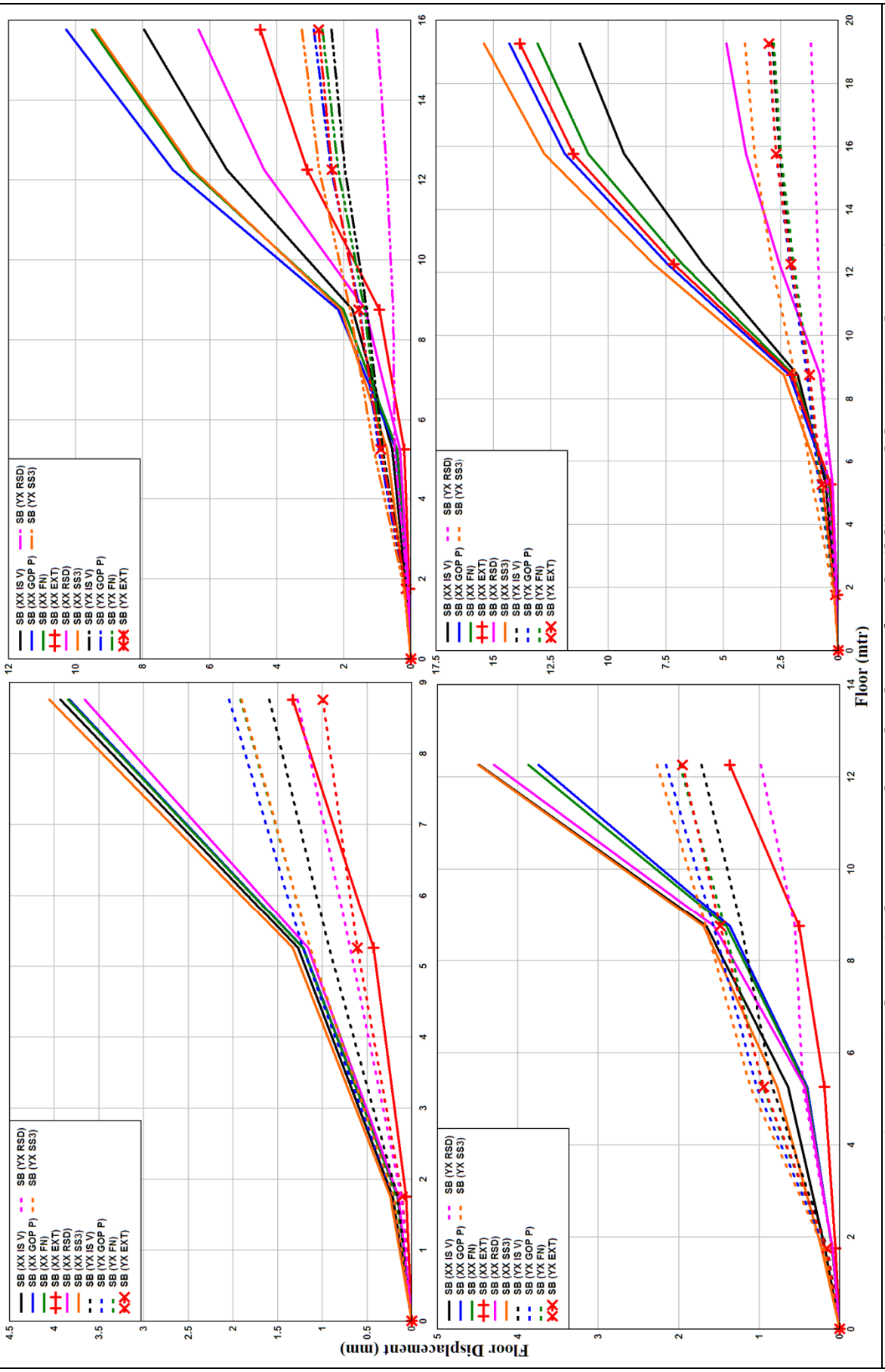

Figure 5.33. Floor Displacements along the slope of SB building models at Gopeshwar Site

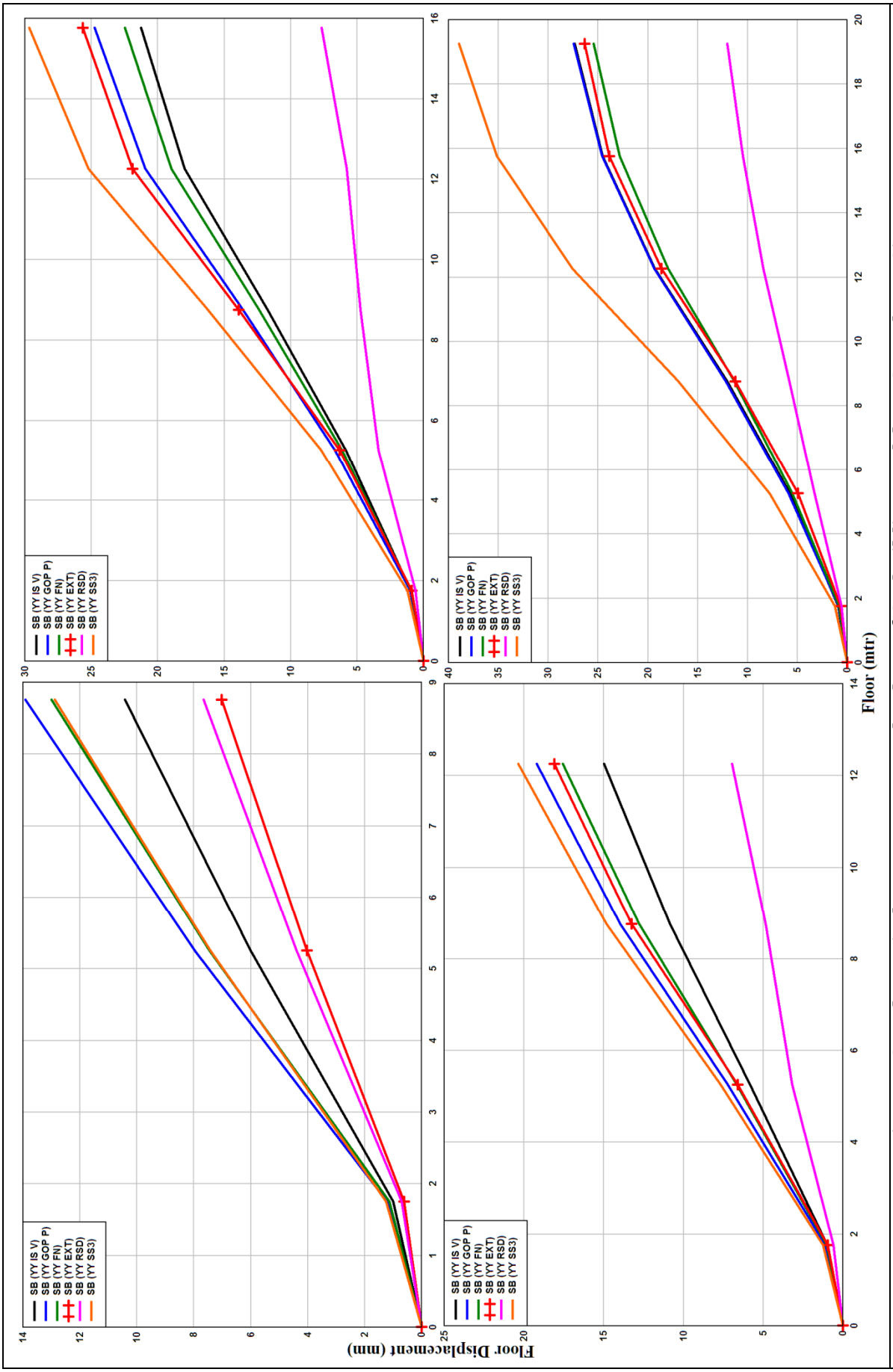

Figure 5.34. Floor Displacements across the slope of SB building models at Gopeshwar Site

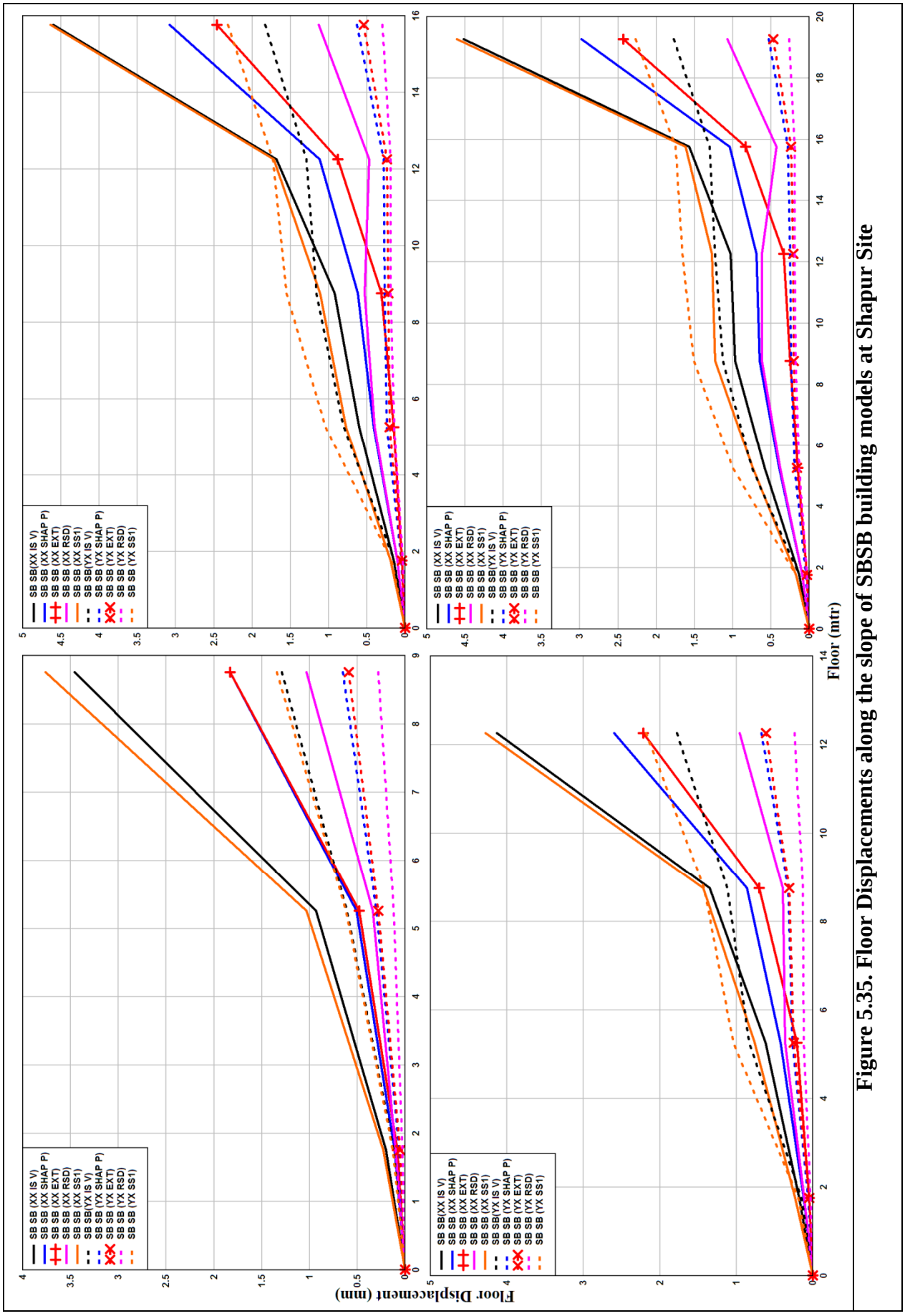

Figure 5.35. Floor Displacements along the slope of SBSB building models at Shapur Site

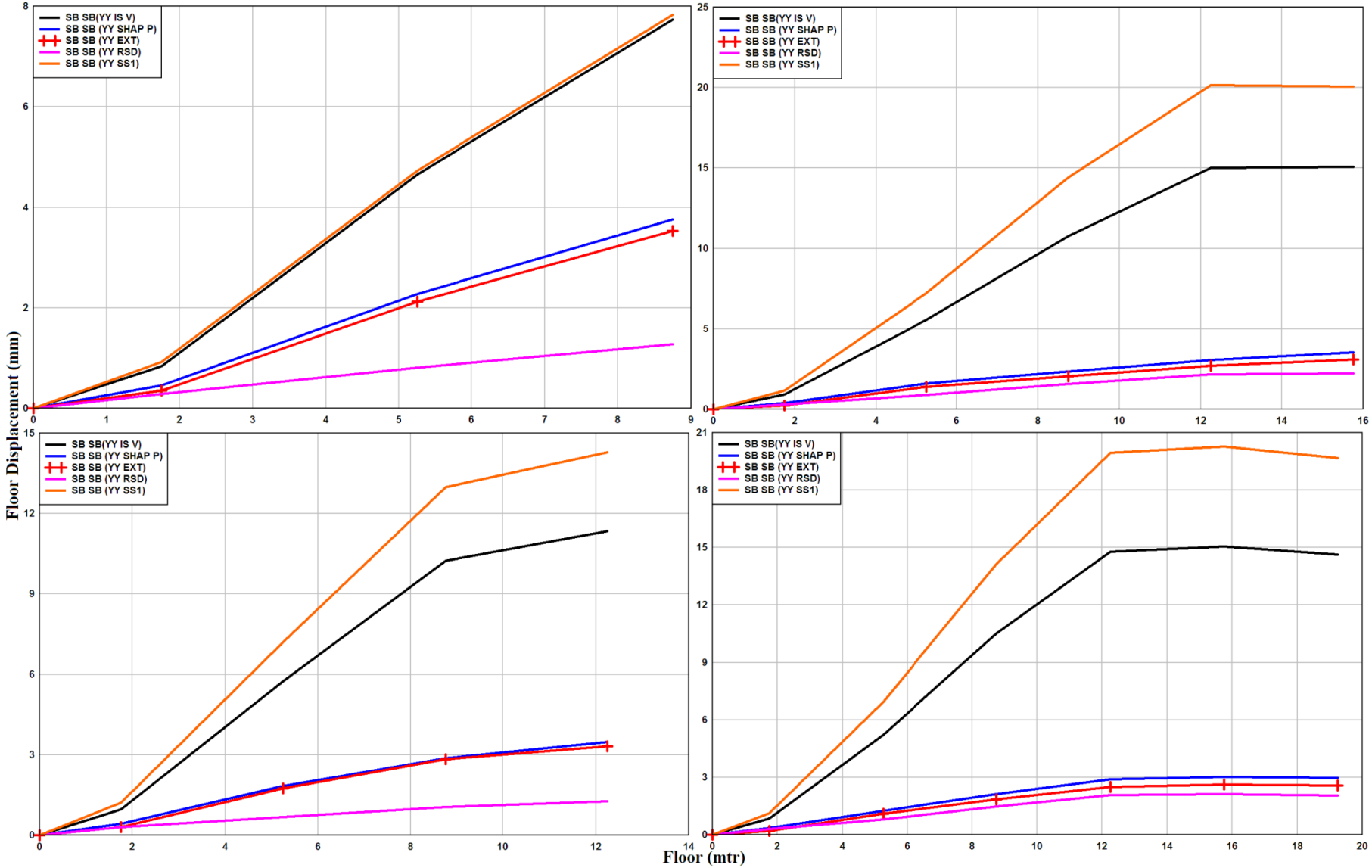

Figure 5.36. Floor Displacements across the slope of SBSB building models at Shapur Site

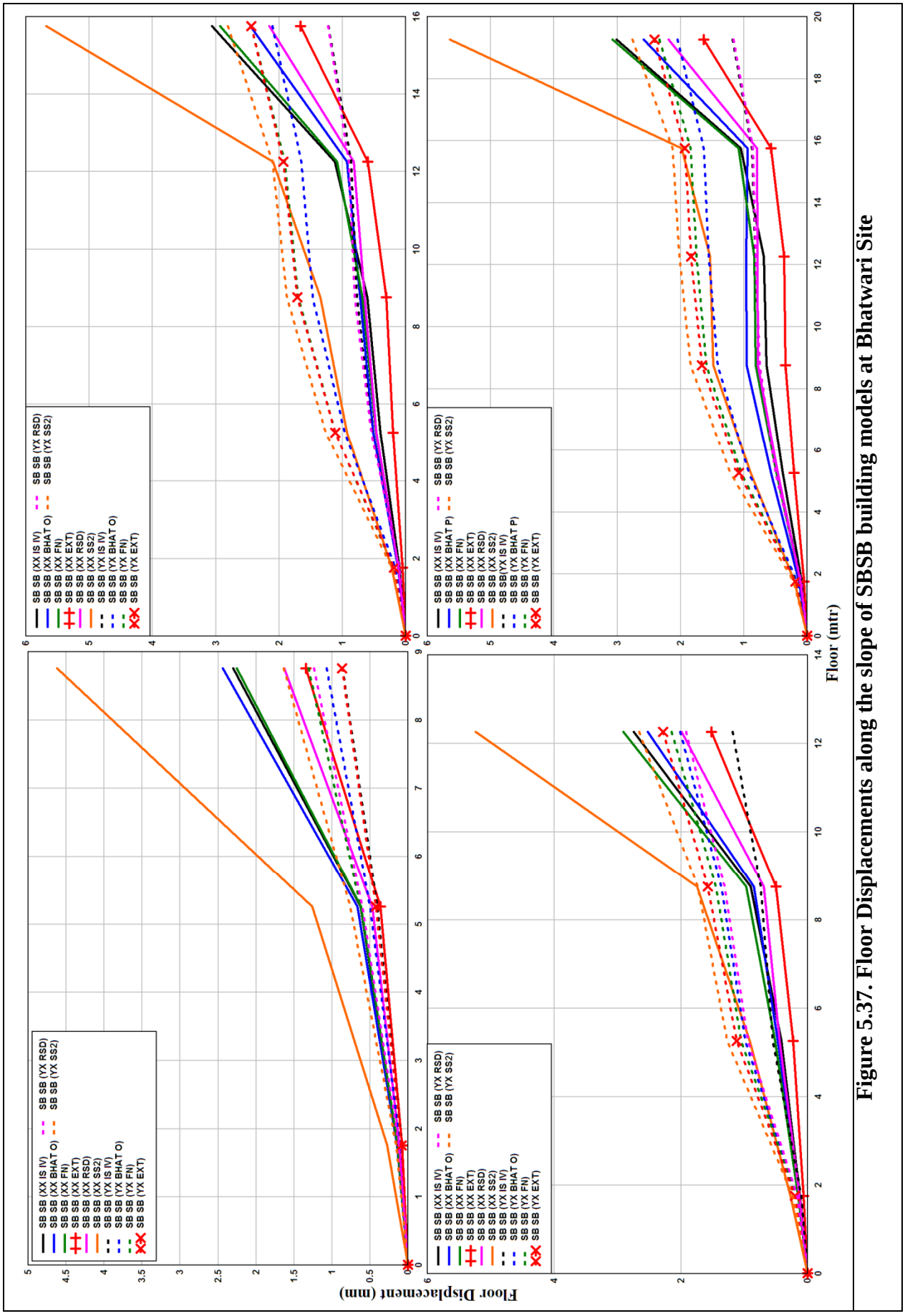

Figure 5.37. Floor Displacements along the slope of SBSB building models at Bhatwari Site

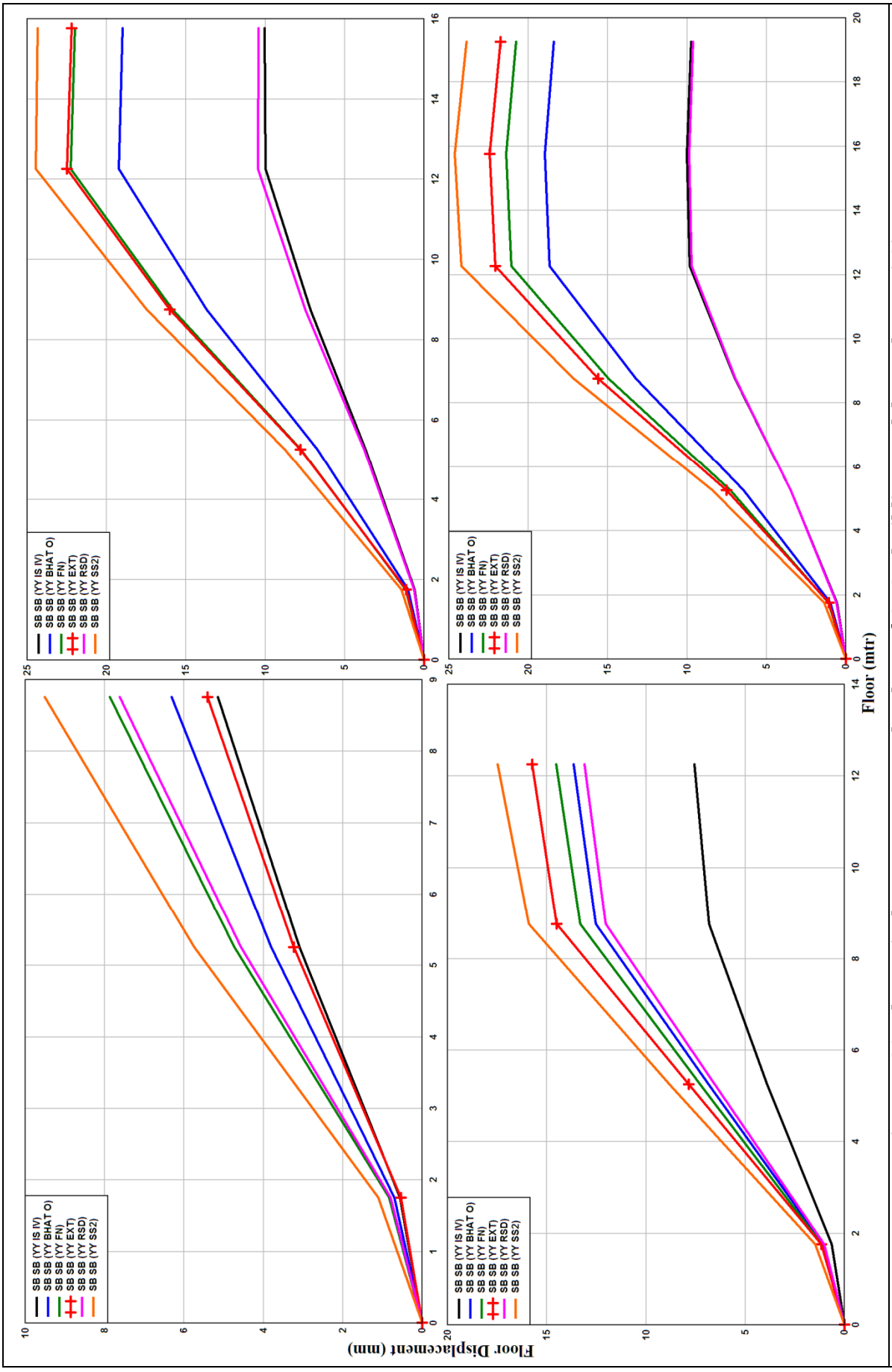

Figure 5.38. Floor Displacements across the slope of SBSB building models at Bhatwari Site

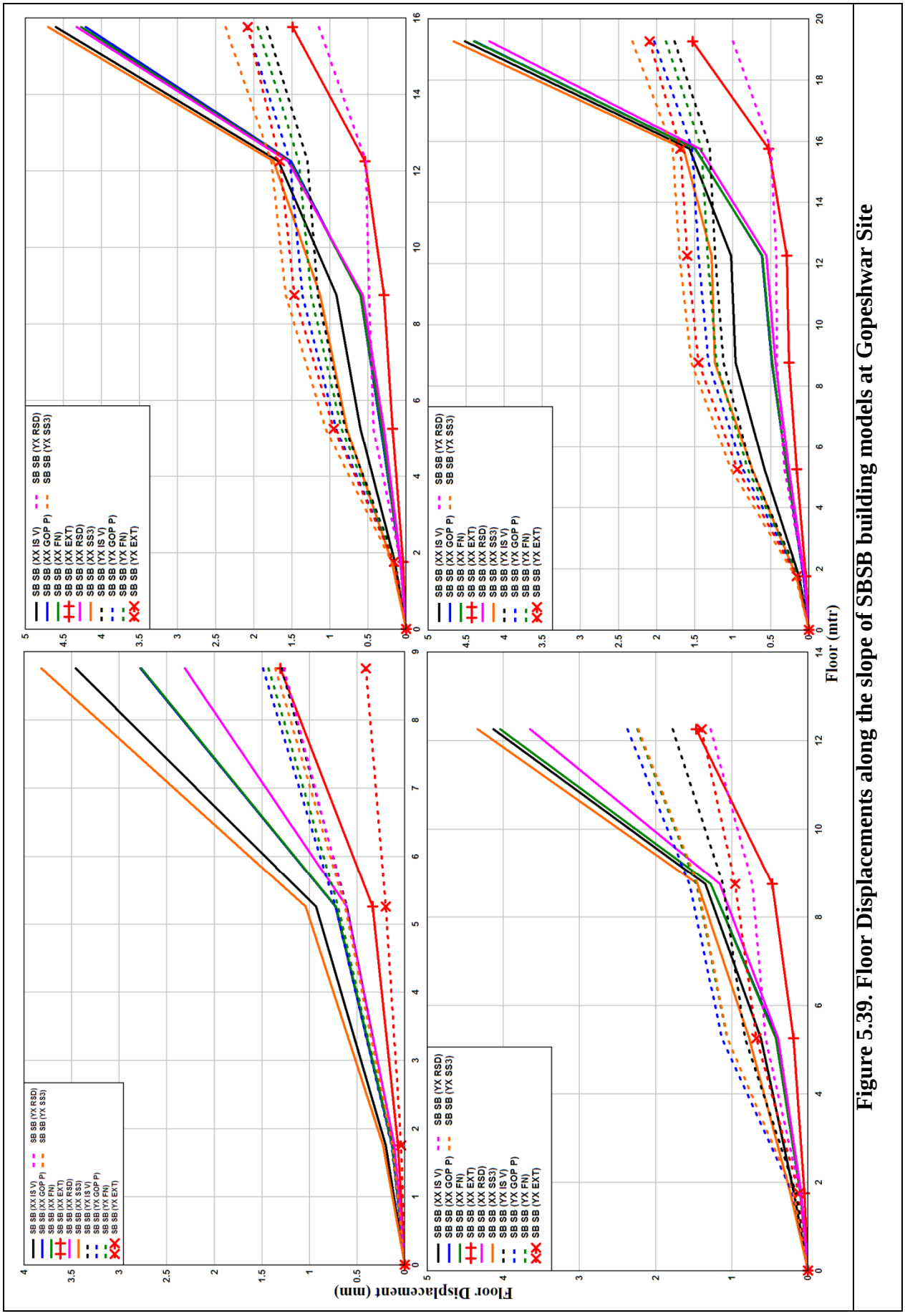

Figure 5.39. Floor Displacements along the slope of SBSB building models at Gopeshwar Site

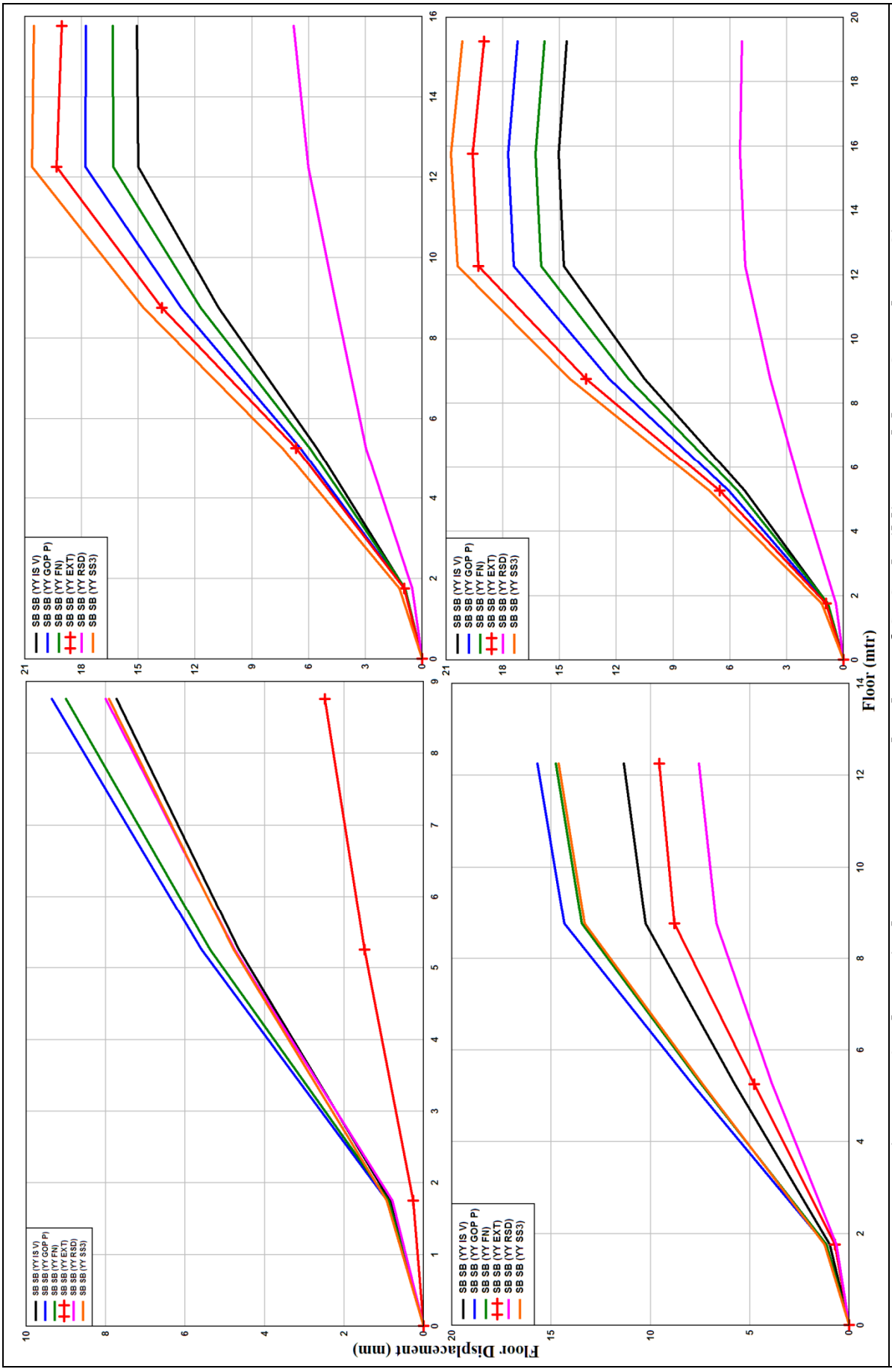

Figure 5.40. Floor Displacements across the slope of SBSB building models at Gopeshwar Site

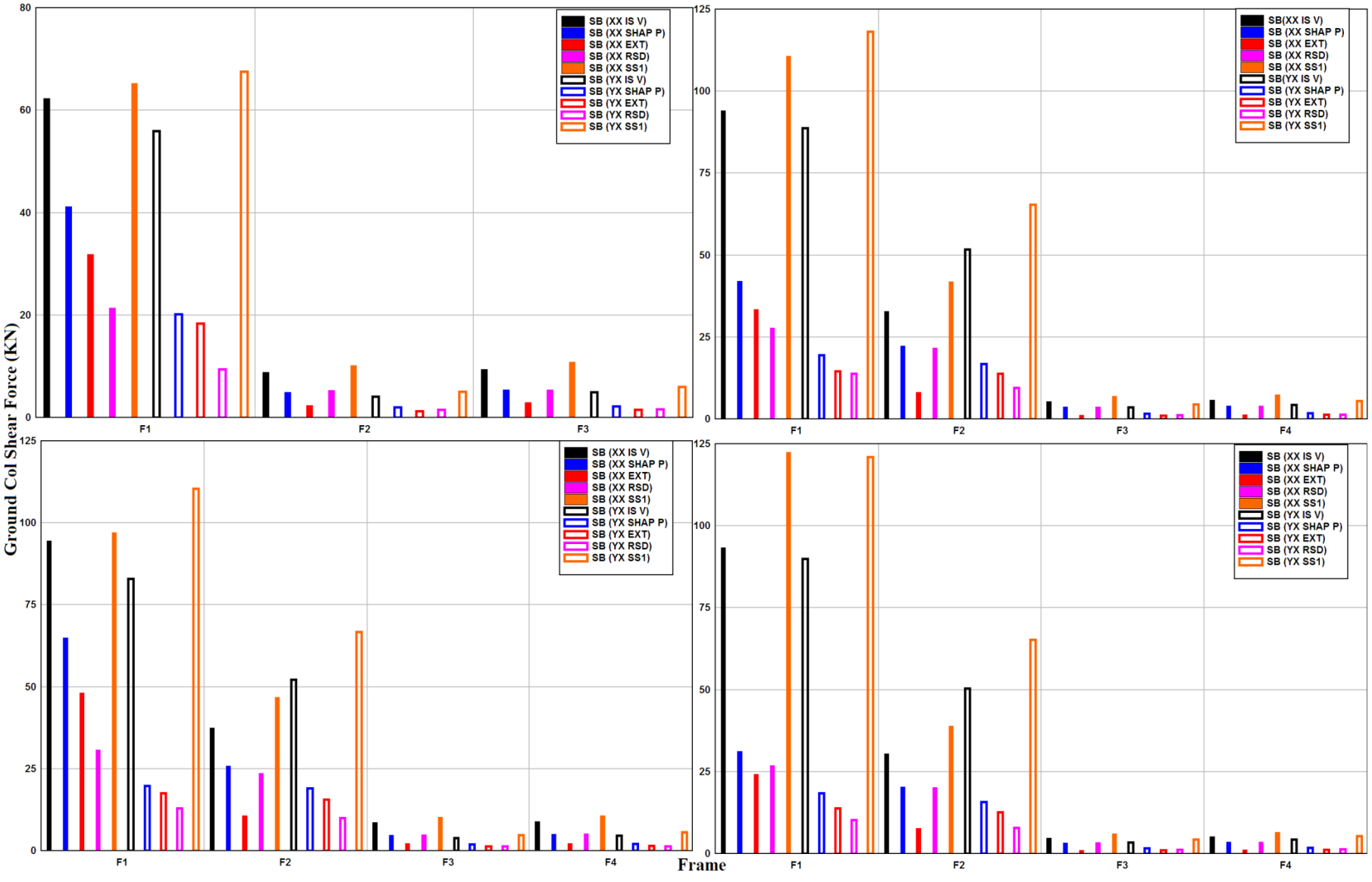

Figure 5.41. Ground Column Shear Force along the slope of SB building models at Shapur Site

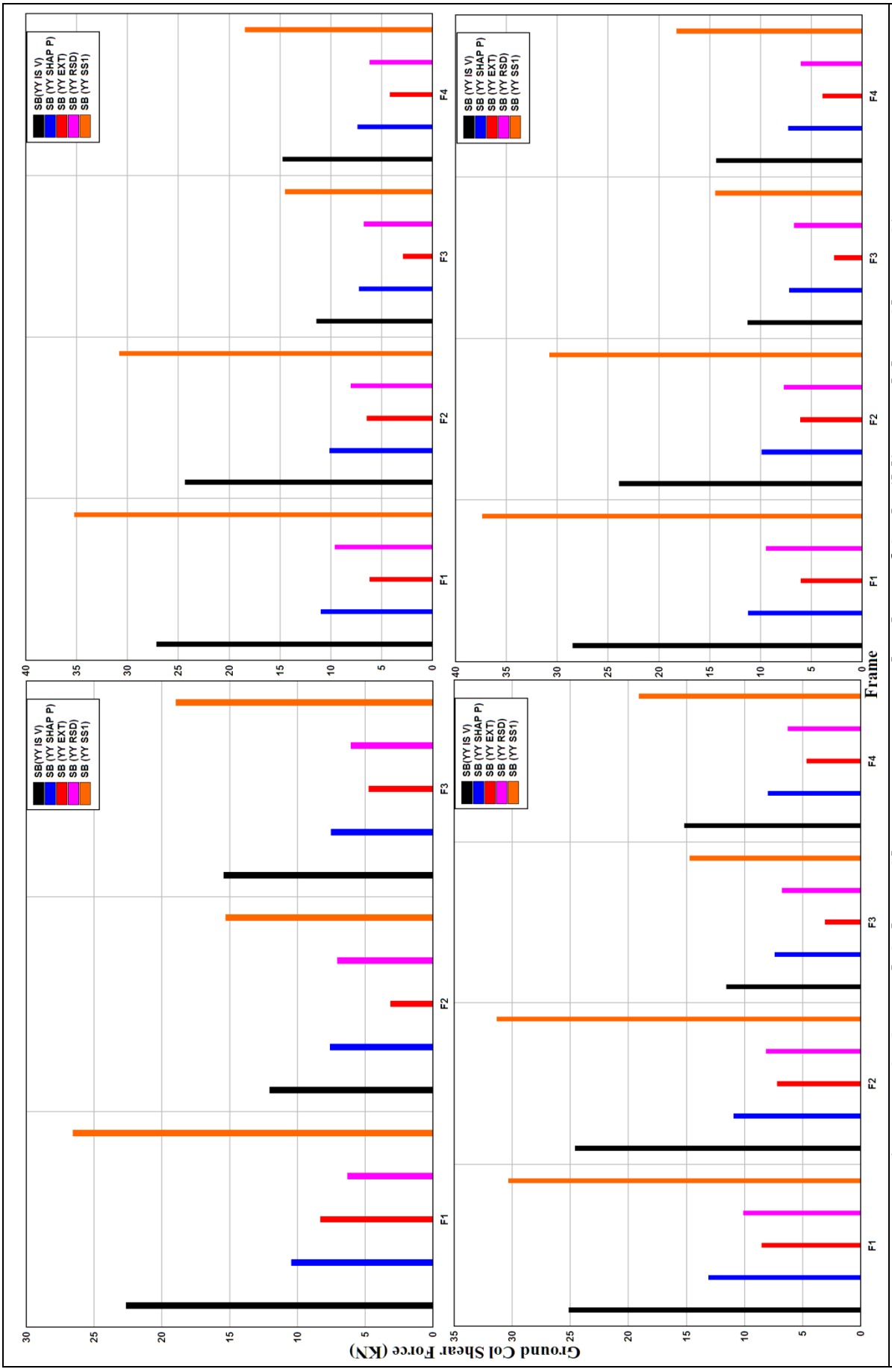

Figure 5.42. Ground Column Shear Force across the slope of SB building models at Shapur Site

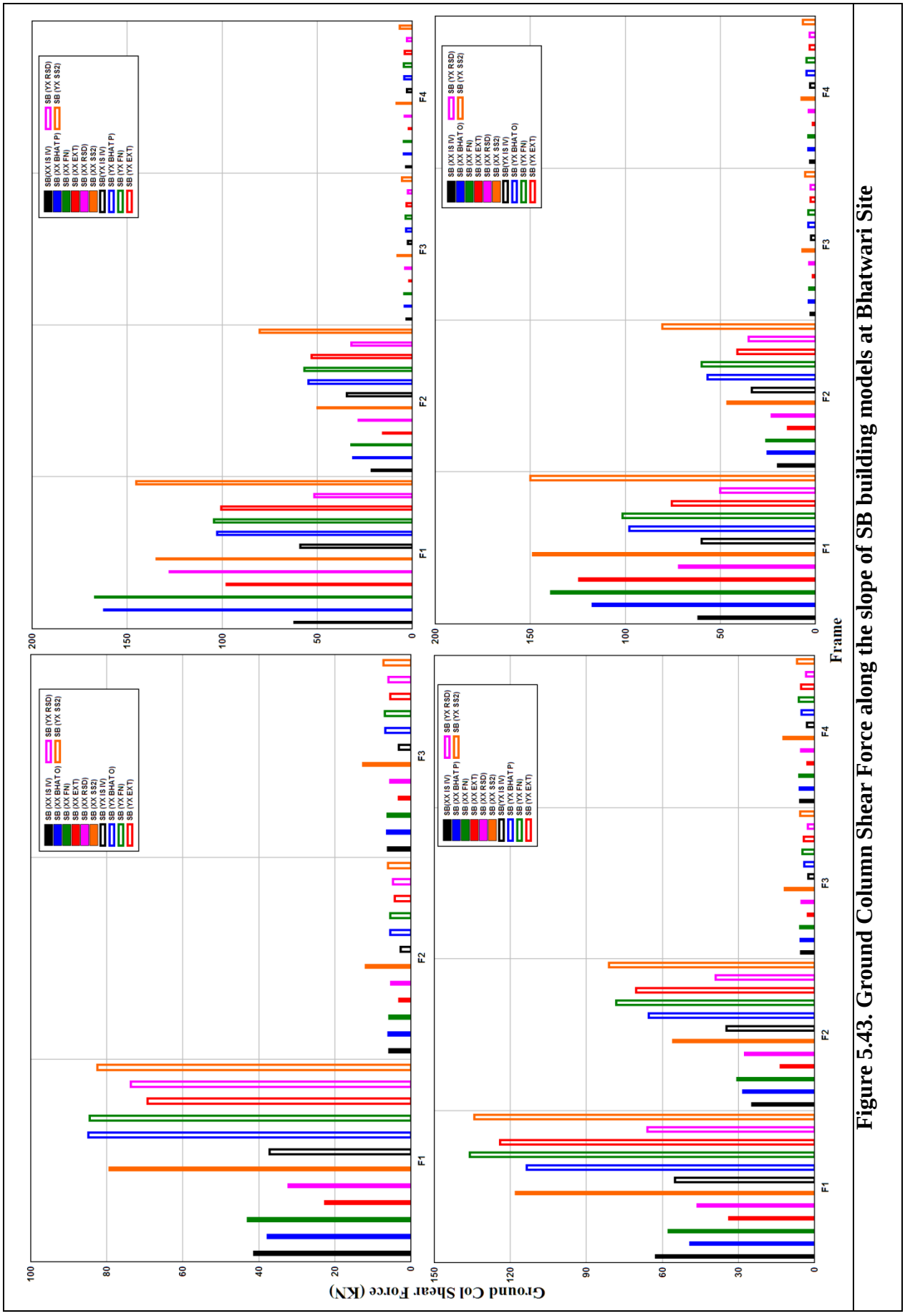

Figure 5.43. Ground Column Shear Force along the slope of SB building models at Bhatwari Site

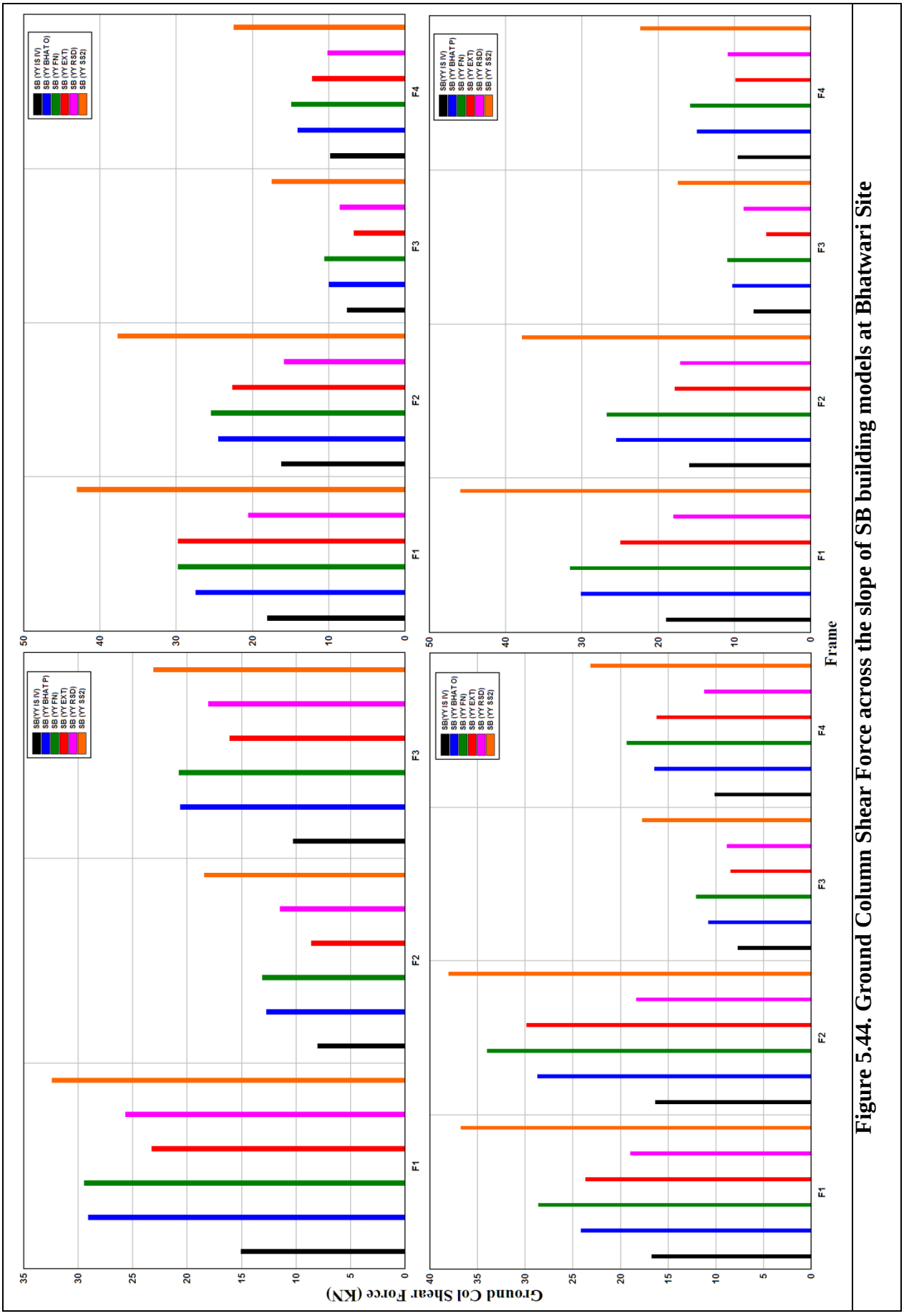

Figure 5.44. Ground Column Shear Force across the slope of SB building models at Bhatwari Site

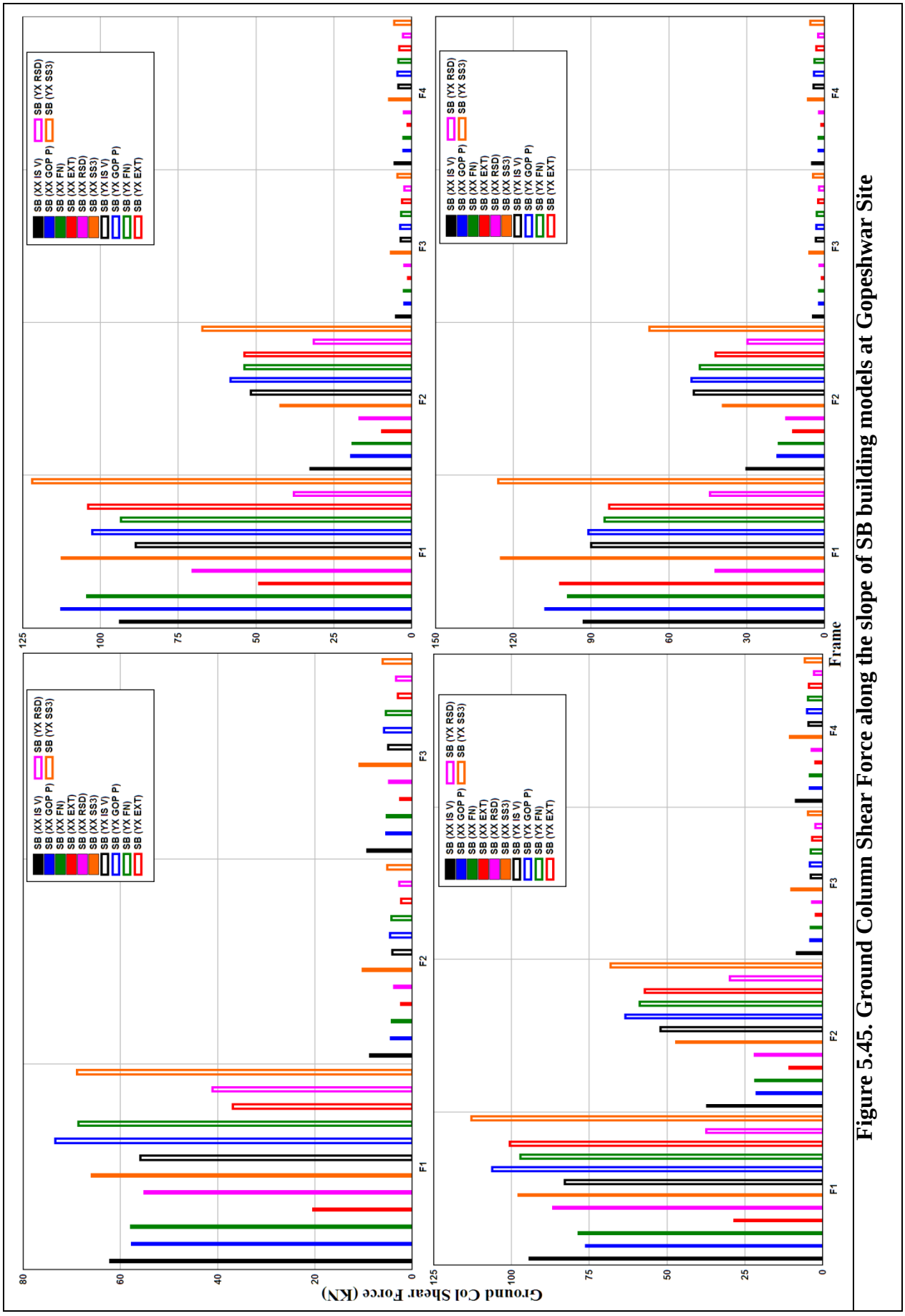

Figure 5.45. Ground Column Shear Force along the slope of SB building models at Gopeshwar Site

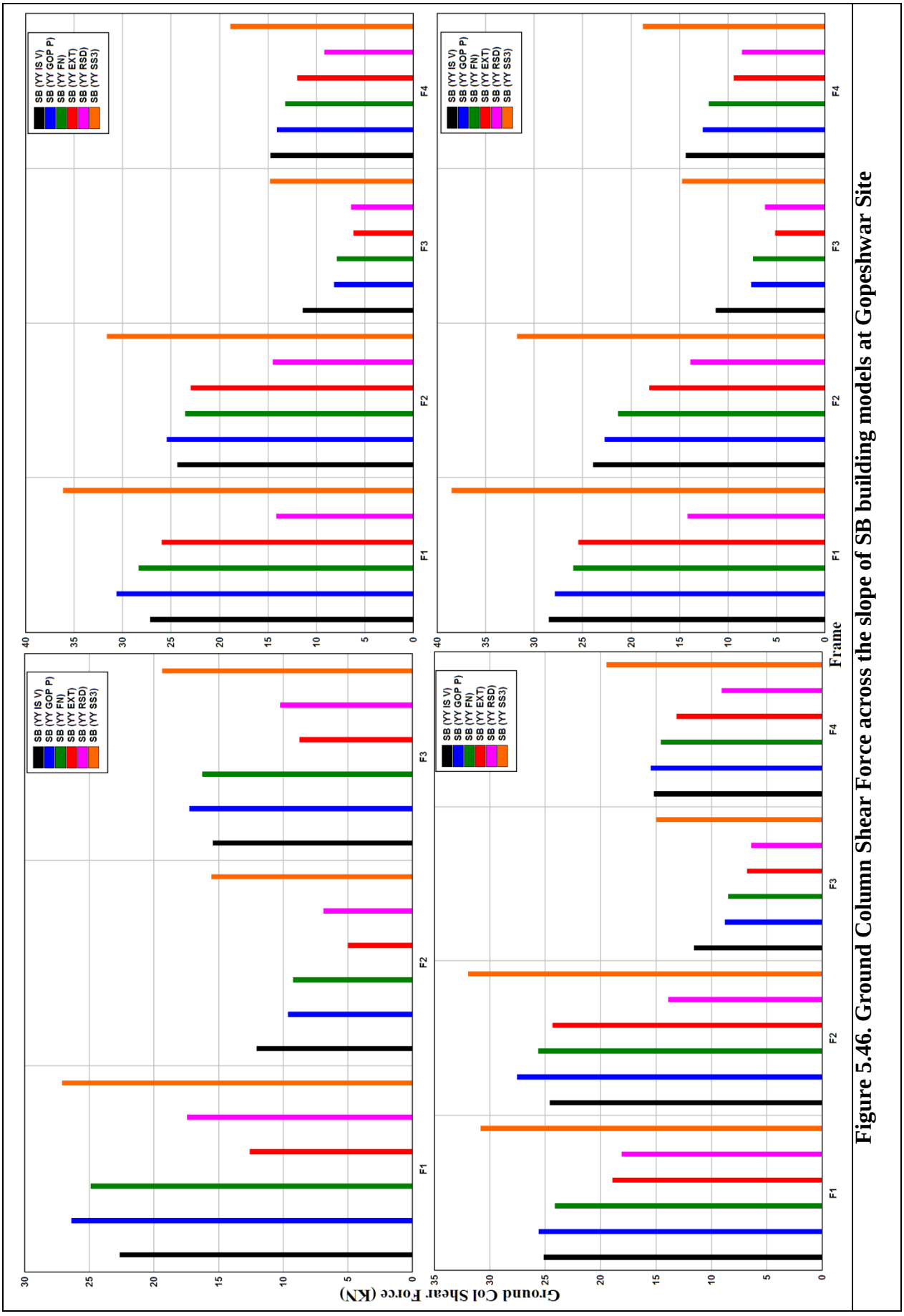

Figure 5.46. Ground Column Shear Force across the slope of SB building models at Gopeshwar Site

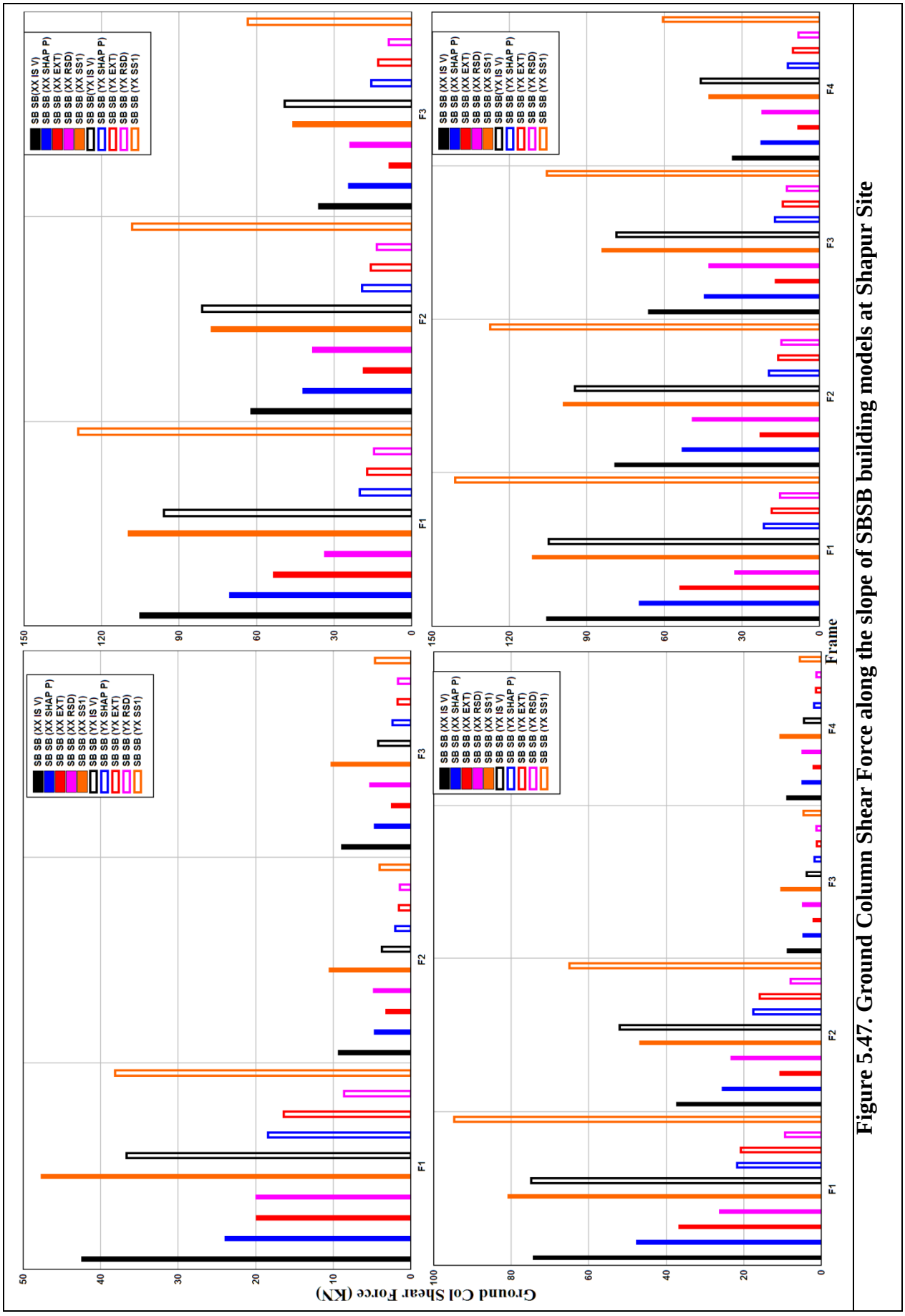

Figure 5.47. Ground Column Shear Force along the slope of SBSB building models at Shapur Site

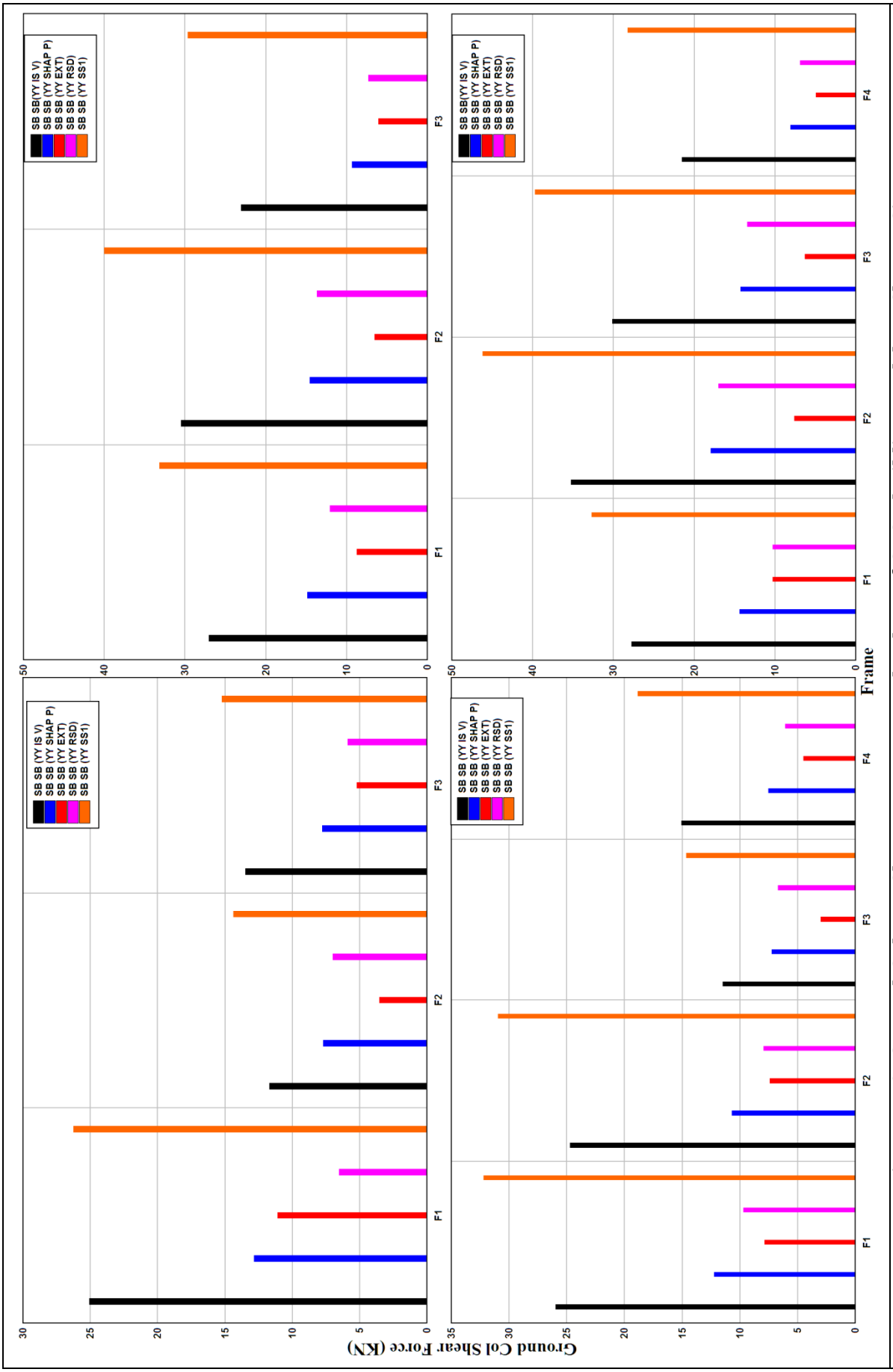

Figure 5.48. Ground Column Shear Force across the slope of SBSB building models at Shapur Site

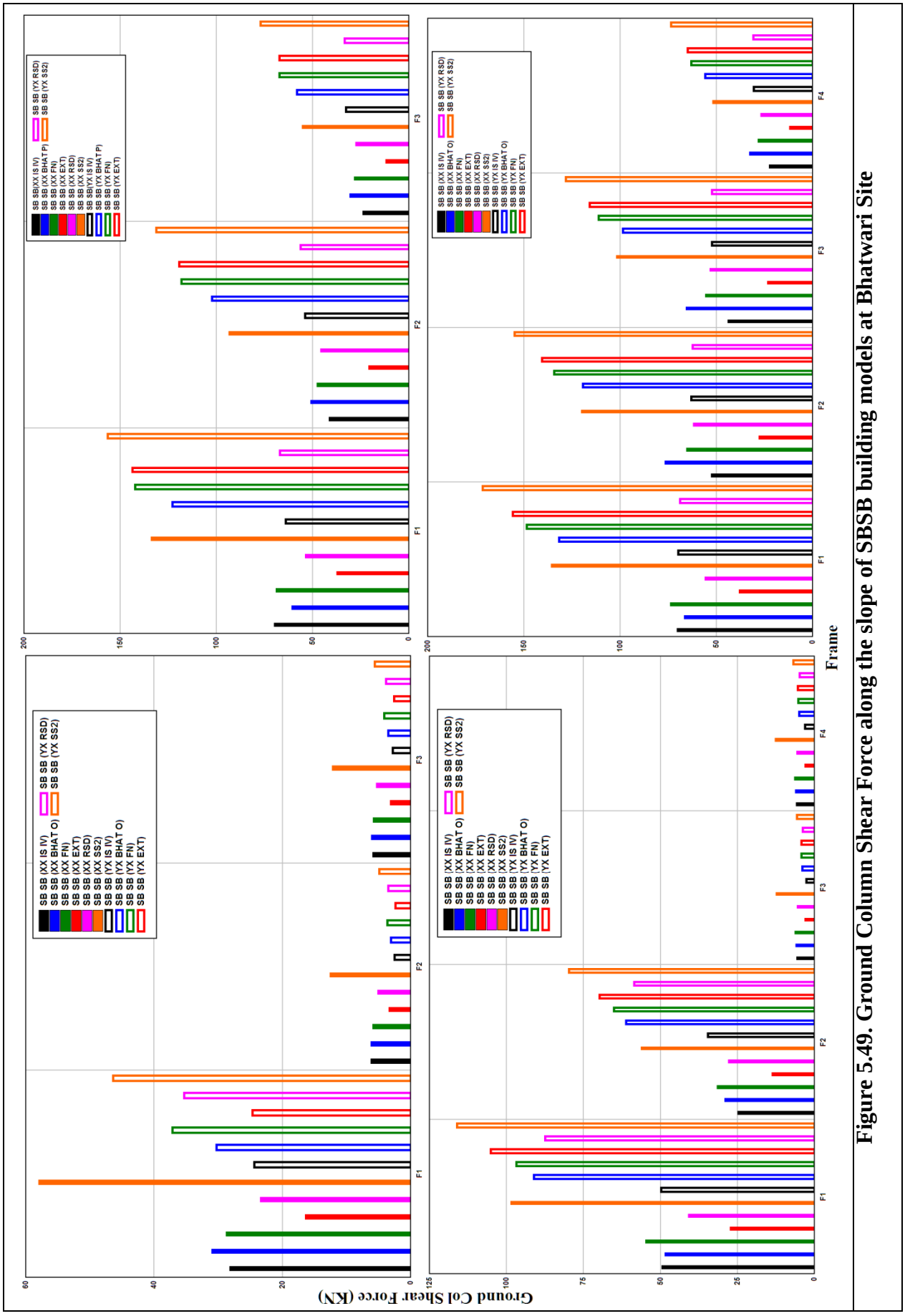

Figure 5.49. Ground Column Shear Force along the slope of SBSB building models at Bhatwari Site

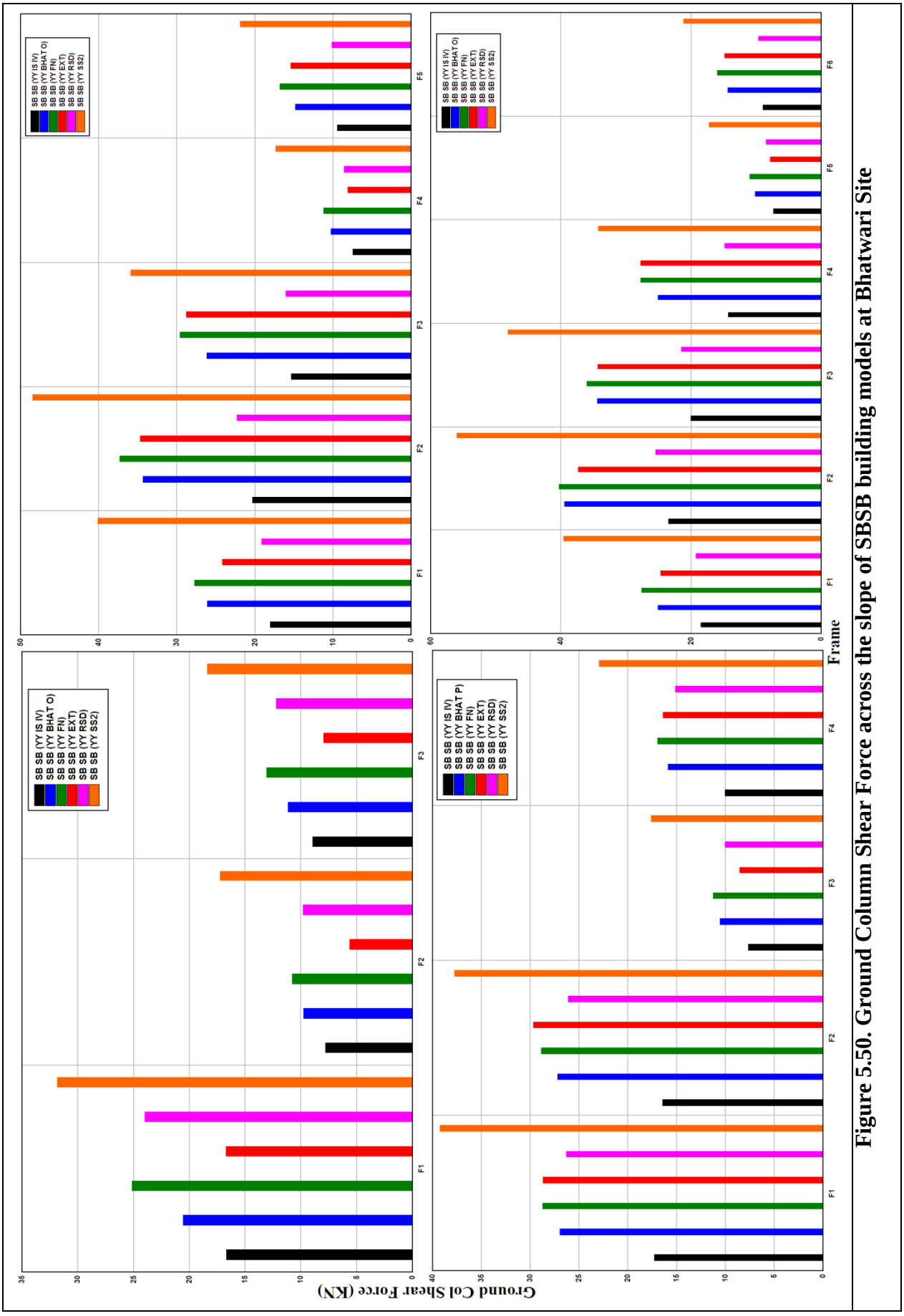

Figure 5.50. Ground Column Shear Force across the slope of SBSB building models at Bhatwari Site

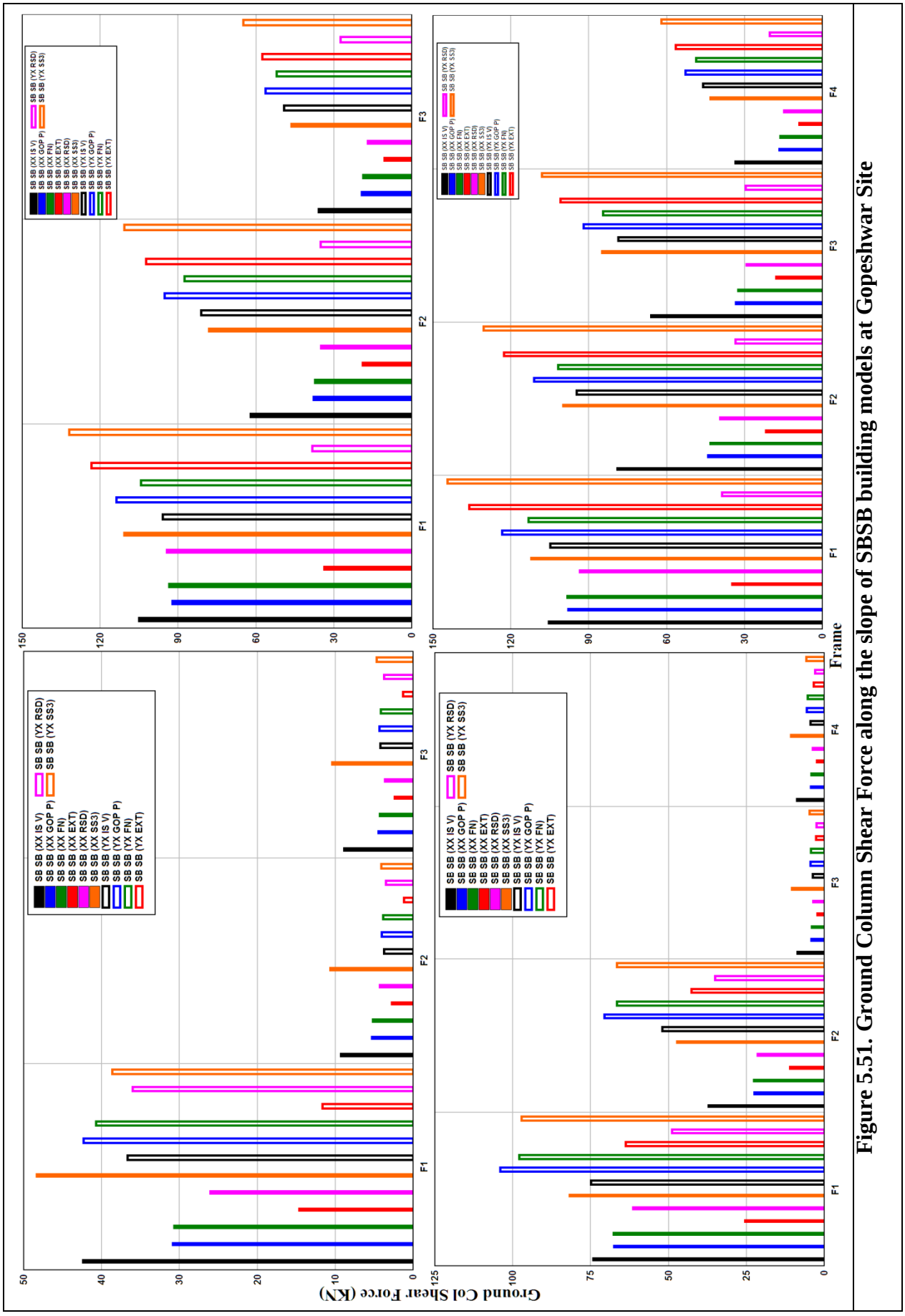

Figure 5.51. Ground Column Shear Force along the slope of SBSB building models at Gopeshwar Site

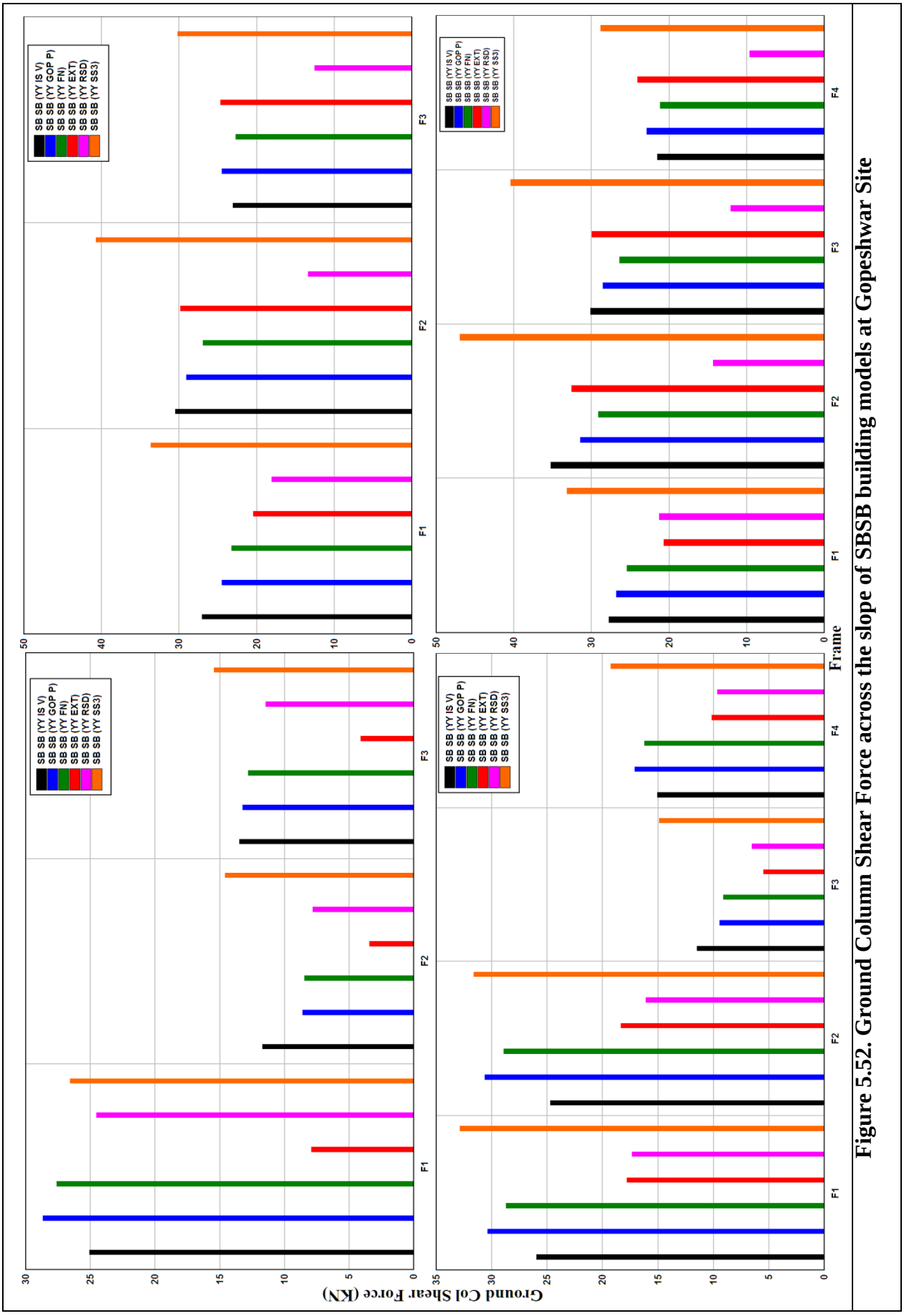

Figure 5.52. Ground Column Shear Force across the slope of SBSB building models at Gopeshwar Site

5.4.4 Results and Discussion of Modal Time History Analysis

The main objective in carrying out the modal time history analysis of considered building models is to study the change in response trends with respect to the responses obtained from response spectrum analysis. The modal time history analysis has been carried out by using various types of seismic inputs, namely, recorded pulse-type ground motions, FN-components, extracted pulses (EXT), residual (RSD) part of ground motions, codal compatible time histories, and compatible time histories of estimated site-specific response spectrum. The maximum floor displacements at various floor levels and maximum ground column shear forces have been obtained for seismic excitation along the slope and across the slope. The results obtained from the dynamic structural response (seismic analysis) of considered buildings (SB and SBSB) are discussed on the basis of observed trends. The computed results are expressed in terms of peak values of two parameters: floor displacements (horizontal) and shear forces in the ground columns. In the figures, symbols XX, YX and YY stands for, seismic input in X, Y, Y directions and computed response parameters in X, X, Y directions, respectively.

The results obtained at Bhatwari and Gopeshwar sites are only discussed because the ground motions obtained at these two sites are relatively stronger compared to ground motion obtained at Shapur site during the 1986 Dharamshala earthquake (M_w 5.5). However, at Shapur site, responses obtained due to compatible time history of estimated site-specific ground motion at the site showed maximum response compared to other seismic inputs at the site. Further, the spectral-amplitudes of NFGM recorded at Shapur station are by and large compatibile with IS code spectra in the period range of 0.1 sec to 0.5 sec, barring one peak at 0.16 sec with a spectral value of 2.91. However, as the period increases beyond 0.5 sec, the spectral values are low compared to the codal spectral values.

a) Floor Displacements of Step-Back Building Models along and across the Slope.

XX: Response along the slope (X-Dir) when seismic excitation along the slope (X-Dir).

For Bhatwari Site, in the modal time history analysis (THA), the floor displacements (FDs) in the X-direction due to considered seismic inputs for all the SB building models show almost same trend as obtained during response spectrum analysis (RSA). Whereas, in 4 storey building model, the response due to site-specific ground motion (SS2) is found slightly lower than obtained in RSA (**Figure 5.53**).

At Gopeshwar site, the comparable FDs observed due to the codal-compatible time history (CCTH) and residual part (RSD) of ground motion in 2 storey building model and are in similar trend as obtained during RSA. However, the responses due to SSGM (SS3), FN-component and recorded ground motion are higher than the responses due to CCTH and residual part (RSD) in THA (**Figure 5.55**). In 3 storey building model, it is found that responses due to SSGM (SS3), FN-component, recorded ground motion (GOP P) and residual part (RSD) are following similar trend as obtained in RSA with slightly higher response due to CCTH at top floor. In 4 storey building model, the responses due to all seismic inputs following same trend as obtained during RSA (**Figure 5.55**). In 5 storey building model, similar trend has been observed between residual (RSD) part, CCTH, FN-component and recorded ground motion (GOP P); while, the response due to extracted pulse (EXT) comes closer to the CCTH response, and the response due to recorded ground motion (GOP P) becomes comparable with SSGM (SS3) (**Figure 5.55**).

YX: Response along the slope (X-Dir) when seismic excitation across the slope (Y-Dir).

For Bhatwari Site, when the seismic inputs are applied in Y-direction and FDs in X-direction, it is observed that the FDs due to all the considered seismic inputs are in same trend as of RSA. In 2 and 3 storey building models, the effect of torsion is more clearly seen compared to 4 and 5 storey building models (**Figure 5.53**).

At Gopeshwar site, in THA of 212SB model, similar trend has been obtained between extracted pulse (EXT), residual (RSD) part, CCTH, FN-component and recorded ground motion (GOP P), as obtained during RSA; while, the response due to SSGM (SS3) found lower and comparable to the response due to the CCTH. In 313SB building model, similar trend has been observed between the responses due to residual (RSD) part and CCTH; while, FN-component and recorded ground motion (GOP P) showed higher response values at top floor level compare to SSGM (SS3) (**Figure 5.55**). It is also observed that response due to extracted pulse (EXT) get lowered and closer to the response due to CCTH. In 413SB model, the similar trend has been observed between the responses due to the residual (RSD) part, CCTH and extracted pulse (EXT). However, the responses due to the FN-component and recorded ground motion (GOP P) are highest. In 513SB model, the responses due to all the considered seismic inputs show almost similar trend as observed in RSA (**Figure 5.55**).

YY: Response across the slope (Y-Dir) when seismic excitation across the slope (Y-Dir).

For Bhatwari site, in all the SB building models the FDs in Y-direction, due to application of all considered seismic inputs show the same trend of response as obtained during RSA (**Figure 5.54**).

At Gopeshwar site, in THA of 212SB model, similar response trends have been observed as obtained in RSA. However, the responses due to FN-component and recorded ground motion (GOP P) are higher than the response due to the SSGM (SS3). In 313SB model, the response due to residual (RSD) part, CCTH, FN-component and recorded ground motion (GOP P) follows same trend as obtained in RSA. However, the responses due to FN-component, recorded ground motion (GOP P) and SSGM (SS3) show comparable values; whereas, the response due to the extracted-pulse (EXT) found to be closer to the response due to the CCTH (**Figure 5.56**). In 413SB model, the similar trend has been observed between the responses due to the residual-part (RSD), CCTH and extracted (EXT) pulse, and the responses due to SSGM (SS3), FN-component, recorded pulse-type ground motion (GOP P) and extracted (EXT) pulse are higher than the response due to the CCTH. These observations are also obtained during RSA. However, the responses due to SSGM (SS3) and recorded pulse-type ground motion (GOP P) are highest and also have comparable values; whereas, responses due to extracted pulse (EXT) and FN-component are comparable, and lower than the responses due to SSGM (SS3) and recorded pulse-type ground motion (GOP P). In 513SB model, almost similar trend between the responses have been observed as obtained in RSA, but the difference is only that the response due extracted pulse (EXT) comes slightly below the response due to the FN-component (**Figure 5.56**).

b) Floor Displacements of Step-Back-Set-Back Building Models along and across the Slope.

XX: Response along the slope (X-Dir) when seismic excitation along the slope (X-Dir).

For Bhatwari site, the responses of all the SBSB building models due to considered seismic inputs in THA are in similar trend as obtained in RSA (**Figure 5.57**).

At Gopeshwar site, in THA, all the SBSB building models show almost similar response trend due to the considered seismic inputs as obtained in RSA. However, in 212SBSB model, the responses due to CCTH and SSGM (SS3) come closer (**Figure 5.59**).

YX: Response along the slope (X-Dir) when seismic excitation across the slope (Y-Dir).

For Bhatwari site, as the building storey increases from 3 to 5, the FDs along the slope due to application of seismic inputs across the slope show significantly higher FDs-YX at all the intermediate floor levels for all types of seismic inputs compared to FDs (XX) obtained along the slope when these seismic inputs were also applied along the slope. This shows the significance of torsional effect. Further, the response trend in THA found similar to that of RSA (**Figure 5.57**).

At Gopeshwar site, in THA of 212SBSB and 313SBSB building models, the responses due to all considered seismic inputs show similar pattern as obtained during RSA. However, in 313SBSB model, the response due to SSGM (SS3) gets lower down and closer to the CCTH response. The 414SBSB and 515SBSB building models, show similar response pattern as obtained in RSA. However, in these two models, the response due to extracted pulse (EXT) get lower down and comes closer to the CCTH response; while, response due to SSGM (SS3), FN-component and recorded pulse-type ground motion (GOP P) are higher and comparable too (**Figure 5.59**).

YY: Response across the slope (Y-Dir) when seismic excitation across the slope (Y-Dir).

For Bhatwari site, in the THA, the FDs-YY due to seismic excitations across the slope found almost in similar trend as obtained in RSA. However, in 4 and 5 storey building models the FDs obtained due to extracted pulse (EXT) & FN-component found closer to the FDs due to the SSGM (SS2) compared to RSA (**Figure 5.58**).

At Gopeshwar site, in THA of 212SBSB model, similar trend has been observed between the responses due to the residual-part (RSD), FN-component, recorded pulse-type ground motion (GOP P) and extracted-pulse (EXT) as obtained in RSA; while, the response due to SSGM (SS3) gets lowered than the responses due to CCTH and residual-part (RSD) (**Figure 5.60**). In 313SBSB model, similar trend between the responses due to the residual-part (RSD), CCTH, FN-component and recorded pulse-type ground motion (GOP P) has been observed. However, the responses due to the extracted-pulse (EXT) and SSGM (SS3) get lower down and come closer to the responses obtained due to the residual-part (RSD) and CCTH, respectively. In THA of 414SBSB & 515SBS building models, similar trend has been observed between the responses due to the residual-part (RSD), CCTH and SSGM (SS3), and between the responses due to the CCTH, FN-component and recorded pulse-type ground motion (GOP P), as obtained

in RSA (**Figure 5.60**). However, in both the building models, the time history responses due to FN-component and recorded pulse-type ground motion (GOP P) get closer to SSGM (SS3), while the response due to extracted-pulse (EXT) goes lower and closer to that response obtained due to the CCTH and FN-component of ground motion (**Figure 5.60**).

c) Ground Column Shear Force in Step-Back Building Models along and across the Slope.

XX and YX: Response along the slope (X-Dir) when seismic excitation along the slope (X-Dir) and Response along the slope (X-Dir) when seismic excitation across the slope (Y-Dir).

For Bhatwari site, the shear force in ground columns in frame F1 attracts much higher forces compare to other frames because of short column effect. THA shows almost similar trending responses for all building models, as obtained in RSA (**Figure 5.61**).

XX: Response along the slope (X-Dir) when seismic excitation along the slope (X-Dir).

At Gopeshwar site, during the THA, almost similar trend in responses are obtained for 3 and 4 storey building models, as obtained in RSA. However, in 212SB building model, response due to the CCTH goes slightly lower than that of response due to FN-component and recorded pulse-type ground motion (GOP P) in frame "F1". While, in 513SB building model, responses due to CCTH and FN-component of ground motion slightly exceeds the response due to extracted-pulse (EXT) (**Figure 5.63**).

YX: Response along the slope (X-Dir) when seismic excitation across the slope (Y-Dir).

At Gopeshwar site, in THA, the 212SB building model shows similar pattern of responses as obtained in RSA. However, in 3, 4 and 5 storey building models almost similar trend obtained between the responses due to the FN-component, recorded pulse-type ground motion (GOP P), residual-part (RSD), SSGM (SS3) and CCTH; while, the response due to the extracted-pulse (EXT) gets lowered down and not remain comparable to the responses due to FN-component and recorded pulse-type ground motions (GOP P) (**Figure 5.63**).

YY: Response across the slope (Y-Dir) when seismic excitation across the slope (Y-Dir).

For Bhatwari site, in THA, the application of seismic inputs across the slope (Y-direction) has brought out that the shear forces across the slope in all the building models showed closer match with the responses as obtained in RSA. However, the reverse responses are obtained

between the residual (RSD) part of ground motion & extracted pulse (EXT) in 2 storey building model (**Figure 5.62**).

At Gopeshwar site, in THA, the 413SB building model shows similar pattern of responses as obtained in RSA. However, in 513SB building model response due to extracted-pulse (EXT) goes down and has lower response compared to residual-part (RSD) of ground motion in frames 'F2' and 'F4'. Further, in 212SB building model, the response due to residual-part (RSD) get lowered and becomes almost same that of extracted-pulse (EXT) response with slight difference in frame 'F1'; while in frames 'F2' and 'F3', the responses between extracted-pulse (EXT) and residual-part (RSD) of ground motion get reversed. In 313 building model, the response due to extracted-pulse (EXT) goes lowered and showed lower response compared to response obtained due to residual-part (RSD) (**Figure 5.64**).

d) Ground Column Shear Force in Step-Back-Set-Back Building Models along and across the Slope.

XX: Response along the slope (X-Dir) when seismic excitation along the slope (X-Dir).

For Bhatwari site, for all the SBSB building models, "XX" component of shear force due to considered seismic inputs in THA show close matching response trend that of RSA (**Figure 5.65**).

At Gopeshwar site, for all the SBSB building models, 'XX' component ground-column shear forces due to considered seismic inputs in THA show matching response trend that of RSA. However, in 3, 4 and 5 storey SBSB building models, the response due to the CCTH shows significantly higher value compared to other seismic inputs; and in 212SBSB building model the response due to the CCTH shows significantly lower value compared to other seismic inputs and becomes closer to the response due to the recorded pulse-type ground motion (GOP P) (**Figure 5.67**).

YX: Response along the slope (X-Dir) when seismic excitation across the slope (Y-Dir).

For Bhatwari site, in all the SBSB building models, YX-response due to all considered seismic inputs exceeds respective XX-response due to torsional effect, except response due to SSGM (SS2) in frame F1 of 2 storey building model. Further, it is observed that the responses due to all seismic inputs in all building models are in similar pattern as obtained during RSA. However, in frame "F1" of 414SBSB building model, the response due to FN-component & extracted pulse (EXT) shows higher values than SSGM (SS2) compared to the RSA; and in

frames “F1” and “F2” of 515SBSB building model, the response due to FN-component and extracted pulse (EXT) shows almost comparable values to the response due to SSGM (SS2). Whereas, in RSA, the responses due to FN-component and extracted pulse (EXT) were lower than the response due to SSGM (SS2) (**Figure 5.65**).

At Gopeshwar site, it is observed that the responses due to all seismic inputs in 313SBSB building model are in similar pattern as obtained during RSA. However, 212SBSB building model, response due to the CCTH found highest, and response due to residual-part (RSD) exceeds the response due to SSGM (SS3) and FN-component, and has comparable response to recorded pulse-type ground motion (GOP P). Further, in 414SBSB and 515SBSB building models, the response due to the extracted-pulse (EXT) showed lower response compared to FN-component and RGM, but is comparable to FN-component in 515SBSB building model (**Figure 5.67**).

YY: Response across the slope (Y-Dir) when seismic excitation across the slope (Y-Dir).

For Bhatwari site, in THA, the responses obtained across the slope are found almost in similar pattern as obtained in RSA for all the seismic inputs. However, the responses due to extracted pulse (EXT) & residual part (RSD) of ground motion are slightly higher in frame “F1” of 3 storey building model. Further, in 515SBSB model the responses due to FN-component and recorded pulse-type ground motion are showing significantly higher values compared to the responses obtained in the RSA (**Figure 5.66**).

At Gopeshwar site, in THA, the responses obtained across the slope are found almost in similar pattern for 2 and 3 storey building models, as obtained in RSA for all the seismic inputs. However, in 4 and 5 storey building models, the response due to extracted-pulse (EXT) get lowered down to that of responses due to the CCTH, FN-component and recorded pulse-type ground motion (GOP P). Further, the response due to the CCTH goes higher compared to FN-component, recorded pulse-type ground motion (GOP P) and extracted-pulse (EXT) ground motion in 5 storey building model (**Figure 5.68**).

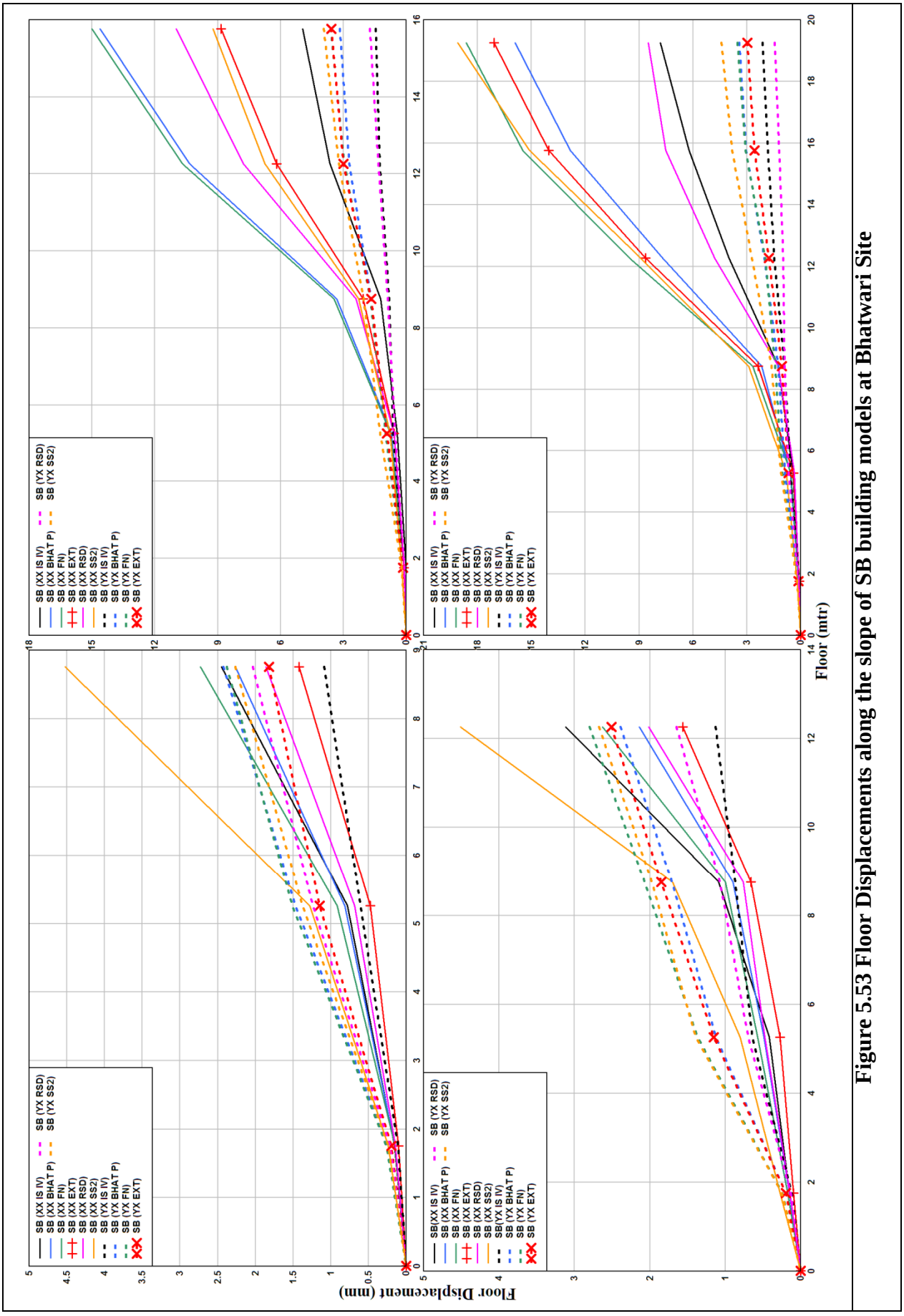

Figure 5.53 Floor Displacements along the slope of SB building models at Bhatwari Site

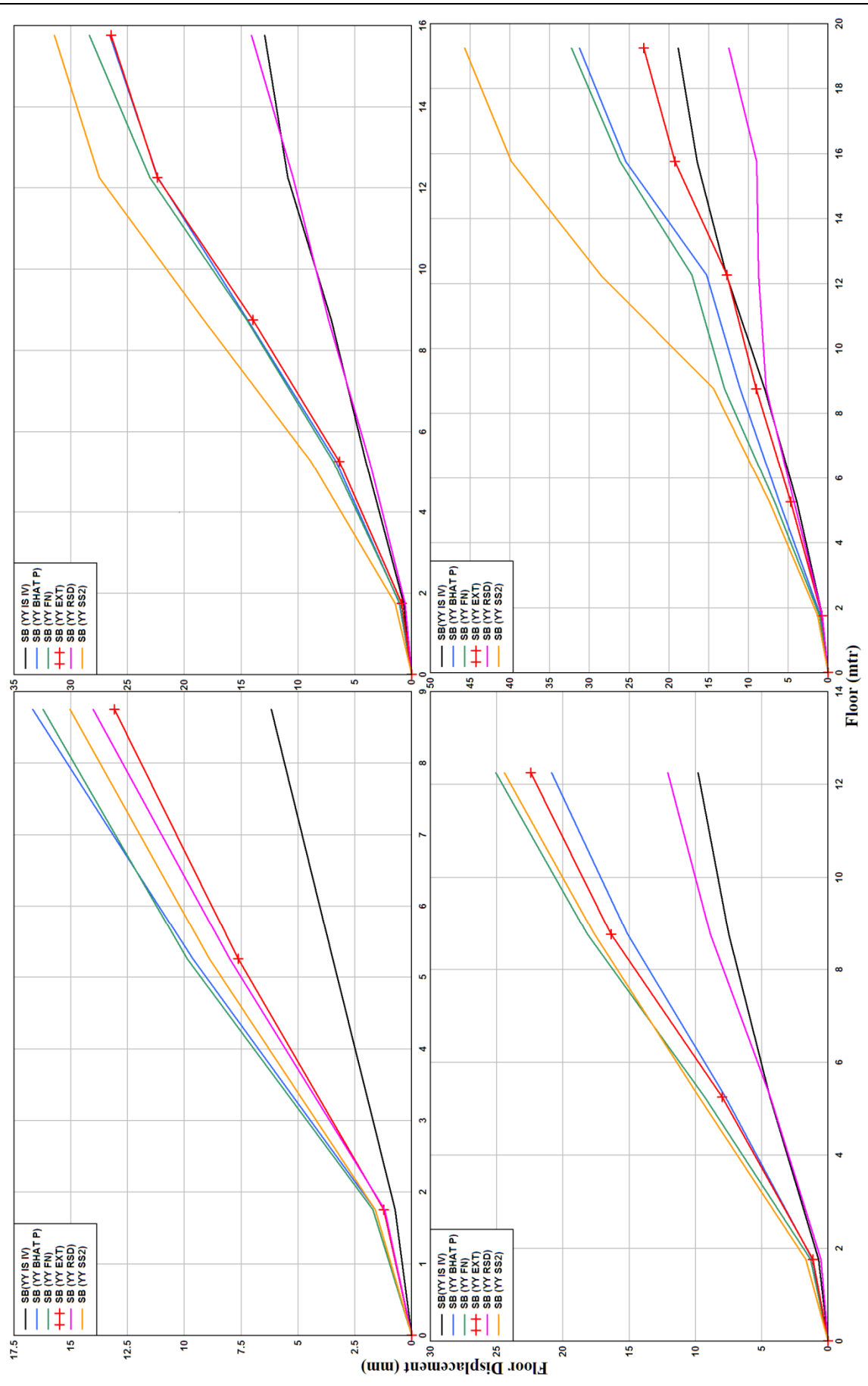

Figure 5.54 Floor Displacements across the slope of SB building models at Bhatwari Site

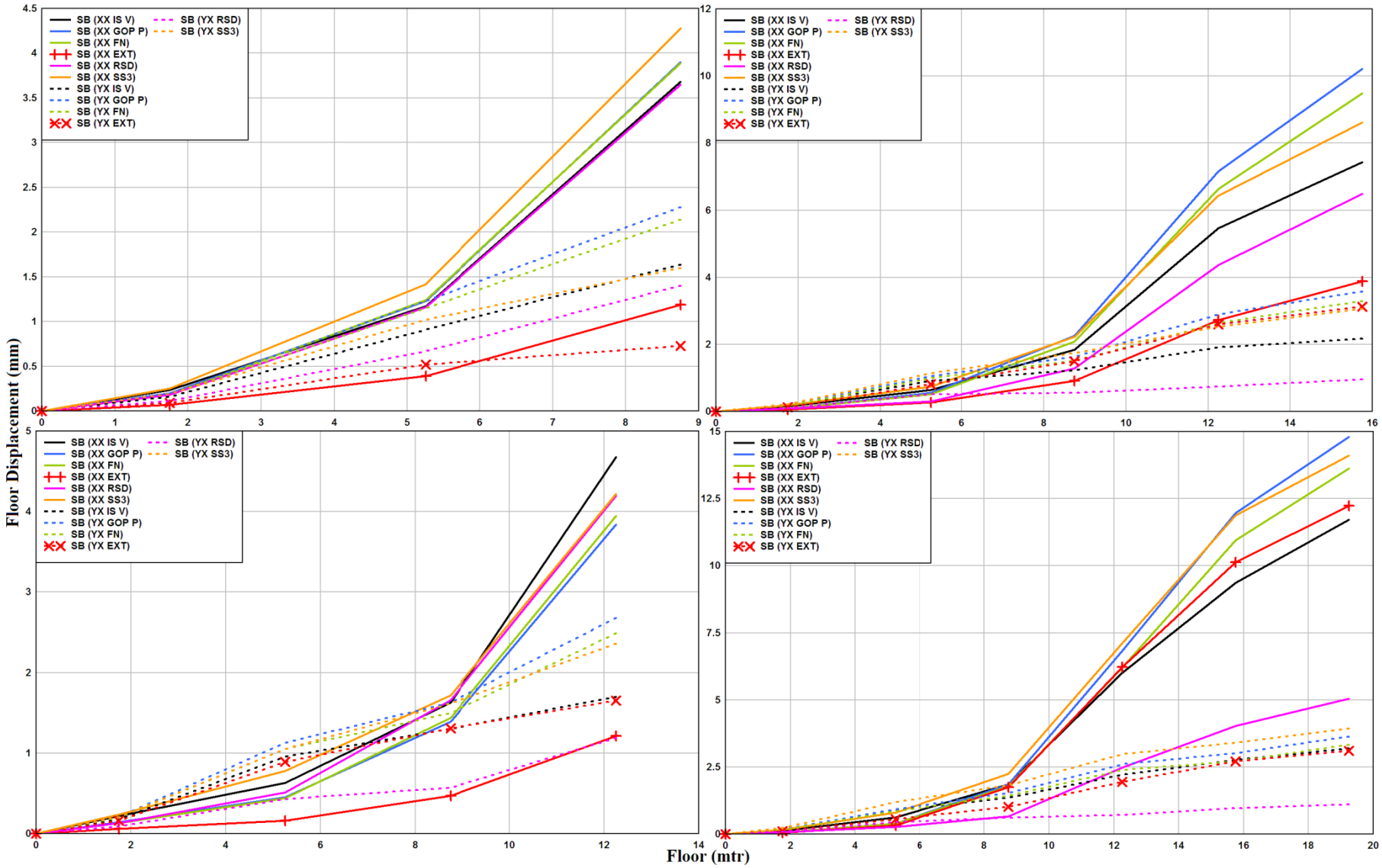

Figure 5.55 Floor Displacements along the slope of SB building models at Gopeshwar Site

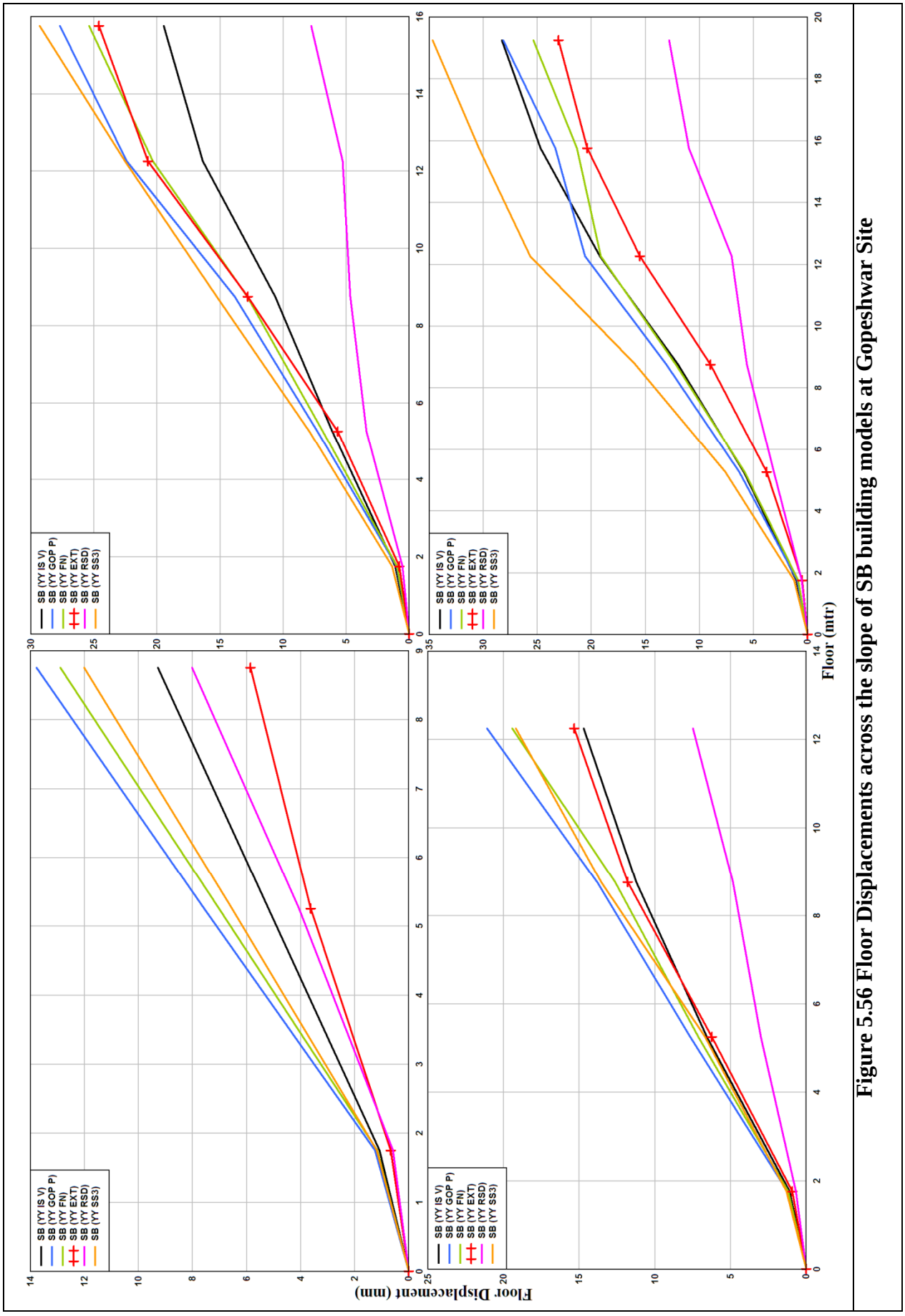

Figure 5.56 Floor Displacements across the slope of SB building models at Gopeshwar Site

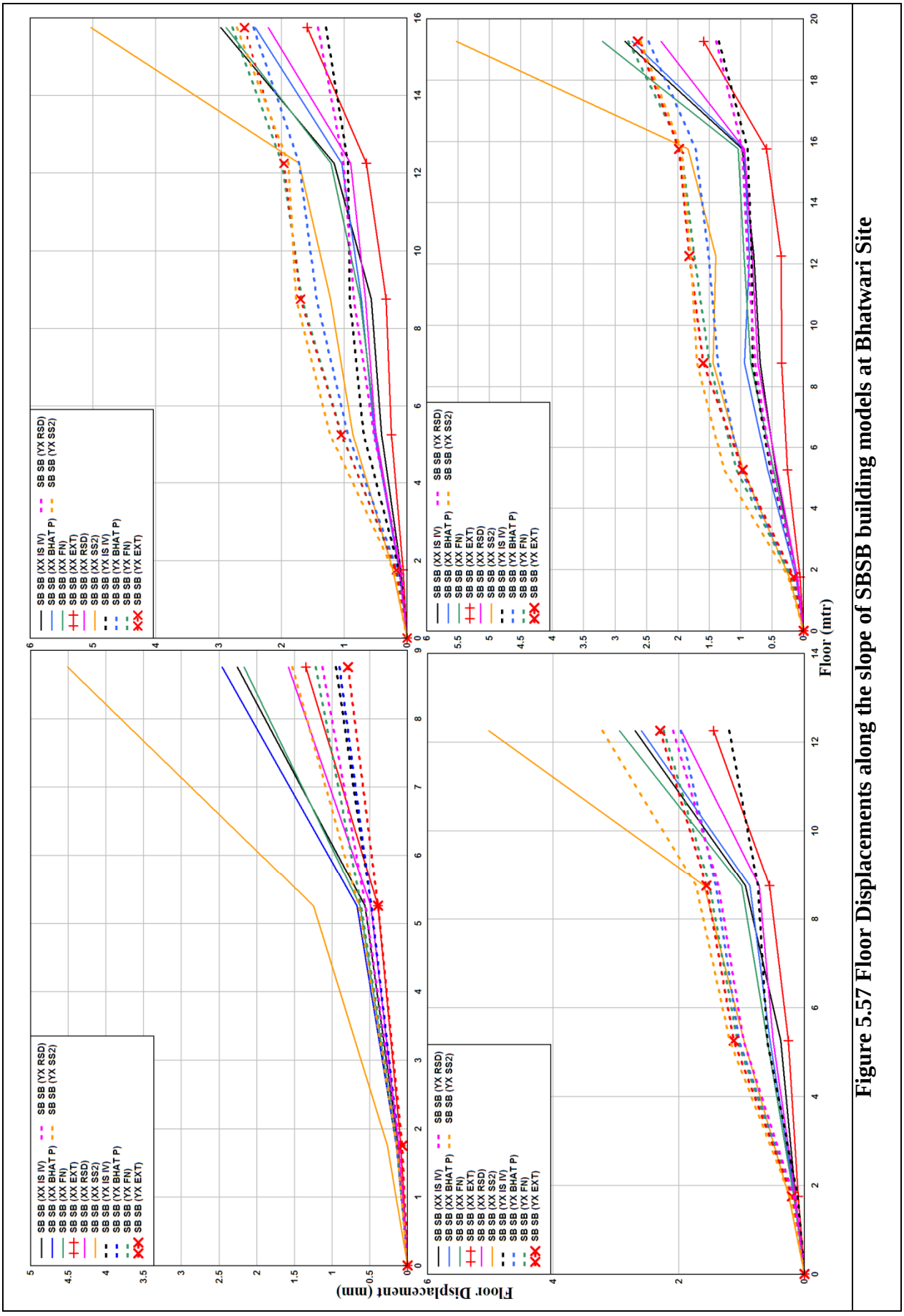

Figure 5.57 Floor Displacements along the slope of SBSB building models at Bhatwari Site

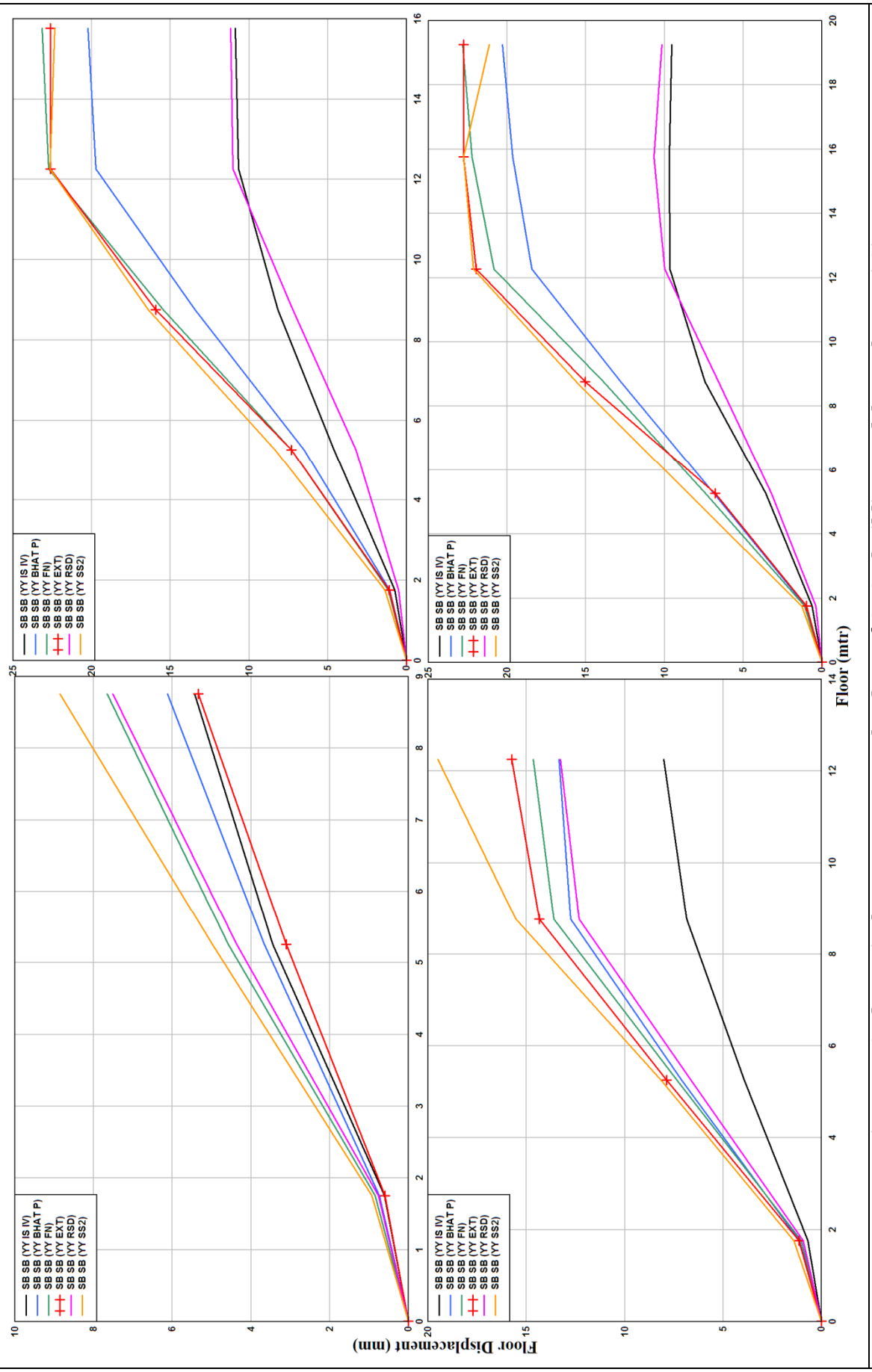

Figure 5.58 Floor Displacements across the slope of SBSB building models at Bhatwari Site

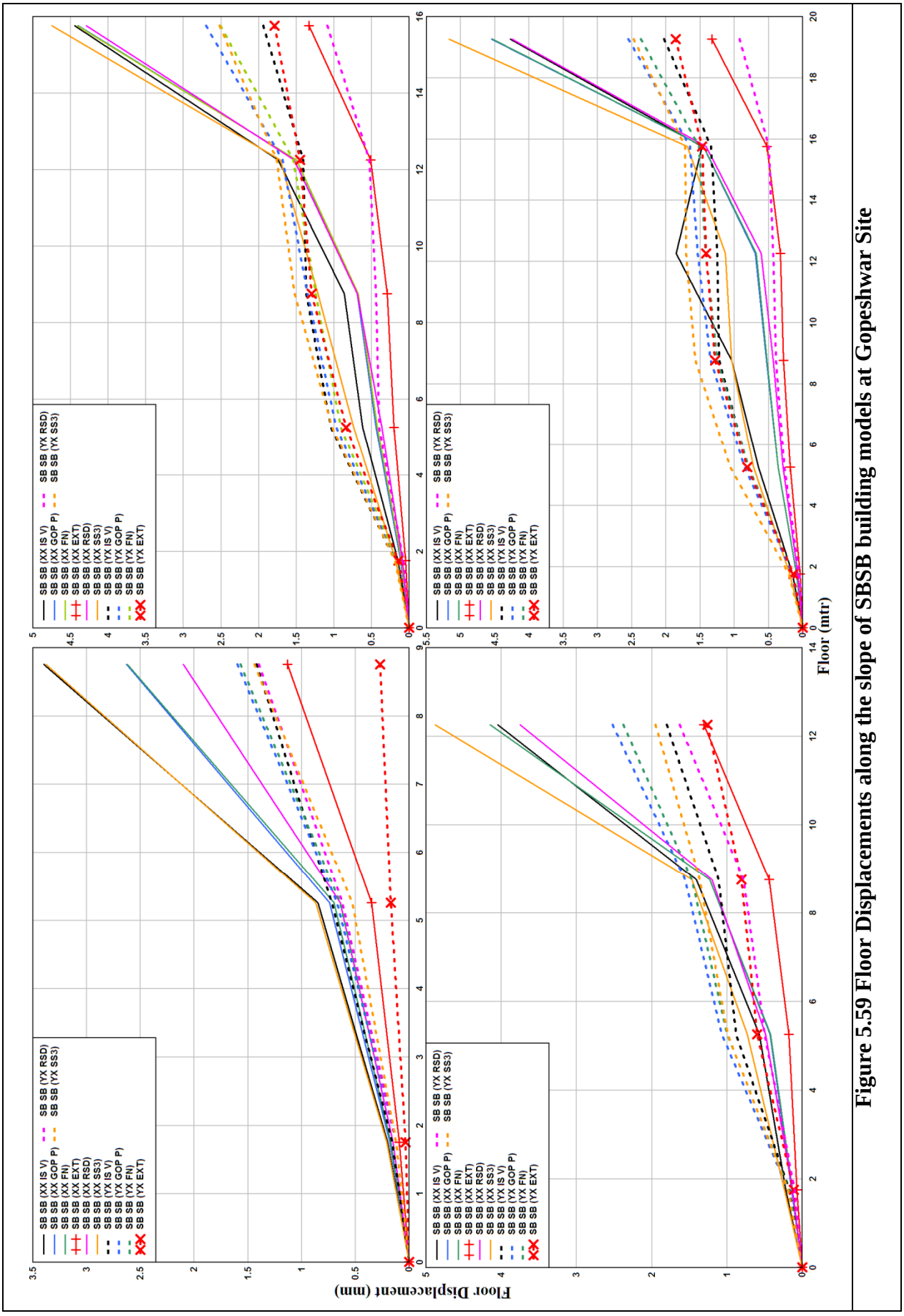

Figure 5.59 Floor Displacements along the slope of SBSB building models at Gopeshwar Site

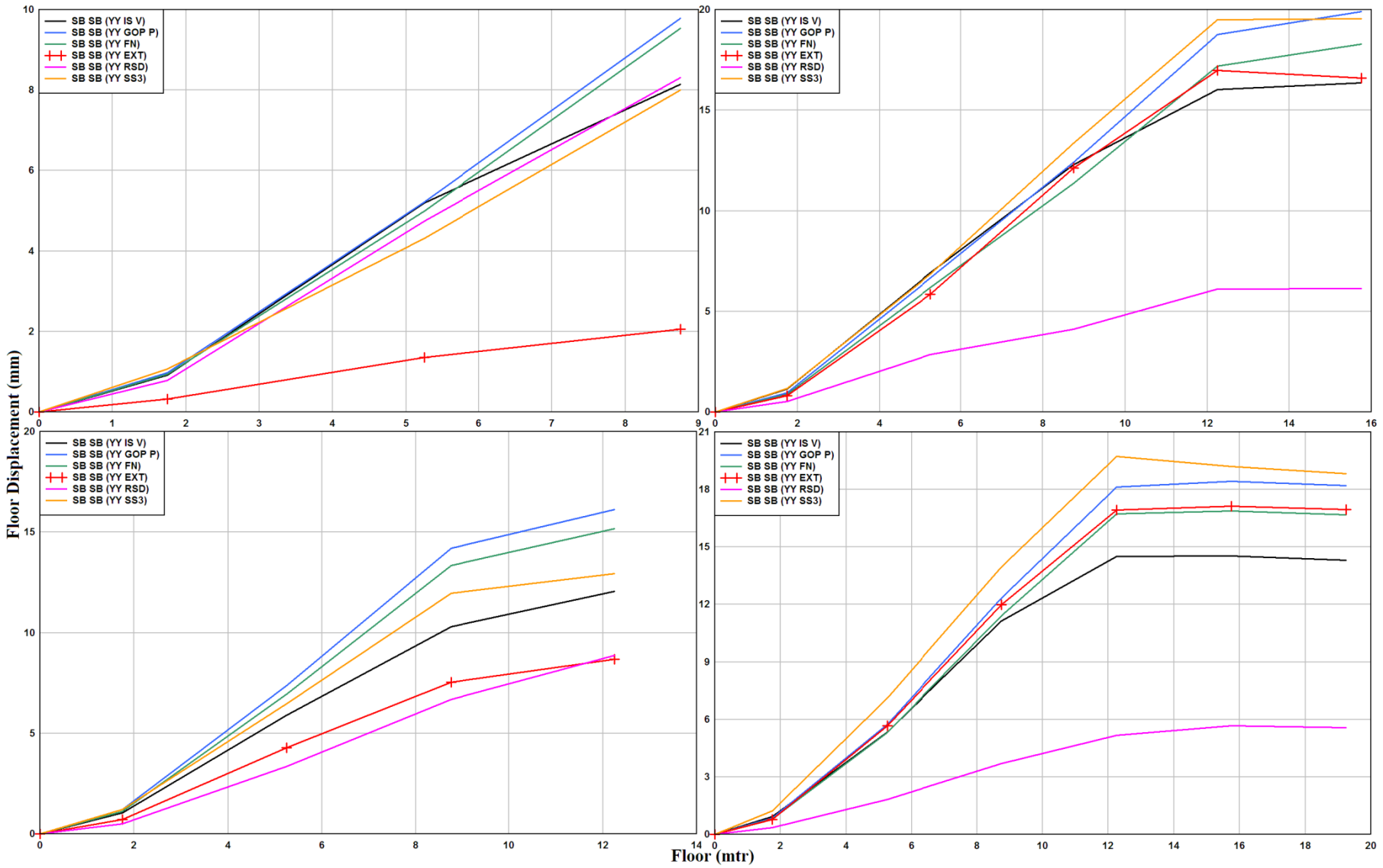

Figure 5.60 Floor Displacements across the slope of SBSB building models at Gopeshwar Site

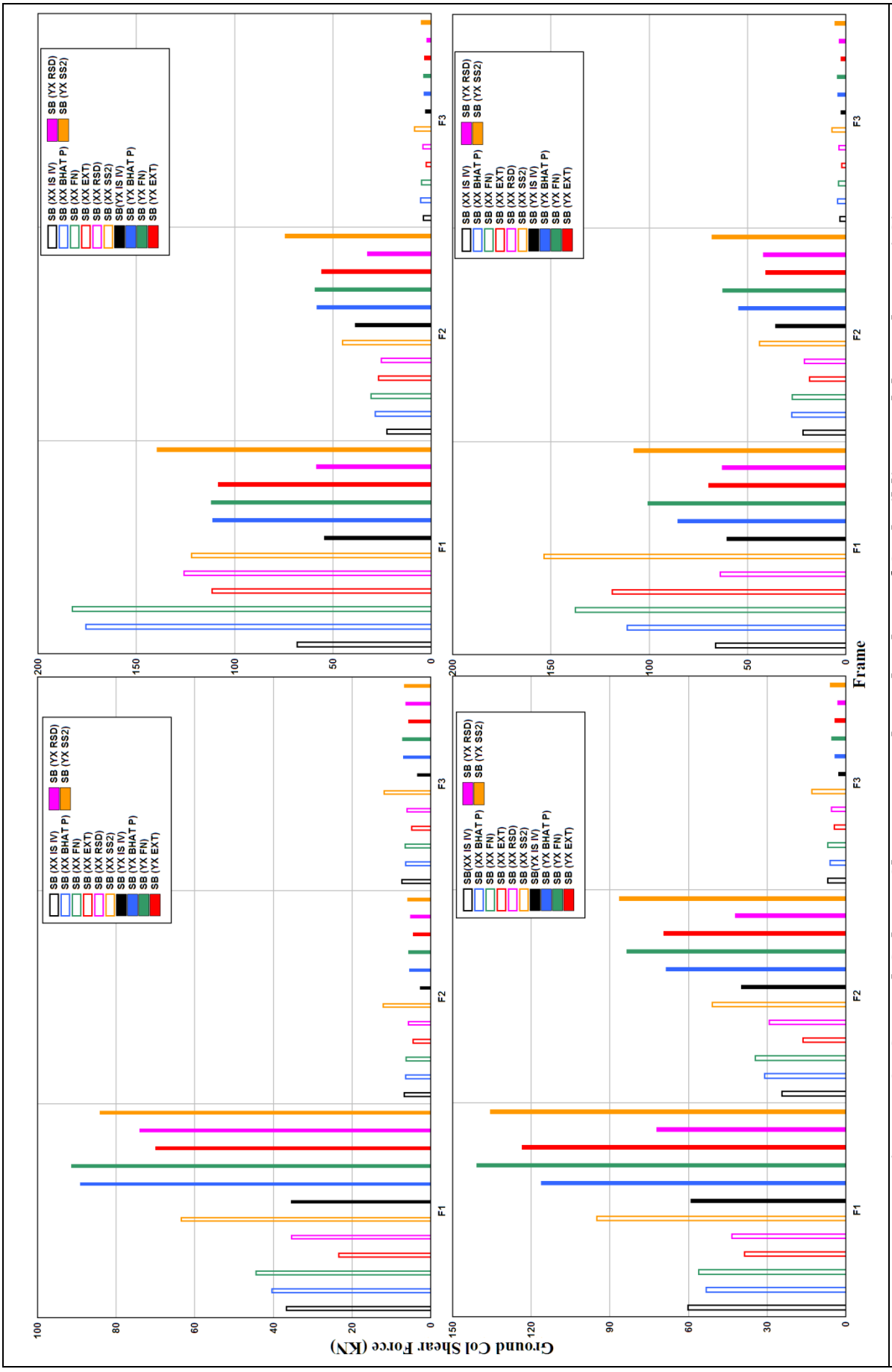

Figure 5.61 Ground Column Shear Force along the slope of SB building models at Bhatwari Site

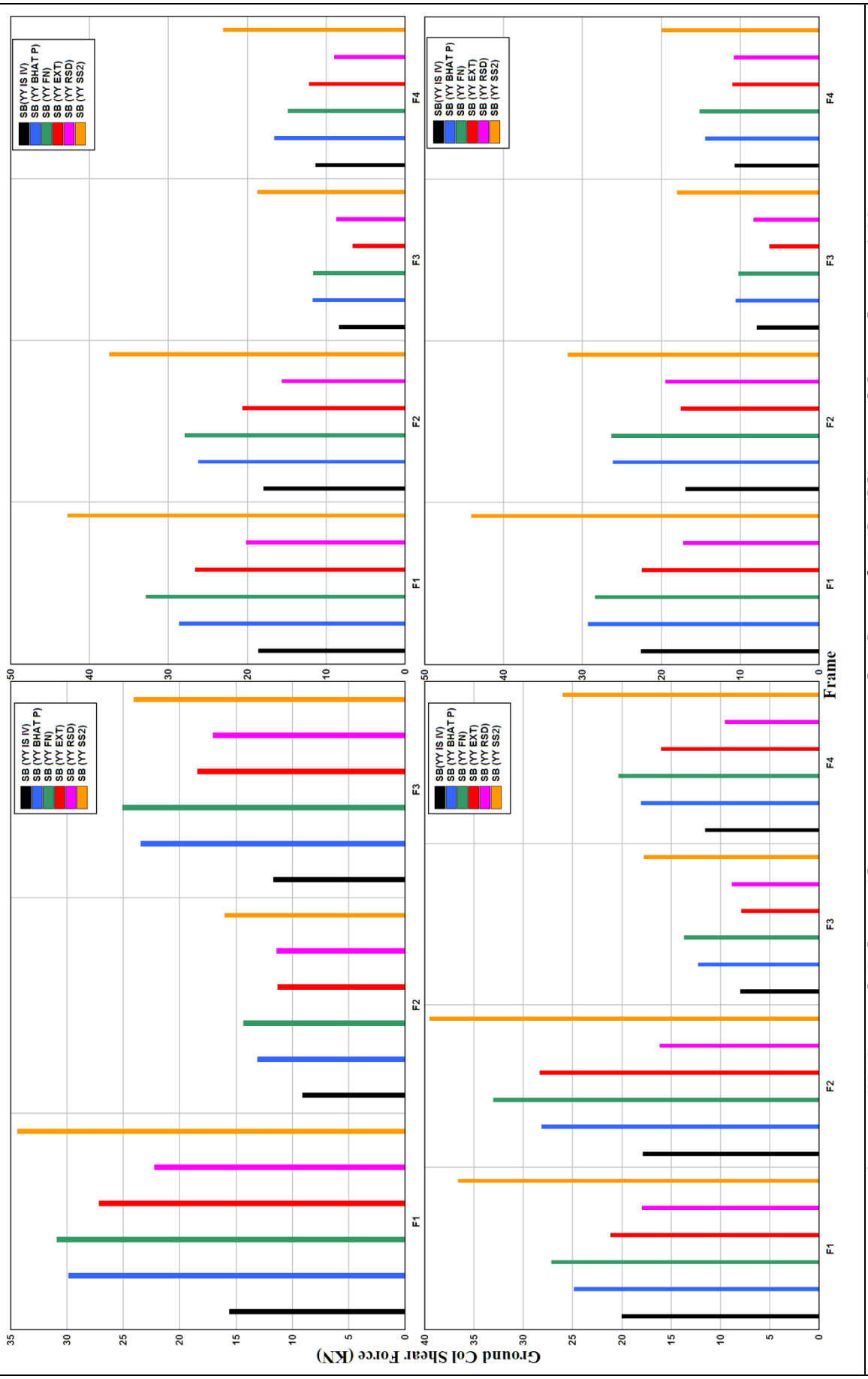

Figure 5.62 Ground Column Shear Force across the slope of SB building models at Bhatwari Site

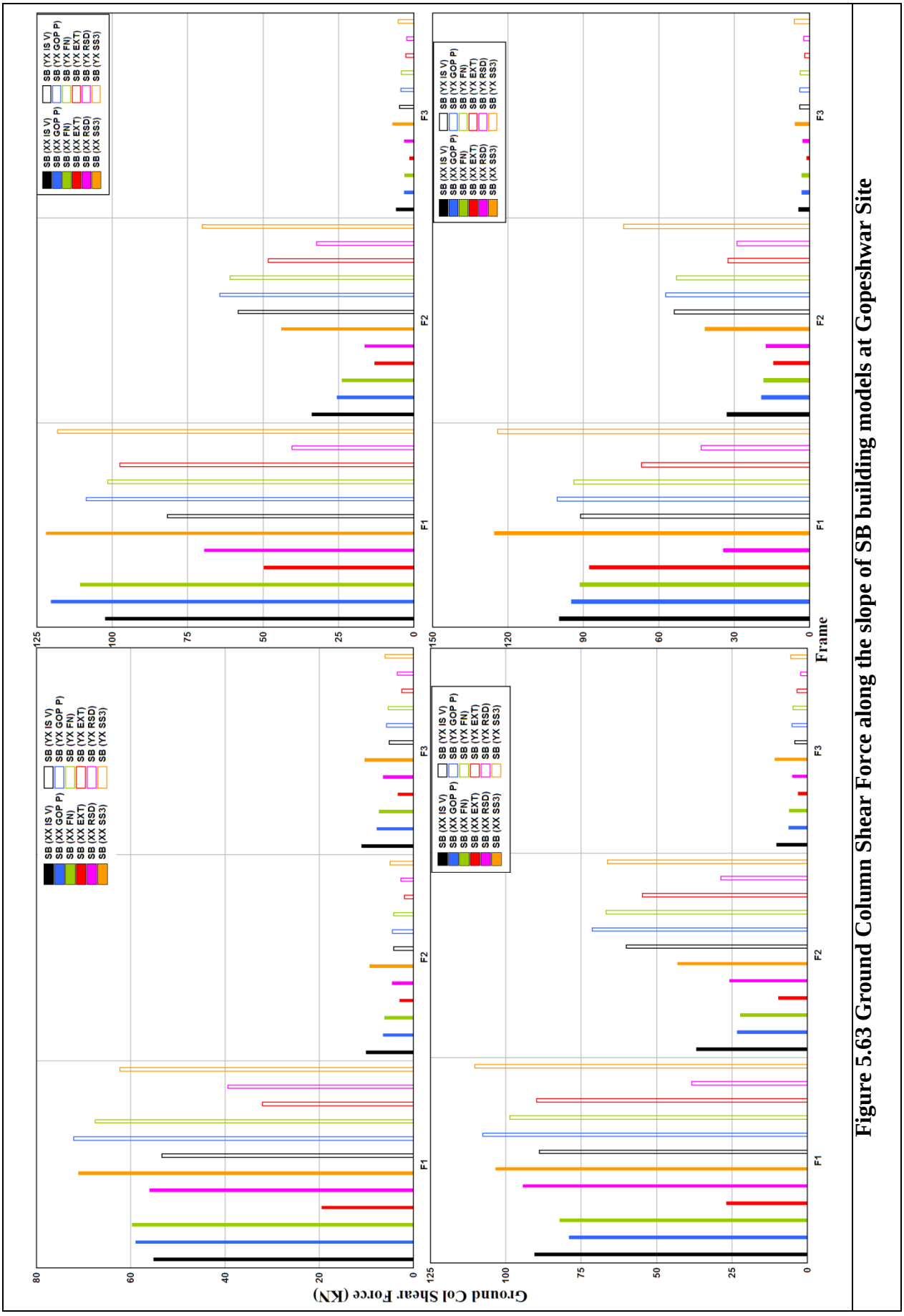

Figure 5.63 Ground Column Shear Force along the slope of SB building models at Gopeshwar Site

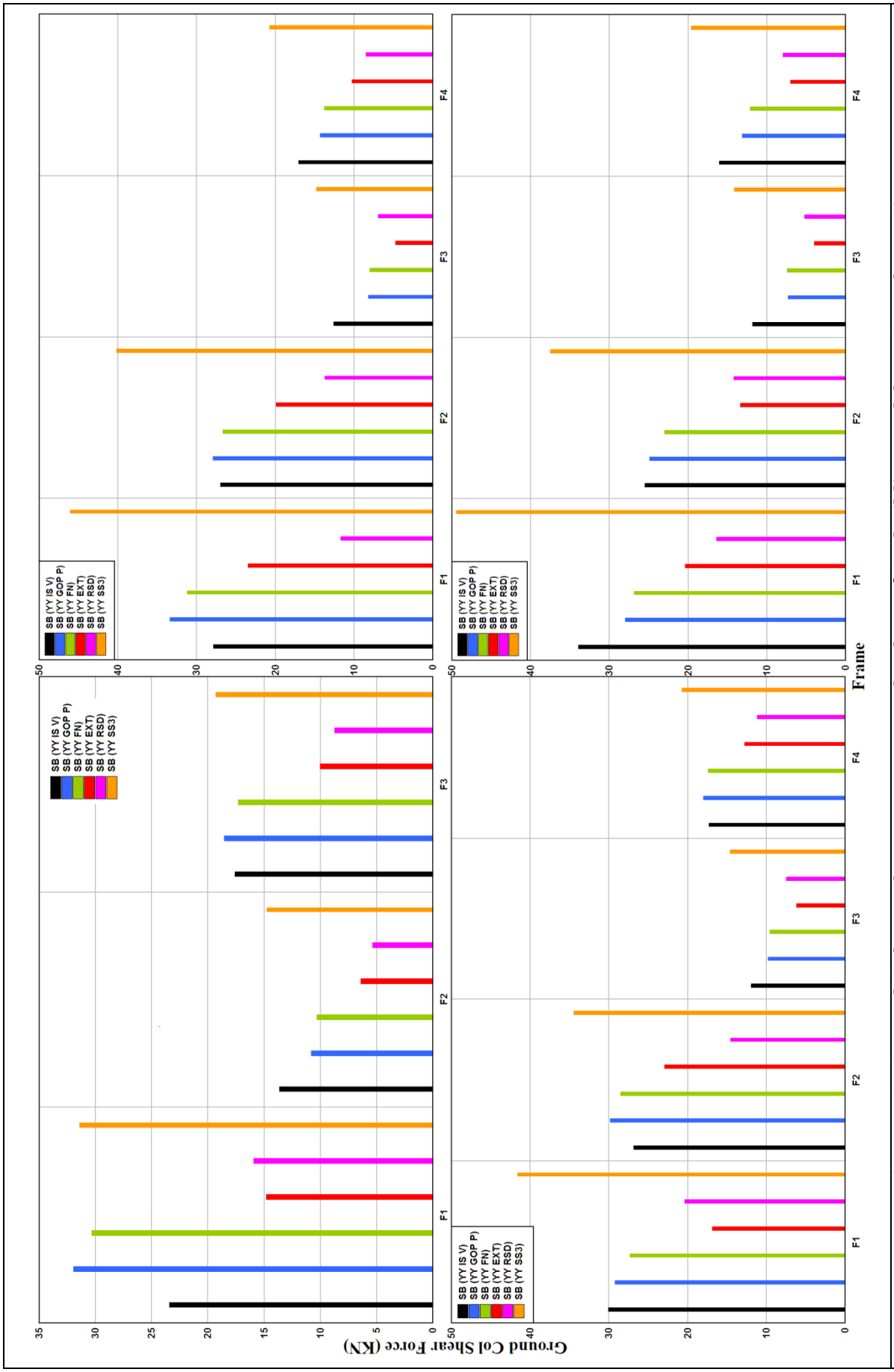

Figure 5.64 Ground Column Shear Force across the slope of SB building models at Gopeshwar Site

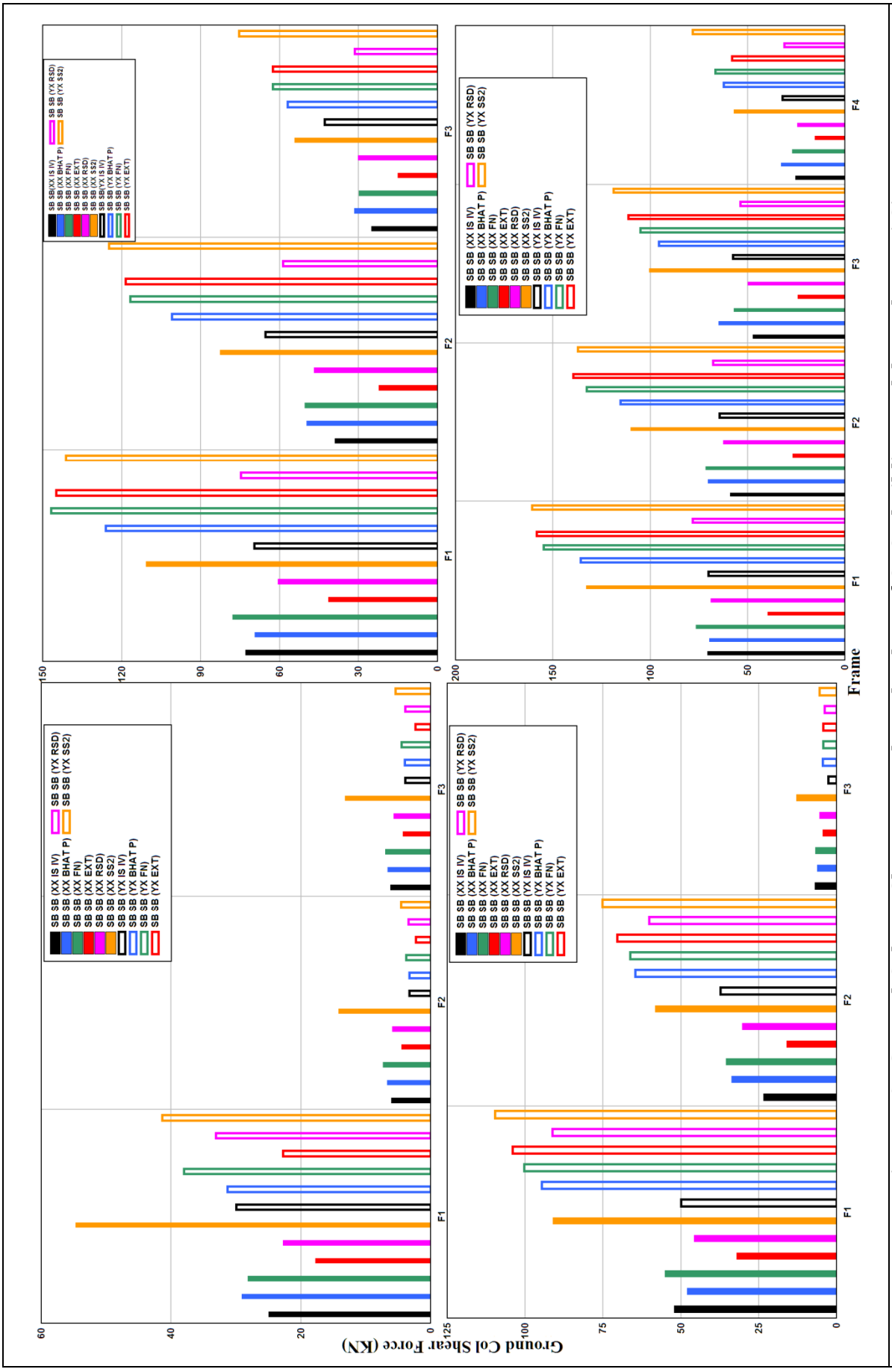

Figure 5.65 Ground Column Shear Force along the slope of SBSB building models at Bhatwari Site

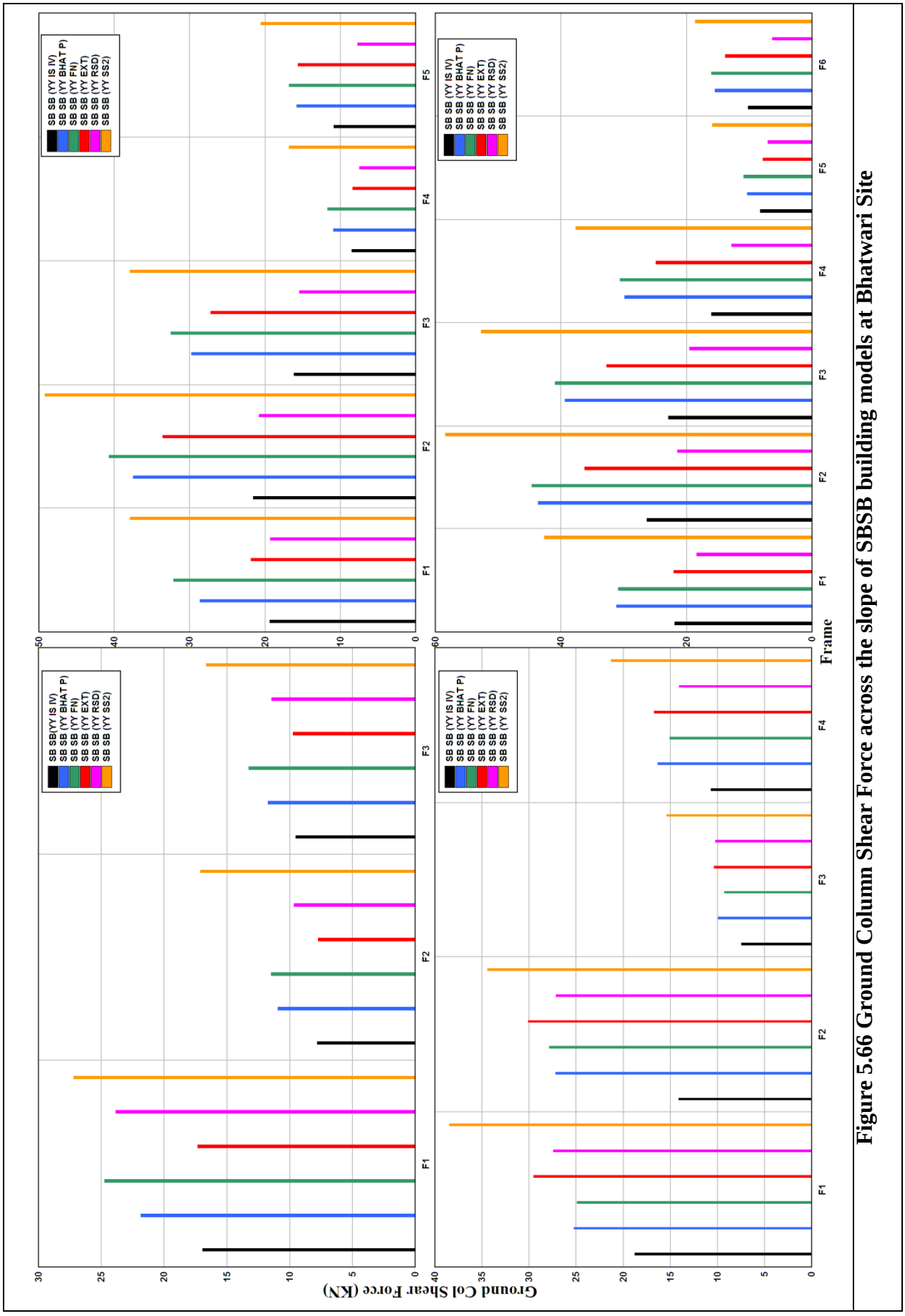

Figure 5.66 Ground Column Shear Force across the slope of SBSB building models at Bhatwari Site

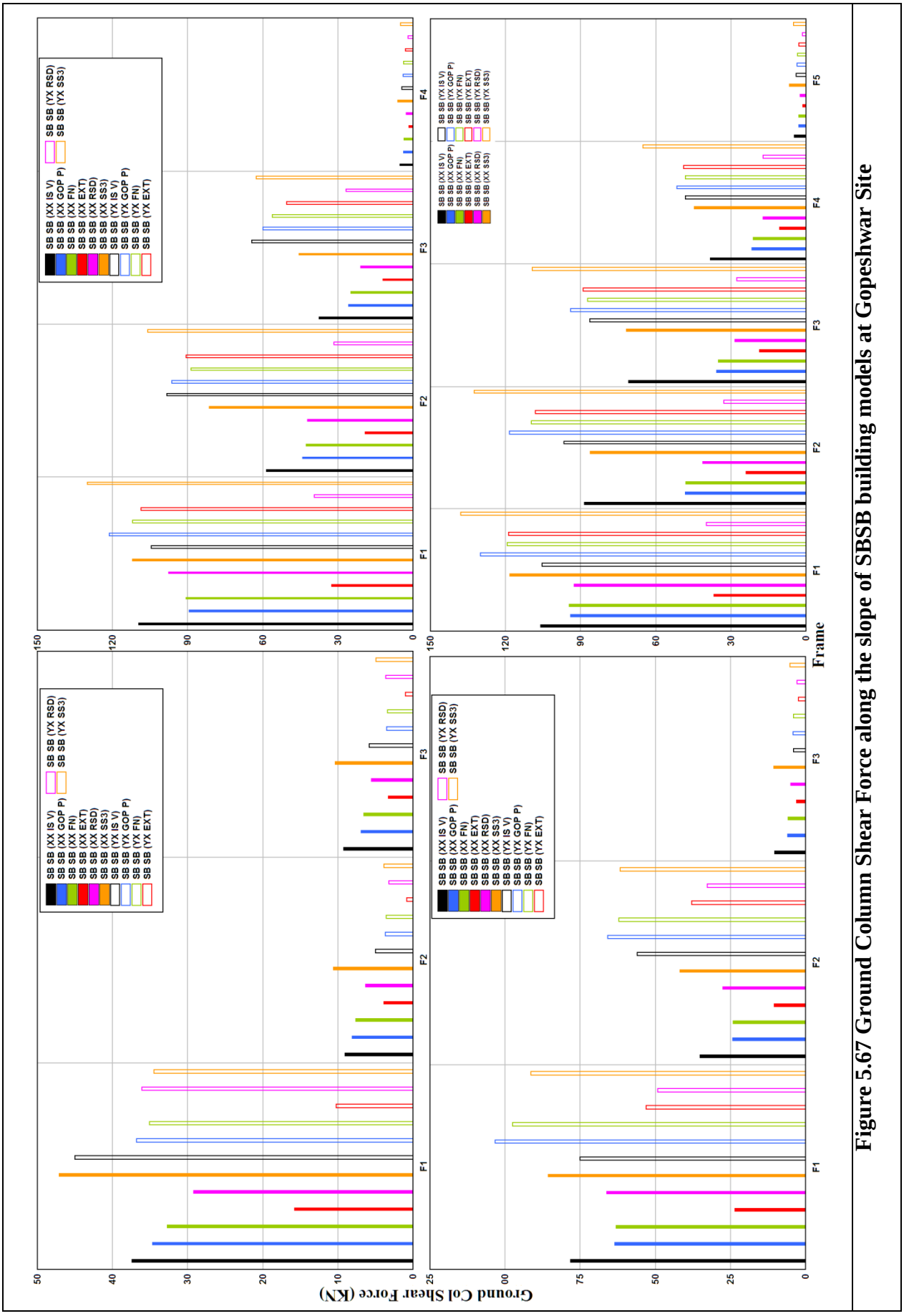

Figure 5.67 Ground Column Shear Force along the slope of SBSB building models at Gopeshwar Site

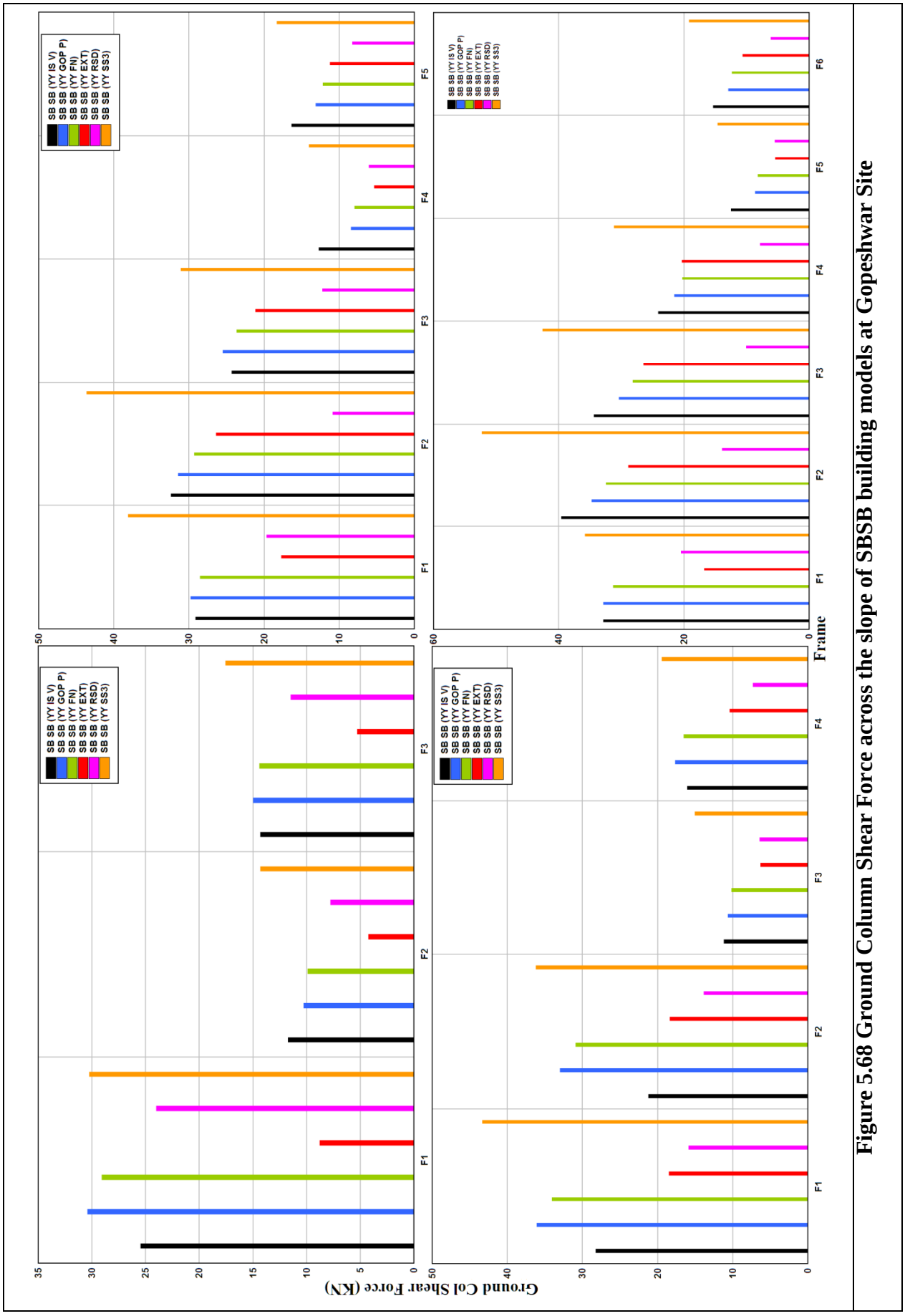

Figure 5.68 Ground Column Shear Force across the slope of SBSB building models at Gopeshwar Site

5.5 Concluding Remarks

In SB building models, as the number of storeys increases, the fundamental time periods, i.e., across the slope, increases significantly. Whereas, there is not much variation in the time period along the slope, i.e., third-mode, for 212SB and 313SB building models, however, the 413SB and 513SB building models show increase in time period, and much higher time periods compared to 212SB and 313SB building models. In SBSB building models, as the number of storeys increases, the fundamental time periods across the slope, increases significantly, but not much variation have been found in 414SBSB and 515SBSB building models. Whereas, there is not much variation in the fundamental time periods along the slope, i.e., third-mode, for 212SBSB building model, fourth-mode for 313SBSB and 414SBSB building models, and fifth-mode for 515SBSB building model. Response of two types of building models (SB & SBSB) have brought out that as the number of storeys increase from 2 to 5, the extracted pulse response increases compared to response due to residual component GM; because as the height of the building increases the time-period also increases resulting in decrease of high-frequency response. This is only true when the seismic inputs are across the slope (Y-direction) and direction of displacements is observed in the in-plane (X) and out-of-plane (Y) directions. However, for 2 to 4 storey "SBSB" buildings, the response due to residual component is always higher than the extracted pulse response when the ground motion is applied in X-direction (along the slope) because there is no significant variation in the time periods of the models in X-direction. For similar type of earthquake loadings, the five story building (SBSB) the response due to extracted pulse ground motion is higher compared to RSD response.

At Bhatwari site located in seismic zone IV as per IS code, the responses of all buildings of both types due to codal type ground motion found highly un-conservative compared to pulse-type ground motion and site-specific ground motion. However, at Gopeshwar site located in seismic zone V, as the SB buildings storey increases beyond 3 storeys, i.e., for 4 and 5 storey building models the response along the slope due to codal type ground motion found highly un-conservative compared to pulse-type ground motion and site-specific ground motion. The same observation also found when the response considered across the slope for 2, 3, and 4 storey SB building models. Further, in all SBSB building models, the response across the slope due to codal type ground motion found lower than the responses due to pulse-type ground motions and site-specific ground motion.

The Indian codal spectra needs modification and the effects of pulse-type ground motion due to moderate, large, and great earthquakes should be incorporated for sites in the vicinity of near-fault regions particularly for the Himalaya region.

CHAPTER 6

SUMMARY AND CONCLUSIONS

6.1 Introduction

The aim of the study is to investigate the NFGM characteristics of the three moderate Himalayan earthquakes, and to compute and interpret the response of buildings on hillslope subjected to pulse-type ground motion. For this purpose 33 strong motion recordings obtained from the Dharamshala, Uttarkashi and Chamoli earthquakes have been analyzed. The objectives of the study include investigating the pulse-type characteristics of strong ground motion in terms of pulse-period, pulse indicator and type of pulse of these earthquakes, estimating site-specific ground motion (SSGM) at three sites incorporating the near-fault factor, studying the dynamic response of the Step-Back (SB) and Step-Back-Set-Back (SBSB), and comparing the dynamic response of buildings on hillslope computed from pulse-type ground motion with the response computed using IS codal spectra and estimated site-specific ground motion. The results are summarized below.

6.2 Summary of Results on the NFGM Characteristics of Three Himalayan Earthquakes

6.2.1 The study showed that moderate Himalayan earthquakes contain NFGM characteristics. At Bhatwari, Gopeshwar and Shapur sites the pulses have been identified applying the criteria of threshold levels of six ground motion parameters.

6.2.2 It is found that Daubechies wavelets of order four and seven are more efficient compared to other mother wavelets in extracting the pulse-type characteristics that include pulse-indicators (PI), pulse-periods (T_p) and spectral pulse-periods ($T_{v\text{-}p}$) from the strong motion recordings.

6.2.3 It is found that the spectra of long-period pulses extracted using Daubechies mother wavelet of order seven (db7) are closer to the long-period spectral amplitudes of the FN components of ground motions at three sites.

6.2.4 The estimated pulse-periods for fault-normal components of ground motion at Bhatwari and Gopeshwar stations are 1.30 sec and 1.39 sec respectively. For the Dharamsala earthquake, fault-normal component of ground motion at Shapur station contains pulse-type ground motion with the pulse-period (Tp) 0.52 sec.

6.2.5 The estimated pulse-periods by and large conform to the world-wide dataset but are on lower side than the average pulse-periods. This could be attributed to compressional tectonic environment and thrust-type focal mechanism of the Himalayan earthquakes.

6.3 Summary of Results on Comparison of Near-Fault Response Spectra with the IS Codal Spectra

6.3.1 The acceleration-sensitive region in the response spectra extends up to 0.65 sec and 0.53 sec because of high PGV/PGA ratios at Bhatwari and Gopeshwar stations. These values are higher than the codal value (0.40 sec).

6.3.2 As a consequence of widening of the acceleration-sensitive region the structures designed to be flexible in the intermediate-period and long-period range will behave as stiff structures, and subjected to increased base shear because of NFGMs in the Himalaya.

6.3.3 Spectral characteristics of near-fault pulse-type ground motions due to the Uttarkashi and Chamoli earthquakes have illustrated that the IS code is deficient in addressing the long-period near-fault ground motions, particulary for the Himalayan regions. Therefore, the IS code needs modification, and the effect of NFGM in terms of increasing spectral amplitudes towards long-periods should be incorporated in the design spectrum. Because of lack of sufficient number of near-fault recordings, the present study is unable to recommmend a specific design spectra for near-fault sites. In the future when sufficient data shall be available, it may be possible to arrive at a specific NFGM design spectra.

6.4 Summary of Results on Estimated Site-Specific Ground Motion Spectra Incorporating Near-Fault Factor

6.4.1 At all the three sites, the estimated site-specific ground motion incorporating the near-fault factor showed much higher Peak Horizontal Accelerations (PHA) compared to NFGM recordings. This is attributed to deterministic approach that considered the worst scenario earthquakes at these sites.

6.4.2 At Bhatwari site the spectral shapes of estimated site-specific ground motion exceeds the codal spectral values at all time periods. However, spectral shapes of recorded pulse-type ground motion (transverse component), FN component, and extracted pulse component of recorded ground motion showed higher values between 0.5 and 1 sec compared to estimated site-specific ground motion spectra. This shows that the dynamic response of structures falling in this fundamental period range will be more when subjected to recorded pulse-type ground

motion, FN component, and extracted pulse component of recorded ground motion as compared to estimated site-specific ground motion.

6.4.3 At Gopeshwar and Shapur sites the spectral shapes of estimated site-specific ground motion show higher values at time periods ranging from 0.1 to 0.35 sec and 0.55 to 4.0 sec as compared to codal spectral values.

6.4.4 At Gopeshwar site, recorded pulse-type ground motion (transverse component) and FN component of recorded ground motion show higher spectral values between 0.40 and 0.90 sec as compared to estimated site specific ground motion.

6.4.5 At Shapur site, the spectral values of recorded pulse-type ground motion (transverse component), FN component, extracted pulse, and residual component of recorded ground motion are below the spectral envelope of estimated site-specific ground motion and codal spectral amplitude. This is because of smaller magnitude of Dharamshala earthquake (M_w 5.5) compared to Uttarkashi and Chamoli earthquakes.

6.5 Summary of Results on Dynamic Response of Buildings on Hillslope and Comparison with IS code

6.5.1 Response of two types of building models, namely, the Step-Back (SB) and Step-Back-Set-Back (SBSB) models, have brought out that as the number of storeys increase from 2 to 5, the extracted pulse response increases compared to response due to residual component of ground motion. This happens because as the height of the building increases the time-period also increases resulting in decrease of high-frequency response. However, this is only true when the seismic inputs are across the slope (Y-direction) and directions of displacements are observed in the in-plane (X) and out-of-plane (Y) directions.

6.5.2 For all SBSB building models, the response along the slope due to residual (RSD) component is always higher than the extracted (EXT) pulse response when the ground motion is applied in X-direction (along the slope) because there is no significant variation in the time periods of the models in the X-direction. However, the 3 to 5 storey building models showed that the response due to extracted (EXT) pulse ground motion is higher compared to residual-part of the ground motion when the similar type of earthquake loadings are applied across the slope.

6.5.3 At Bhatwari site, for both building configurations (SB and SBSB) the response parameters, namely, the floor displacements and ground column shear forces, computed using codal spectra show lowest values compared to those obtained from other seismic inputs. For SBSB building models, the response parameters (across the slope), due to extracted pulse

ground motion in both directions show increasing trend and closely match the response due to estimated site-specific ground motion. Further, it is found that as the number of storeys increase, the difference between the response due to extracted pulse ground motion, FN component of ground motion, and recorded pulse-type ground motion reduced.

6.5.4 At Gopeshwar site located in seismic zone V, as the SB buildings storey increases beyond 3 storeys, i.e., for 4 and 5 storey building models the responses along the slope due to codal type ground motion are found to be highly un-conservative compared to pulse-type ground motion and site-specific ground motion. The same observation was also found when the response was considered across the slope for 2, 3, and 4 storey SB building models. Further, in all SBSB building models, the response across the slope due to codal type ground motion found lower than the responses due to pulse-type ground motions and site-specific ground motion.

6.5.5 At Shapur site, because of smaller magnitude of the 1986 Dharamshala earthquake, the recorded pulse-type ground motion, EXT pulse, and residual part of ground motion showed lower response compared to estimated site-specific ground motion response and codal based spectra response. Further, as the number of storeys increase the responses due to recorded ground motion, residual part of ground motion, and extracted pulse ground motion become closer for both types of building forms (SB & SBSB).

6.6 Conclusions

6.6.1 The estimated pulse-periods of three moderate Himalayan earthquakes by and large conform to the world-wide dataset but are on lower side than the average pulse-periods computed using various worldwide relationships between magnitude and pulse period. This could be attributed to compressional tectonic environment and thrust-type focal mechanism of the Himalayan earthquakes.

6.6.2 With the increasing period of buildings, response due to extracted long-period pulse at three sites is in close agreement with responses due to recorded pulse-type ground motions & FN component of ground motions. This illustrates the adequacy of representation of NFGM with extracted long-period pulse.

6.6.3 At Bhatwari site that lies located in seismic zone IV as per IS code, the responses of all buildings of both types due to codal type ground motion found highly un-conservative compared to recorded pulse-type ground motion, fault-normal component and site-specific ground motion.

6.6.4 The Indian codal spectra needs modification to incorporate the effects of pulse-type ground motion due to moderate, large, and great earthquakes for sites in the vicinity of fault regions particularly for the Himalaya region.

6.6.5 Spectral characteristics of near-fault pulse-type ground motions due to the Uttarkashi and Chamoli earthquakes have illustrated that the IS code is deficient in addressing the long-period near-fault ground motions, particularly for the Himalayan regions. Therefore, the IS code needs modification, and the effect of NFGM in terms of increasing spectral amplitudes towards long periods should be incorporated in the design spectrum.

6.7 Limitations of the Study

Because of lack of sufficient number of near-fault recordings, the present study is unable to recommend specific design spectra for near-fault sites. In the future when sufficient data shall be available, it may be possible to arrive at a specific NFGM design spectra.

6.8 Suggestions for Future Work

In the present study the dynamic response of asymmetric buildings on hillslope has been computed adopting the linear analysis. It recommended that the dynamic analysis should be carried out using pushover analysis and nonlinear time history analysis to further knowledge of such structural forms so that appropriate modifications can be incorporated in the applicable IS codes.

LIST OF BIBLIOGRAPHY

1 Abrahamson NA and Silva WJ (2008). "Summary of the Abrahamson & Silva NGA Ground-Motion Relations," Earthquake Spectra, 24(1) 67–97.

2 Abrahamson NA and Somerville PG (1996). "Effects of the Hanging Wall and Foot Wall on Ground Motions Recorded During the Northridge Earthquake," Bulletin of the Seismological Society of America, 86(1B) 93-99.

3 Abrahamson NA, Shedlock KM (1997). "Some Comparisons between Recent Ground Motion Relations," Seismological Research Letters, 68(1) 9-23.

4 Agrawal AK, He WL (2002). "A Close-Form Approximation of Near-Fault Ground Motion Pulses for Flexible Structures" 15th ASCE Engineering Mechanics Conference, Columbia University, New York, Paper No. 367.

5 Alavi G and Helmut K (2001). "Effects of Near-Fault Ground Motions on Frame Structures," The John A Blume Earthquake Engineering Center, Stanford University, Report No. 138.

6 Alavi G and Krawinkler H (2000). "Consideration of Near-Fault Ground Motion Effects in Seismic Design," Proceedings 12WCEE, New Zealand.

7 Amirzehni E, Taiebat M, Finn WDL, and Devall RH (2013). "Effect of Near-Fault Ground Motions on Seismic Response of Deep Basement Walls," 4th ECCOMAS Thematic Conference on Computational Methods in Structural Dynamics and Earthquake Engineering, Greece.

8 Anderson J and Bertero V (1978). "Uncertainties In Establishing Design Earthquakes," ASCE Journal of Structural Engineering, 113(8) 1709-1724.

9 Anderson J, Bertero V, and Bertero R (1999). "Performance Improvement of Long Period Building Structures Subjected to Severe Pulse-Type Ground Motion," PEER Center, University of California, Berkeley, Report No. PEER-1999/09.

10 Anderson JG, P Bodin, J Brune, J Prince, and Singh SK (1986). "Strong Ground Motion and Source Mechanism of the Mexico Earthquake of September 19, 1985," Science, 233 1043-1049.

11 Baker JW (2007). "Quantitative Classification of Near-Fault Ground Motions Using Wavelet Analysis," Bulletin of Seismological Society of America, 97(5) 1486-1501.

12 Bertero V, Mahin S, and Herrera R (1978). "Aseismic Design Implications of Near-Fault San Fernando Earthquake Records," Earthquake Engineering and Structural Dynamics, 6(1) 31-42.

13 Birajdar BG and Nalawade SS (2004). "Seismic Analysis of Buildings Resting on Sloping Ground," Proceedings of 13WCEE, Canada, Paper no. 1472.

14 Bolt BA and Abrahamson NA (2003). "Estimate of Strong Seismic Ground Motions," International Handbook of Earthquake and Engineering Seismology, IASPEI, Part B.

15 Boore DM and Atkinson GM (2008). "Ground-Motion Prediction Equations for the Average Horizontal Component of PGA, PGV, and 5%-Damped PSA at Spectral Periods between 0.01 s and 10.0 s," Earthquake Spectra, 24(1) 99–138.

16 Boore DM and Atkinson GM (2008). "Ground-Motion Prediction Equations for the Average Horizontal Component of PGA, PGV, and 5%-Damped PSA at Spectral Periods between 0.01 s and 10.0s," Earthquake Spectra, 24(1) 99-138.

17 Boore DM, Joyner WB (1982). "The Empirical Prediction of Ground Motion," Bulletin of the Seismological Society of America," 72(6) 43-60.

18 Boore DM, Joyner WB and Fumal TE (1997). "Equations for Estimating Horizontal Response Spectra and Peak Acceleration from Western North American Earthquakes: A Summary of Recent Work," Seismological Research Letters, 68(1) 128–153.

19 Bozorgnia Y, Niazi M, and Campbell KW (1995). "Characteristics of Free-Field Vertical Ground Motion During the Northridge Earthquake," Earthquake Spectra, 11(4) 515-525.

20 Bray JD and Marek AR (2004). "Characterization of Forward-Directivity Ground Motions in the Near-Fault Region," Soil Dynamics and Earthquake Engineering, 24(11) 815-828.

21 Caldwell WB, Klemperer SL, Lawrence JF, Rai SS, and Ashish (2013). "Characterizing the Main Himalayan Thrust in the Garhwal Himalaya, India with Receiver Function CCP Stacking," Earth and Planetary Science Letters, 367 15–27.

22 Caltran (2012a). "Methodology for Developing Design Response Spectrum for Use in Seismic Design Recommendations," Division of Engineering Services, Geotechnical Services.

23 Campbell KW (1981). "Near-Source Attenuation of Peak Horizontal Acceleration," Bulletin of the Seismological Society of America, 71(6) 2039-2070.

24 Campbell KW (1985). "Strong Motion Attenuation Relations: A Ten-Year Perspective," Earthquake Spectra, 1(4) 759–804.

25 Campbell KW (1997). "Empirical Near-Source Attenuation Relationships for Horizontal and Vertical Components of Peak Ground Acceleration, Peak Ground Acceleration, Peak Ground Velocity, and Pseudo-Absolute Acceleration Response Spectra" Seismological Research Letters, 68(1) 154-179.

26 Campbell KW (2003). "Strong-Motion Relations," International Handbook of Earthquake & Engineering Seismology, Academic Press, 1003-1030.

27 Campbell KW and Bozorgnia Y (2008). "NGA ground Motion Model for the Geometric Mean Horizontal Component of PGA, PGV, PGD and 5% Damped Linear Elastic Response Spectra for Periods Ranging from 0.01 to 10 s," Earthquake Spectra, 24(1) 139–171.

28 Chandrasekekran AR (1988). "Strong Motion Arrays in India," 9WCEE, Japan (Vol. VIII).

29 Chandrasekekran AR and Das JD (1995). "Strong Motion Records from Uttarkashi Earthquake," Geological Society of India, 30 133-147.

30 Chik Z, Islam T, Rosyidi SA, Sanusi H, Taha MR, and Mustafa MM (2009). "Comparing the Performance of Fourier Decomposition and Wavelet Decomposition for Seismic Signal Analysis," European Journal of Scientific Research, 32(3) 314-328.

31 Chiou BS-J and Youngs RR (2008a). "An NGA Model for the Average Horizontal Component of Peak Ground Motion and Response Spectra," Earthquake Spectra, 24(1) 173–215.

32 Chiou BS-J and Youngs RR (2008b). "NGA Model for the Average Horizontal Component of Peak Ground Motion and Response Spectra," Pacific Earthquake Engineering Research Center, University of California, Berkeley, PEER Report No. 2008/09, 293.

33 Chopra AK and Chintanapakdee C (1998). "Accuracy of response spectrum estimates of structural response to near-field earthquake ground motions: Preliminary results [C/CD]," Proceedings of the ASCE Structures World Conference, Elsevier Science Ltd Oxford, England, Paper No. T136-1.

34 Chopra AK and Chintanapakdee C (2001). "Comparing Response of SDF System to Near-Fault and Far-Fault Earthquake Motions in the Context of Spectral Regions," Earthquake Engineering and Structural Dynamics, 30(12) 1769-1789.

35 Datta TK (2010). "Seismic Analysis of Structures," John Wiley, pp 472.

36 Deb SK (2008). "Base Isolation and Energy Dissipation, Chapter-14," Handbook on Retrofit of Reinforced Concrete Building, Narosa Publication.

37 Douglas J (2011). "Ground-Motion Prediction Equations 1964–2010," Final report RP-59356-FR (PEER Report 2011/102), BRGM, Orléans, France.

38 Egan JA, Makdisi FI and Rosidi D (1994). "Near-Field Vertical Ground Motions from the 17 January 1994 Northridge Earthquake; Were They Unusual? Program Abstracts, Annual Meeting," Seismological Society of America, Pasadena, California, April 5 -7.

39 Elgohary M and Ghobarah A (2003). "Seismic Response of Structures to Near Fault Ground Motion," OECD/NEA Workshop on the Relations between Seismological Data and Seismic Engineering, Istanbul.

40 Finn WDL (2000). "State-of-the-Art of Geotechnical Earthquake Engineering Practice," Soil Dynamics and Earthquake Engineering, 20(1-4) 1–15.

41 Finn WDL, Ventura CE, and Schuster ND (1995). "Ground Motions During the 1994 Northridge earthquake," Canadian Journal of Civil Engineering, 22(2) 300–315.

42 Galal K and Ghobarah A (2006). "Effect of Near-Fault Earthquakes on North American Nuclear Design Spectra," Nuclear Engineering and Design, 236(18) 1928–1936.

43 Garini E and Gazetas G (2013). "Damage Potential of Near-Fault Records: Sliding Displacement against Conventional Intensity Measures." Bulletin of Earthquake Engineering, 11(2) 455–480.

44 Garini E, Makris N, and Gazetas G (2014). "Elastic and Inelastic Systems Under Near-Fault Seismic Shaking: Acceleration Records Versus Optimally-Fitted Wavelets," Bulletin of Earthquake Engineering, 13(2) 459-482.

45 Gazetas G, Garini E, Anastasopoulos I, and Georgarakos T (2009). "Effects of Near-Fault Ground Shaking on Sliding Systems," Journal of Geotechnical and Geoenvironmental Engineering 135(12) 1906–1921.

46 Geological Survey of India (2000). "Seismotectonic Atlas of India and Its Environs," Geological Survey of India.

47 Gerolymos N, Apostolou M, and Gazetas G (2005). "Neural network analysis of overturning response under near-fault type excitation," Earthquake Engineering and Engineering Vibration, 4(2) 213–228.

48 Ghahari SF, Jahankhah H, and MA Ghannad (2010). "Study on Elastic Response of Structures to Near-Fault Ground Motions through Record Decomposition," Soil Dynamics and Earthquake Engineering, 30(7) 536-546.

49 Ghasemi A and Shakib H (2008). "Behavior of Asymmetric Multi-Story Buildings Subjected to Near-Fault Ground Motions," 14WCEE, Beijing, China.

50 Ghasemi A and Shakib H (2011). "The Improvement of Structural Adequacy against Large Demands of Near-Fault Ground Motions," Arabian Journal for Science and Engineering, 36(2) 185–202.

51 Ghobarah **A** (2004). "Response of Structures to Near-Fault Ground Motion," 13WCEE, Paper-1031.

52 Ghobarah **A**, El Sheikh, and M Elgohary (2003). "Effect of Near-Fault Ground Motion on the Response of Concrete Structures," International Symposium on Seismic Evaluation of Existing Nuclear Facilities, Austria.

53 Gurley K and Kareem A (1999). "Application of Wavelet Transformations in Earthquake, Wind and Ocean Engineering," Engineering Structures, 21(2) 149-167.

54 Haigh SK, Teymur B, Madabhushi SPG, and Newland DE (2002). "Application of Wavelet Analysis to the Investigation of the Dynamic Behavior of Geotechnical Structures," Soil Dynamics and Earthquake Engineering, 22(9-12) 995-1005.

55 Hall JF (1995). "Near-Source Ground Motion and Its Effects on Flexible Buildings," Earthquake Spectra, 11(4) 569-605.

56 Housner GW (1984). "An Historical View of Earthquake Engineering," Proceedings of the 8th World Conference on Earthquake Engineering, San Francisco, 25–38.

57 Huang CT and Shi SC (2000). "Near-Field Characteristics and Engineering Implication of the 1999 Chi-Chi Earthquake," Earthquake Engineering and Engineering Seismology, 2(1) 23-41.

58 Idriss IM (2008). "An NGA Empirical Model for Estimating the Horizontal Spectral Values Generated by Shallow Crustal Earthquakes," Earthquake Spectra, 24(1) 217–242.

59 IS 1893-Part 1 (2002). "Criteria for Earthquake Resistant Design of Structures–General Provisions and Buildings," Bureau of Indian Standards, New Delhi.

60 Iwan W (1997). "Drift Spectrum: Measure of Demand for Earthquake Ground Motions," ASCE Journal of Structural Engineering, 123(4) 397-404.

61 Jain SK and Das S (1993). "Analysis of Strong Motion Records from Uttarkashi Earthquake for Assessment of Code Provisions for Different Seismic Zones," Earthquake Spectra, 9(4) 739-754.

62 Jain SK, Murty CVR, Arlekar JA, Rajendran CP, Rajendran K, and Sinha R (1999) "The Chamoli, India, Earthquake of March 29, 1999," EERI Special Earthquake Report, EERI Newsletter, 33(7) 1-8.

63 Jangid RS and Datta TK (1995). "Performance of Base Isolation Systems for Asymmetric Building Subject to Random Excitation," Engineering Structures, 17(6) 443–454.

64 Jangid RS and Datta TK (1995). "The Stochastic Response of Asymmetric Base Isolated Buildings," Journal of Sound and Vibration, 179(3) 463–473.

65 Joshi A (2000). "Modeling of Rupture Planes for Peak Ground Accelerations and its Application to the Isoseismal Map of MMI scale in Indian Region," Journal of Seismology, 4(2) 143-160.

66 Joshi A (2003). "Predicting Strong Motion Parameters for the Chamoli Earthquake of 28th March, 1999, Garhwal Himalaya, India, from Simplified Finite Fault Model," Journal of Seismology 7(1) 1–17.

67 Joshi A (2006). "Analysis of Strong Motion Data of the Uttarkashi Earthquake of 20th October 1991 and the Chamoli Earthquake of 28th March 1999 for Determining the Q Value and Source Parameters," ISET Journal of Earthquake Technology, 43(1-2) 11-29.

68 Joshi A, S Singh, and K Giroti (2001). "The Simulation of Ground Motions Using Envelope Summations," Pure Applied Geophysics, 158(5-6) 877-901.

69 Kaklamanos J, Boore DM, Thompson EM and Campbell KW (2010). "Implementation of the Next Generation Attenuation (NGA) Ground-Motion Prediction Equations in Fortran and R," U.S. Geological Survey Open-File Report 2010–1296, Reston VA.

70 Kalkan E and Kunnath SK (2006). "Effects of Fling Step and Forward Directivity on Seismic Response of Buildings," Earthquake Spectra, 22(2) 367–390.

71 Khattri KN (1987). "Great Earthquake, Seismicity Gaps and Potential for Earthquake Disaster along the Himalaya Plate Boundary," Tectonicphysics, 138(1) 79–92.

72 Khattri KN and Tyagi AK (1983). "Seismicity Pattern in the Himalayan Plate Boundary and Identification of Areas of High Seismic Potential," Tectonophysics, 96(3-4) 281–297.

73 Kumar D, Sarkar I, Sriram V, Khattri KN (2005). "Estimation of the Source Parameters of the Himalaya Earthquake of October 19, 1991, average effective shear wave attenuation parameter and local site effects from accelerograms," Tectonophysics 407(1-2) 1–24.

74 Kumar D, V Sri Ram, and KN Khattri (2006). "A Study of Source Parameters, Site Amplification Functions and Average Effective Shear Wave Quality Factor Qseff from Analysis of Accelerograms of the 1999 Chamoli Earthquake, Himalaya," Pure and Applied Geophysics, 163(7) 1369-1398.

75 Kumar N, Arora BR, Mukhopadhyay S, Yadav DK (2013). "Seismogenesis of Clustered Seismicity beneath the Kangra–Chamba Sector Of Northwest Himalaya: Constraints from 3D Local Earthquake Tomography," Journal of Asian Earth Sciences, 62(30) 638–646.

76 Kumar P, Kumar A, and Pandey AD (2010). "Near-Fault Ground Motion-An Engineering Perspective," 14SEE, IIT Roorkee, 167-177.

77 Kumar P, Kumar A, and Pandey AD (2012). "Characteristics of Near Fault Ground Motion of Dharamsala Earthquake of 1986," ISET Golden Jubilee Symposium, IIT Roorkee, Paper No. A013.

78 Kumar P, Kumar A, and Pandey AD (2014). "Comparison of Seismic Response of Buildings on Slopes," NCETEST-2014, Roorkee, India.

79 Kumar P, Sharma S, and Pandey AD (2012). "Effect of Soil-Structure Interaction on Building Response in Hilly Areas," The IUP Journal of Structural Engineering, 5(4) 7-27.

80 Kumar P, Sharma S, and Pandey AD (2012). "Influence of Soil-Structure Interaction in Seismic Response of Step Back-Set Back Buildings," ISET Golden Jubilee Symposium, IIT Roorkee, Paper No. C012.

81 Kumar P, Sharma S, and Pandey AD (2012). "Influence of Soil-Structure Interaction in Seismic Response of Step-Back Buildings," ISET Golden Jubilee Symposium, IIT Roorkee, Paper No. C013.

82 Kumar S (1996). "Seismic Analysis of Step-back and Set-back Buildings," PhD Thesis, University of Roorkee, India.

83 Kumar S and Mahajan AK (1991). "Dharamsala Seismotectonic Zone–Neotectonics and State of Stress in the Area," Himalayan Geology, 2(1) 53–57.

84 Kumar S and Mahajan AK (2001). "Seismotectonics of the Kangra Region, Northwest Himalaya," Techonophysics, 331(4) 359-371.

85 Kumar S and Paul DK (1994). "3-D Analysis of Irregular Buildings with Rigid Floor Diaphragms," Bulletin of Indian Society of Earthquake Technology, 1(3) 141-154.

86 Kumar S and Paul DK (1994). "Dynamic Analysis of Stepback and Setback Buildings," Tenth Symposium on Earthquake Engineering, University of Roorkee, v.1 341-350.

87 Kumar S and Paul DK (1997). "A State of Art: Seismic Safety of Step Back and Set Back Buildings," Bulletin of the ISET, 34(2) 47-74.

88 Kumar S and Paul DK (1999). "Hill Building Configuration from Seismic Consideration," Journal of Structural Engineering, 26(3) 179-185.

89 Kunnath SK and Zhao H (2009). "Effects of Near-Fault Vertical Accelerations on Highway Bridge Columns," Proceedings of the US-Japan Bridge Engineering Workshop.

90 Kunnath SK, Erduran E, Chai YH, and Yashinsky M (2008). "Effect of Near-Fault Vertical Ground Motions on Seismic Response of Highway Overcrossings," Journal of Bridge Engineering, 13(3) 282–290.

91 Lilhanand K and Tseng WS (1988). "Development and Application of Realistic Earthquake Time Histories Compatible with Multiple-damping Design Spectra," Proceedings of the Ninth World Conference on Earthquake Engineering, Tokyo-Kyoto, Japan, International Association for Earthquake Engineering, Tokyo, 819-824.

92 Lili X, Longjun X, and Marek AR (2005). "Representation of Near-Fault Pulse-Type Ground Motions," Earthquake Engineering and Engineering Vibration, 4(2) 193-199.

93 Longjun X, Marek AR, and X Lili (2006). "Design Spectra Including Effect of Rupture Directivity in Near-Fault Region," Earthquake Engineering and Engineering Vibration, 5(2) 159-170.

94 Mahajan AK, Kumar S (2004). "Linear Features Registered on the Landset Imagery and Seismic Activity in Dharamsala-Palampur Region (NW Himalayas)" Geofizika, 11(1) 15-25.

95 Mahesh P, Rai SS, Sivaram K, Paul A, Gupta S, Sharma R, and Gaur VK (2013). "One-Dimensional Reference Velocity Model and Precise Locations of Earthquake Hypocenters in the Central (Kumaon–Garhwal) Himalaya," Bulletin of the Seismological Society of America, 103 328–339.

96 Mahin S, Bertero V, Chopra A, and Collins R (1976). "Response of the Olive View Hospital Main Building during the San Fernando Earthquake," Earthquake Engineering Research Center, University of California, Berkeley, Report No.UCB/EERC-76/22.

97 Makris N and Roussos Y (1998). "Rocking Response and Overturning of Equipment Under Horizontal Pulse-Type Motion," PEER Report 1998-05. Berkeley, Collage of Engineering, University of California, 1-81.

98 Malhotra PK (1999). "Response of Building to Near-Field Pulse-Like Ground Motions," Earthquake Engineering and Structural Dynamics, 28(11) 1309-1326.

99 Maniatakis CA, Taflampas IM, and Spyrakos CC (2008). "Identification of Near-Fault Earthquake Record Characteristics," 14WCEE, Beijing, China.

100 Mark RK (1977). "Application of Linear Statistical Models of Earthquake Magnitude Versus Fault Length in Estimating Maximum Expectable Earthquakes," Geology, v.5 464-466.

101 Mavroeidis GP (2004). "Modeling and Simulation of Near-Fault Strong Ground Motions for Earthquake Engineering Applications," PhD Dissertation, State University of New York, Buffalo.

102 Mavroeidis GP and Papageorgiou AS (2003). "A Mathematical Representation of Near-Fault Ground Motions," The Bulletin of the Seismological Society of America, 93(3) 1099-1131.

103 Mavroeidis GP, Dong G, and Papageorgiou AS (2004). "Near-Fault Ground Motion and the Response of Elastic and Inelastic Single-Degree-of-Freedom (SDOF) Systems," Earthquake Engineering and Structural Dynamics, 33(9) 1023-1049.

104 Meena M, Shinde R, Sapre A, Sinha R, Goyal A, Deb SK, Dasgupta K, Kaushik HB, Dhang N, Chakrabarty S, Deb A, Menon A, Prasad AM, Menon D, Murty CVR, Krrishnan DR, Uma N, Singh Y, Paul DK, Haldar P, Rahul A, and Sood A (2013). "Seismic Vulnerability Assessment of Building Types in India," User Manual for Survey of Buildings, National Disaster Management Authority Government of India.

105 Menun C and Fu Q (2002). "An Analytical Model for Near-Fault Ground Motions and the Response of SDOF Systems," [C/CD]//EERI, 7th US National Conference on Earthquake Engineering. Boston, Paper No. 00011.

106 Ministry of Construction (2001). "Code for Seismic Design of Building GB50011-2001," Beijing, China Architecture and Building Press, 16-18.

107 Mittal H, Kumar A, and Ramhmachhuani (2012). "Indian National Strong Motion Instrumentation Network and Site Characterization of its Station," International Journal of Geosciences, 3(6A) 1151-1167.

108 Mohammad AH and Ramancharla PK (2013). "Modelling of Buried Faults Using Applied Element Method," International Journal of Earthquake Engineering and Science, 3(1) 1-16.

109 Molnar P and Lyon-Caen H (1989). "Fault Plane Solutions of Earthquakes and Active Tectonics of the Tibetan Plateau and its Margins," Geophysical Journal International, 99(1) 123-153.

110 Mukherjee S and Gupta VK (2002). "Wavelet-Based Generation of Spectrum-Compatible Time-Histories," Soil Dynamics and Earthquake Engineering, 22(9) 799-804.

111 Mukhopadhyay S and Kayal JR (2003). "Seismic Tomography Structure of the 1999 Chamoli Earthquake Source Area in the Garhwal Himalaya," Bulletin of the Seismological Society of America, 93(4) 1854–1861.

112 Nason R, Benfer NA, Coffman JL and Bernick JR (Editors (1973). "Increased Seismic Shaking Above A Thrust Fault, San Fernando, California, Earthquake of February 9, 1971, in Geological and Geophysical Studies," U.S. Dept. of Commerce, Natl. Oceanic Atmos. Adm., Environ. Res. Lab., Washington, D.C., 3, 123–126.

113 Ni J, Barazangi M (1984). "Seismotectonics of the Himalayan Collision Zone: Geometry of the Under-Thrusting Indian Plate beneath the Himalayas," Journal of Geophysical Research, 89(B2) 1147–1163.

114 Oglesby DD, Archuleta RJ and Nielson SB (1998). "Earthquakes on Dipping Faults: the Effects of Broken Symmetry," Science, 280 1055–1059.

115 Oglesby DD, Archuleta RJ and Nielson SB (2000). "The Three Dimensional Dynamics of Dipping Faults," Bulletin of the Seismological Society of America, 90(3) 616–628.

116 Pachuau LZ (1992). "Seismic Response of RC Framed Building on Hill-Slopes," M.E Dissertation, Department of Earthquake Engineering, University of Roorkee.

117 Pandey AD, Kumar P, and Sharma S (2011). "Seismic Soil-Structure Interaction of Buildings on Hill Slopes," International Journal of Civil and Structural Engineering, 2(2) 535-546.

118 Pandey MR, Tandukar RP, Avouac JP, Lavfi J and Massot JP (1995). "Interseismic Strain Accumulation on the Himalayan Crustal Ramp (Nepal)" Geophysical Research Letters, 22(7) 751-754.

119 Paul A, Sharma ML, and Singh VN (1998). "Estimation of Focal Parameters of Uttarkashi Earthquake Using Peak Ground Horizontal Accelerations," ISET Journal of Earthquake Technology, Paper No. 372, 35(1-3) 1-8.

120 Petersen MD, Frankel, AD, Harmsen SC, Mueller CS, Haller KM, Wheeler RL, Wesson RL, Zeng Y, Boyd OS, Perkins DM, Luco N, Field EH, Wills CJ and Rukstales KS (2008) "Documentation of the 2008 Update of the United States National Seismic Hazard Maps," U.S. Geological Survey Open-File Report 2008-1128, 61 .

121 Power M, Chiou B, Abrahamson N, Bozorgnia Y, Shantz T and Roblee C (2008). "An Overview of the NGA Project," Earthquake Spectra, 24(1) 3-21.

122 Rajendran K, Rajendran CP, Jain SK**,** Murty CVR, and Arlekar JA (2000). "The Chamoli Earthquake, Garhwal Himalaya: Field Observations and Implications for Seismic Hazard," Current Science, 78(1) 45-51.

123 Ramancharla PK and Meguro K (2006). "3D Numerical Modeling of Faults for Study of Ground Surface Deformation Using Applied Element Method," Current Science, 91(8) 1026-1037.

124 Ramancharla PK, Hatem TD, and Meguro K (2004). "Dynamic Modeling of Dip-Slip Faults for Studying Ground Surface Deformation Using Applied Element Method," 13WCEE, Canada, Paper No. 832.

125 Rathje EM, Faraj F, Russell S, and Bray JD (2004). "Empirical Relationships for Frequency Content Parameters of Earthquake Ground Motions," Earthquake Spectra, 20(1) 119-144.

126 Rautela P, Thakur VC, (1992). "Structural Analysis of the Punjal Thrust Zone, Himachal Himalaya, India," J. Him. Geol, 3(2) 195–207.

127 Reiter L (1990). "Earthquake Hazard Analysis-Issues and Insights," New York: Columbia University Press, pp 254.

128 Rezai M and Ventura CE (2002). "Analysis of Strong and Weak Ground Motions Recorded at Two Sites during Loma Prieta Earthquake by Wavelet Transform," Canadian Journal of Civil Engineering, 29(1) 157-170.

129 Rodriguez MA (2000). "Near Fault Seismic Site Response," PhD Thesis, Civil Engineering, University of California, Berkeley.

130 Ruegg JC, Kasser M, Tarantola A, Lepine JC and Chouikrat B (1982). "Deformations Associated with the El Asnam Earthquake of 10 October 1980; Geodetic Determination of Vertical and Horizontal Movements," Bulletin of the Seismological Society of America, 72 (6A) 2227–2244.

131 S K Deb **(**2004). "Seismic base isolation–An overview," Special Section: Geotechnics and Earthquake Hazards, Current Science, 87(10) 1426-1430.

132 Sabegh SY (2010). "Detection of Pulse-Like Ground Motions Based on Continues Wavelet Transform," Journal of Seismology, 14(4) 715-726.

133 Shakib H and Datta TK (1993). "Inelastic Response of Torsionally Coupled System to an Ensemble of Nonstationary Random Ground Motion," Engineering Structures, 15(1) 13–20.

134 Shakib H and Ghasemi A (2007). "Considering Different Criteria for Minimizing Torsional Response of Asymmetric Structures under Near-Fault and Far-Fault Excitations," International Journal of Civil Engineerng, 5(4) 247–265.

135 Shakib H and Tohidi RZ (2002). "Evaluation of Accidental Eccentricity in Buildings Due To Rotational Component of Earthquake," Journal of Earthquake Engineering, 6(4) 431–445.

136 Shrikhande M, Basu S, Mathur BC, Mathur AK, Das JD and Bansal MK (2000). "Strong motion data. Report on Chamoli Earthquake of March 29, 1999," Department of Earthquake Engineering, University of Roorkee, Roorkee, 27-43.

137 Shrikhande M, Rai DC, Narayan JP, and Das J (2000). "The March 28, 1999 Earthquake at Chamoli, India," 12WCEE, Auckland-New Zealand, Paper No. 2838.

138 Shuang L and XIE Li (2007). "Progress and Trend on Near-Field Problems in Civil Engineering," Acta Seismologica Sinica, 20(1) 105-114.

139 Silva WJ and Lee K (1987). "State-of-the-Art for Assessing Earthquake Hazards in the United States: WES RASCAL Code for Synthesizing Earthquake Ground Motions," Miscellaneous Paper S-73-1, Report 24, U.S. Army Engineer Waterways Experiment Station, Vicksburg, MS.

140 Singh SK, Bansal BK, Bhattacharya SN, Pacheco JF, Dattatrayam RS, Ordaz M, Suresh G, Kamal, and Hough SE (2003). "Estimation of Ground Motion for Bhuj (26 January 2001; M_w 7.6) and for Future Earthquakes in India," Bulletin of the Seismological Society of America, 93(1) 353-370.

141 Singh SK, Iglesias A, Dattatrayam RS, Bansal BK, Rai SS, Campos XP, Suresh G, Baidya PR, and Gautam JL (2006). "Muzaffarabad Earthquake of 8 October 2005 (Mw 7.6): A Preliminary Report on Source Characteristics and Recorded Ground Motions," Current Science, 91(5) 689-695.

142 Singh SK, Mena E, and Castro R (1988). "Some Aspects of Source Characteristics of the 19 September 1985 Michoacan Earthquake and Ground Motion Amplification in and Near Mexico City from Strong Motion Data," Bulletin of the Seismological Society of America, 78(2) 451-477.

143 Singh SK, Mohanty WK, Bansal BK, and Roonwal GS (2002). "Ground Motion in Delhi from Future Large/Great Earthquakes in the Central Seismic Gap of the Himalayan Arc," Bulletin of the Seismological Society of America, 92(2) 555–569.

144 Singh SK, Ordaz M, and Pacheco JF (2003). "Advances in Seismology with Impact on Earthquake Engineering," Chapter- 67, International Handbook of Earthquake & Engineering Seismology, Part B, 1081-1095.

145 Singh SK, Ordaz M, Anderson JG, Rodriguez M, Quaas R, Mena E, Ottavian M, and Almora D (1989). "Analysis of Near-Source Strong-Motion Recordings along the Mexican Subduction Zone," Bulletin of the Seismological Society of America, 79(6) 1697-1717.

146 Sinha R, Goyal A, Murty CVR, Krishna C, Meena M and Shinde R (2014). "Mw=8.0 Mandi Earthquake Scenario: Multi-State Exercise and Awareness Campaign," National Disaster Management Authority, Government of India.

147 Sinha R, Murty CVR, Goyal A, Krishna C and Vishnoi P (2012). "Mw=8.0 Mandi Earthquake Disaster Scenario for Disaster Risk Management," National Disaster Management Authority, Government of India.

148 Somerville P (1998). "Development of an Improved Ground Motion Representation for Near Fault Ground Motions," SMIP98 Seminar on Utilization of Strong-Motion Data, Oakland, CA.

149 Somerville P (2000). "Characterization of Near Fault Ground Motion," US-Japan Workshop on Effects of Near-Field Earthquake Shaking, San Francisco, CA.

150 Somerville P, Smith N, Graves R, and Abrahamson N (1997b). "Modification of Empirical Strong Ground Motion Attenuation Relations to Include the Amplitude and Duration Effects of Rupture Directivity," Seismological Research Letters, 68(1) 180-203.

151 Somerville PG (2002). "Characterizing Near Fault Ground Motion for the Design and Evaluation of Bridges," Proceedings of the 3th National Seismic Conference and Workshop on Bridges and Highways, State University of New York at Buffalo, 137–148.

152 Somerville PG (2003). "Magnitude Scaling of the Near Fault Rupture Directivity Pulse," Physics of the Earth and Planetary Interiors, 137(1-4) 201–212.

153 Somerville PG, Irikura K, Graves R, Sawada S, Wald D, Abrahamson N, Iwasaki Y, Kagawa T, Smith N, Kowada A (1999). "Characterizing Crustal Earthquake Slip Models for the Prediction of Strong Ground Motion," Seismological Research Letters, 70(1) 59-80.

154 Sri Ram V, Kumar D, Khattri KN (2005). "The 1986 Dharamsala Earthquake of Himachal Himalaya – Estimates of Source Parameters, Average Intrinsic Attenuation and Site Amplification Functions" Journal of Seismology, 9(4) 473-485.

155 Srivastava HN, Dube RK, Raj H (1987). "Space and Time Variation in the Seismicity Patterns Preceding Two Earthquakes in the Himachal Pradesh, India" Tectonophysics, 138(1) 69–77.

156 Thakura VC (1998). "Structure of the Chamba Nappe and Position of the Main Central Thrust in Kashmir Himalaya," Journal of Asian Earth Sciences, 16(2–3) 269–282.

157 U.S.A.C.E (1999). "EM 1110-2-6050: Engineering and Design Response Spectra and Seismic Analysis for Concrete Hydraulic Structures," Engineer Manual, Department of the Army U.S. Army Corps of Engineers Washington.

158 Uniform Building Code (1997). International Conference of Building Officials, Whittier, California.

159 Ventura CE, Archila M, Bebamzadeh A and Finn WDL (2011). "Large Co-seismic Displacements and Tall Buildings," The Structural Design of Tall and Special Buildings, 20(S1) 85–99.

160 Verma RK (1989). "Earthquake Response Spectrum Analysis of Buildings on Hill Slopes," M.E Dissertation, Department of Earthquake Engineering, University of Roorkee.

161 Wang GQ, Zhoua XY, Zhangb PZ, and Igelc H (2002). "Characteristics of Amplitude and Duration for Near Fault Strong Ground Motion from the 1999 Chi-Chi Taiwan Earthquake," Soil Dynamics and Earthquake Engineering, 22(1) 73-96.

162 Wells DL and Coppersmith KJ (1994). "New Empirical Relationships among Magnitude, Rupture Length, Rupture Area and Surface Displacement," Bulletin of Seismological Society of America, 84(4) 974-1002.

163 Xin-le LI and Xi ZHU (2004). "Study on Equivalent Velocity Pulse of Near-Fault Ground Motion," Acta Seismologica Sinica, 17(6) 697-706.

164 Xin-le LI, Hui-juan D, and Xi ZHU (2007). “Response Spectrum of Seismic Design Code for Zones Lack of Near-Fault Strong Earthquake Records,” Acta Seismologica Sinica, 20(4) 447-453.

165 Yu-ji T, Qing-shan Y, and LU Ming-qi (2007). “Simulation Method of Near-Fault Pulse-Type Ground Motion,” Acta Seismologica Sinica, 20(1) 80-87.